Cyclone Reactors for Selective Non-Catalytic Reduction of NO_x

Svith, Casper Stryhn

Publication date:
2020

Document Version
Publisher's PDF, also known as Version of record

Ph.D. Thesis

Cyclone Reactors for Selective Non-Catalytic Reduction of NO_x

2020

Casper Stryhn Svith

Technical University of Denmark

Department of Chemical and Biochemical Engineering

Combustion and Harmful Emission Control Research Center

Casper Stryhn Svith
2020

Combustion and Harmful Emission Control Research Center
Department of Chemical and Biochemical Engineering
Technical University of Denmark

Søltofts Plads 228A
2800 Kongens Lyngby
Danmark
Phone: +45 4525 2822
Email: kt@kt.dtu.dk

Abstract

The objective of this thesis is to investigate the performance of cyclone reactors, focusing on Selective Non-Catalytic Reduction of NO_x (SNCR), outlining the existing knowledge and improving the understanding.

Cyclone reactors provide an opportunity for process intensification, by facilitating gas-particle separation, gas-solid heat exchange, and reaction in a single unit simultaneously. One important application of cyclone reactors is the NO_x abatement by SNCR in combustion processes. Cyclone SNCR is commonly utilized in the cyclones for CFBC (Circulating Fluidized Bed Combustor) boilers, and in cyclone preheater systems for cement and mineral wool production.

A literature study on cyclone reactors has been conducted to describe the current state-of-the-art of cyclone reactors as well as the current knowledge gap in understanding and modelling cyclone reactors, as well as the SNCR process. Analysis of the available literature on industrial applications of cyclone reactors showed that cyclone reactors are primarily used for high temperature processes, such as combustion, gasification, pyrolysis, pyro-metallurgical smelting processes, and flue gas cleaning by SNCR. Many other potential applications have been investigated in laboratory or pilot scales. The available literature on modeling of cyclone reactors showed a lack of detailed reactor models and a lack of experimental verification of existing models. From the SNCR literature, the published results on ammonia slips are scarce both experimentally and theoretically.

A pilot scale cyclone reactor has been modified and used to conduct a series of SNCR experiments at different reactor conditions. The overall performance of SNCR was tested. The temperature profiles and the concentration profiles inside the cyclone reactor were mapped at various conditions. The temperature in the cyclone inlet varied between 866 and 1023 °C, while the inlet NO concentration was kept at ~500 ppm. Gaseous NH_3 was injected in the cyclone inlet using nitrogen as carrier gas, with the NH_3/NO molar ratio varied between 0 and 7. The carrier gas flow rate was varied between 0 and 1.5 Nl/min and the injection tube position in the inlet was also varied. The optimal conditions for NO_x reduction were found to be at an inlet temperature of 982 °C, NH_3/NO molar ratio of 1.6, and carrier gas flow of 1.5 Nl/min. At these conditions, a NO reduction of 69 % was achieved with only 4 ppm ammonia slip. The temperature profiles showed large temperature drops in the cyclone reactor of close to 400 °C from the top to the bottom of the cyclone, suggesting that the main reaction zone of the cyclone was the inlet section and the upper parts of the cyclone chamber. This was confirmed by the concentration profiles measured inside the cyclone reactor, which showed very little or even no NO reduction in the lower part of the cyclone. Despite the low temperatures (600-800 °C) in the lower part, a significant ammonia conversion was still observed in this region. Based on the concentrations measured in the outer and inner vortex and in the outlet, it was concluded that a large fraction of the flue gas bypass' the majority of the cyclone volume due to lip leakage.

The pilot scale experiments were modelled using both simple and detailed kinetics combined with simple reactor models, and a compartment reactor network model was also developed. The qualitative trends of NO reduction and ammonia slip were captured by the models using detailed kinetics. However, NO reduction and the ammonia slip were significantly over-predicted for most of the experimental results. The modeling results were insensitive to the choice of reactor model and mixing model, while the influences of temperature, gas composition and kinetics model were significant. The simple kinetics of Duo et al. [1] showed the best quantitative fit with the experimental results. The developed compartment model were able to adjust the flow pattern and represent the temperature distribution in the cyclone reactor. Furthermore, the model was able to qualitatively reproduce the internal concentration profiles caused by the double vortex flow in the cyclone reactor, using both detailed and simple kinetics. The simple kinetics generally showed a good quantitative agreement for the NO concentrations, but unsatisfactory for the ammonia.

Industrial scale measurements of the SNCR process were conducted in a preheater cyclone system. In the measurement campaign, raw NO_x emissions, flue gas composition, temperatures, and the performance of SNCR were measured. The system were modelled using the measurement data, simple reactor models and detailed chemical kinetics. Experimentally the SNCR process achieved a NO_x reduction of up to 70 % without exceeding ammonia slip limits of 40 ppmv for the standard preheater conditions. When operating at low temperatures in the preheater system, the SNCR performance was insufficient for meeting the emission limits, due to high ammonia slips. The mixing limitations in the riser was found to be severe and only 0-15 % NO_x conversion occur in the riser, meaning the cyclone chamber is the largest contributor to the conversion. The models could predict the overall trends of the SNCR process using the measured temperature and gas composition data as input. However, the NO_x removal and the ammonia slip were over-predicted, as also observed in the pilot scale results.

Danish abstract

Målet med denne afhandling er at undersøge brugen af cyklonreaktorer, med fokus på selektiv ikke-katalytisk reduktion af NO_x (SNCR-processen), ved at redegøre for den eksisterende viden samt indsamling af ny for at forbedre forståelsen.

Cyklonreaktorer giver mulighed for procesintensivering, ved at muliggøre gas-partikel separation, gas-partikel varmeudveksling samt reaktion samtidigt i en enkelt enhedsoperation. En vigtig brug af cyklonreaktorer er fjernelse af NO_x fra forbrændingsprocesser ved SNCR. Cyklon SNCR bruges oftest i cykloner til cirkulerende fluid bed kedler og i cyklon forvarmer systemer til cement og stenulds produktion.

Et litteraturstudie om cyklonreaktorer er blevet udført for at beskrive den nuværende state-of-the-art for cyklonreaktorer, samt det nuværende vidensgab i forståelsen af og modelleringen af cyklonreaktorer, samt SNCR-processen. En gennemgang af den tilgængelige litteratur om industriel anvendelse af cyklonreaktorer viste, at cyklonreaktorer primært bruges til forbrændings- og højtemperaturprocesser, som forgasning, pyrolyse, metallurgisk smeltning og røggasrensning ved SNCR. Mange andre potentielle anvendelser er blevet undersøgt i laboratorie- og/eller pilotskala. Den tilgængelige litteratur om modellering af cyklonreaktorer viste at en mangel på detaljerede reaktormodeller og de eksisterende modeller manglede eksperimentel verifikation. Fra litteraturen om SNCR-processen, var der kun få publicerede resultater om koncentrationerne af uomdannet ammoniak, både i eksperimentelle og teoretiske resultater.

En pilotskala cyklonreaktor er blevet modificeret og brugt til at udføre en række SNCR forsøg, under forskellige betingelser. Temperatur- og koncentrationsprofilerne inde i cyklonreaktoren, samt den overordnede ydeevne blev målt under forskellige betingelser. Indgangstemperaturerne varierede mellem 866 og 1023 °C, mens en baggrundskoncentration af NO blev holdt på ~500 ppmv. Ammoniak gas blev injiceret i cyklonens indløb sammen med nitrogen som injektionsgas, med et NH_3/NO-molforhold på mellem 0 og 7, en strøm af injektionsgas på mellem 0 og 1.5 Nl/min, og injektionsrørets position blev varieret. De optimale betingelser for SNCR-processen blev fundet til at være en indgangstemperatur på 982 °C, et NH_3/NO-molforhold på 1.6, og en strøm af injektionsgas på 1.5 NL/min. Under disse betingelser blev en reduktion af NO på 69 % opnået med en koncentration af uomdannet ammoniak på kun 4 ppmv. Temperaturprofilerne viste store temperaturfald i cyklonreaktoren på tæt på til 400 °C fra top til bund af cyklonen, dette antydede at cyklonens primære reaktionszone var i indgangssektionen og den øvre del af cyklonkammeret. Koncentrationsprofilerne målt inde i cyklonen bekræftede dette, da kun lidt eller intet NO blev fjernet i den nedre del af cyklonen. På trods af de lave temperaturer (600-800 °C) i den nedre del af cyklonen blev der observeret en betydelig omdannelse af ammoniak i dette område. Baseret på koncentrationerne målt i den ydre og indre vortex, samt i cyklonreaktorens udgang, kunne det konkluderes at en stor del af gassen ikke passerede størstedelen af cyklonens volumen, men i stedet strømmede ud af cyklonen umiddelbart under vortex finderen.

Pilotskalaforsøgene blev modelleret ved anvendelse af både simpel og detaljeret kinetik kombineret med enkle reaktormodeller, og en reaktor netværksmodel blev udviklet. Reaktor modellerne kunne estimere de kvalitative tendenser for NO-reduktionen og uomdannet ammoniak, ved hjælp af detaljeret kinetik. NO-reduktionen og det uomdannede ammoniak blev dog signifikant overestimeret for størstedelen af forsøgsresultaterne. Modelleringsresultaterne var ufølsomme over for valget af reaktormodel og opblandingsmodel, mens følsomheden for temperatur, gassammensætning og kinetikmodel var signifikant. De bedste kvantitative modelresultater, ved sammenligning med de eksperimentelle, blev opnået med den simple kinetik model af Duo et al. [1]. Den udviklede reaktor netværksmodel var i stand til at justere strømningsmønstret og repræsentere temperaturfordelingen i cyklonreaktoren. Modellen var i stand til kvalitativt at gengive koncentrationsprofilerne forårsaget af strømningsmønsteret, både ved brug af detaljeret og simpel kinetik. Den simple kinetik havde gode kvantitative resultater for NO koncentrationsprofilerne, mens resultaterne for NH_3 koncentrationsprofilerne var utilfredsstillende.

Målinger af SNCR-processen i et forvarmer cyklonsystem blev foretaget i industriel skala. I målekampagnen blev, baggrunds NO_x-emissionerne, røggassammensætningen, temperaturerne og den overordnede ydeevne af SNCR-processen målt. Systemet blev modelleret ved hjælp af måledata, enkle reaktormodeller og en detaljeret kinetiks model. Ved standardbetingelserne i systemet kunne en 70 % reduktion af NO_x opnås, uden at overskride grænsen for ammoniakudledning på 40 ppmv. Ved drift med lavere temperaturer i systemet, var det ikke muligt at overholde emissionsgrænserne ved hjælp af SNCR, grundet høj ammoniakudledning. Der blev fundet store problemer med opblanding af ammoniak reaktanten i riseren med kun 0-15 % NO_x i indgangen til cyklonen, hvilket betyder at selve cyklonen, er den primære reaktionszone. Modellerne kunne reproducere, tendenserne for SNCR-processen ved brug af de målte temperatur- og røggassammensætningsdata som input. Dog blev NO_x reduktion og koncentrationen af uomdannet ammoniak overestimeret, ligesom i pilotskala resultaterne.

Preface and Acknowledgements

This thesis has been written and submitted as a partial fulfilment of the requirements, for acquiring the Ph.D. degree from the Technical University of Denmark (DTU). The studies for the Ph.D. program have been conducted, in the period from September 2016 to March 2020, at the Combustion and Harmful Emission Control (CHEC) research center, Department of Chemical and Biochemical Engineering at Technical University of Denmark (DTU). Part of the work have been conducted in collaboration with Rockwool International.

The work has been supervised by Professor Kim Dam-Johansen, Associate Professor Weigang Lin, and Associate Professor who I would like thank for their great help and support, both academically and practically.

I would also like to thank to the people at the Department of Chemical and Biochemical Engineering who helped make this possible: Professor Peter Glarborg, for his advice and our discussions on SNCR and reaction modelling; Senior Researcher Peter Arendt, for help coordinating the industrial partnership; the technicians Anders Kjersgaard, Nikolaj Vinterberg Nissen, and Søren Post, without whom the experimental work could not have succeeded; all the great administration staff at KT with special mentions to Anne Helene Juul, Hanne Mikkelsen, Gitte Rossen-Jørgensen, and Klaus Kirstein Haubroe; and all my close colleagues and fellow Ph.D. students both former and present, who have been an inspiration to work with and great support socially, mentally, and academically.

I would like to extent my thanks to the people at Rockwool International, who helped facilitate the industrial measurement campaign, especially Haosheng Zhou.

Finally, thank you to all my friends and family, for their support and willingness to listen to me explain my research for the 100th time, especially my wonderful wife who has a patience that cannot be understated.

Casper Stryhn Svith

Technical University of Denmark

14. March 2020

Table of Contents

List of Figures

List of Tables

Notation

Abbreviations

CFB	Circulating Fluidized Bed
CFBC	Circulating Fluidized Bed Combustor
CFD	Computational Fluid Dynamics
CLD	Chemi-luminescence detector
CSTR	Continuously stirred tank reactor
EU	European Union
FCC	Fluid Catalytic Cracking
FV	Finite Volume
HE	High efficiency / Heat exchanger
LB	Lattice-Boltzmann
LDA	Laser Doppler Anemometry
LES	Large Eddy Simulation
LHV	Lower heating value
MFC	Mass flow controller
PFR	Plug flow reactor
RANS	Reynold averaged Navier-stokes
RNG	Renormalization Group
RSM	Reynold stress model
RTD	Residence time distribution
SCR	Selective Catalytic Reduction
SNCR	Selective non-Catalytic Reduction
UV	Ultraviolet light
QUICK	Quadratic Upstream Interpolation for Convective Kinematics
VOC	Volatile Organic Compounds

List of symbols

Greek letters

α	Bypass fraction	-
β	Stoichiometric ratio	-
β_{lede}	Volume fraction for the lede model	-
Δ	Difference	-
λ	Thermal conductivity	$\mathrm{J\ (m \cdot K \cdot s)^{-1}}$
μ	Dynamic viscosity	Pa s
ρ	Density	$\mathrm{kg \cdot m^{-3}}$
τ	Residence time	s
η_c	Collection efficiency	-

Roman letters

a	Cyclone inlet height	mm, cm, or m
A	Area	$\mathrm{mm^2}$, $\mathrm{cm^2}$, or $\mathrm{m^2}$
b	Cyclone inlet width	mm, cm, or m
B	Dust outlet diameter	mm, cm, or m
d_p	Particle diameter	mm, cm, or m
d	Diameter	mm, cm, or m
D	Cyclone diameter	mm, cm, or m
De	Vortex finder diameter	mm, cm, or m
E_a	Activation Energy	kJ/mol
f	Cumulated fraction	-
Fm	Solid loading ratio	-
Fe	Federov number	-
g	Gravitational acceleration	$\mathrm{m/s^2}$
h	Heat transfer number	$\mathrm{W/m^2K}$
h	Cylinder length	mm, cm, or m
H	Cyclone length	mm, cm, or m
J	Momentum ratio	-
K	Reaction constant	1/s
L	Length of plugflow zone	m
$\dot{m}$	Mass flow	kg/s
$\dot{n}$	Number flow	number/s
Nu	Nusselt Number	-
P	pressure	Pa
Pr	Prandtl Number	-
$\dot{Q}$	Heat flow	W
Re	Reynolds number	-
S	Vortex finder heigth	

Sh	Sherwood number	-
t	Time	s or min
T	Temperature	°C or K
u	Directional velocity	m/s
v	velocity	m/s
V	volume	mm^3, cm^3, or m^3

Subscripts

c	Collected
e	Elutriated
g	Gas
(g)	Gas
H	Hydraulic
i	Inlet/interval
i	Inlet
in	Inlet
k	Section
(l)	Liquid
Lede	Parameter related to lede model
P	Particle
S	Solid
(s)	Solid
t	Terminal
0	Initial/inlet

Chapter 1 – Introduction

Cyclones are primarily known for their industrial application as a separation unit for gas-solid, gas-liquid, or in the case of a hydrocyclone liquid-solid separation. Moreover, cyclones can also be utilized as gas-solid heat exchangers and as reactors. The use as gas-solid heat exchangers is widely applied in mineral processing industry, such as cement, mineral wool, metallurgy etc., while the use as reactors is mainly focused on high temperature processes, such as combustion, gasification, pyrolysis, pyro-processing of metal ores, and Selective Non-Catalytic Reduction [2,3].

Utilization of gas-solid separation cyclone as a reactor offers intensive mixing due to the swirling double vortex flow, comparably long residence time for particles, short residence time for gas, and short contact time between gas and solids. Furthermore, cyclone reactors based on separation cyclones offer an opportunity for process intensification, by achieving gas-particle separation and reaction in a single process unit simultaneously.

One of the important applications of cyclone reactors for process intensification is the NO_x abatement by SNCR (Selective Non-Catalytic Reduction) in stationary combustion processes [3]. In the SNCR process a reduction agent such as ammonia, urea, or cyanuric acid is injected into the hot flue gas stream, thereby reducing NO_x. This is commonly done in the cyclones of CFBC (Circulating Fluidized Bed Combustor) boilers for heat and power generation, and in the preheater cyclone systems of industrial production processes such as cement clinker and stone wool manufacturing.

The overall scope and objectives of this thesis are to improve the understanding of cyclone reactors and specifically the SNCR process in gas-solid cyclone reactors. A literature study is conducted to describe the state-of-the art knowledge of cyclone reactors in terms of industrial applications and research work, and the current knowledge gap in understanding and modelling cyclone reactors. Through experimental work in pilot and industrial scale cyclone reactors and through modeling, a systematic study of the SNCR process in cyclone reactors is carried out in this thesis.

The thesis is structured as follows:

Chapter 2 - Literature study: This chapter starts with a short introduction on cyclone technology in general, followed by a review of cyclone reactors in terms of industrial applications and research work through experiments and modeling, and finally a section about NOx emissions and the SNCR process. Describing the knowledge gap to be addressed.

Chapter 3 - Pilot scale experiments: This chapter describes the materials and methods as well as the results for the pilot scale experiments. The material and methods part contains a description of the pilot setup, the analysis equipment, and the experimental procedures used. The results are presented and discussed.

Chapter 4 - Pilot scale modelling – This chapter describes how the models from literature used in this work is implemented and the development of new models in this work. The model results are tested against each other and the experimental results.

Chapter 5 - Industrial scale work: This chapter presents the work conducted with industrial scale application of SNCR in cyclone preheater systems. First a short introduction to the process followed by a modeling study, based on plant operating data supplied by Rockwool, is presented. Then an industrial measurement campaign, its results and the modeling hereof is detailed and discussed.

Chapter 6 - Conclusions and perspective: Here conclusions on all the work detailed in the thesis will be summarized, and suggestions of future work is given.

Chapter 2 – Literature study

After their development in the late 1800s, cyclones have become a standard unit operation in many industries. The first patented cyclonic particle separation device, the "Dust Collector" by John M. Finch from 1885 [4], looked very different from how a standard cyclone looks today. However, it took only a relatively short time period (for the times) before cyclones roughly resembling the standard cylinder-on-cone shape that we know today were developed. An example of this is the design which O.M Morse filled for patent in 1905 [5]. The original devices were quite complex compared to today's standard cyclones, but Finch's new idea of using centrifugal forces to separate particles from gas is what kicked off the development of cyclones [6]. Before this development, particle separation primarily consisted of "dead air" chambers, with low gas velocities in order to facilitate particle settling, and filtration [6,7]. Compared to other separation technologies, the key advantage of a cyclone, is the ability to continuously separate solid or liquid from the gas phase at high efficiency and low pressure loss with a high throughput for a small size. Cyclones can handle a wide variety of particle sizes and loadings. Furthermore, the simplicity of the design without moving parts ensures low manufacturing and maintenance cost, long lifespan and operability at very high temperature, compared to other separation techniques [6,8].

While cyclones are primarily used as separation devices, they can also act as gas-solid heat exchangers and reactors. The use of cyclones as reactors is a relatively new concept. A cyclone reactor can perform several functions simultaneously e.g., separation, heat transfer and reaction. Cyclone reactors are compact and gives good contact between gas and solid, while still ensuring that the contact time between gas and solid is short [2]. The literature on cyclones focusing on the separation aspects is plentiful and the textbook "Gas Cyclones and Swirl Tubes" by Hoffman and Stein [6] gives an excellent overview of both the basics and the more advanced parts of cyclone separation. As such this literature review will focus on the not so well described use of cyclones as reactors, and only in a summary manner describe the basics of cyclone separator design and operation. The scope and objectives of this review will be to describe and categorize the most used types of cyclone reactors, to describe and review cyclone reactor applications, and to give an overview of existing methods for cyclone reactor modeling, and to finally identify the current knowledge gap, for understanding, modeling, and developing cyclone reactors.

2.1 Cyclone basics

The basic concept behind any cyclonic device for gas-liquid/gas-solid separation is that the particle/droplet containing gas stream is forced into a swirling motion. Due to the rotation of the flow, the dense phase (liquid or solid) will be accelerated towards the wall by the "centrifugal force", while the gas phase will be flow towards the middle of the separation chamber. For simplicity, the focus in this section will be on gas-solid systems, however most of the principles for gas-liquid systems are the same or similar. The most common cyclone depicted and described is the standard reverse-flow, cylinder-on-cone cyclone with a tangential slot inlet. Here the inlet is designed in such a way that the gas stream enters the cyclone

tangentially to the wall thereby inducing the swirling motion. A sketch of such a cyclone is shown in Figure 2.1 [6].

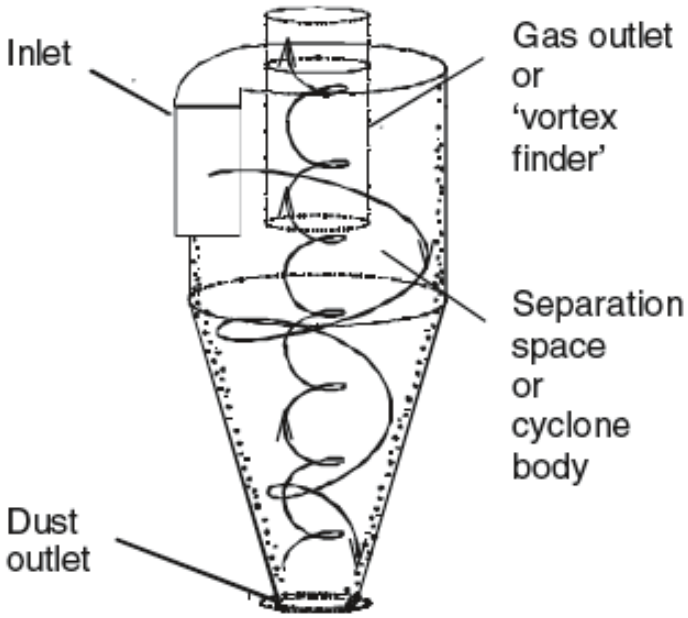

Figure 2.1: Principle sketch of standard reverse-flow, cylinder-on-cone cyclone (from [6]*)*

This section will focus on this design and explain different phenomena and design rules, while other designs and variations will be described shortly.

2.1.1 Flow pattern

Since the invention of cyclones and their wide implementation in industry, the flow pattern has been and continue to be the subject of extensive investigations. This is due to the fact that although the design is relatively simple, the flow pattern inside a cyclone is complicated [6].

2.1.1.1 Gas

The overall gas flow pattern in cyclones is generally well understood from experimental data collected over a long time span for many different geometries and scales by using both simple and advanced measurement techniques [6]. When describing the gas flow pattern it can be divided into the primary flow pattern and secondary flow pattern [6].

The primary flow is the double vortex. The double vortex is made up of a downward moving spiral flow in the outer part and an upward moving spiral flow in the center part. The gas rotates downwards in the outer part of the cyclone while part of the stream gradually flows into the inner part where it rotates upwards into the vortex finder, creating a flow pattern known as the double vortex as illustrated in Figure 2.1 [8,9].

The flow is visualized more detailed by the velocity profiles of the 3 velocity components shown in Figure 2.2, as reported by ter Linden in 1949 [10]. Note that even though these results are old and measured with now considered un-suitable techniques (pitot tube) the trends and

shape of the profiles fit well with newer results measured with more advanced techniques [6,11].

As seen on the left part of Figure 2.2, the vertical velocity is negative in the outer part showing a downward flow, while it is positive and therefore upwards going in the inner part of the cyclone. The right part of the figure is can be seen that the tangential velocity increases inward towards the inner vortex with the maximum being roughly at the edges of the vortex finder in the top and then dropping again toward the center axis. Furthermore, by looking at the radial velocity it can be seen that there is a small inward velocity over the whole length of the cyclone except in the center of the inner vortex. This inward flow gradually transfers the gas flow from the outer vortex to the inner vortex [10].

The general rotating motion of the primary flow gives rise to distinct pressure gradients inside the cyclone chamber, where the highest pressure is seen along the walls, and the pressure decreases inwards toward the center [6]. This behavior is depicted well by the measured data from ter Linden 1949 [10] shown in Figure 2.3. The pressure gradients and the inherent instability of the swirling vortex cause the secondary flow structures [6].

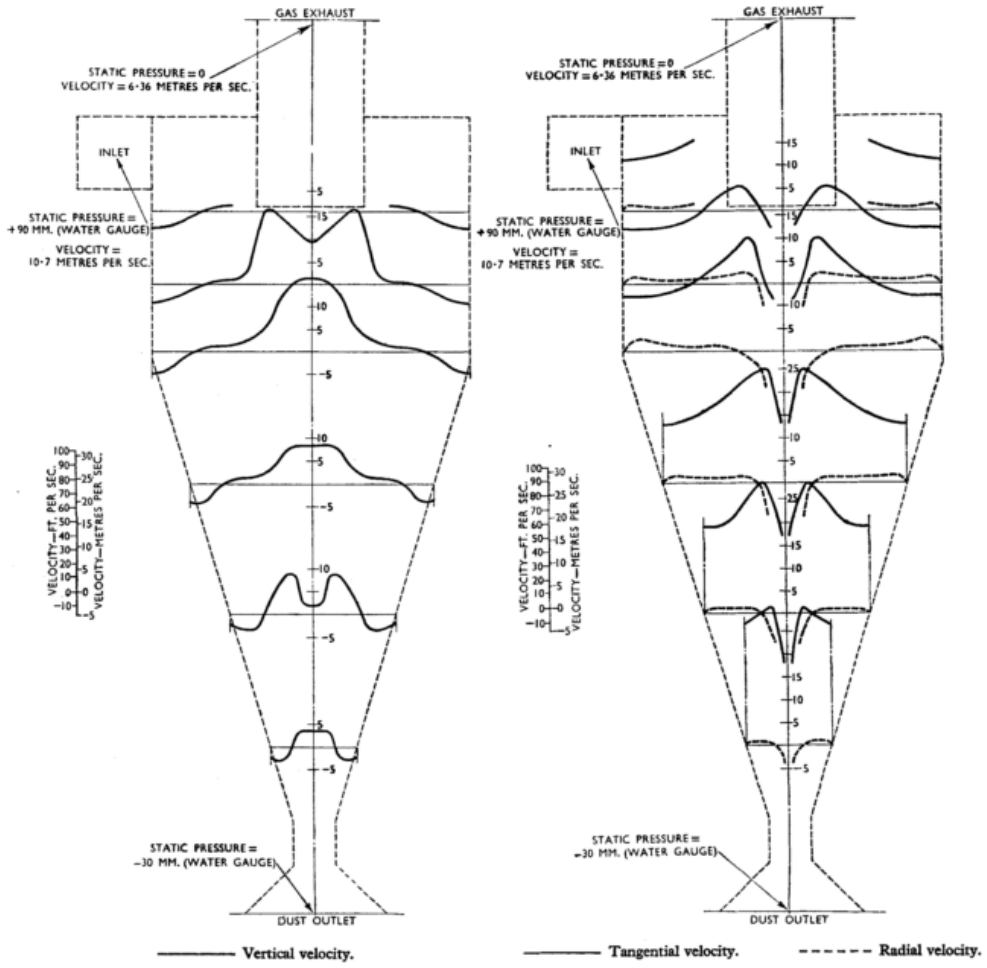

Figure 2.2: Depiction of the profile of the 3 velocity components in a cone-on-cylinder cyclone (from [10]*)*

The secondary flow, caused by the pressure gradients, consists primarily of flow along the walls. This cause a vertically circulating flow between the inner and the outer vortex and a bypass form the outer vortex to the inner vortex over the tip of the vortex finder, a phenomena called lip leakage.

The flow profile in Figure 2.2 and the pressure profile in Figure 2.3, are symmetrical as they are double representations of time averaged measurements between one wall and the axis. In real system the profiles are not symmetrical. Often the vortex will attach itself to a wall of the cyclone or in the chamber or tube below the dust exit and the center of rotation will continuously move around the cyclone. This is referred to as the vortex precessing and reduces the efficiency of the cyclone due to re-entrainment of particles from the wall [6].

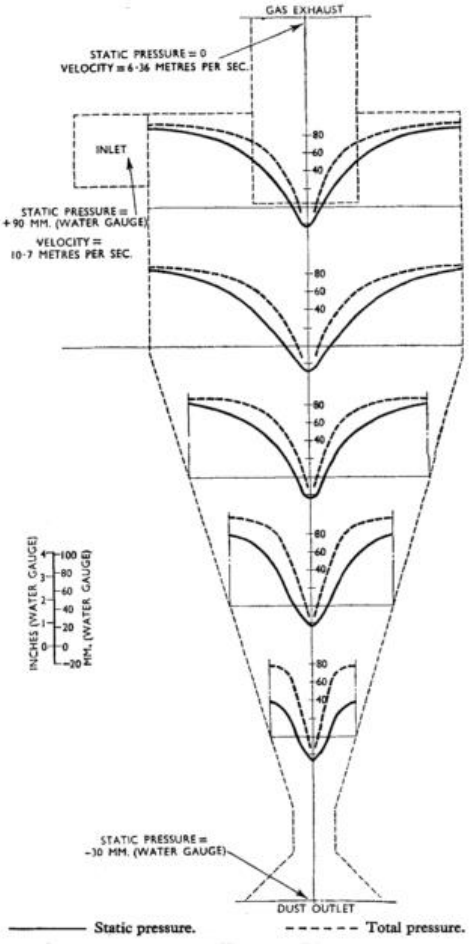

Figure 2.3: Depiction of the pressure profile in a cone-on-cylinder cyclone (from [10]*)*

2.1.1.2 Particles

As particles enter the cyclone, three main forces act upon them namely drag, centrifugal, and gravity. The drag force acts radially inward, tangentially, and either upwards or downwards depending on the position in the cyclone (outer or inner vortex). The centrifugal force acts in the radially outward direction controlled by the tangential velocity of the particle, while the gravity acts downwards irrespective the position and velocity of the particle. The centrifugal and gravitational forces are proportional to the mass of the particle, while the drag force is proportional to the particle projection area. Assuming spherical particles this makes the

centrifugal and gravitational forces proportional to the cube of the diameter, while the drag force is simply proportional to the diameter squared if Stokes' law is applicable [6]. Hence, the particle flows are highly dependent on the size.

Ideally, most of the particles are forced towards the walls due to a higher centrifugal force compared to the inward drag, while traveling down through the outer vortex. At the walls they move downwards, mainly by the downward going gas flow and partly by gravity in a vertical cyclone, and exit through the bottom [6,9]. Some particles will, either due to small size or their initial position, be forced into the inner vortex by the inward drag force on their way down the cyclone. Once the particles enters the inner vortex they are carried upwards into the vortex finder and are not separated [6]. The particle flow patterns are illustrated in Figure 2.4. Moreover some deviations from this general behavior occur, such as particles along the wall being re-entrained due to flow irregularities or particle collisions. Moreover, some particles might circulate between the inner and outer vortex multiple times due to fluctuations in the tangential and radial gas velocities throughout the cyclone etc.

Lede et al. [12] suggested that that the separated particles could be assumed to have plug flow behavior independent of the particle loading. This suggestion was based on results from pulse experiments and hold-up experiments [12]. However, contrary to earlier publications, Kang et al. [13] argued that the particles do not follow a plug flow behavior, due to back mixing of the solid phase inside the cyclone. This was supported by the pulse experiments of tracer particles carried out under constant particle feeding [13].

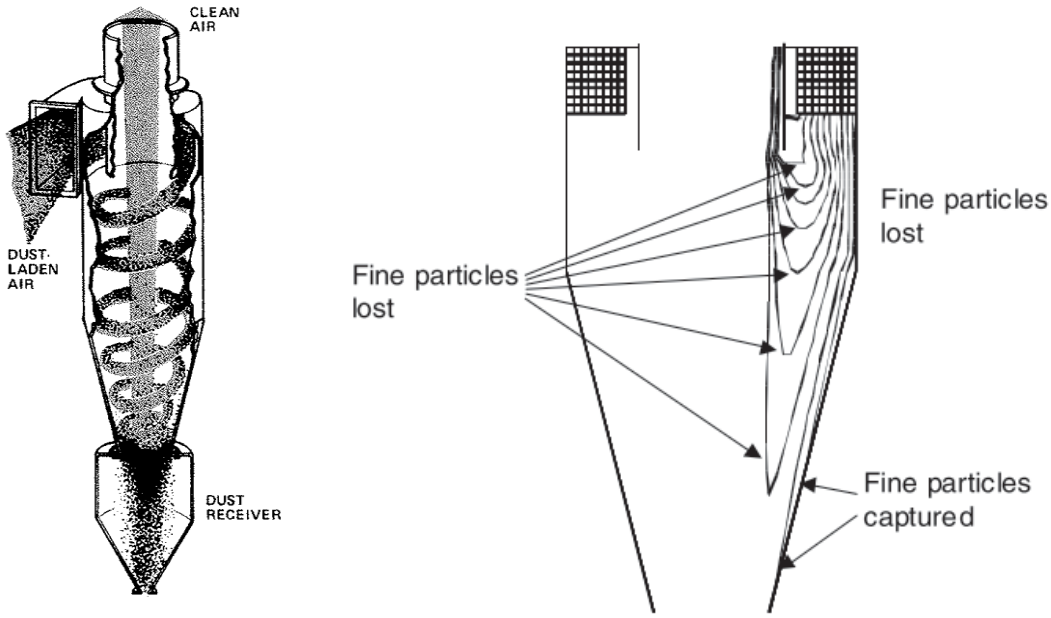

Figure 2.4: Left – idealized illustration of particle flow pattern in cyclone Right – CFD calculated particle paths of fine particles not separated [6]

2.1.2 Cyclone performance

The main function of a cyclone is to separate solids or liquids from a gas stream. Besides the initial installation cost and possible maintenance the main operating cost associated with a cyclone is the pressure drop. Hence, when evaluating the cyclone performance, the two main

parameters to examine are the particle separation efficiency and the pressure drop over the cyclone.

2.1.2.1 Particle collection efficiency

The efficiency or collection efficiency for a cyclone can be defined in various ways. If particles were monodispersed the collection efficiency, η_c, could simply be defined as in eq. 2.1.

$$\eta_c = \frac{\dot{m}_c}{\dot{m}_0} = \frac{\dot{n}_c}{\dot{n}_0} \qquad \textit{eq. 2.1}$$

Where $\dot{m}$ and $\dot{n}$ denotes mass and number flow of particles respectively, and the subscript 0 and c denotes the inlet and collected flows. However, as particles are rarely monodispersed the number efficiency and mass efficiency are not equal. The overall separation of the particles on a mass basis is commonly the critical parameter in industrial use, defined by eq. 2.2 [6]. Where subscript e denotes the elutriated solids, not collected.

$$\eta_c = \frac{\dot{m}_c}{\dot{m}_0} = 1 - \frac{\dot{m}_e}{\dot{m}_0} \qquad \textit{eq. 2.2}$$

However, the overall efficiency is only valid for a specific particle size distribution and does not give sufficient information about how cyclone separation efficiency depends on particle size. Therefore it is common practice to report a grade efficiency which shows the separation efficiency for a range of particle sizes. The grade efficiency can be calculated as shown in eq. 2.3.

$$\eta(d_p) = \frac{\dot{m}_c(d_p)}{\dot{m}_0(d_p)} \qquad \textit{eq. 2.3}$$

However, as particle size analysis is based on size intervals the data used to calculate will be based on distributions. Hence, the value for interval, i, is given by:

$$\eta_c(d_i) = \frac{\dot{m}_{c,i}}{\dot{m}_{0,i}} = \frac{\dot{m}_c\, f_{c.i}}{\dot{m}_0\, f_{0.i}} \qquad \textit{eq. 2.4}$$

Where f is the fraction of the whole sample with a diameter between the lower limit of i and $i+1$, and d_i being the mean diameter of this interval. Alternatively, cumulative distribution data often reported for particle sizes can also be used to calculate the grade efficiency curve. An example of a generic grade efficiency curve is given in Figure 2.5. The curve gives a good picture of the cyclone performance, and cyclones can easily be compared by plotting in the same graph. However, it is often needed to compare different designs on a single value parameter relevant to the application in question; here a cut-off value can be used. This value is simply a particle diameter at which a specified percentage of the particles are separated, and the value can be read directly from the efficiency curve. In Figure 2.5 the diameter at which 50 % of the particles are separated is shown as an example. Alternatively, the separation efficiency of a specified particle size relevant to the application can be used.

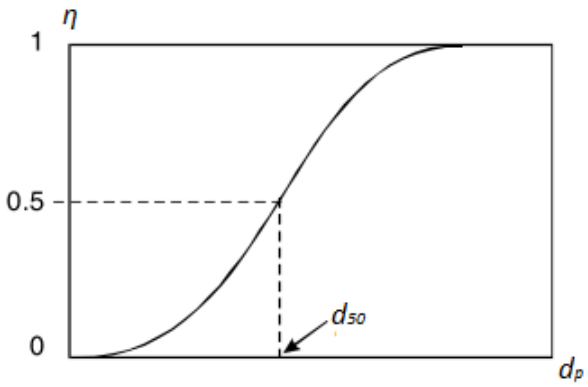

Figure 2.5: Example of typical grade efficiency curve

Overall the main factors which influence the separation efficiency in a cyclone and their effect are:

- Particle density and size – Increasing one or both will cause higher separation efficiency [6,9].
- Rotational speed of the cyclone vortex – An increase in the speed of rotation, for example by increasing inlet velocity, will increase separation efficiency [6,9].
- Cyclone diameter and length – Decreasing the cyclone diameter or increasing the cyclone length gives a higher separation efficiency [6,9].

Other factors such as inlet shape, type, and dimensions; vortex finder shape, and dimensions; and other design, and operational conditions also have an effect, but usually do not have general rules [6,9].

Various models have been developed to calculated the separation efficiency of cyclones based on design and operating conditions. Generally the most used models can be separated into different categories: Equilibrium-orbit models, Time-of-Flight models, and Hybrid models [6]. A good summary of the main models are given in the book by Hoffman and Stein [6].

2.1.2.2 Pressure drop

The pressure drop over a cyclone is a limiting factor for cyclone design as too high pressure losses will lead to increased operating cost, practical problems or decreased efficiency either upstream or downstream of the cyclone.

The standard procedure for measuring the pressure drop over a cyclone is to measure the difference between the static pressure at the inlet duct and the outlet pipe as defined in eq. 2.5.

$$\Delta P_{static} = P_{static,in} - P_{static,out} \qquad \textit{eq. 2.5}$$

However, this does not give a good representation of the actual pressure loss, due to the swirling flow in the gas outlet. This swirling flow gives a higher static pressure along the walls compared to the cross sectional average and considerable dynamic pressure stored in the swirling motion. To fully describe the pressure loss, the total pressure as given by eq. 2.6 at each point should be used as given in eq. 2.7 [6].

$$P_{total} = P_{static} + P_{dynamic} \quad \textit{eq. 2.6}$$

$$\Delta P_{total} = P_{total,in} - P_{total,out} \quad \textit{eq. 2.7}$$

Where $P_{dynamic} = \frac{1}{2}\rho v^2$, which is easily found in the inlet. However, it is nontrivial to calculate for the swirling flow in the outlet and the problem of the non-uniform static pressure in the outlet still exists. The static pressure measured at the wall is very close to the average static pressure that could be measured if all the dynamic pressure stored in the swirling motion were converted loss free to static pressure, i.e. in the case of ideal pressure recovery. Hence, this interpretation should be remembered when evaluating pressures measured in this manner. Furthermore, the result gives the pressure loss in the cyclone plus downstream due to dissipation of the swirling flow [14].

2.1.3 Cyclone dimensions

The dimensions of even a standard cylinder-on-cone cyclone with a rectangular inlet can vary widely. For this type of cyclone, the full design of the cyclone chamber can be described by the dimensions showed in Figure 2.6.

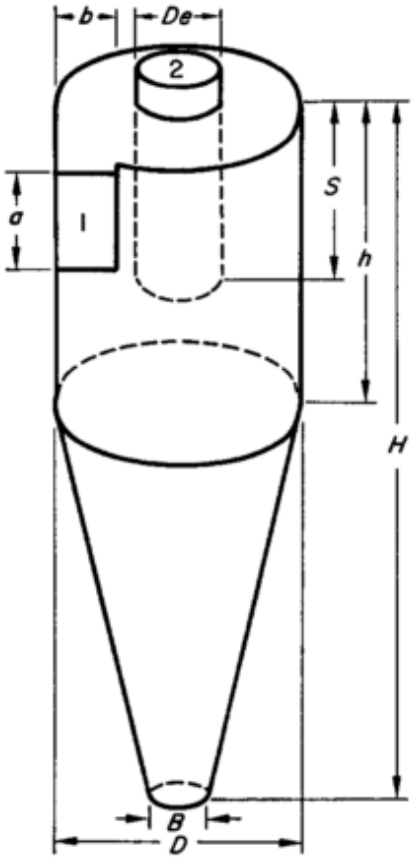

Figure 2.6: Illustration of the dimensions of a standard cylinder-on-cone cyclone with rectangular tangential inlet [9]

To elaborate on Figure 2.6 the dimensions displayed are: the cyclone diameter, D, cyclone length, H, cylinder length, h, vortex finder diameter, De, vortex finder length, S, dust outlet diameter, B, inlet height, a, and inlet width, b. These naming symbol conventions will be used throughout this thesis.

Many different designs exists. To compare these designs over different size ranges, the dimensionless ratio between a certain dimension and the cyclone diameter is used. Many standard designs are referred in literature by name, with some of these are summarized in Table 2.1.

Table 2.1: The dimensional ratio of different cyclones (original data from [15]*)*

Name	De/D	S/D	H/D	h/D	a/D	b/D	B/D
Muschelknautz E	0.25	0.46	1.37	0.25	0.25	0.09	0.34
Muschelknautz D	0.33	0.89	2.42	0.73	0.52	0.15	0.55
Storch 1	0.34	0.39	5.32	1.50	0.27	0.27	0.18
Storch 2	0.48	1.06	4.88	2.06	0.84	0.24	0.37
Storch 3	0.56	1.04	4.28	2.41	0.87	0.31	0.48
Storch 4	0.45	0.68	6.22	3.50	1.00	0.15	0.35
Tengbergen A	0.40	0.57	2.34	0.65	0.49	0.27	0.73
Tengbergen B	0.53	1.07	2.88	1.54	0.85	0.27	0.53
Tengbergen C	0.33	0.43	2.76	0.55	0.30	0.30	0.33
TSN-11	0.39	0.70	2.76	0.63	0.53	0.16	0.44
TSN-15	0.59	1.32	4.23	2.21	0.62	0.23	0.45
Stairmand high efficiency	0.50	0.50	4.00	1.50	0.50	0.20	0.38
Stairmand high flow	0.74	0.87	3.97	1.49	0.74	0.37	0.37
VanTongeren AC	0.31	1.00	3.79	1.34	0.46	0.21	0.40
Vibco	0.39	0.43	2.52	0.80	0.39	0.31	0.23
Lapple GP	0.50	0.63	4.00	2.00	0.50	0.25	0.25

The different designs are usually a choice between high collection efficiency or low pressure drop or a compromise between these two. This is due to the fact that higher collection efficiency often results in higher pressure drops over the cyclone for a given gas flow for a specific dimensions. Alternatively, for a given pressure drop over a similar size cyclone design with high efficiency will not be able to process as much gas as a design with low efficiency [9].

Much research has been conducted to study effects of cyclone dimensions in order to understand how the design affects cyclone performance and to use this knowledge to optimize designs [6,16]. In the following section the general consensus on this will be explained.

2.1.3.1 Cyclone diameter

The cyclone diameter is often referred to as the size of the cyclone. An increase in the cyclone diameter, D, usually increases the particle collection efficiency at fixed inlet flow rate, due to an increase in the angular momentum of the flow and therefore the spin velocity of the vortex core. However, for the same reason the pressure drop will increase [6]. The increase in particle collection efficiency with increasing cyclone diameter has diminishing returns up to a point, where any increase in cyclone diameter becomes unpractical compared to the gain in performance [6,9]. This is illustrated by Figure 2.7, which is based on calculations from empirical cyclone performance models.

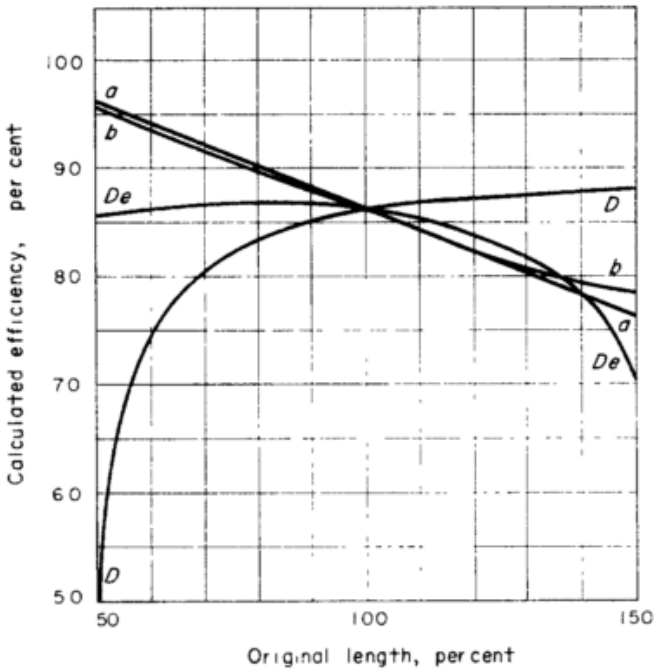

Figure 2.7: Cyclone collection efficiencies dependence on different geometric sizes, original sizes based on Stairmand High Efficiency design calculated by Leith & Mehta [9]

2.1.3.2 Cyclone length

Generally an increase in cyclone length, H, leads to both an increased collection efficiency and a decreased pressure drop. However, when the cyclone becomes longer than the natural vortex length, a decrease of the collection efficiency can be observed [6,9,16]. This can be seen from the experimental data from Hoffmann et al. 2001 [17] shown in Figure 2.8. Similar effect can be obtained by increasing either the cylinder length, h, or the cone length, $H - h$. However the effect is most pronounced for the cylinder length and it is typically better to increase the cylinder length [6,16,18].

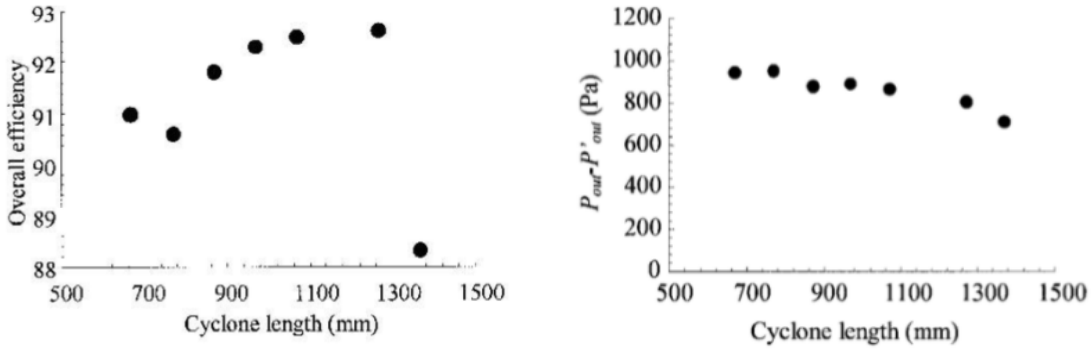

Figure 2.8: Particle collection efficiency and pressure drop dependence on cyclone length [17]

2.1.3.3 Inlet dimensions

The inlet dimensions, height, a, and width, b, have roughly the same effect on the cyclone performance. By lowering the inlet cross section area the velocity at the inlet increases. Thereby the vortex core velocity increases, enhancing the collection efficiency. This effect is illustrated by the calculated efficiencies in Figure 2.7. At the same time, the pressure loss is increased due to the increased frictional losses in both the inlet and from the cyclone walls

[6,9,16]. It is usually recommended not to make the inlet wider than the free space between the cyclone wall and the vortex finder, to avoid flow disturbances and impact erosion due to the high velocity inlet stream hitting the vortex finder.

2.1.3.4 Vortex finder diameter

The vortex finder diameter, De has a significant impact on the collection efficiency of the cyclone, as it controls the diameter of the inner vortex core. Generally, a smaller vortex finder diameter will give higher collection efficiency at the cost of higher pressure loss [6,9,19]. From Figure 2.7, the drop-off in collection efficiency can be seen as De increases. The practical optimum for the diameter considering both efficiency and pressure loss is commonly agreed to be between 1/3 and 1/2 of the total cyclone diameter [16].

2.1.3.5 Vortex finder length

The vortex finder length, S, is usually designed to be similar to the inlet height. Generally, a vortex finder longer than the inlet height gives a higher collection efficiency with roughly the same pressure drop. The optimal length with regards to this has been suggested to be 1.25 times the inlet height. A vortex finder shorter than the inlet height gives a lower pressure loss, at a loss of separation efficiency. This can become severe if the vortex finder is too short, due to short circuiting of the particle laden gas. This is generally a problem if the vortex finder is below half the length of the inlet height [6].

2.1.3.6 Dust outlet

The dimensions of the dust outlet should primarily just be wide enough to allow the collected solids to exit the cyclone without causing any build up. For most designs it has little to no effect on the cyclone performance. Mostly it is not wider than that of the vortex finder, but this is not a necessity [16,20].

2.1.4 Design variations

A number of variations other than geometric ratios to the standard reverse-flow, cylinder-on-cone cyclone with slot inlet shown in Figure 2.6 exist. The variations can be from different inlets, dust outlets and other variations. Some of the most typical variations are described in this section.

2.1.4.1 Inlets

Throughout the years, different inlet types for achieving the transition to swirling flow have been developed [16]. Examples of the main inlet types are shown in Figure 2.9. For these several variations exist. Each inlet type and variation hereof have different advantages and disadvantages, which are summarized below [6].

The tangential inlet in Figure 2.9 A is a simple inlet where the outer wall of the inlet fits tangentially with the cyclone. The tangential inlet exists in two main variations, the slot inlet and the circular pipe inlet. The circular pipe inlet is cheap and simple to produce, and remove the need for making a transition between round piping and rectangular as seen in other inlet types. This comes at the price of reduced separation efficiency compared to the slot inlet, due

to the flow irregularities caused at the inlet. The slot inlet is slightly more difficult and more expensive than the circular pipe inlet to produce. However, it does not suffer from the lower separation efficiency. This inlet type is the most widely used for cyclones in the chemical processing industry [6].

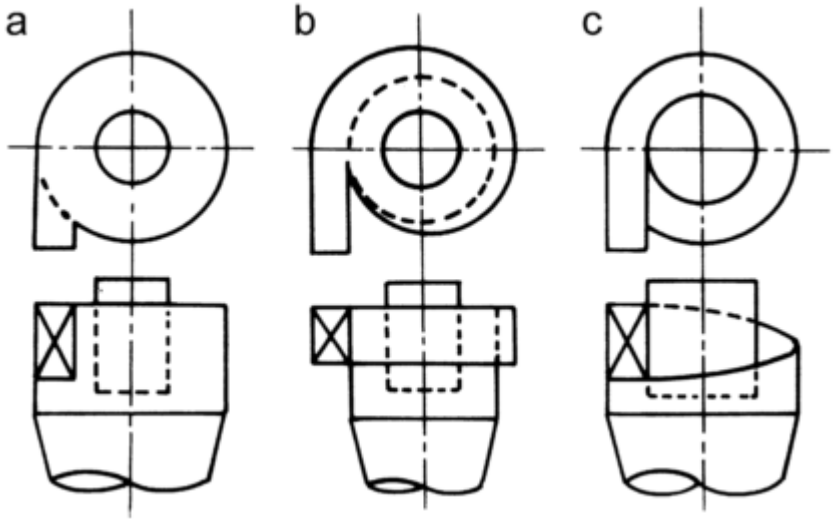

Figure 2.9: Cyclone inlet variations a) tangential, b) scroll, c) helicoidal [15]

The scroll type inlet is often used in high flowrate cyclones. This is done in order to avoid part of the inlet jet to hit the vortex finder, which can cause disturbances in the flow and erosion. Furthermore, the increased initial radius increases angular momentum and the spin velocity in the vortex core. Therefore the separation efficiency is increased compared to cyclones of same diameter but with tangential inlet. By doing this a more compact cyclone can be used for higher gas flow rates without causing flow problems. As a tradeoff, the pressure loss over the cyclone is increased. A scroll inlet can vary in the length it wraps around the cyclone body. This is denoted by the angle from where the curvature on the outer wall of the inlet duct starts, to where the outer wall of the duct meets the outer cyclone wall. The most common types being 90°, 180°, 270°, and 360° [6]. Examples for two circular scrolls are given in Figure 2.10.

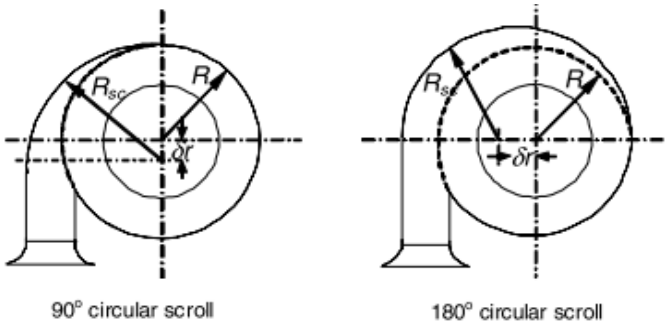

Figure 2.10 illustration of 90° and 180° circular scrolls [6]

Other types of scroll inlet includes the logarithmic scroll where the radius of the curvature of the scroll gradually decreases to meet the cyclone as opposed to the circular scroll where the scroll radius is constant [6].

While the tangential inlet and scroll inlets have a flat cyclone roof, the helicoidal inlet is part of the roof as it gradually angles down from a slot type inlet into the cyclone chamber. This provides a more smooth transition of the flow.

2.1.4.2 Dust outlet

Different variations of the dust outlet for cyclones exist, and combinations of these create a large number of possible outlet configurations. This includes configuration of the solid hopper or dust bin, the use and length of dip legs, the implementation and placement of vortex stabilizers and vortex breakers. Examples of different outlet variations are shown in Figure 2.11. A short discussion of some of these variations and how they affect the cyclone performance is given below.

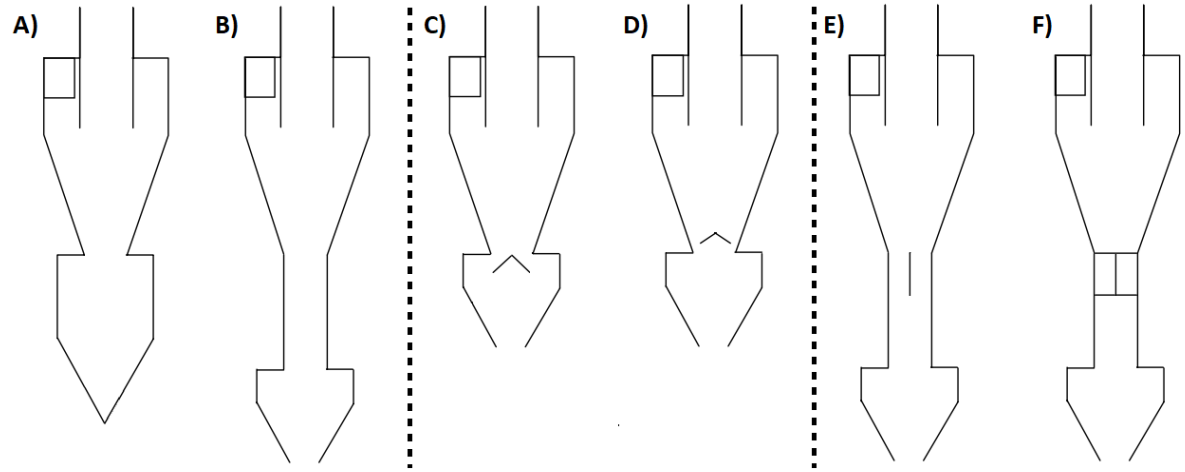

Figure 2.11: Illustration of cyclone outlet variations, (adapted from [6]*), A) dust outlet directily into dust bin, B) dust outlet with dip tube into dust hopper, C) vortex stabilizer below dust outlet, D) vortex stabilizer above dust outlet, E) single plate vortex breaker, F) crossed plates vortex breaker*

In batch operations or for sampling cyclones, the dust outlet often leads into a simple dust bin where the solids are kept until the bin is full or the batch operation is over as seen in Figure 2.11 A). In continuous operation, the dust has to be transported away either continuously or periodically. For this a dust hopper is often used. A dust hopper is usually constructed in a way similar to silos for solid materials with conical walls and an opening below to lead the solid to a vessel or a solid conveying system [6]. Different dust hoppers are shown in Figure 2.11 B)-F). A dust hopper is not a necessity and many cyclones simply have a tube leading directly to the collection vessel or conveying system [20]. A tube section is often placed before the dust hopper or bin, as seen in in Figure 2.11 B, E & F, this is called a dip tube or dip leg. A dip tube reduces entrainment of the solids from the dust hopper/bin from cyclones where the vortex extends beyond the dust exit. However, it also increases pressure loss in these cases [6]. A vortex stabilizer is typically a small conical piece sloping downward inserted just below or above the dust outlet as illustrated by Figure 2.11 C) and D) respectively [6]. This is also sometimes referred to as an apex cone [20]. The purpose of a vortex stabilizer is to provide a smooth surface to which the vortex end can attach itself. This stabilizes the vortex and prevents precessing and re-entrainment of particles from the cone section or dust hopper/bin, thereby increasing the collection efficiency of the cyclone [6,20]. The main disadvantage of a vortex stabilizer is the increased complexity, cost of manufacturing, and risk of blockages in the outlet.

A vortex breaker is usually a simple plate or a cross of plates in the dust outlet as shown in Figure 2.11 E) and F). A vortex breaker stops the vortex from extending into the dust hopper/bin or other outlet configurations in order to reduce erosion. However, the vortex breaker causes high mixing in the lower part of the cyclone and reduces the vortex core spin velocity, both of which is detrimental to the collection efficiency of the cyclone due to re-entrainment and lower centrifugal force, respectively [6,20].

2.2 Cyclone reactors

In an effort to categorize different cyclone reactor designs, they are grouped by the inlet/outlet configuration. An overview of the most common configurations is shown in Figure 2.12.

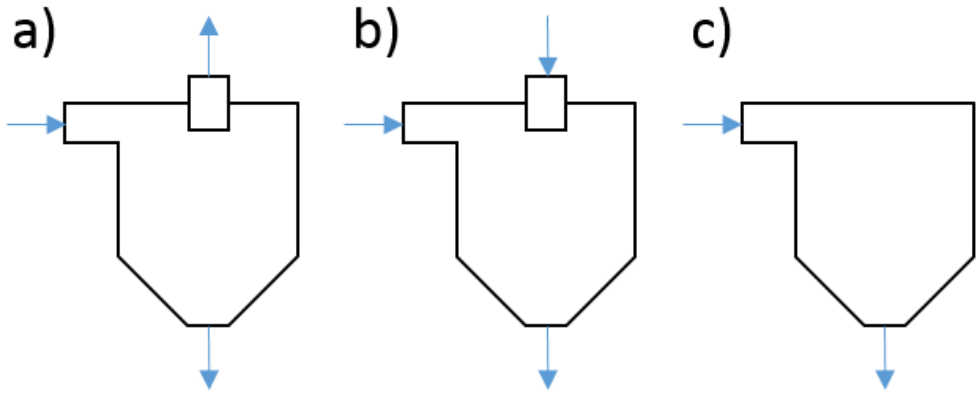

Figure 2.12: Illustrations of common cyclone reactor inlet and outlet configurations – a) standard cyclone configurations b) tangential and axial inlets c) closed top

The three configurations of cyclone reactors shown in Figure 2.12, will be used for reference in this review. Configuration A is the standard reverse flow cyclone configuration, typically vertically oriented with a gas outlet in the form of a vortex finder in the top and a dust outlet in the bottom. It can have one or more tangential inlets.

For some cyclone reactors the final separation of the phases is not the primary function, instead the swirling flow or the separation of the phases inside the reactor chamber is important. This is the case for most cyclone burners for slagging combustion [21–25] and some cyclone smelters for metal pyro processing [26–32]. In these cases, some of the cyclone reactors have only a single outlet for both gas and solid/liquids. This is the case for both configuration B and C. Configuration B has one or more tangential inlets as well as an axial inlet and only a single axial outlet for both the gas and dense phase. Configuration C has one or multiple tangential inlets, and a single axial outlet for both the gas and the dense phase.

Apart from the common design types discussed above additional features might be included to facilitate certain behavior in the reactor. For example external heating of the cyclone reactors surface can be added to provide the necessary heat for reaction [33,34], or cooling can be used control the temperature in the case of highly exothermic reactions and to ensure formation of desired phases of reactants and products.

Non-typical cyclone designs, such as the inverted cyclone [35–38], a type of uniflow cyclone shown in Figure 2.13 can also be utilized as a reactor. Other alternative designs include the

short contact cyclone reactor developed for catalytic processes [39–43] described further in section 2.2.1.7.

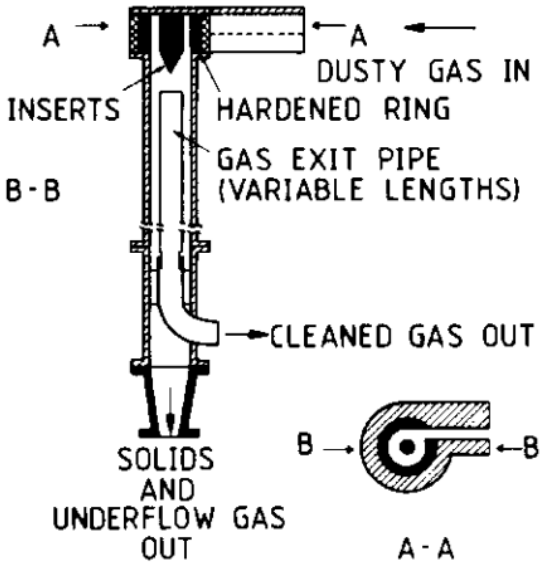

Figure 2.13: Illustration of the inverted flow cyclone design (from Gauthier et al. [35])

2.2.1 Cyclone reactor applications

The following sections describe applications of cyclone reactors that are either in industrial use, have been substantially experimentally validated and proven applicable, or simply investigated through lab scale experiments and modelling.

2.2.1.1 Combustion

Combustion is most commonly used to convert the chemical energy stored as fuels into thermal energy, which can then be directly utilized or converted to power. Combustion is widely used in industrial processes, including power and district heating plants, utility boilers for steam generation, metal ore smelters, glass melters, cement clinker furnaces, and countless other examples [44]. The role of an industrial burner is to mix the fuel and combustion air in a way that achieves stable and efficient combustion. Complete combustion of most fuels can be generalized by the reaction, R2.1 [44].

$$C_xH_y + (x + ½y)\ O_2 \leftrightarrows x\ CO_2 + ½y\ H_2O \qquad R2.1$$

A general overview of typical cyclone combustion process is given in Figure 2.14.

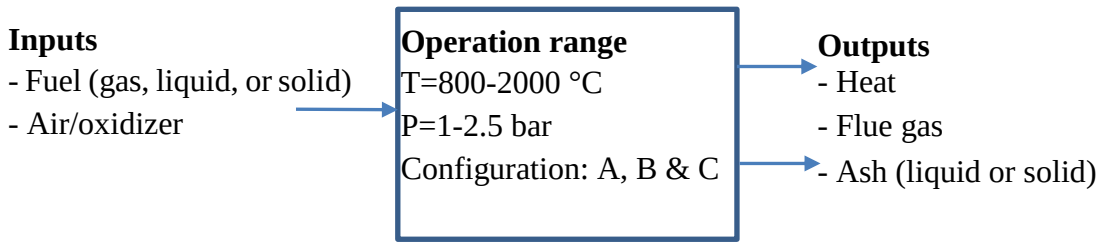

Figure 2.14: General principle of cyclone combustion processes (operating conditions based on Table 2.2)

The use of cyclones or cyclone like devices for combustion is well established. Cyclone burners were first introduced in 1944, by Babcock and Wilcox, in order to efficiently burn fuels, such as crushed or coarse pulverized bituminous and semi-bituminous coals [22,45]. The cyclone burners proved capable of handling difficult fuels, like high ash coals, coals with low ash fusion temperatures and fuels with long burnout time. These fuels caused operational problems in traditional suspension fired boilers, such as incomplete burnout of the fuel and ash deposition on heat transfer surfaces in the boiler. The invention of cyclone burners with slagging combustion solved these problems by increasing the residence time of the fuel particles and removing the ash as a liquid slag continuously [22,25,45,46]. Later the principles have been used in the development of cyclone combustors for burning low-melting ash fuels such as biomass, high sulfur oils, low quality waste gases and for thermal oxidation of mineral ores [47,48]. Apart from the ability to burn fuels with high ash and/or low ash melting temperature, the cyclone burner also has the benefit of being able to handle large fuel particles. As opposed to entrained flow burners where short burnout times are critical, the cyclone burner traps the larger particles while still providing oxygen for combustion through the forced convection. This makes the cyclone burners good for irregular fuels like agriculture waste with large particle sizes and hard to grind coals [22,46–49]. Furthermore, a major advantage of cyclone burners is the ability to separate the ash from the flue gas immediately during combustion [48].

2.2.1.1.1 Design and working principles

The operation of cyclone burners is dependent on the application and the design of the burner. However, a general description of the operation principle for solid fuel cyclone burners is given below.

A cyclone burner typically consists of a cylindrical cyclone combustion chamber. All three cyclone reactor configurations shown in Figure 2.12 are commonly used in cyclone burners. The design and number of inlets, as well as the design of outlets, can vary [25,48]. The fuel can be injected into the combustion chamber either axially of tangentially together with the primary and tertiary air, depending on the configuration. While the secondary air is predominately fed tangentially in order to induce the swirling flow, either in a separate inlet or together with the fuel and primary air [48]. The orientation of the cyclone burner can be either vertical or horizontal [46,47]. The operation of cyclone burners is dependent on the application A general description of the operation principles for solid fuel cyclone burners is given below.

As the fuel enters the combustion chamber, it is mixed into the hot swirling vortex flow starting the heating and combustion processes. The fuel particles will be forced out towards the walls, and due to the force balance between the drag and centrifugal force, will have a long residence time compared to conventional burners [47]. In non-slagging combustion, the burning fuel particles and solid ash will be transported along the walls as in a normal gas-solid cyclone. While in slagging combustion the ash forms a liquid melt on the cyclone walls, and the fuel particles not fully burned hitting the wall are trapped on the surface of the slag [22,25,48,50].

If operating with slagging combustion, the temperature in the combustion chamber must be sufficiently high, typically above 1500 °C, so that the ash formed during combustion forms a liquid slag on the walls and thereby be removed efficiently [22,45,47]. If operating with non-slagging the temperature must be low enough, typically below 1200 °C for the ash to be collected in solid form without sticking to the wall [47]. The gaseous combustion products will exit through the gas outlet. If the burner is operating under slagging combustion, the liquid slag is let out of a tap either in the same end as the gas exit or in the lower part of the chamber. This ensures that any slag in excess of the amount need to line the walls with a thin layer for trapping the fuel particles is removed [21,22,25]. Operating in non-slagging mode can help reduce NO_x emissions by operating at lower temperatures than slagging burners and by using fuel rich conditions inside the cyclone burner with full burnout of the gas performed by a secondary burner [51].

The different designs, operating conditions and applications available in literature are summarized in Table 2.2.

Table 2.2: summary of reactor design and operating conditions for solid fuel cyclone burners available in literature

Application	Reactor configuration	Size (D/V) [m/m^3]	Fuel	Fuel feed rate [kg/h]	Temperature [°C]	Effect [MW]	Ash removal	Source
Slagging combustion for boilers (Patent)	C	0.9/0.87	Coarse bituminous & semi-bituminous coal	1000	1760	8.7	93 %	Kerr 1944 [22]
Slagging combustion for boilers (Patent)	A	0.9/0.87	Coarse bituminous & semi-bituminous coal	1300	1650	6.1	80 %	Kerr 1944 (1) [45]
Slagging combustion for boilers (Patent)	B	1.5/4.0	Coarse bituminous & semi-bituminous coal	3200	1930	21	97.5 %	Bailey 1944 [52]
Slagging combustion for boilers (Patent)	B	-	Coarse bituminous & semi-bituminous coal	-	>1540	-	-	Kerr 1952 [23]
Slagging combustion (industrial scale)	A	0.9/-	Crushed coal	820	-	2-5	70-92 %	Hoy 1958 [50]
Slagging combustion (industrial scale)	B	2.75/	Crushed coal	18000	-	-	-	Steam 1963[21]
Slagging combustion (pilot scale)	A	0.62/-	Coal	-	2000	-	-	Kalishevskii 1967 [53]
Slagging combustion (lab scale)	A	0.15/0.004	bituminous & semi-bituminous coal	3-12	1315-1573	0.08	-	Barnhart 1982 [46]
Non-slagging combustion (pilot scale)	A	-	bituminous coal, anthracite & coke	-	1300	0.3	-	Morgan 1989 [51]
Slagging combustion	A	-	Anthracite	-	1500-1600	-	-	No 1993 [47]
Slagging Co-combustion of waste and gas (patent)	C	-	Paper mill sludge & natural gas	-	-	-	-	Nechvatal 1996 [24]
Slagging combustion for boilers (Patent)	B	-	-	-	-	-	-	Dahl 2000 [25]

2.2.1.1.2 Applications

Due to the highly commercial nature of cyclone burner developments, most of the detailed studies are not easily available in the open literature, and much of the information is found through patent.

The early patented designs of the cyclone burner for slagging combustion developed by Babcock and Wilcox had three types of configurations namely, A [45], B [52] and C [22] ash shown in Figure 2.15. The common feature for these designs is that the recovery of ash components as a liquid slag was substantially improved, compared to the existing burner types at the time [21]. Furthermore, due to the high temperature required for slagging combustion, the walls of the cyclone burners is cooled to avoid damaging the refractories. This is done through both water cooling and air cooling [22,45,52].

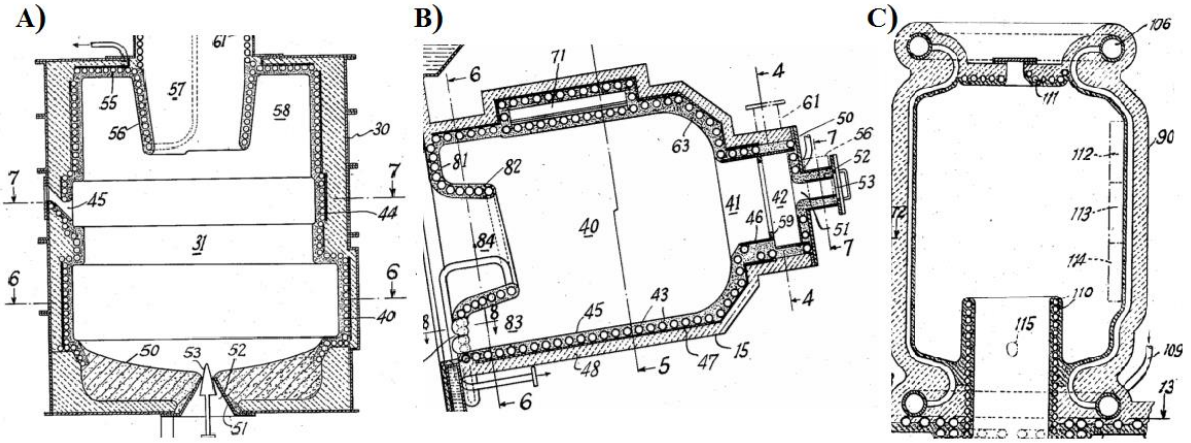

Figure 2.15: Vertical cross section illustrations of early cyclone burner designs – a) B&W patent drawing (US2357302) [45] *b) B&W patent drawing (US2357301)* [52] *c) B&W patent drawing (US2357303)* [22]

The cyclone burner shown in Figure 2.15 (a) is the closest to a standard cyclone separator configuration, i.e. cyclone reactor configuration A. There are two tangential inlets, at different heights. The top one (marked 45) for fuel, primary, and secondary air and the lower one for (the indent at the height marked 6) tertiary air. It is vertically oriented with a slag outlet at the bottom with a valve for controlling the slag accumulation in the burner and in the top a vortex finder and gas outlet [45]. Several units of this burner type would be fitted in the bottom of a furnace chamber. In retrofit application this could enable existing boilers that could not previously handle low melting ash fuels, as the slag handling is build into the cyclone burner [45].

The cyclone burner design shown in Figure 2.15 (c) uses cyclone reactor configuration C with only a single outlet for both flue gas and slag. It has multiple tangential inlets for fuel and air. The inlets were arranged as a row of 3 tangential inlets below each other as marked with the numbers 112 to 114. The top inlet (112) is for fuel and primary air, while the secondary air enters through the two other inlets. As the vortex finder or exit throat protrudes up into the cyclone chamber, a slag drainage hole marked 115 is needed to avoid excessive slag buildup, while keeping a constant level. Several units of this type of cyclone burner were placed above a furnace chamber extension with both the gas and the slag exiting downwards into this. The

slag drops to the furnace floor and is discharged into a slag pit [22]. It could be retrofitted in furnaces with existing liquid slag removal capabilities greatly increasing the ash removal from the hot flue gas. This also meant that by using it in new installations, the furnace chamber could be more compact [22].

The design shown in Figure 2.15 B) uses the cyclone reactor configuration Figure 2.12 B [52]. Later designs of cyclone burners developed by B&W use this basic layout and would become the modern "classical" cyclone burner. Figure 2.16 illustrates the design and principle of a modern B&W cyclone burner.

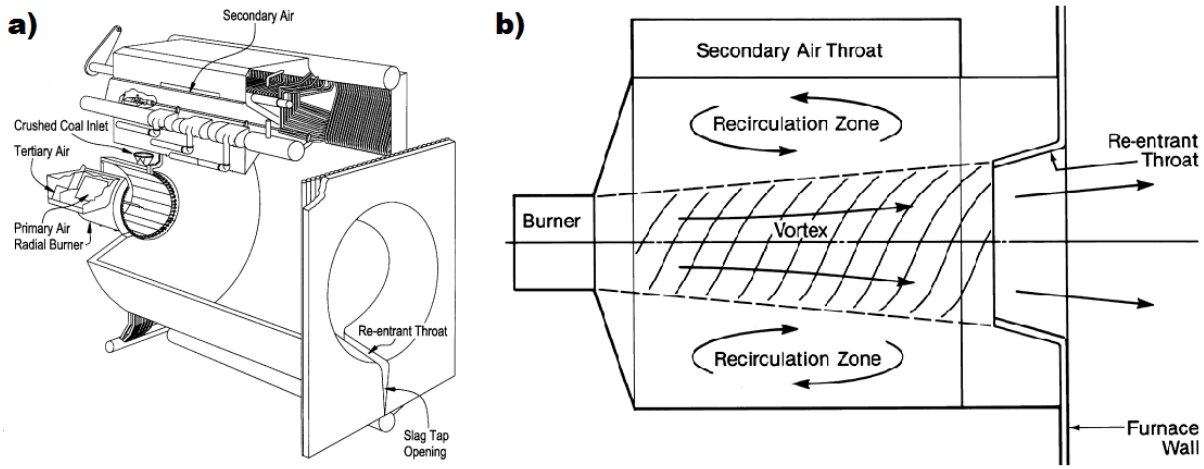

Figure 2.16: Illustration of the "classic" cyclone burner a) modern B&W patent drawing (converted from [25]*) b) sketch of operation principle* [54]

As seen on Figure 2.16 (a) this design has both an axial and a tangential inlet and a single outlet for both gas and slag. The cyclone burner is horizontally oriented [25] or can be slightly slanted downwards [23]. The fuel is fed through the axial inlet together with the primary and tertiary combustion air. In this design the axial inlet is designed as a type of swirl burner, with the primary air introduced tangentially inside the inlet to produce a swirl flow while the tertiary air is introduced from the back of the inlet to provide axial momentum. The majority of the combustion air is the secondary air introduced inside the cyclone burner tangentially. The gas exit, in these drawings called the Re-entrant Throat has an extra slit acting as tap for the molten slag, ensuring a constant slag level in the burner [25,52].

Although cyclone burners of configuration B are the most used in slagging combustion furnaces, many variations of cyclone burner designs, using all 3 cyclone reactor configurations, have been developed throughout the years for different applications. This includes solid fuel cyclone burners for both slagging combustion and non-slagging combustion [47,48]. Examples of some of the common designs of these types are shown in Figure 2.17 [48].

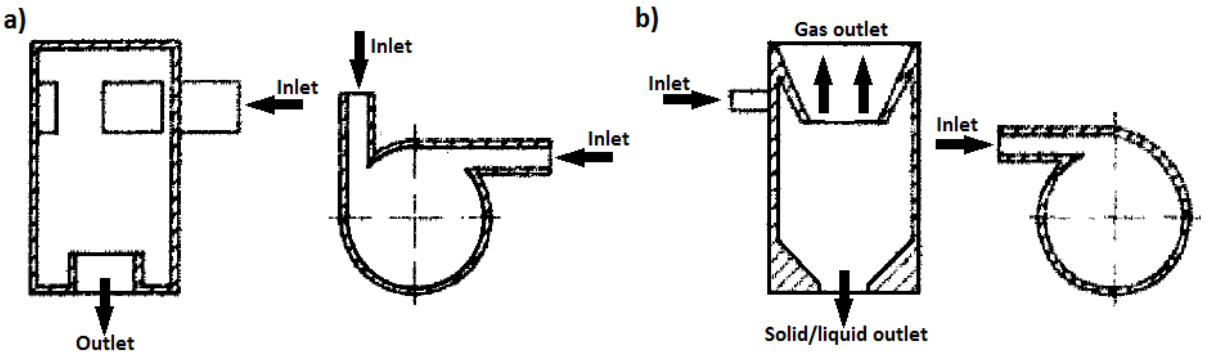

Figure 2.17: Illustrations of different cyclone burner designs (converted from [48]*)*

The design shown in Figure 2.17 a, is a reactor configuration C, therefore lacking a separate dust and gas outlet. This design is not made fuels with high ash content or low melting ash. However, it has the advantages of high mixing and long particle residence times, and are therefore good for solid fuels with long burnout times. The version shown has two tangential inlets. But there are versions with only one or more inlets [48].

Design b on Figure 2.17, is reactor configuration A burner, following a classic cyclone configuration with a gas outlet with a vortex finder in the top and a solid/liquid outlet in the bottom. This design is very versatile and especially good at handling high ash fuels using both slagging and non-slagging combustion depending on the operating temperature and ash properties. The liquid slag or particulate ash will be removed through the outlet in slagging and non-slagging combustion respectively. Therefore, this cyclone burner design are especially well suited for reducing fly ash problems in non-slagging combustion of high ash fuel or in applications where the ash is highly detrimental to the downstream equipment [47,48].

Many more variations of cyclone burners exists for different fuels and operations, for example the pressurized cyclone combustor for gaseous fuel etc. [49].

Furthermore, in combustion plants like circulating fluidized bed boilers the mixing in bigger units can become inadequate and cause incomplete combustion in the fluid bed riser. However, the intense mixing in the cyclone for recirculating the unburnt char and sand can lead to completion of the gas phase combustion reaction inside the cyclone [55].

2.2.1.2 Gasification

Gasification is used to convert solid fuel into a combustible gas that can be used as gaseous fuel or as synthesis gas. Gasification is a kind of sub stoichiometric combustion process, where the fuel is only partially oxidized, to provide heat for the process. Under sub-stoichiometric conditions, it is primarily the volatiles that burn, while the char is converted through gasification reactions. The combustion of the volatiles heats the gas and char, while the gasification agents such as steam or CO_2 can either be supplied together with the combustion air or be supplied by the combustion of the volatiles. The products from gasification processes usually consist of a mixture of gases like CO, H_2 and methane [56]. The primary gasification reaction are given in R2.2, R2.3, and R2.4 [56,57].

$$C + CO_2 \leftrightarrows 2CO \quad R2.2$$

$$C + H_2O \leftrightarrows CO + H_2 \quad R2.3$$

$$C + 2\,H_2 \leftrightarrows CH_4 \quad R2.4$$

The overall goal of a gasification process is to maximize the production of combustible gases (H_2, CO & CH_4), while minimizing the amount of unconverted char. The gasification efficiency is defined as the total LHV (lower heating value) of the produced gas divided by the total LHV of the fed fuel. Unconverted char means wasted carbon that could have been converted into product gas and a carbon efficiency can be used to quantify the performance of a gasifier together with the gasification efficiency. Some unburned volatiles might end up as tars in the product gas. For applications with direct combustion of the gas in a second stage like in turbine combustion this is not a problem as the heating value is utilized. However, in producer and power gas production, where these are condensed together with the water content, their heating value is wasted. Finally, it is desirable and often critical to reduce the amount of ash in the product gas.

The use of gasification technology has had different objectives throughout the years. In the 70's and 80's the global oil crisis led to an increased interest to use the worlds vast coal reserves for applications where oil and natural gas had previously been the preferred fuels and the beginning interest of using alternative (non-fossil) fuels. Coal gasification was and is still used for producing syn-gas, substitute natural gas and power gas. However, recent scientific and industrial development has primarily been driven by the need for fuel- and synthesis gas from renewable resources like biomass or from waste derived fuels. A general overview of cyclone gasification processes is shown in Figure 2.18.

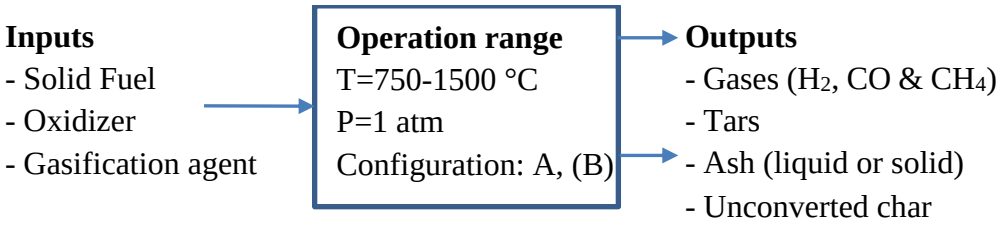

Figure 2.18: General principle of gasification in cyclone reactors (operating conditions based on Table 2.3)

The use of cyclones as gasifiers was inspired by the cyclone combustor. Initially it was the cyclone burners capabilities for handling slower burning fuels, due to the extended residence time and high gas-solid mass transfer as compared to entrained flow reactors, which made the cyclone reactor interesting for gasification [58–60]. This is due to slow gasification reactions compared to combustion reactions [61]. Later the in situ removal of ash from the product gas has become one of the main advantages, compared to other gasification technologies, as fly ash can often cause problems downstream [62–64]. This is especially attractive in the application of cyclone gasifiers for gas turbine combustors [63,64].

2.2.1.2.1 Design and working principles

A cyclone gasifier is designed and operated in much the same way as a cyclone burner with possibility for both slagging and non-slagging operation. The main difference being that the air supply is sub-stoichiometric and steam might be added as a gasification agent. The fuel and gasification agent/air is introduced through one or more tangential inlets for configuration A and in case of configuration B the fuel is introduced axially. A summary of the design, operating conditions used and the results obtained by different studies of cyclone gasifiers are shown in Table 2.3.

2.2.1.2.2 Applications

Early studies of gasification in cyclones were conducted in the 1950's by the US bureau of mines with the goal to evaluate new technologies for producing syn-gas by coal gasification for synthetic production of liquid fuels. The studies was performed in a configuration B cyclone reactor with coal fed from an axial inlet in the top, several tangential inlets for the oxygen/steam mixture used as oxidizer/gasification agent and a single gas outlet in the bottom [46,58,59]. In the first study (Perry et al. 1950 [58]) care was taken to avoid slagging conditions which can cause significant problems in traditional gasification reactors. Overall this study showed poor to mediocre carbon to CO/H_2 efficiencies in the range ~50-75% based on char yield. However, the later study (Elliot et al. 1952 [59]) the reactor was modified to allow for slagging operation and performed substantially better with carbon efficiencies of around 60-90 % due to the increased residence time of the fuel particles caught in the slag layer [59]. At the same time a lot of coal gasification studies were conducted in Germany as part of the development of the Ruhrgas process for producing power gas. A tangentially fed cyclone reactor operating under slagging conditions was used achieving carbon efficiencies between 61 and 80. However, the cyclone was operated in such a way that there was significant char content in the product gas stream. After recycling this the carbon efficiency could be increased to 95 % [60]. A commercial cyclone gasification plant with a capacity of 4000 kg/h was build as part of the Ruhrgas project, but only operated for a short time period [46].

Yagi and Kunii 1957 used basic cyclone design principles to improve the separation efficiency by keeping the design in the standard cyclone separator configuration (reactor configuration A) with the classic cylinder on cone and vortex finder. This were done in and effort to reduce the elutriation of char through the gas outlet and ensure high ash removal. Operating under slagging conditions, using both air/steam and oxygen/steam mixtures as oxidizer and gasification agents in separate experiments, carbon efficiencies between 71 and 98 % were achieved depending on other operational parameters [62]. These results are well in line with results for coal gasification in cyclone reactors later reported in literature [46]. The high carbon efficiencies achieved without recirculation

More recent studies on gasification, including those focusing on cyclone gasifiers, primarily focus on the conversion of alternative fuels such as biomass or waste derived fuels such as; municipal and industrial waste etc.

Cousins & Robinson 1985 [65] used an air blown laboratory cyclone gasifier of reactor configuration B operating under non-slagging conditions for the investigation of sawdust conversion into producer gas for use in retrofitted oil or gas boilers at sawmills. A gasification efficiency of 60 % was obtained slightly lower than the reported values ~65-70 for other gasifier types for the same application. However, with comparable or higher energy density (LHV per volume) than the other listed gasifiers. The char efficiency varied depending on the oxygen equivalence ratio between 0.9 and 0.98 % and the producer gas contained all the ash and unconverted char, due to the used reactor configuration [65]. A more traditional cyclone configuration could might solve this, however the char conversion suffer if the separated char was not utilized either by recirculation or otherwise.

Later studies on cyclone gasifiers has primarily focused on application for direct turbine combustion.

Gabra et al. 2001 [63,64,66] investigated the use of a configuration A cyclone gasifier for making producer gas from different sugar cane residue in the form of bagasse [63] and cane trash [64]. Steam and air was used for gasification agent and oxidzer and the gasifier was operating under non-slagging conditions to avoid volatilization of corrosive elements such as sodium and potassium. These are characteristic of biomass derived fuels and can be problematic in many applications. The producer gas is meant for direct firing in a gas turbine for power generation. This is exemplifies one of the gasification applications where the in situ removal of fly ash particles and non-converted char residue is important as these are highly detrimental to turbine combustion. The heating values of the producer gas was sufficient for turbine combustion. However, the carryover of fly ash was deemed too great for direct turbine firing [63,64]. In a comparison the cyclone gasifier showed superior alkali retention (~70 %) compared to fluidized bed gasification (4-12 %)operating under similar conditions and temperature. However, the alkali content in the producer gas was still too high for turbine combustion [66]. The doctoral thesis by Fredrikssons studies the same process in depth but for woody biomass gasification. The conclusions are similar, but design guidelines for improving cyclone gasifiers are given [67].

Recently cyclone gasifier have received a lot of attention again for gasification of alternative fuels such as different biomass fuels, both from industrial and agricultural waste. This is driven by a need to find fuel flexible gasification technologies for local small scale gasification units primarily for power generation and secondarily for syn-gas production.

He et al 2012 [68] studied the gasification of biomass char from industrial pyrolysis units [68]. Gao et al 2012 [69] studied gasification of sawdust both experimentally and through CFD modeling [69]. Zhao et al. [70] studied the effect of fuel staging in cyclone gasifiers for wood powder [70]. Risberg et al. 2014 [71] studied the effect of the fuel type on the producer gas quality, carbon and gasification efficiency in a cyclone gasifier using 5 different fuels; stem wood, peat, rice husk, bark and terrified spruce [71]. Zhao et al. 2017 [72] studied a novel design for cyclone gasifiers with 3 inlets along the length of the cyclone for air staging with

rice husks as raw materials. The results where in the same range as standard designs [72]. Further results from the same gasifier with rice husk where reported in Sun et al. 2018 [73].

A commercial cyclone gasification plant were commissioned in 2012 in Hortlax, Sweden, operating as a combined heat and power plant. Powdered wood chips and pellets are gasified in an air blown cyclone gasifier operating at 950 °C. The producer gas is then cooled and cleaned and used in a gas piston engine for electricity production, while the heat recovered from the cooling of the producer gas and heat recovery of the engine flue gas is used for district heating, providing at max capacity 1.3 MW and 2.4 MW electricity and district heating respectively. With a max fuel consumption corresponding to an energy input of 4.5 MW, the plant have an overall fuel energy efficiency of 82 % [74].

Table 2.3: summary of reactor design and operating conditions for cyclone gasifiers available in literature

Application	Reactor configuration	Tangential inlets	Size D/V [m/m^3]	Atmosphere	Heat source	Temperature [°C]	Fuel rate [kg/h]	Carbon efficiency [-]	Gasification efficiency [%]	Ash removal [%]	Source
Non-slagging coal gasification for syngas	B		0.61/ 0.27	O_2/H_2O	Partial combustion	<1000	18	† 0.65	-	0	Perry 1950 [58]
Slagging coal gasification for syngas	B		0.61/ 0.27	O_2/H_2O	Partial combustion	1000-1500	18	† 0.80	-	0	Elliot 1952 [59]
Slagging coal gasification for producer gas	A		0.8/-	Air/H_2O	Partial combustion	>1200	570	0.80 0.95 (recycle)	64 %	66%	Traencker 1953 [60]
Slagging coal gasification	A		0.2/-	Air/H_2O	Partial combustion	1250	1.4	0.89	-	80%	Yagi 1957 [62]
Slagging coal gasification	A		0.2/-	O_2/H_2O	Partial combustion	1250	1.6	0.91-0.98	-	70%	Yagi 1957 [62]
Slagging coal gasification	A		0.15/ 0.004	Air	Partial combustion	1500	10	0.83	45 %	-	Barnhart 1982 [46]
Non-slagging sawdust gasification	B		-/-	Air	Partial combustion	1000	-	0.90-0.985	50-60 %	0 %	Cousins 1985 [65]
Non-slagging wood powder gasification	A		0.16/-	Air	Partial combustion	750-1050	6-18	-	-	70-80%	Kallner 1994 [75]

Application	Reactor configuration	Tangential inlets	Size D/V [m/m^3]	Atmosphere	Heat source	Temperature [°C]	Fuel rate [kg/h]	Carbon efficiency [-]	Gasification efficiency [%]	Ash removal [%]	Source
Non-slagging wood powder gasification	A	2	0.21-0.25/0.0338-	Air/H_2O	Partial combustion	820-1000	26-36	-	-	26%	Fredriksson 1999 [67]
Non-slagging Sugar cane bagasse gasification	A	2	0.2/0.046	Air/H_2O	Partial combustion	800-850	39-52	-	-	60-70%‡	Gabra 2001 [63]
Non-slagging Sugar cane trash gasification	A	2	0.2/0.046	Air/H_2O	Partial combustion	820-850	39-52	-	-	60-70%‡	Gabra 2001[64]
Non-slagging biomass char gasification	A	1	-/-	Air/H_2O	Partial combustion	800-1000	12	0.52-0.93	-	-	He 2012 [68]
Non-slagging sawdust gasification	A	1	2/-	Air	Partial combustion	800-1000	19.4	0.77-0.942%	53.6-63 %	-	Gao 2012 [69]
Non-slagging gasification of wood powder with fuel staging	A	2	0.2/-	Air	Partial combustion	800-1000	-	0.844-0.911	54-63.7 %	-	Zhao 2013 [70]

Application	Reactor configuration	Tangential inlets	Size D/V [m/m^3]	Atmosphere	Heat source	Temperature [°C]	Fuel rate [kg/h]	Carbon efficiency [-]	Gasification efficiency [%]	Ash removal [%]	Source
Non-slagging gasification of torrefied spruce, peat, rice husk, bark and wood	A	1	-	Air	Partial combustion	800	70-97	0.7-0.95	43-52 %	63-100 %	Risberg 2014 [71]
Non-slagging rice husk gasification	A	3	-	Air/H_2O	Partial combustion	800-900	36.6	0.62-0.72	40-51 %	-	Zhao 2017 [72]
Non-slagging rice husk gasification	A	3	-	Air	Partial combustion	750-850	18-50	0.50-0.55	30.6-36 %	-	Sun 2018 [70]
Non-slagging sawdust gasification	A	1	0.1/-	Air	Partial combustion & electrical heating	700-900	0.32-0.47	0.2-0.3	39-68 %	-	Vongsvarnrungruang 2018 [76]
Industrial non-slagging wood powder	A	2	-	Air	Partial combustion	950	4.5 MW	-	82 %	-	Jafari 2020 [74]

† calculated based on carbon available after partial oxidation (combustion) (mole gas/mole carbon)

‡ based on alkali content of fuel and the alkali content in the collected ash and char residue

2.2.1.3 Pyrolysis

Another thermal fuel conversion process is pyrolysis. Pyrolysis most commonly refers to processes where the heat is supplied externally either by heated gas, particles or walls and the raw material is only partially converted by the release of volatiles leaving the char. The products from pyrolysis is a mixture of primarily condensable volatiles consisting of a mixture of higher carbon hydrates, generally referred to as pyrolysis oil or tars, and some non-condensible gases including similar products as from gasification [56]. Traditionally pyrolysis has been used to produce charcoal by a slow process with oxygen limited combustion, since ancient times. In more modern times the gaseous products released from coal pyrolysis the process became the product of interest for the chemical industry with the leftover cox used for heating. While liquid fuels had been produced from coal pyrolysis earlier. The 70's and 80's the global oil crisis led to an increased interest to use the worlds vast coal reserves for applications where oil and natural gas had previously been the preferred fuels. Furthermore, it started the interest in using alternative (non-fossil) fuel and recent scientific and industrial development has primarily been driven by the need for liquid fuels from renewable resources such as bio-oil or waste derived fuels [77].

The overall goal of pyrolysis processes for bio-oil production is to achieve high oil yield and high quality oil. The oil quality refers to different factors including; high energy density, stable viscosity, low solid content, low oxygen content and low solid/ash contamination [33,78]. The oil yield and quality are dependent on different factors including; heating rate, reaction temperature, product gas residence time, carrier gas composition and the nature of the raw material [78,79]. A general overview of cyclone pyrolysis processes is shown in Figure 2.19.

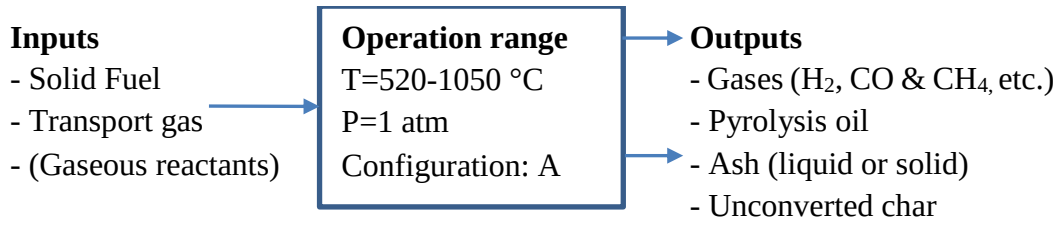

Figure 2.19: General principle of pyrolysis in cyclone reactors (operating conditions based on Table 2.4)

Pyrolysis was traditionally a slow process with high gas residence time, which caused low oil yields due to the cracking of the volatilized tars. However, the development of fast and flash pyrolysis changed this, small particles in the sub millimeter range is heated at rates high of ~10-200 K/s and >1000 K/s for fast and flash pyrolysis respectively [78,80]. Generally high heating rates and low gas residence time yields more and higher quality pyrolysis oil, while high reaction temperature favors gas production due increased rate of secondary reactions. The carrier gas used is based on the desired product mixture; it can be combustion flue gas favoring production of gaseous products due to the presence of oxygen and gasification agents CO_2 and H_2O [78,79] and, hydrogen for hydropyrolysis often catalyst assisted [81], or an inert gas such as nitrogen to reduce secondary reactions. The product gas residence time is important as too high residence time facilitate unwanted secondary reactions such as tar cracking and repolymerization favoring gas and char yields [78]. The heat transfer method has a large

influence on the product, as the heat transfer rate and therefore reaction temperature influence product composition and yield as well as the rate of the secondary reactions. Fast pyrolysis is currently the most popular process for bio-oil production and is commonly performed in fluidized bed reactors, FBR, CFBR or BFBR where the heating is either achieved through contact with a hot gas or heated inert particles [34,77,78].

Compared to combustion and gasification in cyclone reactors, where the ash removal, the intense mixing and long particle residence time is the main advantages, cyclone reactors provide further advantages for pyrolysis. One of the advantages for using a cyclone reactor compared to other technologies such as fluidized beds and entrained flow reactors, is the decoupling of the gas and the solid residence time. The long residence time of the solids ensures ample time for conversion of the raw material, while the short residence time for the gas limits secondary gas phase reactions, thus improving tar and therefore oil yield [56]. Another advantage hypothesized is the short contact time between the produced tars and the leftover chars. This reduces the secondary tar cracking reactions catalyzed by the char and ash components present in it. Giving a product a higher oil yield as less higher molecular hydrocarbon would be converted into non-condensibles [33].

2.2.1.3.1 Design and working principles

Contrary to cyclone burners and gasifiers cyclone pyrolysis is mainly carried out in reactors of Type A referring to Figure 2.12, with a classic reverse flow separation cyclone inlet-outlet configuration. The fuel and carrier-gas enters through one or multiple tangential inlets. Here the fuel particles are heated and react along the wall, while the gaseous pyrolysis products is quickly transported away from the leftover char, into the inner vortex and out of the gas outlet. The char is collected in the bottom.

The heating of the fuel to facilitate the pyrolysis can be achieved through various methods. The most popular method is using the heated inerts in the form of hot sand as it provides effective heat transfer and using a cold fluidization/transport gas will quench the formed volatiles reducing unwanted secondary reactions. The sand is separated out together with the char fraction and is heated in a separate burner by combustion of the char reusing the sand for heat transfer an utilizing the heat value of the formed char [34,77,78].Using sand as heat transfer medium has the disadvantage that it requires effective gas cleaning to avoid sand fines and ash in the oil even in a cyclone reactor. Furthermore, the char cannot easily be used for other purposes as it is mixed with the [34,77,78].

An alternative to using heated particles or gas are reactors capable of ablative heat transfer, among these are the cyclone reactor [34,77,78]. The principle behind ablative heat transfer is that the fuel particles are forced against a hot surface facilitating direct heat conduction across the surfaces. This can be achieved in a cyclone reactor where the cyclone walls are externally heated by a heating jacket or otherwise and the centrifugal force imparted on the particle from the vortex flow force the particles against the heated wall [34,77,78]. The advantages of the ablative method, is that very high heating rates can be achieved even for larger particles the

char residue can be collected in the bottom of the cyclone as a “pure” char, and that sand particles will not be partly entrained gas stream ending up as solid residue in the pyrolysis oil. The collected char can be burned as normal to provide heat for the process or as it is easier to process further, be used for making activated charcoal or used in a pulverized fuel combustor, as it is not mixed with sand

A summary of referenced designs, operating conditions and results for different cyclone pyrolyzers found in the literature are shown in Table 2.4.

Table 2.4: summary of reactor design and operating conditions for cyclone pyrolysers available in literature

Application	Reactor configuration	Tangential inlets	Size D/V [m/m^3]	Atmosphere	Heat transfer method	Temperature [°C]	Fuel rate [kg/h]	Oil/Tar yield [%]	Gas yield [%]	Solid yield [%]	Source
Patent for coal pyrolysis	A	3	-	Combustion flue gas	Hot sand	500-1000	-	-	-	-	Choi 1979 [82]
Flash pyrolysis of sawdust	A	1	$0.028/4.6\cdot10^{-5}$	Steam	Ablative (heated wall)	792 1054	0.25-0.5	61 † 3 †	36 93	2.8 3.6	Lede 1986 [83]
Fast pyrolysis of beech wood sawdust	A	1	$0.028/4.6\cdot10^{-5}$	Steam	Ablative (heated wall)	520-1054	0.14-0.36	16	79	3.93	Lede 2000 [77]
Fast pyrolysis of beech wood sawdust	A	1	$0.04/1.41\cdot10^{-4}$	Steam	Ablative (heated wall)	807-917	0.25-0.48	15	78	4.71	Lede 2000 [77]
Flash pyrolysis of wood sawdust	A	1	$0.06/0.47\cdot10^{-3}$	Nitrogen	Ablative (heated wall)	627- 710	0.33-0.71	75	16.7	10.5	Lede 2007 [84]

Application	Reactor configuration	Tangential inlets	Size D/V [m/m^3]	Atmosphere	Heat transfer method	Temperature [°C]	Fuel rate [kg/h]	Oil/Tar yield [%]	Gas yield [%]	Solid yield [%]	Source
PyRos reactor for biomass pyrolysis	A	1	0.4	Combustion flue gas	Hot sand	500-600	30	45-70	<15	-	Brem 2007 [85]
Fast pyrolysis of stem wood powder	A	1	0.39/	Nitrogen	Ablative (heated wall)	750	20	55	20	19	Wiinikka 2015 [34]
Fast pyrolysis of various biomass feedstock	A	1	0.39	Nitrogen	Ablative (heated wall)	675-775	20	35-50	11-28	27-6	Sandström 2016 [86]

†the amount of water in the collected oil is not given in the article

2.2.1.3.2 Applications

Lin et al. 1987 investigated the use of a cyclone reactor with heated gas as heat transfer medium for pyrolysis of bitumen-impregnated sandstone, through simple reactor modeling and concluded that the heating rate and particle residence time in the investigated reactor would not be sufficient for full conversion [87].

Choi 1978 & 1979 [82,88] patented a cyclone reactor with 3 separate inlets merging into one helicoidal inlets for coal pyrolysis using heated sand as heat transfer medium. Apart from the benefit of simultaneous reaction and separation it is suggested that the high heating rate and low gas residence would provide good conditions for producing high quality pyrolysis oil. The patents also claims the invention useful for agglomerating coals normally problematic for pyrolysis processes due to the high velocity shearing action of the sand particles [82,88]. Figure 2.20 shows the patent drawings where the concept of the 3 inlets is illustrated in part 1. The inlets marked 32 and 40 are heated inert at 'high' and 'low velocity respectively, while the inlet marked 34 is the coal inlet. The idea is that the difference in velocity and location would layer the coal between two hot inert layers, while the outer inert layer would ensure no sticking to the reactor wall [82,88]. No results of the oil yield or quality or other experimental data were published with the patent.

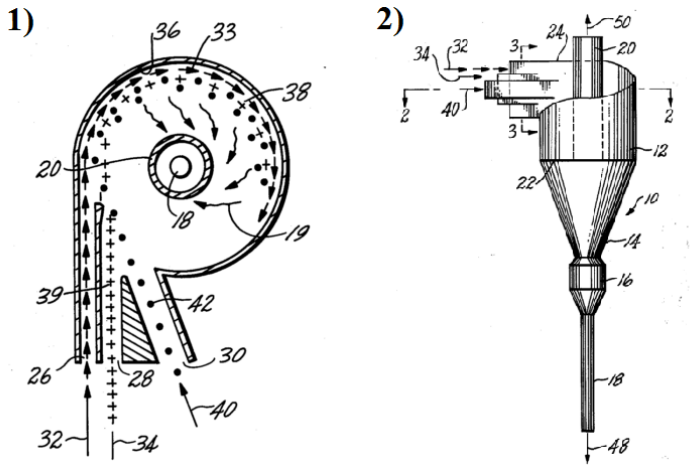

Figure 2.20: Patent drawings of cyclone pyrolyzer from Choi [82,88]

The Thermal Engineering group at Twente has developed cyclone flash pyrolysis process using the hot sand heat transfer method, called the PyRos process. They have overcome the some of the issues of this method by greatly improving the cyclones separation efficiency by using a rotating filter in place of the vortex finder thereby reducing the sand and char/ash particulates ending up in the condensed bio-oil without further hot gas cleaning or oil filtration [85].

Galiasso et al. 2014 [36] studied the use of an inverted cyclone reactor for hydropyrolysis of biomass by modelling. The setup modelled used heated carrier gas and inert particles as heat transfer medium, while the modelling was based on a kinetic pyrolysis model and reactor models based on a cold reactor setup [36].

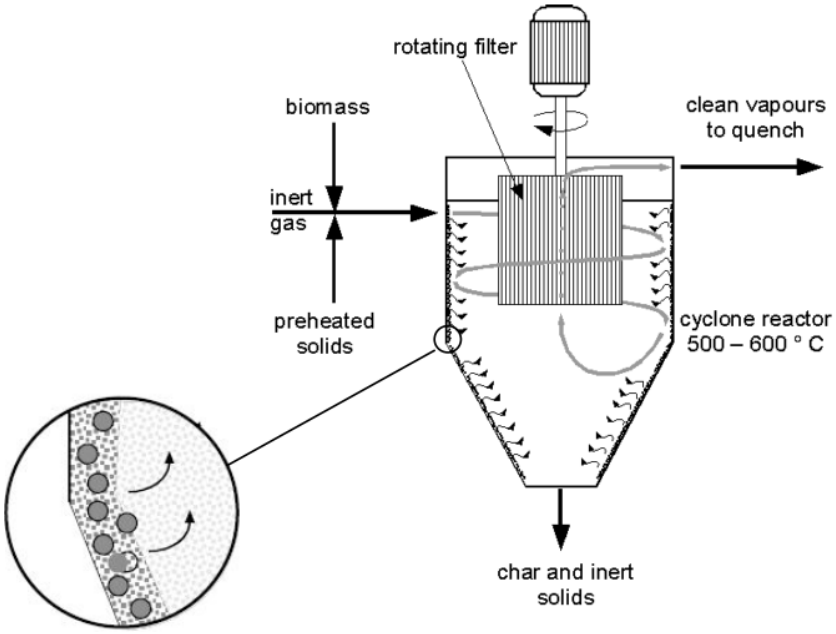

Figure 2.21: simplyfied process scheme of the PyRos procees (from [85]*)*

As some of the first Lede et al. 1986 [83] investigated the applicability of the ablative cyclone reactor for flash pyrolysis (or fast pyrolysis) of wood into fuel gas/syngas and pyrolysis tar in a lab scale reactor, primarily with focus on the gas production. Ablative heat transfer were used with the walls of the cyclones heated to different temperatures and the pyrolysis happening in a steam atmosphere as further reactions would be gasification reactions increasing the gas yield. The fuel conversion was above 94 % at wall temperatures of 1065 K and above with tar and gasification yields of 61 % and 36 % respectively at 1065 K and 3 % and 93 % respectively at the highest temperature of 1327 K [83]. Nothing is noted about the quality of the pyrolysis oil, as the focus was on the gasous products.

Lede et al. 2000 [77] compared the effects of operating conditions in two different lab scale cyclone reactors for ablative flash pyrolysis using the data from the study mentioned above in 1986 [83] and data from a study published in a phd thesis. The yield results and gas quality are comparable for both setups when conditions were similar. However, the results includes data from a run where the carrier gas was recycled product gas in order to avoid the use of steam and dilution of the product. However, the results from this show that the increased residence time of the product gases causes a drop in oil yield while increasing the gas yield. Overall both cyclone reactors show a very high capacity for the size of cyclone, compared to other pyrolysis reactors [77].

Lede et al. 2007 [84] investigated the oil quality and yield from fast pyrolysis in a lab scale ablative pyrolysis cyclone reactor again showing high volumetric capacity. This time with high oil yields [84].

Wiinikka et al. 2015 [34] studied the fast pyrolysis of pulverized wood biomass in a pilot scale cyclone reactor using ablative heat transfer and in a nitrogen atmosphere (carrier gas). As opposed to the focus on the gasous product in the earlier experimental studies [77,83] the focus

is on the production of pyrolysis oil for direct use or as raw material for liquid fuel synthesis. At a wall temperature of 750 °C the pyrolysis oil yield was 55 % and a solids yield of 23 % with the solid residue composed of char, ash and partially unconverted biomass. The energy yield of the oil was 53 %, 22 % for the solids and 9 % for the gas. The heat for the wall is partially supplied by the combustible uncondesable gas from the pyrolysis process which is mixed with liquefied petroleum gas (LPG) in order to ensure stable combustion and ensure enough heat input. Significant entrainment of ash and char was detected in the condensed oil suggesting that the separation in the cyclone was not optimal [34]. With a higher conversion of the raw material the energy yield of the gas could be higher and supply more of the needed energy for the pyrolysis, meanwhile the char fraction could easier be used for co-firing or other purposes. Further studies where made showing comparable results with different biomass feedstocks [86], while the quality and composition of the pyrolysis oil was analyzed and published in another study [33].

2.2.1.4 Ore and mineral processing

In the refining of metal ores pyro processing is often used to convert the ores from their mixed mineral form to a usable metal. This includes converting mixtures of metal sulfides and oxides into forms where the different metals can be separated physically or chemically to remove impurities. These processes involves heating the materials to high temperature and contacting it with a gas of a specific composition depending on the application and often also melting the solid ore. These processes are known under the common name smelting.

The potential for using cyclone reactors for processing mineral ore was realized after the invention of the first cyclone burners in the 1940's. It was realized that the combustion process was similar to the oxidation of sulfide concentrates used in some metallurgical process and the use of the principles from cyclone burners for was suggested in the 1950's [26,27]. Since then the cyclone reactor has seen use in various mineral refining process. An overview of cyclone smelting processes is given in Figure 2.22.

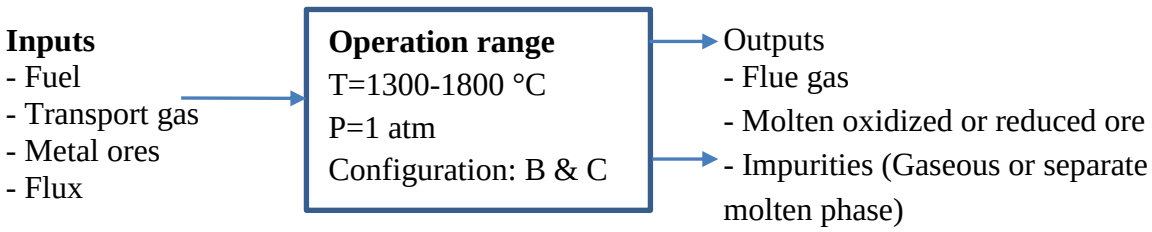

Figure 2.22: General principle of cyclone smelters (operating conditions based on Table 2.5)

2.2.1.4.1 Design and working principle

Cyclone smelters are designed and functions very similar to slagging cyclone burners using cyclone reactor configurations B and C from Figure 2.12, with a cylindric chamber that has a single outlet for both gas and smelt in the bottom, one or more tangential inlets and in the case

of configuration B an axial inlet. Fuel, ore, flux[1] , and combustion air (or oxygen) is injected into the cyclone smelter chamber tangentially [26–32], while some gas in the case of configuration B might be injected axially [27–29]. The mixture is mixed into the hot swirling vortex igniting the fuel and starting to heat up the ore and flux for reaction and melting. Both molten and un-molted ore and un-combusted fuel particles are forced toward the wall where a melt layer is formed, which catches the solids extending their residence time [26–32], similar to the slag in slagging combustion. The high tangential velocity and turbulence ensuring good mass and heat transfer to the molten layer and any particles trapped in it. The melt slowly flows down through the cyclone smelter and out into a molten bath for further processing [26–32]. A summary of the designs, operating conditions and applications for different cyclone smelters found in the literature are shown in Table 2.5.

[1] Compounds used for enhancing the flow properties of the melt and removing impurities

Table 2.5: summary of reactor design and operating conditions for cyclone reactors for ore and mineral processing available in literature

Process application	Reactor configuration	Tangential inlets	Size D/V [m/m^3]	Raw material	Atmosphere	Temperature [°C]	Capacity	Source
Volatilization smelting of antimony - pilot test	C	-	-/0.13	Antimony sulfide concentrates	Oxidizing	1300-1450	3.45 $\left[\frac{\text{ton}}{\text{h}\cdot\text{m}^3}\right]$	Tian-cong 1988 [26]
KIVCET - Copper smelting	B	-	1.4/-	Impure copper sulfide concentrates	Oxidizing	1500-1800	14.6 $\left[\frac{\text{ton}}{\text{h}}\right]$	Melcher 1976 [27]
CONTOP – Copper smelting	B	-	1.8/-	Impure Copper sulfide concentrates	Oxidizing	1500-1800	3.9 $\left[\frac{\text{ton}}{\text{h}}\right]$ †	Moskalyk 2003 [28]
CONTOP – Copper smelting	B	-	-	Impure Copper sulfide concentrates	Oxidizing	1500-1800	25 $\left[\frac{\text{ton}}{\text{h}}\right]$	Sauert 2000 [29]
CONTOP – Molybdenum concentrate roasting	B	-	-	Molybdenum Sulfide concentrates	Oxidizing	-	0.625 $\left[\frac{\text{ton}}{\text{h}}\right]$	Sauert 2000 [29]
Flame Cyclone Reactor- Copper smelting- Pilot test	C	1	1/1.2	Impure copper sulfide concentration	Oxidizing	1500-1800	3.2 $\left[\frac{\text{ton}}{\text{h}}\right]$	Ruehl 1986 [30]
Flame cyclone reactor- Copper smelting	C	1	-/-	Impure copper sulfide concentration	Oxidizing	1500-1800	9 $\left[\frac{\text{ton}}{\text{h}}\right]$	Emicke 1986 [31]
Flame Cyclone Reactor – Copper smelting –	C	1	-/-	Impure copper sulfide concentration	Oxidizing	1500-1800	10 $\left[\frac{\text{ton}}{\text{h}}\right]$	Ruehl 1986 [30]
Cyclone Converter Furnace – steel smelting	B‡	-	-	Iron ore	Reducing	1500	-	Langen 1993 [32]
Reduction of iron ore – lab scale	B	2	0.25	Low grade iron ore (Taconite)	Reducing	1400-1600	2.4 $\left[\frac{\text{kg}}{\text{h}}\right]$	Taylor 1993, 1994 [89,90]

† assuming 8000 operating hours per year

‡ Axial inlet is a gas inlet and liquid outlet

2.2.1.4.2 Applications

The cyclone reactor has seen use in the refining of antimony where it has been used for the Volatilization smelting step. Here antimony sulfide, Sb_2S_3, is oxidized to antimony oxides, Sb_2O_3 and Sb_2O_4, partly through gas-solid, gas-liquid and pure gas phase reactions of the volatilized antimony sulfide with oxygen at high temperatures. The overall reaction can be written as reaction R2.5 [26].

$$2\ Sb_2S_{3\ (s)} + 9\ O_{2\ (g)} \rightarrow 2\ Sb_2O_{3\ (g)} + 6\ SO_{2\ (g)} \qquad R2.5$$

The antimony sulfide is injected together with coal and fluxes into the air flow in the inlet pipe of a cyclone reactor of configuration C where combustion and the smelting process takes place. The antimony sulfide, coal ash, flux compounds and some of the produced antimony oxide will form a liquid melt on the cyclone reactor wall, where any un-melted solids will be caught and held in place, providing ample residence time. Most of the antimony oxide will stay in the gas phase. Both gas phase and liquid phase exits in the bottom through the same outlet into a settling chamber where the melt separates into 2 phases a slag and a matte, insoluble in the slag, while the gas phase enters a cooling system where the antimony oxides are recovered for further processing. The slag contains little antimony but most of the impurities and the matte consists of antimony sulfides and some impurities and can be recirculated to the smelting cyclone. The advantages of the cyclone reactor is the intense combustion in a small volume with good mass and heat transfer provided and the simultaneous separation of the gas and liquid phase. Temperatures in the reactor has been reported to reach 1300-1450 °C and a raw material smelting capacity of 3.45 tonnes antimony sulfide concentrate per hour per m^3 reactor volume [26].

The cyclone reactor has also been used extensively in copper production with mainly 3 different process developed, the KIVCET, CONTOP and Flame Cyclone Reactor [28,90]. In the 1960's the KIVCET process was developed in the Soviet Union. The KIVCET process used a cyclone for flash smelting copper concentrates with significant impurities of zinc, nickel and lead [27]. In the developed process the copper concentrates consisting mainly of sulfides of copper, CuS, and iron, FeS_2 & FeS and impurities of zink, nickel and lead sulfides, ZnS, NiS & PbS is smelted. In the smelting process the sulfides of the impurities and part of the iron sulfides is converted to their oxides and the material is melted. The overall reactions can be written as reactions R2.6-R2.10.

$$FeS_2 + O_{2\ (g)} \rightarrow FeS_{\ (l)} + SO_{2\ (g)} \qquad R2.6$$

$$2\ FeS_{\ (s\ \&\ l)} + 3\ O_{2\ (g)} \rightarrow 2\ FeO_{\ (l)} + 2\ SO_{2\ (g)} \qquad R2.7$$

$$2\ ZnS + 3\ O_{2\ (g)} \rightarrow 2\ ZnO_{\ (l)} + 2\ SO_{2\ (g)} \qquad R2.8$$

$$2\ PbS + 3\ O_{2\ (g)} \rightarrow 2\ PbO_{\ (l)} + 2\ SO_{2\ (g)} \qquad R2.9$$

$$2\ NiS + 3\ O_{2\ (g)} \rightarrow 2\ NiO_{\ (l)} + 2\ SO_{2\ (g)} \qquad R2.10$$

The copper concentrate and flux is fed axially to a vertical cyclone reactor of configuration B where it is caught in the vortex flow of pure oxygen fed tangentially. The suspended particles

starts reacting with the oxygen and are forced towards the wall by the centrifugal action. The oxidation of the sulfides is highly exothermic heats the material and the gas to temperatures above 1800 °C melting the materials. The melted particles are caught in a slow moving melt along the wall of the cyclone finally flowing down into the settling chamber. Both the melt and the gas exits into a settling chamber where the gas is separated out. The gas phase is SO_2 rich and can easily be utilized for producing liquid SO_2 or pure sulfur. The melt separates into 2 immiscible liquid phases, a slag of iron oxides and flux containing the oxidized impurities and small amounts of dissolved copper sulfides and oxides, which can be further processed to recover both the copper and some of the impurities, and finally a copper rich matte of copper and iron sulfides for further processing [27].

The CONTOP process developed in Germany in the 1970's uses a similar cyclone smelter as the KIVCET process the main difference being the design of the subsequent chambers for further treatment of the melt and slag [28,91]. The CONTOP process is well suited for copper concentrates with volatile impurities such, Arsenic, As, Antimony, Sb, and Bismuth, Bi, or co-products such as Zinc, Zn, Lead, Pb, or Molybdenum, Mo, due to the post cyclone treatment system [28,92,93]. After development the CONTOP reactor has been used for various other applications such as treating; sulfide concentrates of antimony and tin, Molybdenum concentrates and zink residues [29].

The flame cyclone reactor differs slightly from the KIVCET and CONTOP cyclone designs. The main difference is that oxidizing reactions take place inside the tangential inlet of a horizontally oriented cyclone, as the gas, copper concentrate and fuel is all mixed in the inlet shaft, only a single inlet is needed [28,30,31].

The cyclone smelter has also been used for Zinc and tin, volatilization smelting in processes similar to the antimony case described above [93].

The main advantages of the cyclone smelters over traditional flash smelting for the above mentioned processes is the high volumetric capacity, due to high thermal loads per volume up to 10 times higher than traditional flash smelters [93]. Furthermore, the higher operational temperature and lower surface area of the collected melt facilitates vaporization and prevents re-condensation of volatile impurities or products evaporated during combustion [91,93].

In the early 1990'is a consortium of British, Dutch, Belgian and Italian steel producers developed the cyclone converter furnace for smelting of iron ores [32]. In iron smelting the goal is to reduce the iron ore consisting mainly of oxides, the overall reaction for this is shown in equation R2.11.

$$Fe_2O_3 + 3\,CO_{(g)} \rightarrow 2\,Fe_{(l)} + 3\,CO_{2\,(g)} \qquad R2.11$$

In the cyclone converter furnace, this is achieved by pre-reduction in a cyclone reactor followed by full reduction in a melt bath below. Fine iron ore together with oxygen is injected tangentially into a cyclone, facilitating the swirling flow. Here it meets combustible gas from

coal gasification in the melt bath, thereby the iron oxides is partially reduced through reactions R2.12 and R2.13, simultaneously with combustion of some of the gas ensuring high heat release and melting of the iron oxides. The iron oxide particles/droplets is forced toward the wall through the cyclone action and forms a melt on the cyclone wall [32].

$$3\,Fe_2O_3 + CO_{(g)} \rightarrow 2\,Fe_3O_{4\,(l)} + CO_{2\,(g)} \qquad R2.12$$

$$Fe_3O_4 + CO_{(g)} \rightarrow 3\,FeO_{\,(l)} + CO_{2\,(g)} \qquad R2.13$$

The partially reduced melt flows down into the bath, where it is fully reduced by coal gasification in the melt bath mainly through reactions R2.14 and R2.15, and partly through reaction R2.13, for not fully pre-reduced material [32].

$$C_{(s)} + CO_{2(g)} \rightarrow 2CO_{(g)} \qquad R2.14$$

$$FeO_{\,(l)} + CO_{(g)} \rightarrow Fe_{\,(l)} + CO_{2\,(g)} \qquad R2.15$$

Around the same time as the joint European development Taylor et al. 1993 developed and patented an iron smelting process specifically for taconite ore in the US [89] and published experimental results from a small pilot scale test of the process [90].

2.2.1.5 SNCR

The SNCR or Thermal DeNO$_x$ process is a widely used method to reduce the NO$_x$ emissions from stationary combustion equipment [94,95]. Here ammonia or urea is mixed with the flue gas in the right temperature range reducing NO selectively [94–96]. The process only occurs when oxygen is present, which is generally the case for flue gas from stationary combustion equipment, as they operate at fuel lean conditions. Beside the reduction reaction a parallel reaction pathway oxidizing ammonia into NO occur. The oxidation pathway is favored at higher temperatures. The two pathway can be written as a simplified global reaction scheme as seen in R2.16 & R2.17 [1].

$$4\,NO + 4\,NH_3 + O_2 \rightarrow 4\,N_2 + 6\,H_2O \qquad R2.16$$

$$4\,NH_3 + 5\,O_2 \rightarrow 4\,NO + 6\,H_2O \qquad R2.17$$

Generally the temperature interval that favors NO$_x$ reduction is between 850 and 1100 °C [95]. In reality the process is a lot more complex and involves the initial breakdown of NH$_3$ into radicals and interacts with other species and radicals inherent to combustions systems [97]. These other species such as CO etc. alter the rates, the ratio between the 2 global reactions and the efficient temperature window [94]. A more detailed description of the SNCR process is given in section 2.3.

Especially in CFB boilers the SNCR process is often carried out in the cyclone separator by injecting the reduction reagent at the cyclone inlet, thereby making it a gas phase cyclone reactor [98,99]. Although the temperature in the cyclone of CFBs is sometimes below 850 °C where the standard window for SNCR process start, SNCR has been shown to work effectively. This is due to stratification causing the presence of CO and other combustibles that often only

fully combust in the cyclone due to the intense mixing [3]. SNCR is also applied in cyclone preheaters for high temperature industrial processes like mineral wool production [100] and cement production [101]. An overview of cyclone SNCR process is given in Figure 2.23.

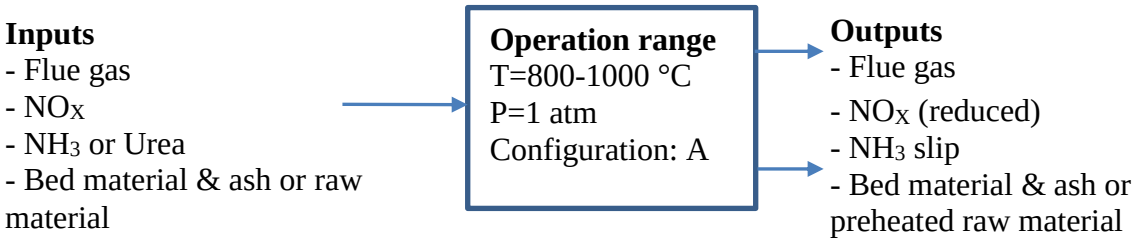

Figure 2.23: General principle of cyclone SNCR (operating conditions based on Table 2.6)

2.2.1.5.1 Design and working principles

The design of cyclones used for SNCR is generally not based on the goal of NO_x reduction, as the primary function of the cyclone is either separating out bed material from the flue gas for CFBs [3,98,99] or acting as a gas solid heat exchanger for preheater cyclones [100,101]. Hence, the cyclone is of the standard reverse flow separator design, configuration A. The reduction reagent is injected either in the cyclone inlet or in the riser before the cyclone.

A summary of the operating conditions and emission results for different cyclone SNCR processes found in the literature are shown in Table 2.6.

Table 2.6: summary of operating conditions and results for SNCR in cyclones available in literature

Application	Cyclone configuration	Tangential inlets	Size D/V [m/m^3]	Temperature [°C]	Reagent	Injection point	CO inlet concentration [ppm]	NO reduction [%]	NH_3 slip [ppm]	source
12-MW CFB boiler	A	1	2/-	850-890	Ammonia gas	Cyclone inlet	~1000	40-60	<15	Leckner 1991 [3]
12-MW CFB boiler	A	1	2/-	850-890	Ammonia water 25 %	Cyclone inlet	~1000	37-50 %	<15	Leckner 1991 [3]
20-MW CFB boiler	A	1	3.2/-	900-994	Ammonia water 25 %	Cyclone inlet	~1000	41 %	9	Ljungdahl 2001 [98]
20-MW CFB boiler	A	1	3.2/-	900-994	Ammonia water 25 %	Cyclone center	~1000	56 %	13	Ljungdahl 2001 [98]
Cement plant preheaters	A	1	-	-	Ammonia water	Cyclone riser	-	54-84 %	-	Horton 2006 [101]
Cement plant preheater	A	1	-	-	Urea	Cyclone riser	-	15-71%	-	Horton 2006 [101]

2.2.1.5.2 Applications

Leckner et al. 1991 [3] investigated how the injection method, injection point and additives affected the SNCR efficiency in the cyclone of 12-MW CFB boiler with inlet temperature from 735 to 890 °C. They found that the injection of ammonia as gas with recirculated flue gas as carrier gas were more effective compared to injection of ammonia in water and that additives such as hydrogen, methane, ethane and butane reduced the SNCR efficiency in most cases. Furthermore, they found that, by injection in the cyclone inlet as compared to in the cyclone outlet led to slightly better SNCR reductions while having very limited adverse effect. The ammonia slip was below 5 ppm and increase in CO emissions less than 10 % for NH_3/NO ratios up to 4 while the NO_x reduction were between 40 and 60 % for inlet feeding. Feeding in the outlet at feed ratios of 2 already led to ammonia slips above 15 ppm and CO emission increase of more than 50 % while at this feed ratio having achieved NO_x reduction between 35 and 45 % [3].

Ljungdahl and Larfeldt 2001 [98] studied the influence of ammonia injection point in on the efficiency of SNCR in the cyclone of a commercial CFBC boiler. Modeling results based on cold flow pilot scale measurements and the full scale test suggested that under the SNCR efficiency could be improved by moving the ammonia injection point to inside the vortex finder or just beyond its opening. Industrial scale measurements in the cyclone of a 20 MW CFB-boiler were performed. At full load the temperature in the cyclone increased from 900 °C in the inlet to ~985 °C in the outlet due to combustion of CO and other combustibles. The measurement results showed that by moving the ammonia injection from the cyclone inlet, to the inner vortex of the cyclone, the NO_x reduction improved from 41 % to 56 %, while the ammonia slip were stable. During low load operation where no combustion in the cyclone was observed, no improvement in NO_x reduction were found by moving the injection point. This showed that in cases with high CO concentration and combustion in the cyclone the SNCR performance can be improved by injecting the ammonia after the initial mixing in the outer vortex. The model results were not compared to the industrial scale experimental results, but mainly used as an explorative investigation [98].

Horton et al. 2006 [101] evaluated the use of SNCR for NO_x reduction in the cyclone preheater system at 5 different cement plants, using ammonia and urea. NO_x reduction between 10-90 % were achieved depending on the size and layout of plant, the position of injection, the number of nozzles, the used reagent, and the raw material used. The overall trends showed: the larger the plant the less effective the SNCR were; injection in the riser before the bottom preheater cyclone achieved the highest NO_x reduction, while injection after the bottom cyclone achieved the lowest NO_x reduction; increasing the number of injection nozzles from 2 to 4 did not improve the SNCR performance, in some cases the performance decreased; using ammonia water as reagent achieved better NO_x reduction than urea; the trend between plants suggested that higher iron content in the raw material improved the SNCR performance. The ammonia slip were not reported [101].

2.2.1.6 Dry scrubbing

HCl and SO_x other acidic/toxic gases generated in industrial combustion processes are have traditionally been removed from the flue gas through wet scrubbing, due to higher efficiency compared to dry scrubbing. However, the use of dry and semi-dry scrubbing technology is becoming more widespread due to simpler implementation and reduction of waste generation in the form of wastewater [102]. A good example is the injection of limestone sorbents into fluidized bed combustors for desulphurization of flue gas [103]. At low to moderate temperatures 150-315 °C in-duct sorbent injection have been used for HCl adsorption after fluegas cooling in the downstream equipment after which the solid sorbents are collected in electrostatic precipitators or bag filters [102].

A series of papers investigates the use of cyclone reactors for simultaneous HCl removal and sorbent separation for process intensification and easier sorbent recirculation to improve the efficiency and reduce the sorbent costs [102,104–106].

In 2001 Fonseca et al. [104] investigated the use of a small lab modified stairmand HE cyclone with a diameter of 2 cm, and slightly reduced inlet and vortex finder width, as a reactor for adsorption of HCl with hydrated lime $Ca(OH)_2$ at low temperatures (50-130 °C). The results were promising showing that full HCl removal could be achieved with a sorbent/HCl molar ratio of around 2-3 times the stoichiometric ratio at 50 °C with a bit lower performance at 130 °C [104].

In 2007 Chibante et al. [105] tested the use of recirculating RS_VHE cyclone reactor with a diameter of 2 cm and the staimand HE cyclone from the previous study for adsorption of HCl with hydrated lime $Ca(OH)_2$ at 53 °C. The recirculating of the elutriated fines did not have an effect on the HCl capture, as both reactors performed near identically for adsorption. The performance where overall lower than the previous study, with a linear dependency on the stoichiometric ratio (R/SR) as shown in Figure 2.24 a. The recirculating system did however have higher solid removal efficiency and lower pressure drop, as compared to the standard system [105].

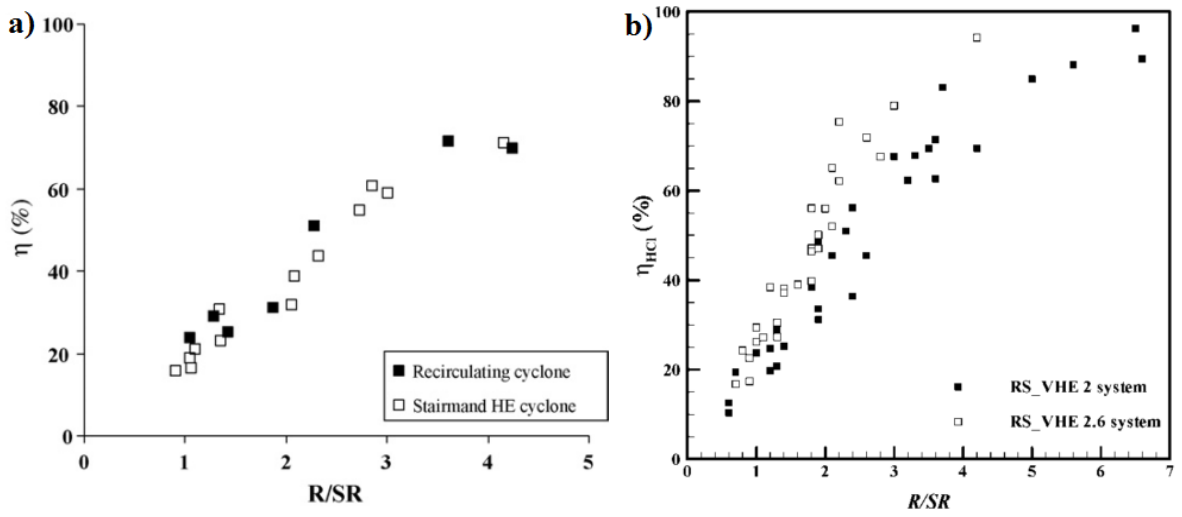

Figure 2.24: dependence of HCl adsorption efficiency on the stoichiometric ratio for different cyclone reactor configurations with hydrated lime a) recirculating RS_VHE D=2 cm and modified Stairmand HE D=2 cm (from [105]) b) recirculating RS_VHE D=2 cm and D=2.6 cm (from [102])

In 2009 Chibante et al. [102] tested the effect of cyclone size on the HCl scrubbing efficiency of the recirculating system described above, by comparing similar system with diameters of 2 cm and 2.6 respectively. They found that higher HCl adsorption were achieved at lower stoichiometric ratio's for the larger cyclone as seen in Figure 2.24 b. This were found to be due to increased conversion degree of the solids likely caused to longer residence time of the solid sorbents [102].

Overall the process show great promise in lab scale although the sorbent requirements are still quite high. Recirculating parts of the captured sorbents instead of just the elutriated should be investigated to reduce the sorbent requirement. This would meaningfully increase the sorbent load in the reactor without increasing the overall sorbent use. Furthermore, larger scale experiments must be conducted to ensure that the process works in practical scales. The move from 2 cm to 2.6 cm in diameter with improved efficiency is insufficient to conclude that the process would work at even pilot scale.

2.2.1.7 Catalytic reactor

In some catalytic processes such as fluid catalytic cracking (FCC), it is important to strictly control both solid and gas residence time, as well as provide sufficient contact between the gas phase reactants and the catalyst but limit the contact of the products with the catalyst. Much effort has been put into designing an optimizing both riser and downer reactors for this. Relative recently a short-contact cyclone reactor has been developed and patented [39]. The reactor consists of 2 separate compartments a type B cyclone reactor where the gas and solid exit is connected to swirl vanes acting as the inlet for a type A cyclone reactor. A drawing is shown in Figure 2.25.

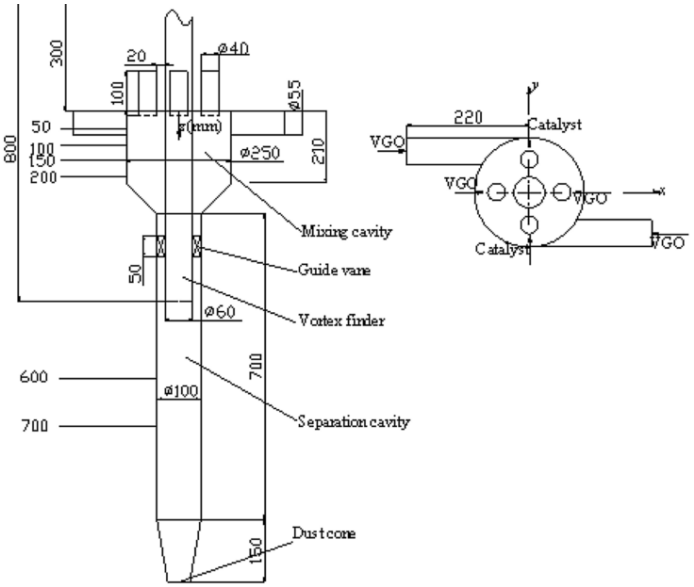

Figure 2.25: drawing of short-contact cyclone reactor [43]

The top compartment has 4 axial inlets for catalysts and 2 radial inlets for the vaporized crude oil and acts as the mixing and reaction chamber with the vortex finder of the second chamber going all the way through the upper chamber. The bottom chamber acts as a standard reverse flow cyclone with swirl vanes as inlet to provide the swirling flow a vortex finder as outlet for the product gas and a conical section for the solid catalyst outlet [40–43].

A series scientific studies of the reactor using CFD to model and test against experimental data measured on both cold flow models and overall reactor performance have been published [40–43].

Zhang et al. [40] investigated the solid and gas flow fields both experimentally and using CFD, showing reasonable agreement between modeling and experiments [40]. In a later study the residence time distribution of particles where measured using colored tracer particles and different CFD models were used to simulate the experimental results and parameters for models were evaluated to find best fit. Both model and experimental data for the residence time showed a short residence time for the catalyst. [41]. A simplified kinetic scheme were implemented into the CFD model in order to simulate the conversion of the crude oil into the different product categories such as; diesel, gasoline, coke and so forth. A comparison is made with experimental data for the exit concentrations, however the source or the method of producing the experimental data is not given. [43]. Finally, the latest study investigates particle trajectories of the catalyst in the reactor using CFD modeling [42].

The CFD studies of the short-contact cyclone reactor shows promise for future FCC application of the reactor. The short residence time of the catalyst and little to no back mixing is highly promising. However, the lack of available experimental data on actual reactor performance makes full potential hard to evaluate.

2.2.1.8 Aerosol Ceramic Reactor

Manenti and Masi 2011 [107], used CFD to investigate the possibility of producing fine ceramic powders through the vapour-phase aerosol process in a type A cyclone reactor. The process modelled was the production of titania micro-powder through the reaction shown below.

$$TiCl_{4\,(g)} + 2\,H_2O_{\,(g)} \rightarrow TiO_{2\,(s)} + 4HCl_{\,(g)} \qquad R2.18$$

In the process the reactants are fed separately to the reactor and reacts in a similar manner to non-premixed flames. The advantage sought from using a cyclone reactor instead of the traditional aerosol reactors, is to avoid back mixing of the nucleated particles common for the turbulent flow regimes in these reactors, where the particles reenter the flame zone and grows or agglomerate further. By separating the particles by the centrifugal forces in a cyclone reactor the back mixing is reduced, hereby further particle growth is avoided and the particle size distribution is narrowed, improving the product quality. This hypothesis was supported by the modeling work [107]. However, no experimental data is currently available.

2.2.1.9 Decarbonation of sodium bicarbonate

In 1992 Lede et al. [108] studied the decarbonation reaction of sodium bicarbonate ($NaHCO_3$) shown in R2.19 in a small 4 cm diameter lab scale type A cyclone reactor at various conditions [108].

$$2\,NaHCO_3 \rightarrow Na_2CO_3 + CO_2 + H_2O \qquad R2.19$$

From the results the use of lab scale cyclone reactors for studying kinetics of solid phase decomposition reactions. Furthermore, it was concluded that cyclone reactors was promising for industrial processes involving such reactions [108].

2.2.1.10 Sublimation of isocyanuric acid

In 1996 Lede et al. [109] studied the use of cyclone reactors for fast sublimation reactions with ablation heat transfer using isocyanuric acid in a small 4 cm diameter lab scale type A cyclone reactor with heated walls. Showing that complete sublimation could be reached if wall temperatures where sufficient, in the studied case 1000 kelvin [109].

2.2.1.11 Non-catalytic naphta cracking

Lucena et al. 2017 [38] modeled the use of an inverted cyclone reactor for for non-catalytic cracking of light naphta using heated inert particles as heat carrier, with simple reactor modeling methods. The idea was to prevent coke formation on the walls, which is a problem in traditional naphta cracking reactors, by having it form on the heated particles. The particles with the coke would be separated in the reactor and heat recoved from the coke by burning it to reheat the solids. The modeling results showed poor reactor performance for both conversion and selectivity compared to current industrial standards [38].

2.2.1.12 Production of niobium powder

Luidold et al. 2007 [110] experimentally investigated the production of niobium powder from niobium oxides using magnesiothermic reduction in a type A cyclone reactor. The reduction reaction are given in R2.20.

$$NbO_2 + 2Mg \rightarrow Nb + 2MgO \qquad R2.20$$

The used cyclone reactor had a diameter of 10.7 cm and was externally heated to 1130 °C. Niobium oxide and magnesium powder where fed to a heated argon stream at the cyclone inlet and the produced mixture of niobium and magnesium oxide powder where collected in the dust bin off the cyclone. Afterwards the Magnesium oxide and residue magnesium where leached using hydrochloric acid. Overall results of the experiments showed that the process was feasible, but the resulting product were quite impure and additional purification step where necessary [110].

2.2.2 Modeling Cyclone Reactors

Reactor modeling is an important tool for designing, optimizing and understanding the behavior of reactors. This is no less the case for cyclone reactors. Literature on modeling of cyclone seperators are plentiful. Models for cyclone reactors are a bit more scarce and not as well developed, due to cyclone reactors being somewhat of a niche and most models are not general, but have been developed for very specific applications. This section gives and overview of the available literature and models first in the form of empirical and engineering models and then in the form of computational fluid dynamics (CFD).

2.2.2.1 Emperical and engineering models

Many empirical models have been suggested for flow patterns, cyclone efficiency and pressure drop. Some of which has proven highly useful and now forms the theoretical basis for cyclone design, selection and dimensioning. Authors such as Shepherd and Lapple, Alexander, Stairmand, Barth and Musselknaus continuation of Barths work must be mentioned. For detailed description of the models, the theoretical considerations and implications and the history of the developments the reader is referred to the excellent monograph by Hoffman and Stein [6] or in shorter form the review article by Cortes and Gil [15].

When modeling a reactor, different factors can be important depending on the type of reaction carried out. Residence time of the gas and/or solid phase, heat transfer and mass transfer. Furthermore, the flow behavior/mixing must be represented by an actual reactor model. An overview of the available models and literature known to the author are given in this section.

2.2.2.1.1 Residence time distribution.

From the mean residence time of ideal reactors, it is possible to model any reaction system as long as the kinetic model is available. However, for real reactor this is not the case as the assumption of no back mixing or perfect mixing rarely holds. For non-ideal reactor where the assumptions of a CSTR or PFR reactor does not hold, residence time distributions can yield important information about the mixing behavior, bypass streams and dead volumes. Furthermore, empirical reactor models can be developed based on residence time distributions.

This section gives an overview of the published models for predicting the residence time distribution of the different phases in cyclone reactors.

2.2.2.1.1.1 Gas phase residence time

Lede et al. [111] performed gas phase residence time distribution experiments using tracer gas impulse responses in 4 different cyclones between 2.8 and 30 cm in diameter with slightly different geometric ratios and inlet designs. The experiments were performed under different temperatures, different gases and different inlet flowrates. A residence time model was suggested consisting of a PFR followed by a CSTR with a variable bypass which size is dependent on the flow conditions. An illustration of the model is shown in Figure 2.26.

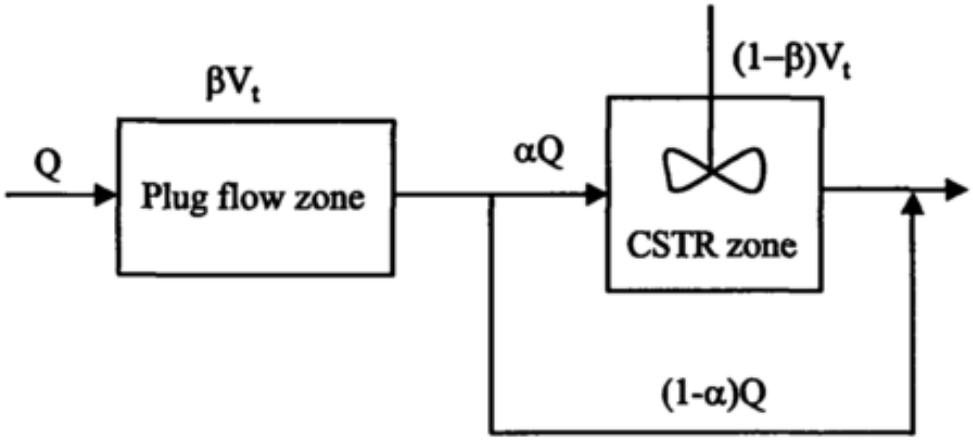

Figure 2.26: Illustration of reactor model suggested by Lede et al. [111] (adapted from [2]*)*

Here Q is the volumetric flowrate, V_t is the total reactor volume, β is the distribution of the reactor volume into PFR and CSTR zone and α is the fraction not bypassing the CSTR zone. In the rest of this work β_{lede} and α_{lede} is used in place of β and α for clarity. Initially it was suggested that β_{lede} could be calculated from the geometrical design of the cyclone by eq. 2.8 [111].

$$\beta_{lede} = \frac{\frac{\pi}{4} D_H^2 L}{V_t} \qquad \textit{eq. 2.8}$$

Where D is the hydraulic diameter of the cyclone, L, is the length of the plug flow zone, defined as the distance from the bottom of the vortex finder, to where the cylinder meets the cone, hence $L = h - S$ according. But analysis of the results showed that both parameters needed empirically fitting [111]. Figure 2.27 shows examples of the measured inlet an outlet tracer signal from the residence time distribution experiment, together with the predicted result for the model and the parameters fitted.

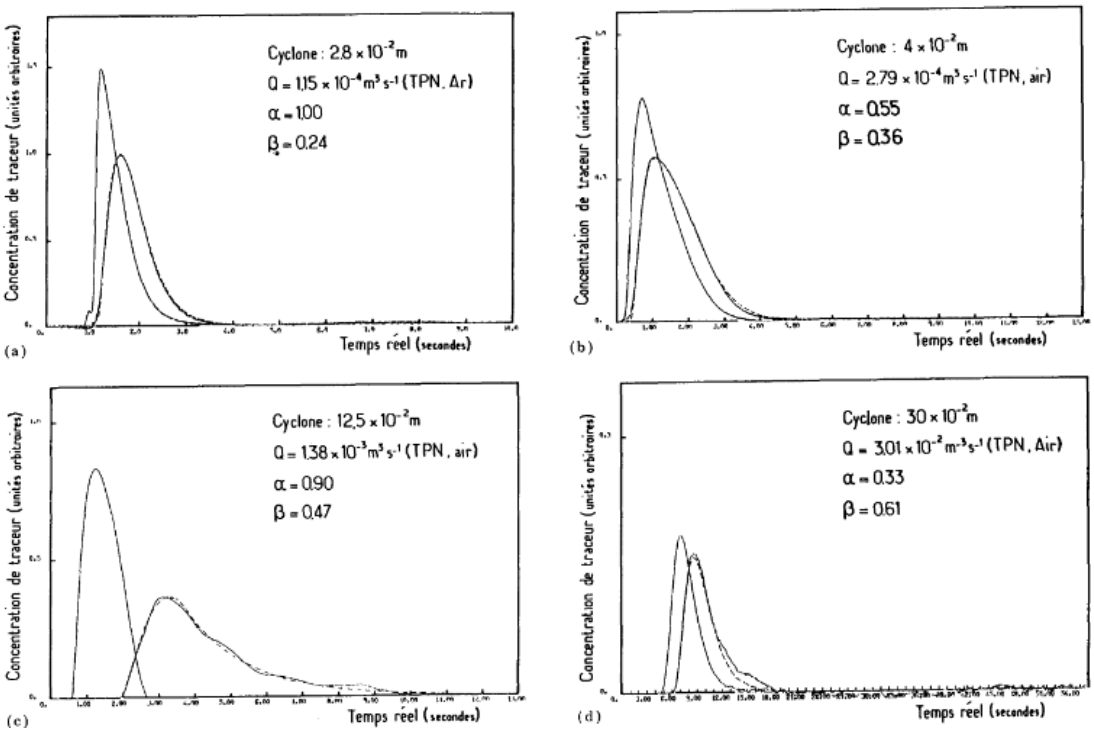

Figure 2.27: Measured tracer inlet and outlet signal (solid lines) and modeled outlet tracer signal (dashed line) for four different cyclones, shown with cyclone diameter, gas flowrate and fitted model parameters.(from [111])

Based on the best fit for the parameters, α_{lede} and β_{lede}, for experiments in these 4 cyclone with varying gases, tracers, flowrates and temperatures an empirical correlation based on the inlet Reynolds number, Re_0, defined as eq. 2.9, were suggested.

$$Re_0 = \frac{4\overline{m_g}}{\pi d_{\mathrm{H},0}\mu} \qquad \textit{eq. 2.9}$$

Where Q_{MG} are the mass flow of gas and d_0 is the hydraulic diameter of the cyclone inlet. The fitted parameters for the experiments are shown in Figure 2.28, plotted against the inlet Reynolds number. β_{lede} proved to be independent from, Re_0, and a value of $\beta_{lede} = 0.42$ were found be the best overall fit for a generalized model, while α_{lede} were best described by a discontinuous function defined by eq. 2.10 and eq. 2.11 [111].

$$\alpha_{lede} = 1, \quad Re_0 \leq 1700 \qquad \textit{eq. 2.10}$$

$$\alpha_{lede} = \frac{35.9}{Re_0^{0.48}}, \quad Re_0 > 1700 \qquad \textit{eq. 2.11}$$

The model have not been widely tested for other cyclone geometries than those in the original study [111].

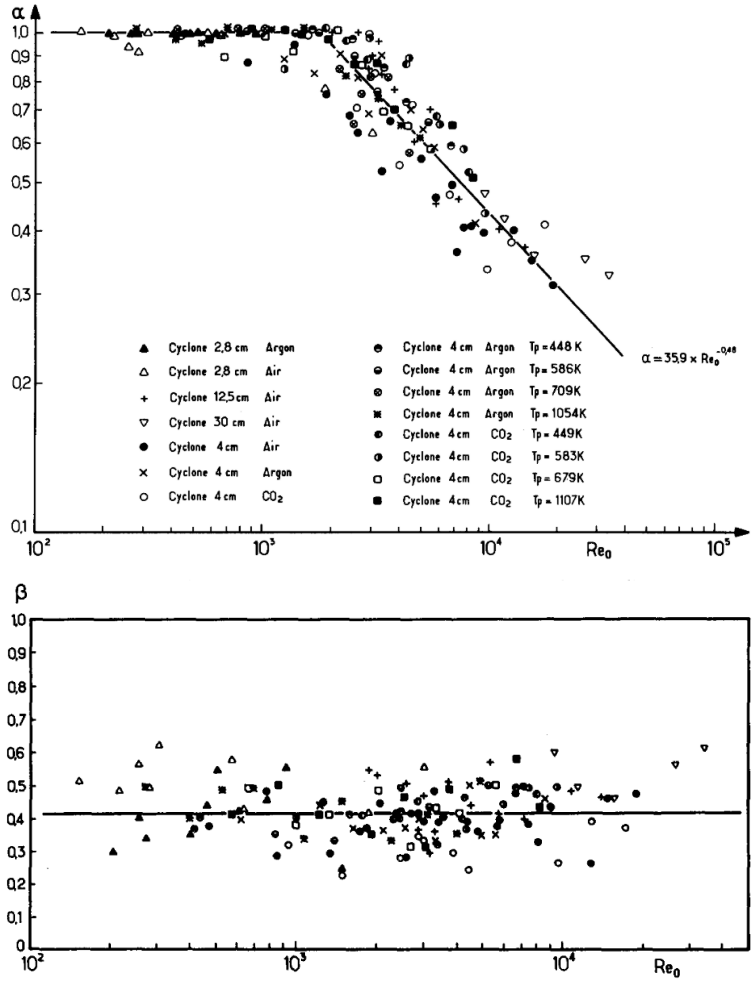

Figure 2.28: Optimal parameter fits (symbols) against inlet Reynolds number, Re_0, for α_{lede} (top) and β_{lede} (bottom), for the gas residence time model (from [111])

2.2.2.1.1.2 Solid phase residence time

Lede et al. 1987 [12] used 4 different methods to measure the average particle residence time with varying inlet gas velocity. The methods used were; single particle detection by phototransistors, impact of a pulse of particles on piezocrystal probes, analysis of particles vertical velocity profile by use of cameras, measurement of the space time of the particles by a hold-up method. The experiments was carried out under ambient conditions (temperature and pressure) in a 12.5 cm diameter standard Lapple cyclone of glass. The expression for calculating the mean solid residence time, τ_s, presented in eq. 2.12 was suggested [12].

$$\tau_s = 1.06 \cdot 10^{-4} Re_0 + 0.037 + t_\infty \qquad \textit{eq. 2.12}$$

Where, t_∞, is the particle settling time for the cyclone height from the middle of the particle inlet, assuming terminal velocity. Later Lede et al. 1989 [112] performed more experiment at different conditions (temperature, inlet velocity and particle sizes) in cyclones from 2.8 cm to 40 cm in diameter. Using the same methods as before, with an additional method of timing the particles with a watch in the cyclones with large residence time. From this work a general

empirical correlation given in equation eq. 2.13, was suggest. This based on the inlet Reynolds number, Re_0, for the cyclone, valid in the range $400 < Re_0 < 250000$ [112].

$$\tau_s = 4 \cdot 10^{-5} (Re_0)^{1.09} + t_\infty \qquad \textit{eq. 2.13}$$

Except for the solid hold up method all the methods used by Lede et al. [12,112] operate in an empty cyclone beyond the measured particles.

Kang et al. 1989 [13] studied the residence time distribution of particles in a series of cyclone with varying cylinder heights from 0.55 to 1.5 m and a diameter of 0.125 m and all other dimensions kept constant. This was done for different process parameters such as inlet gas velocity, particle size and density. The experiments were carried out under continuous operation with feeding of the bulk particles upstream of the inlet. Instead of the dust collector a narrow sample tube was placed at the dust outlet. The residence time distribution was measured by feeding a pulse of tracer particles coated in KCl. As the particles are collected they build up in the sample tube. The distribution of the tracer particles were tested by taking thin slices along the sample cylinder, soaking the particles in demineralized water and finding the KCl concentration via electric conductivity measurements. Based on the experimental data the empirical correlation for the mean residence time of particles given in eq. 2.14 [13].

$$\frac{\tau_s}{\bar{t}_g} = 0.032\, Re_p^{0.43} \left(\frac{v_{g,inlet} - v_t}{v_t}\right)^{0.7} \left(\frac{\rho_s - \rho_g}{\rho_g}\right)^{0.42} \left(\frac{\mathrm{H}}{\mathrm{H} - \mathrm{h}}\right)^{-1.76} \qquad \textit{eq. 2.14}$$

The fit between experimental and calculated values is shown in Figure 2.29.

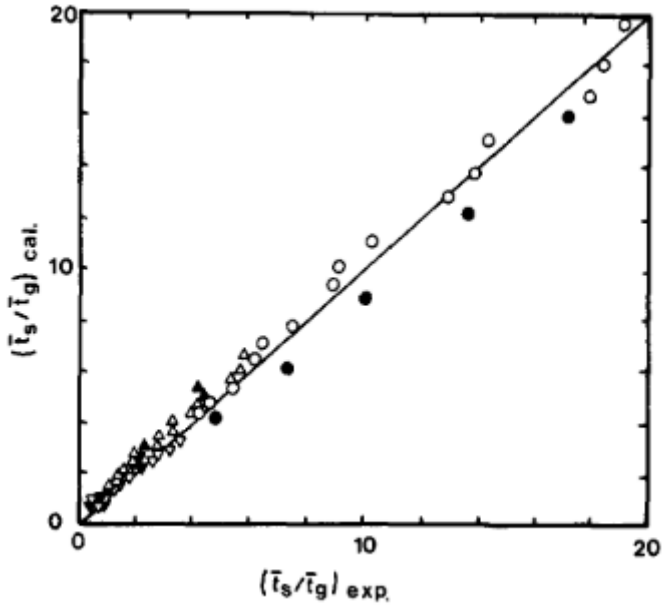

Figure 2.29: Comparison between measured and calculated values for solid residence times (from [113][13]*)*

Even though the distribution were measured no correlation for the spread in residence time where suggested. The main weakness of the method used in Kang et al. 1989 [13] is that the dust collector is removed to make room for the sample tube. In this way the influence of the

dust collector geometry on the cyclone behavior, which is well established in literature, is altered. This may lead to a skewing of the residence time results obtained.

Both of these correlations lack any dependency on the particle loading. Several authors using different measurement techniques for particle residence time measurement have reported a decrease in particle residence time with increase particle loading [114].

2.2.2.1.2 Heat transfer

Heat transfer is of critical importance in many of the applications cyclone reactors are used for, that being pyrolysis, gasification, combustion and smelting etc. Due to wide interest in using the cyclone as a gas-solid heat exchanger in for example the preheater towers for calcination plants several empirical correlations for the interphase heat transfer has been proposed [115–118].

Szekely & Carr 1966 [115] studied the heat transfer between a heated cyclone wall and the gas particle suspension fed cold into the cyclone. For pure gas flow the following Nusselt number correlations were found.

$$Nu = 0.042 \cdot Re_0^{0.8} \qquad \textit{eq. 2.15}$$

$$Nu = \frac{h_g\, D_H}{\lambda_g} \qquad \textit{eq. 2.16}$$

$$h_g = \frac{\dot{Q_g}}{A_{cyclone}\overline{\Delta T}} \qquad \textit{eq. 2.17}$$

Where $\overline{\Delta T}$ is the arithmic mean temperature difference between the wall, T_w, (constant temperature) and the gas inlet and outlet temperature, $T_{g,in}$ & $T_{g,out}$.

$$\overline{\Delta T} = ½\left(2T_w - T_{g,in} - T_{g,out}\right) \qquad \textit{eq. 2.18}$$

With particles it was found that the overall heat transfer from the wall to the gas-solid suspension increased with increasing solid loading. However, the wall to gas heat transfer was significantly reduced, as the particles shielded the gas-wall contact and took up most of the heat. The wall-solid heat transfer coefficient increased with increasing solid flow [115].

Lede et al. 1990 [116] also studied the heat transfer between gas and cyclone wall using the same method as Szekely & Carr [115], suggesting a Nusselt number correlation for wall to gas heat transfer as given in eq. 2.19.

$$Nu_H = 0.08.8 \cdot Re_H^{0.9} \qquad \textit{eq. 2.19}$$

Where Re_H is based on the hydraulic diameter of the cyclone [116].

Jain et al. 2006 [118] studied the heat transfer between hot air and cold sand particles fed into the gas stream just before the cyclone inlet. In their work a total particle heat transfer coefficient is defined by eq. 2.20.

$$h_p = \frac{\dot{Q}_s}{A_{s,total}\,\overline{\Delta T_l}} \qquad \textit{eq. 2.20}$$

Here the area, $A_{s,total}$, is the total particle area inside the cyclone at a given time and the logarithmic mean temperature difference, $\overline{\Delta T_l}$, like in a co-current heat exchanger, as the particles are assumed to move in parallel with the gas phase in plug flow. These two are defined as shown in eq. 2.21 and eq. 2.22 respectively.

$$\mathrm{A} = \frac{6m_s}{\rho_s d_p} \qquad \textit{eq. 2.21}$$

$$\overline{\Delta T_l} = \frac{\left(T_{g,in} - T_{s,in}\right) - \left(T_{g,out} - T_{s,out}\right)}{\ln\left(\frac{T_{g,in} - T_{s,in}}{T_{g,out} - T_{s,out}}\right)} \qquad \textit{eq. 2.22}$$

Where the solid mass holdup, m_s, can either be measured experimentally or found using a residence time model discussed in section 2.2.2.1.1.2. The particle Nusselt number is defined by eq. 2.23.

$$Nu_p = \frac{h_p d_p}{\lambda_g} \qquad \textit{eq. 2.23}$$

The following empirical correlation was proposed.

$$Nu_p = 0.0047 Fe^{1.45} Fm^{0.375}(2 + 0.664 Re_p^{0.5} Pr^{0.33}) \qquad \textit{eq. 2.24}$$

Where Fe is the Federov number and Fm is the solid loading ratio, defined as shown in eq. 2.25 and eq. 2.26. The inlet gas velocity is used as the characteristic velocity in the particle Reynolds number, Re_p.

$$Fe = d_p \left[\frac{4g\rho_g^2}{3\,\mu_g^2}\left(\frac{\rho_p}{\rho_a} - 1\right)\right]^{1/3} \qquad \textit{eq. 2.25}$$

$$F_m = \frac{m_s}{m_g} \qquad \textit{eq. 2.26}$$

The correlation developed fitted well with both their own experimental data and with a bit more deviation when using data from previous authors with other cyclone geometries [118].

Hence, one should be careful using the correlation for other cyclone geometries as the only effect cyclone geometry has on the model is in the estimated mass holdup and the inlet velocity used for calculating the particle Reynolds number.

2.2.2.1.3 Mass transfer

Mass transfer between phases in a reactor is an important factor for heterogeneous reactions such as catalysis and char combustion etc. Experimental literature on mass transfer between gas and solids in cyclone reactors are rare. However, some exists for the mass transfer between the wall and gas phase [2].

Lede et al. 1990 [116] investigated the mass transfer between the gas phase and the cyclone wall, by measuring ozone decomposition in a cyclone with walls of nickel oxide. The study where carried out without particles in a 4 cm diameter cyclone.

$$Sh_0 = 5.17 \cdot 10^{-3} \cdot Re_0^{0.97} \qquad \textit{eq. 2.27}$$

Note that this expression is only valid for a cyclone with the same ratio between inlet hydraulic diameter and cyclone hydraulic diameter. Converting it to using cyclone hydraulic diameter from the dimensions in the experiment gives the following correlation.

$$Sh_H = 0.194 \cdot Re_H^{0.97} \qquad \textit{eq. 2.28}$$

If the heterogeneous reactions are fast and the rate is controlled by large scale mass transport, this might be used to approximate the mass transfer from the bulk gas to the particle rich zone near the wall. If this is not the case it might be possible to use some of the Nusselt number correlations developed for heat transfer and use the principle of similarity for estimating Sherwood numbers and thereby mass transfer coefficients.

2.2.2.1.4 Reactor models

In order to model chemical reactions in a reactor, a reactor model must be formulated. The ideal reactor models might not be realistic, but sometimes they can give reasonable results.

Leckner et al. [3] modeled a cyclone reactor for SNCR using both a CSTR or PFR showing little difference in model results at the investigated conditions [3].

Ljungdahl and Larfeldt [98] used a simple CSTR model to model the gas phase reactions inside the cyclone reactor [98].

The residence time model given in section 2.2.2.1.1 can be used as a basis for a reactor network model for the gas phase, or to give the plug flow residence time for the solid phase. However, these correlations have not been tested with experimental data for reactive systems, but are purely based on residence time measurements.

2.2.2.2 CFD modeling of cyclone reactors

The development of CFD techniques and the availability of computational capacity has led to a "revolution" in chemical reactor research, as with so many other engineering subjects. The results obtained from CFD studies of reactors have significantly increased the understanding of chemical reactors and proved to be a cost effective way to test ideas and investigate phenomena that would be impractical or too expensive to test experimentally. This have led to many developments in reactor engineering through the last decades where CFD modeling have become more commonplace. As with the empirical and engineering models for cyclone reactors, CFD studies of cyclone reactors are also quite rare. Most CFD studies for cyclones studies primarily the flow field and to some extent to particle separation and to pressure drop. Much of the research in cyclones using CFD has been focused solely on describing the gas flow pattern as this can and have yielded results not previously obtained with experimental

methods. And a good description of the flow of the continuous flow is key to describing all other phenomena in the cyclone.

The main focus of CFD studies regarding cyclones have been focused on the cyclone as a separator. Cortés & Gil [15] gives a good review of the methods used for CFD modeling of cyclone separators and the developments up until 2007 [15]. Many studies have been published on accurately modeling the gas flow field in the cyclone without solids, using various turbulence models and discretization schemes.

As methods became more advanced it has been found that for accurate prediction of the gas flow field, transient models had to be used due to the inherent instability of the swirling flow. Furthermore, it has been found that second order discretization are needed to avoid numerical diffusion. The turbulence closure models must have higher order for accurate predictions, with Large Eddy Simulation (LES) being the most recommended model showing great results and the Reynolds Stress Models (RSM) being the cost effective Reynolds Average Navier-Stokes (RANS) alternative [15].

Gronald & Derksen [119], simulated the gas phase flow in a cyclone, using different turbulence models and discretization schemes, comparing it to the Laser Doppler Anemometry (LDA) measurements of Obermair [120]. Both RANS and LES turbulence models were used. The RANS model where the RSM using QUICK discretization scheme. At first the steady state formulation were tried, but failed to converge, so the transient formulation were used instead. Two LES models were used, one using finite volume discretization with the central difference scheme (FV-LES), while the other used Lattice-Boltzmann discretization (LB-LES). All the models performed equally well for the axial velocity (vertical), while the LES models performed best for both radial and tangential velocity as well as for the size and frequency of velocity fluctuations caused by the turbulence and vortex core precession [119] .

The modeling of a cyclone is not complete without description of the solid phase behavior. Traditionally this have been done using Lagrangian particle modeling, first with only gas to solid coupling and later with 2 way coupling. This is mainly valid in dilute gas-solid flows as it fails to account for the solid-solid interactions, which become dominant as distance between particles becomes smaller. As the particles in cyclones are concentrated along the wall, the solid-solid interactions should be taken into account [15].

More recently the use of multiphase CFD models (Eulerian-Eulerian) formulations for gas solid flows popularized for fluidized bed simulations, received a lot of attention and been used for great effects in other. However, the use in cyclone modeling is still scarce, with Lagrangian modeling still dominating [15]. The Eulerian models are mainly used in modified CFD codes developed for steady state prediction of cyclone performance (separation and pressure drop), using various simplifications in order to solve optimization procedures for cyclone geometry [121].

The pro's and con's of two solid phase formulation is described in more detail in the review on CFD simulation in dense particulate reaction systems [122]. Overall the Eulerian-Eulerian models describe the overall flow behavior of the solids and their effect on the gas phase flow in dense particle systems best. But the change of particle properties due to reaction or the modeling of particles of different sizes are problematic. This is less problematic in Lagrangian-Eulerian modeling as each particle and its properties are tracked individually, but the effect of particle-particle interactions are reduced to at maximum collision based [122].

The implementation of chemical reactions in CFD models for cyclone reactors have only received attention recently. Due to the transient nature of cyclone flow either the reactions must be solved for each timestep or the reactions must be implemented in post processing for time averaged data.

Kang et al. 2017 [123] studied the SNCR reaction in a cyclone for an industrial CFB boiler, by applying a reduced kinetic mechanism to the time averaged gas flow field. The flow field was found using RSM turbulence model and a lagrangian particle model with 2 way coupling [123]. The method seemed promising; however, there were no validation data of either flow field or reaction used and turbulence-reaction interaction is not implemented.

Zhang et al. 2013 [40] modeled the solid and gas flow field in the short-contact cyclone reactor illustrated in Figure 2.25 in section 2.2.1.7. They used Eulerian-Eulerian solid phase description with the Gidaspow drag model and the RNG κ-ϵ turbulence model, and the results for velocity profiles and volume fractions were in good agreement with the experimental data [40].

Zhang et al. 2015 [41] modeled the solid-phase residence time using Eulerian-Eulerian solid phase description with species transport in the granular phase. 3 different drag models; the Gidaspow, the Wen and Yu, and the Syamlal-O'Brien models where tested, and the results where compared with experimental data. Of the 3 drag models the Gidaspow performed best [41].

Zhang et al. 2017 [43] implemented a reduced kinetic scheme for FCC into the model described above and simulated the reactor in transient simulations. And investigated different operating conditions effect on the outlet concentrations of the different products [43].

2.3 NO_x emissions and Selective non-catalytic reduction (SNCR)

This section gives an overview of the emission sources of NOx, the underlying formation mechanisms, various emission reduction techniques and finally a more detailed discussion of SNCR as it is the primary reaction system investigated in this work.

2.3.1 NO_x emissions sources and formation mechanism

NO_x is a collective term for a number of oxides of nitrogen, the most common referred to are nitric oxide NO, nitrogen dioxide NO_2, and nitrous oxide, N_2O, which are potent pollutants [97]. After emission to the atmosphere NO is converted into NO_2, which through reaction with

VOC (Volatile Organic Compounds) produces photochemical smog, an contribute to acidification [97,124]. N_2O is a greenhouse gas and contributes to depletion of the ozone layer [125].

NO_x released to the atmosphere due to human activity comes from a variety of sources. However, most of which can be grouped under combustion, which also produces most of the emissions [126].

The most important causes for NO_x generation in combustion processes is the initial formation of NO through three different sources. These three sources are thermal NO_x, Prompt-NO_x and fuel bound nitrogen. A simplified diagram of the reaction pathways for these sources are shown in Figure 2.30 [97].

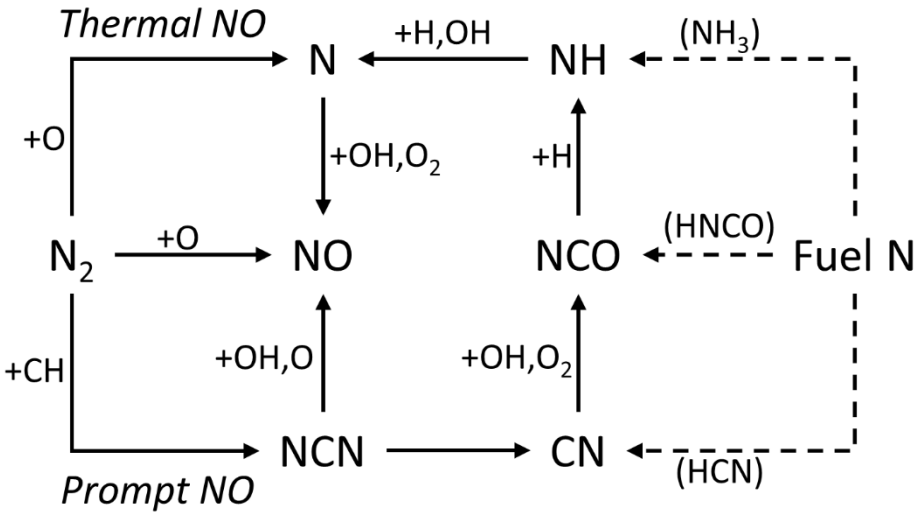

Figure 2.30: Diagram of the simplified reaction path for thermal, prompt, and fuel NO formation. (adapted from [97]*)*

2.3.1.1 Thermal NO_x

Thermal NO_x is generated in combustion systems through a series of reactions starting with the reaction between molecular nitrogen from the combustion air and oxygen atoms at high temperatures [97]. The mechanisms for this, first suggested by Zeldovich [127] as R2.21 & R2.22 and later extended to account for fuel rich conditions by reaction R2.23 [128].

$$N_2 + O \leftrightarrows NO + N \qquad R2.21$$

$$N + O_2 \leftrightarrows NO + O \qquad R2.22$$

$$N + OH \leftrightarrows NO + H \qquad R2.23$$

Thermal NO_x is mainly important at high temperatures, as the high activation energy of the initiation reaction R2.21, $E_a \approx 318\,kJ/mol$ [129], must be overcome and ample atomic oxygen must be present. Due to this one of the strategies for low NO_x combustion is reducing both the peak temperatures and the overall temperature in the flame zone. Thermal NO_x is the main contributor for NO_x formation in high-temperature gas combustion, where the fuel nitrogen content is negligible and the temperature is sufficiently high [97].

2.3.1.2 Prompt-NO_x

Prompt NO_x first by described Fenimore [130], is generated in hydrocarbon flames where CH_n radicals attack the N_2 triple bond. Initially it was believed that the reaction formed HCN and N radical's, but it is now through reaction R2.24, initiating a branching chain of reactions leading to the generation of NO and N_2O [97].

$$N_2 + CH \leftrightarrows NCN + H \qquad R2.24$$

Prompt NO_x is mainly important in turbulent diffusion flames [97], which also makes up the majority of practical flames from an industrial viewpoint.

2.3.1.3 Fuel-N

Fuel NO_x comes from fuel bound nitrogen, most often found in solid and liquid fuels. The carbon-nitrogen bonds of fuel bound nitrogen is more easily broken than the diatomic triple bonds of molecular nitrogen. Therefore fuel NO_x is not as dependent on the temperature as prompt and thermal NO_x. However, the speciation of the fuel nitrogen mainly into NH_3, HNCO and HCN, leads to a complex chemical reaction network where NO is both generated and consumed [97]. Therefore, the stoichiometry in the combustion zone is important to the NO_x generation. Thus another strategy for low NO_x combustion is the staging of fuel and air to control the stoichiometry in a beneficial manner [96,97].

2.3.2 Selective Non-Catalytic Reduction (SNCR)

While various combustion control strategies, such as reducing the NO_x generation by combustion modification and removing part of the generated NO_x by fuel staging, can reduce emissions by up to 50 %, secondary measures are often needed in order to adhere to the emission requirements [96]. SNCR is a well known NO_x abatement technique and is a widely used method to reduce the NO_x emissions from stationary combustion processes [94]. The SNCR process first discovered in 1972 by Exxon Research and Engineering Company and were commercially demonstrated in 1974 [95]. The process is cheap to implement, compared to other solution like SCR (selective catalytic reduction) or wet scrubbing systems [96]. In SNCR a reduction agent in the form of ammonia, urea or cyanuric acid is injected into the high-temperature flue gas. The reagent then react primarily with the NO and converts it to N_2 and H_2O [96,97]. High temperature gas phase reactions between NO and NH_3 had been known before Exxon's discovery, but the studies had been performed under conditions not conducive to selective reduction of NO [96]. The selective NO reduction only occurs when oxygen is present, which is generally the case for flue gas from stationary combustion equipment, as they operate at fuel lean conditions [1,96]. The NO reduction reaction pathways can be simplified to the global reaction shown in R2.25 [1].

$$4\,NO + 4\,NH_3 + O_2 \rightarrow 4\,N_2 + 6\,H_2O \qquad R2.25$$

The reagents for SNCR are also the precursors to NO_x production from fuel NO, as seen in Figure 2.30, hence parallel to the reduction, an alternate reaction pathway producing NO occur, this is illustrated for ammonia by the simplified global reaction R2.26 [1].

$$4\,NH_3 + 5\,O_2 \rightarrow 4\,NO + 6\,H_2O \qquad R2.26$$

The process is much more complicated than that, this is illustrated by Figure 2.31, showing the most important reaction pathway's for the SNCR process with ammonia as reduction reagent, also called the Thermal $DeNO_x$ process [96,97].

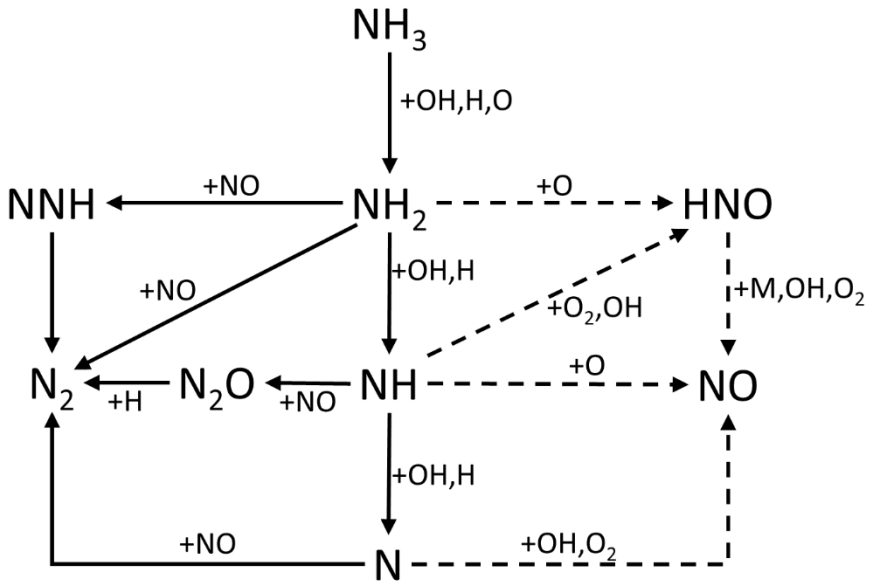

Figure 2.31: Diagram of reaction pathway's for ammonia in the SNCR process. Solid lines denoted pathways for NO reduction, while dashed lines denote pathways for NO production important at high temperatures (adapted from [97]*)*

The process is initiated by the conversion of NH_3 to NH_2 for which the main reaction in practical systems is R2.27 [96,97].

$$NH_3 + OH \leftrightarrows NH_2 + H_2O \qquad R2.27$$

Both this initiation reaction and the oxidation pathways are highly dependent on the presence of especially OH radical. Thus, the lower temperature, above which NH_3 is converted to NH_2 at sufficient rates, and the upper temperature, above which too much NH_2 is oxidized to NO, for the SNCR process is influenced by flue gas species affecting the radical pool such as oxygen, water and combustibles often in the form of CO or hydrocarbons [1,94,96,97]. Generally the lower limit is considered to be between 730 °C and 800 °C if combustion is complete, while the upper limit is around 1200 °C [96]. The optimal temperature is often found to be around 950-980 °C above which the NO producing pathway starts to become more dominating and at some point the upper limit is reached where more NO is generated than removed [96].

Three important factors that govern the reduction of NO by the SNCR process are, the temperature, the residence time and the stoichiometric ratio of reactant to NO. For SNCR with ammonia, the stoichiometric factor, β, also called the feed ratio, is defined as the amount of reduction agent over the NO content before any reaction takes place, given as: $\beta = [NH_3/NO]_0$ for ammonia. The influence of stoichiometric ratio on the NO reduction at different temperature is illustrated in Figure 2.32. From this it is clear that the NO reduction increases with increasing stoichiometric ratio in the temperature window, and that increasing

stoichiometric ratios lower the temperature where maximum NO reduction is achieved. It can also be observed, that after a certain point, in this case $\beta > 2.5$, the increase in NO reduction is negligible. The optimal temperature is observed to be around 950-980 °C in this case.

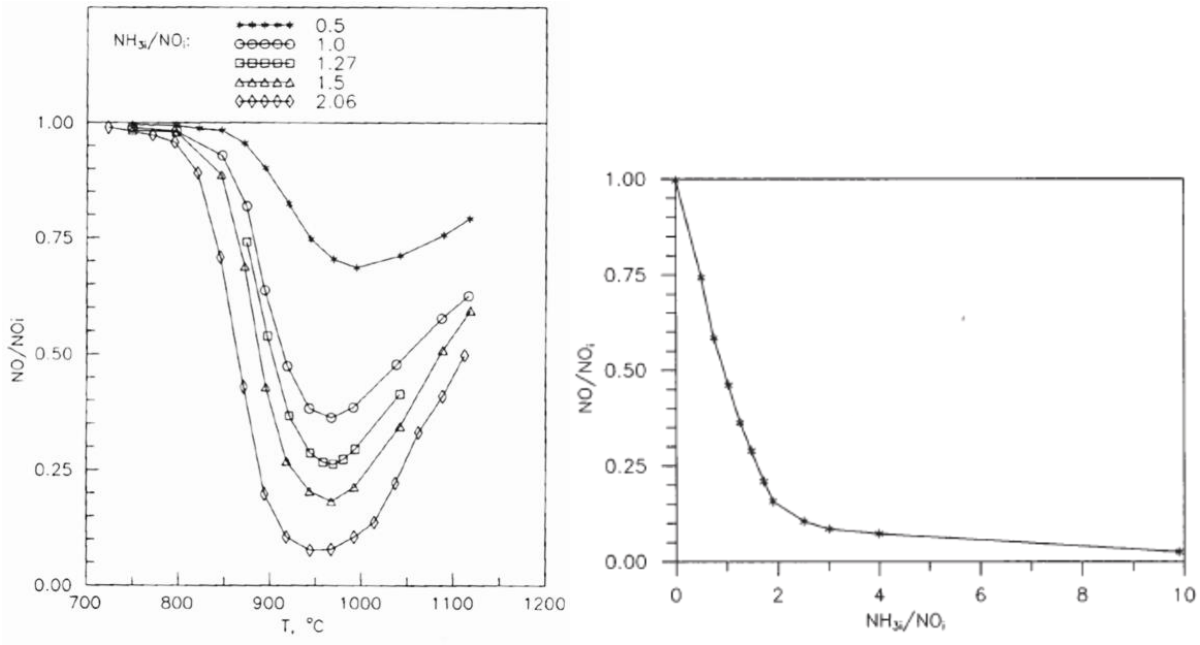

Figure 2.32: Influence of stoichiometric ratio NO reduction, over a temperature range (left) and at 940 °C (right) for SNCR with ammonia Inlet conditions: NO, 507 ppm and O_2, 4%; residence time=0.077 s at 940 °C [131]

While NO reduction through SNCR with ammonia is a fast reaction, the time needed for full conversion is quite important as the residence times in practical systems can be limited. The temperatures influence of temperatures on the rate of conversion and the conversion time is illustrated by Figure 2.33, for a stoichiometric ratio of $\beta = 1.64$.

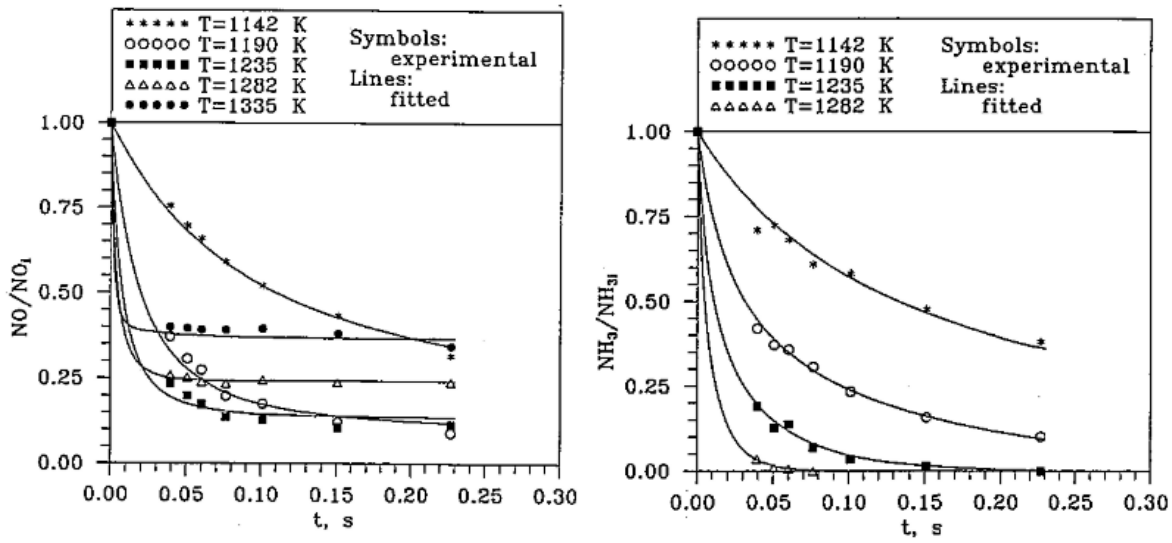

Figure 2.33: Influence of temperature on the time profiles for NO reduction (left) and NH_3 conversion (right) for SNCR with ammonia, Inlet conditions: NO, $5.15 \cdot 10^{-3}\ mol/m^3$; NH_3, $8.45 \cdot 10^{-3}\ mol/m^3$; and O_2, $0.405\ mol/m^3$ [1]

In order to further illustrate this and to further compare with the influence of the stoichiometric ratio shown in Figure 2.32, the NO reduction and NO conversion dependency on temperature for various residence times are shown in Figure 2.34, for a stoichiometric ratio of $\beta = 1.64$. From Figure 2.33 and Figure 2.34 it can be seen that the lower the temperature, the more important the residence time and vice versa. As seen on Figure 2.33 at $\beta = 1.64$ full conversion of the ammonia is achieved at 1282 K after just 0.07 seconds, while at 1235 K it takes more than twice as long at ~0.17 seconds for full conversion, but with a higher NO conversion. From Figure 2.34 it can be observed that the optimal temperature is reduced when residence time is increased sufficient ammonia present. It is also clear that to achieve the best possible NO reduction while avoiding ammonia slip, the stoichiometric ratio must be adapted to the available residence time and temperature.

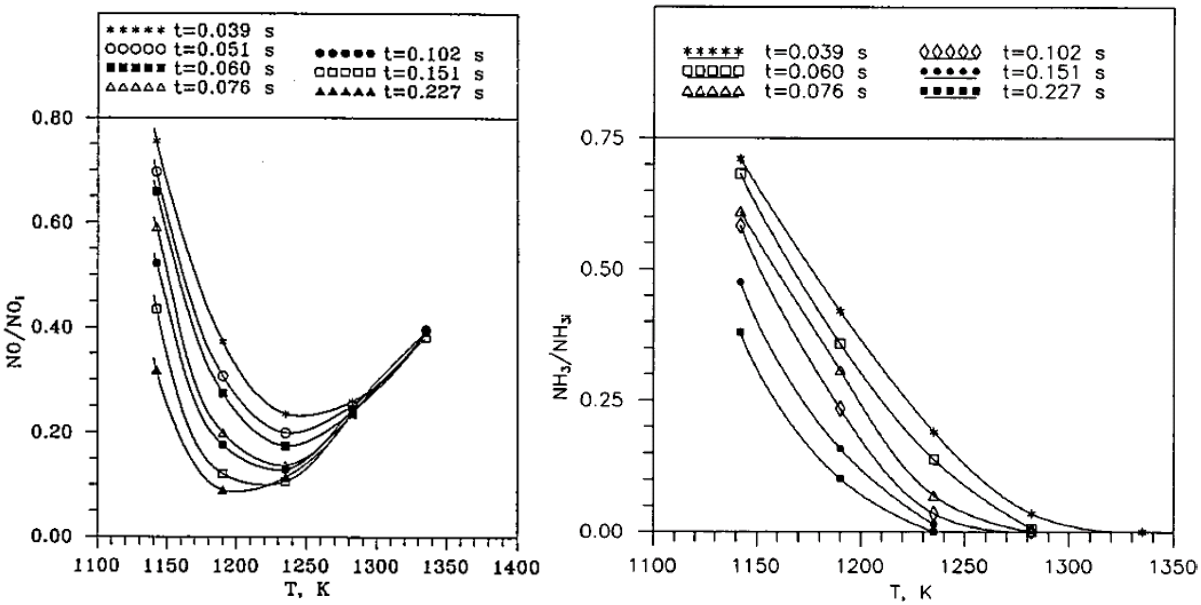

Figure 2.34: Influence of residence time and temperature on NO reduction (left) and NH_3 conversion for SNCR with ammonia (right) Inlet conditions: NO, $5.16 \cdot 10^{-3}\ mol/m^3$; NH_3, $8.45 \cdot 10^{-3}\ mol/m^3$; and O_2, $0.405\ mol/m^3$ [131]

Besides the temperature, residence time, and the stoichiometric ratio, the gas phase composition in terms of major flue gas components has a high influence on the temperature window and the selectivity of the reaction, through their effect on the radical pool as illustrated by Figure 2.31. The influence of oxygen content on the NO reduction is illustrated in Figure 2.35. From this it is clear that practical application of SNCR is only possible when oxygen is present. It can also be concluded that the highest NO reduction can be achieved at low oxygen concentrations, while higher temperatures are needed, as more oxygen concentration shifts the window towards lower temperatures. Furthermore, it can be seen that the influence of oxygen is highest at low oxygen concentration, with large shift of the temperature window with only little change of the oxygen concentration, while at around 4 % oxygen, the temperature window is much less sensitive to any further increase.

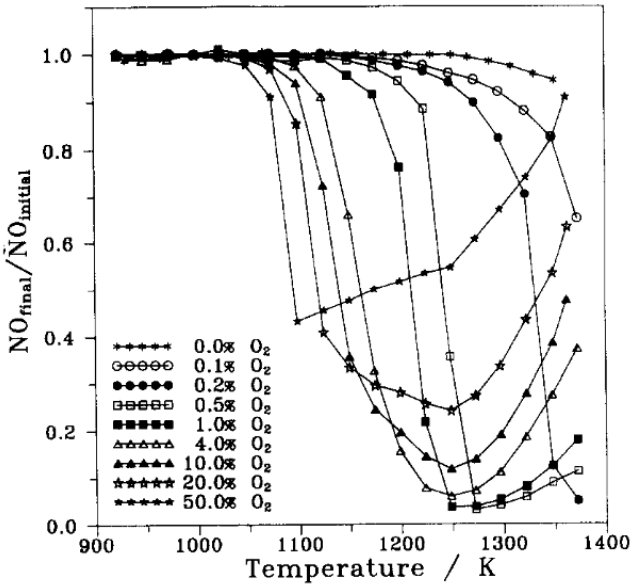

Figure 2.35: Influence of oxygen content and temperature on NO reduction by SNCR with ammonia, Inlet conditions; NO, 500ppm; NH_3, 1000 ppm; and H_2O 5%, Residence time=88.0/T from [139]

Gas phase water content influence the radical pool at high temperature and thereby the SNCR process. The effect of this, is illustrated by Figure 2.36. While the influence of water is minor compared to oxygen, the difference between dry gas and 2.7 % water content is noticeable, with a slightly higher NO reduction above 875 °C and lower NO reduction below. Increasing the water content further shows the opposite effect.

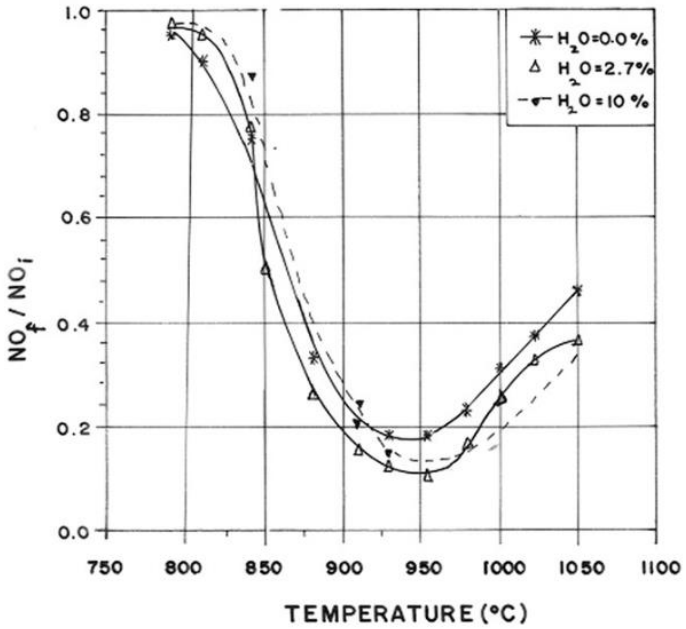

Figure 2.36: Influence of water content and temperature on NO reduction for SNCR with ammonia, Inlet conditions: NO, 507 ppm; NH_3, 832 ppm; and O_2, 4 %[131]

The presence of CO and other combustibles has a significant impact on the reaction kinetics, lowering the temperature window for SNCR [94,97,131] and narrowing it [97]. This is caused by the replenishment of the radical pool, due to the chain branching reactions from the oxidation of the combustibles. This increases the rate of both the reductive and oxidative reaction pathways is increased [97].

Most of the above figures and observations are based on experiments conducted in lab reactors designed to minimize the effects of mixing. This is not possible in practical industrial applications, where the conditions impart mixing limitations due to length scales and flow structure. Hence, the influence of mixing is important when studying larger scales or designing industrial applications.

Østberg et al. [132–134]. studied the effects of mixing of gaseous ammonia injected into a hot flue gas flow as a gas jet, through both experiments and modeling [132–134]. The experiments were conducted in a flow reactor consisting of a tube with a 50 mm diameter and the ammonia injection were done through 2 different nozzles, 1 and 1.9 mm, placed flush with the wall, using different carrier gas types, pure nitrogen and air, different carriers gas flowrates and different temperatures. The conclusions from the experimental results showed that the carrier gas flowrate and injection nozzle had a significant effect on the SNCR performance, which is illustrated by Figure 2.37.

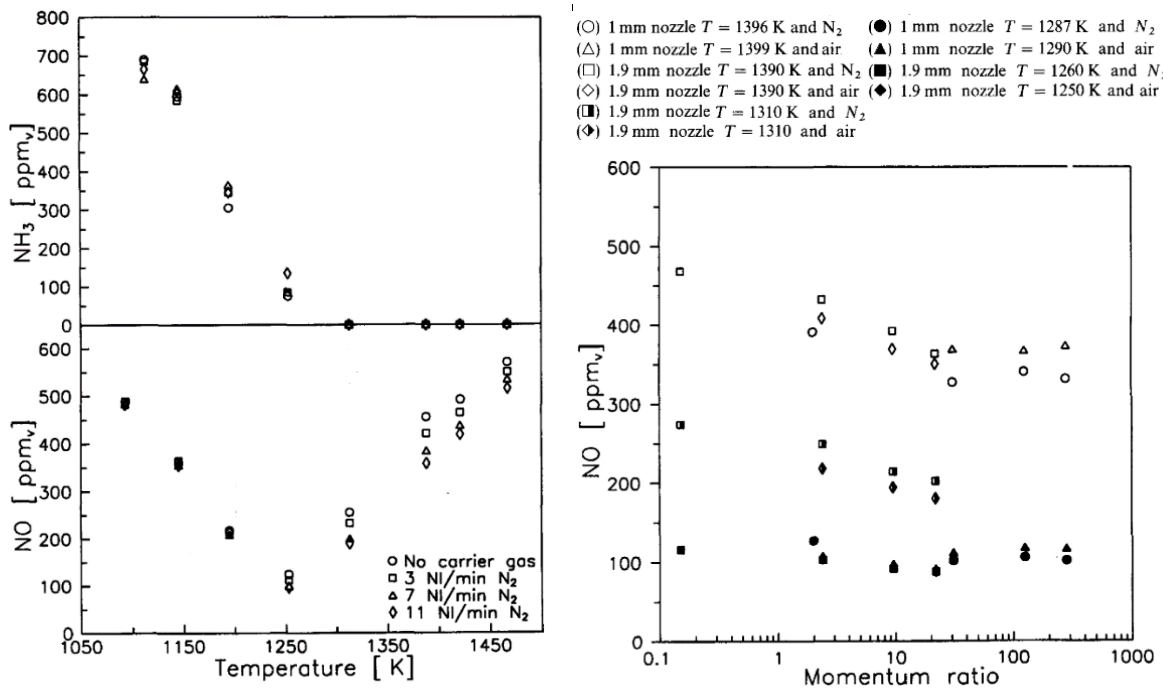

Figure 2.37: The effect of mixing on the SNCR process Inlet concentration: NO, 550 ppm_v; NH_3, 1000; residence time 0.1 seconds at 1200 K (Left) NO and NH_3 outlet concentrations as a function of temperature for the 1.9 mm nozzle (Right) NO outlet concentration as a function of the momentum ratio between injected jet and bulk gas [133]

From Figure 2.37 it can be seen that an increase in carrier gas (improved mixing) increases the NO reduction, until the temperatures where the oxidation pathway for NH_3 is dominant. A slight increase in ammonia slip is observed with increased carrier gas flow [133]. Additionally

it can also be observed that when increasing the momentum ratio between the injected gas and the bulk flow, defined as, $J = \frac{\rho_i u_i^2}{\rho_b u_b^2}$, and thereby improving the mixing, a point where no further improvement of the NO reduction is achieved. This point is influenced by the temperature, but for the investigated system, the overall point to be reached to rule out mixing limitations were stated to be at least $J = 20$ [133,134].

2.3.3 Modeling SNCR

Throughout the years various kinetic models have been suggested for modelling the SNCR process. Since the 1980's detailed kinetic models for the nitrogen chemistry in burners and engines and later for modeling NO_x reduction by various SNCR technology [135,136]. From this kinetic models have been expanded to include the known elemental reactions and updated with regards to reaction rates and thermochemical parameters using both experimental and theoretical results [97]. From this reduced kinetic models, based on sensitivity analysis of the full detailed models, focusing only on the most important reaction pathways, have been developed [94]. Thereby reducing the complexity of the model and the computational cost. However, the sensitivity analysis is carried out under conditions relevant to the specific objective of the reduced model, making the model optimal for those conditions, but reducing its flexibility and accuracy for conditions outside these. Finally, simple kinetics using global reactions with kinetic parameters fitted to a limited set of reaction conditions have been suggested [1,131].

The detailed kinetic model used in this work, constitutes the latest version of the full nitrogen combustion chemistry model presented by Glarborg et al. [97]. This reaction scheme accounts for 151 separate species reacting through 1397 different reactions. It is based on 40 years of research, and the experimental results from hundreds of studies, under various conditions, and theoretical calculations for the elemental reactions which cannot be measured. This makes it applicable over a wide range of conditions, as it have not been fitted to one particular system [97]. For SNCR with ammonia particular the model shows good quantitative results for well controlled lab scale reactors over a wide range of oxygen content from 1-50 % and for the presence of unburned combustibles such as CO [97], which have a large effect on the temperature window [131,137]. However, there are still limitations and important phenomena in nitrogen chemistry not yet fully captured, which can make its strength flexibility, a weakness in certain cases. As an example, the models prediction of the temperature window for SNCR is sensitive to the gas phase water content [97], because of its effect on the radical pool, while experimental results have shown only minor influence [97,138,139]. This is exemplified by the following cases:

- At 4% O_2 and 5 % H_2O the optimal temperature for NO reduction at, inlet concentrations 500 ppm NO and 1000 ppm NH_3, $\beta = 2$, is predicted to be at 1210 K [97], while experimentally it is measured at 1250 K by Kasuya et al. [139].

- At 10% H_2O and 4% O_2 the lower limit is shifted 50 K up to 1125 K compared to 1075 K at 0% water [97], while the experimental data from Rota et al. [138] show little to no effect.

Due to the large size of the model in regards to number of reactions, it will not be presented here, instead refer to the original work [97].

Brouwer et al. 1996 [94] suggested a reduced mechanism for SNCR with ammonia, urea and cyanuric acid, based on the detailed mechanism by Miller and Bowman [136]. The mechanism assumes instantaneous breakdown of urea and cyanuric acid into ammonia (NH_3) and iso-cyanic acid (HNCO). By assuming equilibrium of the H, OH, and O radical pool the mechanism were reduced to the 7 reactions given in R2.28-R2.34.

$$NH_3 + NO \rightarrow N_2 + H_2O + H \quad \textit{R2.28}$$
$$NH_3 + O_2 \rightarrow NO + H_2O + H \quad \textit{R2.29}$$
$$HNCO + M \rightarrow H + NCO + M \quad \textit{R2.30}$$
$$NCO + NO \rightarrow N_2O + CO \quad \textit{R2.31}$$
$$NCO + OH \rightarrow NO + CO + H \quad \textit{R2.32}$$
$$N_2O + OH \rightarrow N_2 + O_2 + H \quad \textit{R2.33}$$
$$N_2O + M \rightarrow N_2 + O + M \quad \textit{R2.34}$$

The reduced mechanism by and Brouwer et al. [94], is in this work converted to a simple kinetic model simply using the two reactions related to ammonia and NO conversion, R2.28 and R2.29.

The simple kinetics derived by Duo et al. [1] uses the global reactions given in R2.25 and R2.26, from experimental data with NO and ammonia in, am atmosphere of 4 % oxygen and the rest nitrogen.

2.3.4 Mixing

Østberg divided the mixing into macro and micro mixing and investigated both through modeling and comparison with experimental results. The influence of macro mixing was investigated by modelling non-ideal macromixing in an “extreme” way. The bulk flow is divided into two parallel volumes flows with identical residence time with the injected reactant fully mixed into and one with no reactant mixed into. After the mixing time the two flows are fully mixed. This leads to two important conditions, it gives a higher local concentration of the injected reactant (ammonia), while limiting the amount of NO available for conversion. Due to the simplicity of the reactor model this was done using both simple and detailed kinetics [133,134].

The droplet diffusion model was developed to describe the micro mixing assuming ideal macromixing. The droplet diffusion model uses diffusive transport of all reactive species and have only used with simple kinetics. This was investigated experimentally in a flow reactor setup and through modeling using both simple and detailed kinetics, ideal reactors and a droplet diffusion model developed for the purpose [132,133,140].

Røjel [141] investigated the effect of mixing on the SNCR both experimentally and by modeling. Existing bench scale data from Østberg [132,133,140] was used together with new lab scale and industrial scale data collected. A macro-mixing model based on bulk flow being entrained in a jet was developed based on a Zwietering reactor model [141].

2.4 Summary and conclusions

Cyclones are not simply separation units, but can also act as gas-solid heat exchangers, chemical reactor, or all three.

An overview of the most common cyclone reactor configurations have been given and sorted into categories, based on their inlet and outlet configuration. The available literature on the current industrial applications of cyclone reactors, their design and operating conditions have been summarized. From this it is clear that cyclone reactors are currently primarily used for high temperature processes.

For heterogeneous gas-solid reactions, the solid fuel combustion and pyro-processing of mineral ores applications are quite similar with the majority involving molten phases forming on the cyclone walls trapping unconverted particles thereby improving the residence time and conversion efficiency. They are mainly performed in cyclones without reverse flow, and either a closed top or axial inlet in one end, several tangential inlets and a common outlet for gas and melt phase. Both cyclone burners and metal pyro-processing in cyclone smelters have been applied widely in industry since the 1940's and the 1960's respectively. Since the mid 1950's, research has been conducted on conversion of solid fuels through both gasification and pyrolysis in cyclone reactors, for producer gas, syngas and liquid fuel oil production, with renewed interest from time to time. The focus in gasification research has moved away from high temperature slagging gasification in systems similar to cyclone burners, to non-slagging conditions in cyclone reactors designed similarly to reverse flow cyclone seperators. Cyclone gasification have had its commercial breakthrough for gasification in combined heat and powerplants. In Pyrolysis the focus have moved from producing mainly gas and char to achieving high oil yields for biofuel synthesis.

For gas phase reactions the main industrial application is SNCR in reverse flow cyclone separators for emission reduction in combustion units. Even though there is a large base of SNCR related literature, only few studies specifically focused on the application in cyclones are available. Cyclone SNCR mainly used in CFBCs and cyclone preheater systems, achieving process intensification by performing several tasks in the same equipment.

A summary of applications for cyclone reactors still in the very early stages of development and applications briefly investigated in literature have been made. This includes, dry scrubbing of HCl and SO_x from flue gas, the use of cyclone reactors for catalytic processes such as a FCC reactor, non-catalytic cracking of naphta, Aerosol Ceramic Reactor for high quality ceramic powder production and production of pure niobium, sublimation of isocyanuric acid, and decarbonation of sodium biocarbonate.

The available literature on modeling of cyclone reactors have been presented, showing a big gap in the available models and the models needed for more detailed reactor engineering calculations for cyclone reactors. The important points from the progress of CFD modeling from cyclone separators have been given and the few published works about CFD modeling cyclone reactors have been summarized.

A common limitation of both the experimental and model investigations for SNCR both in general and in cyclone reactors is that the results for ammonia slip is generally not reported.

Chapter 3 – Pilot scale experiments

This chapter describes the pilot scale cyclone SNCR experiments conducted in this project. First a description of the experimental setup and the experimental procedures used is given. Then the results are presented and discussed, and finally the conclusions are presented.

3.1 Materials and methods

This section describes the materials and methods used in the experimental work, including the cyclone reactor setup and the analysis equipment, as well as the different experimental methods and the experiments conducted.

3.1.1 Experimental setup

The pilot scale experiments were conducted using a cyclone reactor setup consisting of a gas burner, a combustion chamber, a cyclone reactor, and a flue gas treatment system. A simplified overview of the setup is schematically illustrated in Figure 3.1.

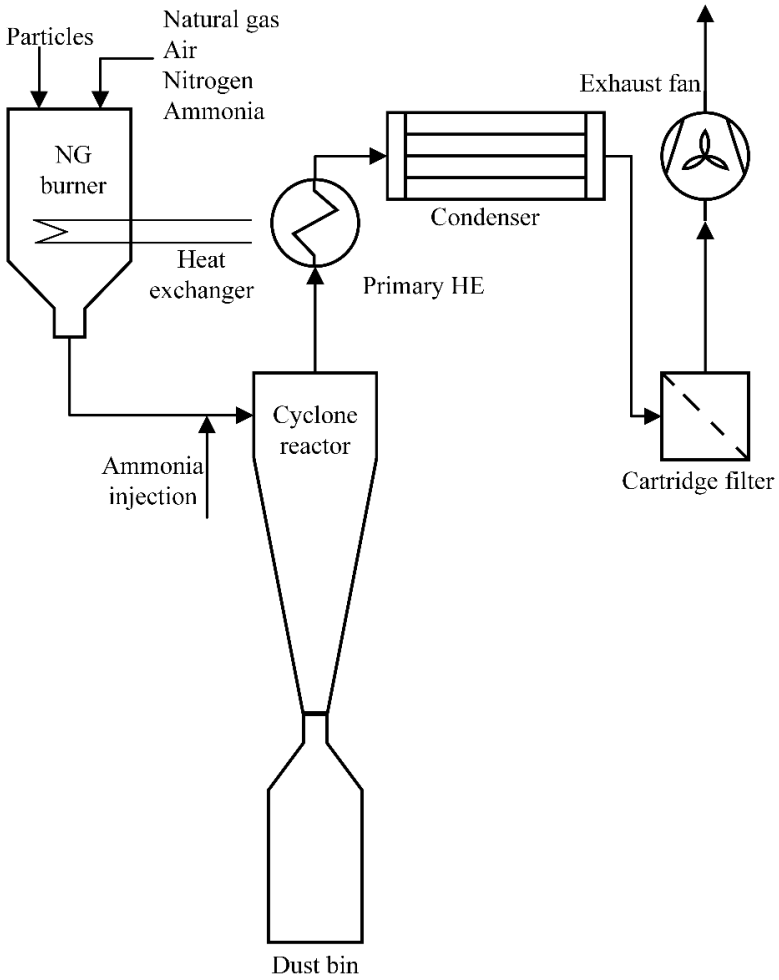

Figure 3.1: Overview of the experimental setup for studying the SNCR process in a cyclone reactor

A picture of the setup the setup is shown in Figure 3.2.

Figure 3.2: Picture of the pilot scale cyclone reactor setup

A more detailed technical overview of the system is given by the PI-diagram given in Figure 3.3, with the individual parts described in detail in the following sections. The part numbers in Figure 3.3 are used in the following sections.

A general feature of the setup is that the interior from the burner to the outlet of the cyclone reactor consists of cast refractory due to the high temperatures present in the system. The refractory consists of the inner most layer of high-density high-temperature resistant cement, surrounded by a low-density insulating refractory, finally encapsulated in the outer steel shell.

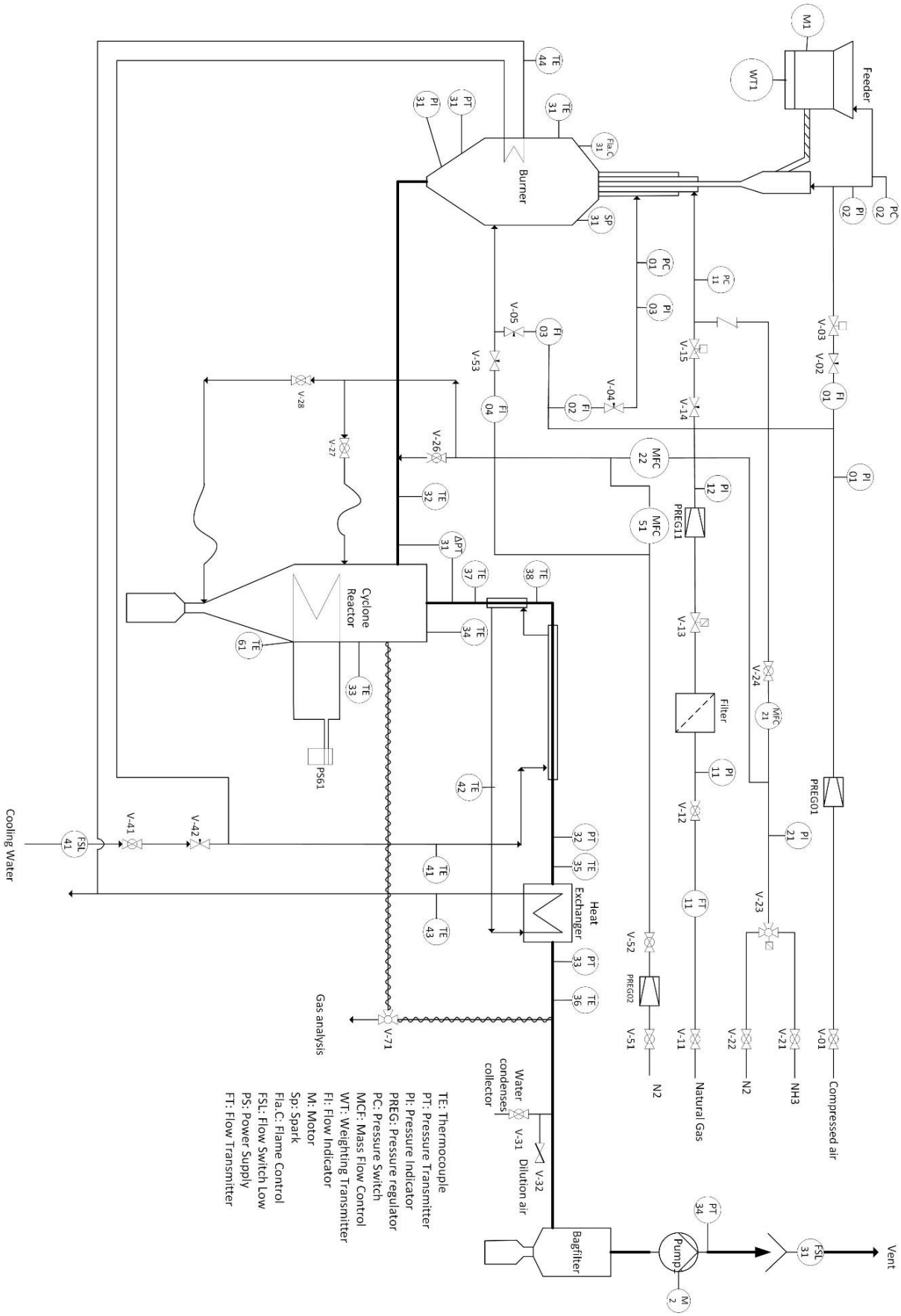

Figure 3.3: P&ID of the cyclone reactor used for the pilot scale experiments

3.1.1.1 Gas burner

The gas burner consists of a fuel and air feeding system, a swirl burner, a combustion chamber, a particle feeding system and control system. An illustration of the combustion chamber and burner is shown in Figure 3.4.

The burner fuel is natural gas, which is fed to the swirl burner, with the flow controlled by a reduction valve V-14 and measured by a flow transmitter, FT11. The natural gas can be doped with pure ammonia gas in order to control the NO_x concentration in the flue gas, as NO_x is generated through the fuel nitrogen mechanism. The ammonia dosing to the fuel line is controlled by a mass flow controller, MFC21. The combustion air is divided into three separate flows, primary, secondary, and tertiary air, with the primary and secondary air being fed to the swirl burner, while the tertiary air is fed to the bottom of the combustion chamber. The tertiary can be diluted with nitrogen, in order to provide further control of the flue gas composition. The flow of primary air, secondary air, tertiary air, and the dilution nitrogen is controlled by separate reduction valves V-02, V-04, V-05, and V-53 and measured with rotameters FI1, FI2, FI3, and FI4 respectively.

The swirl burner, shown on the right in Figure 3.4, has an inner tube for the primary air and an outer annulus with angled swirl vanes for the secondary air in order to create a swirling flow. Between the inner tube and the outer annuls is the fuel annulus for the natural gas. The burner is inserted vertically through the lid of the combustion chamber, while a spark plug, SP31, is inserted at an angle in front of the burner to initiate combustion. Furthermore, an opening through the lid is connected to a small looking glass for an optical flame sensor, Fla.C31, for safety purposes.

The combustion chamber, illustrated on the left in Figure 3.4, is a cylindrical chamber of 610 mm in length and 200 mm in diameter, with a conical bottom section narrowing to 30 mm into the cyclone inlet tube. Beside the openings for the swirl burner, ignition spark, and flame sensor in the lid, the combustion chamber has 5 ports in the side, with 4 of them in use. The second from the top is used for a differential heat exchanger used to control the flue gas temperature, the third for measuring the burner temperature, TE31, the fourth for measuring the burner pressure, PT31, and the bottom port for addition of tertiary air and dilution nitrogen.

The differential heat exchanger used to control the flue gas is a cooling lance, with a constant cooling water flow. The temperature is controlled by moving the lance horizontally in combustion chamber, thereby presenting a smaller or larger surface area for heat transfer from the gas to the cooling water.

The particles is fed to the burner by a screw feeder driven by an electric motor, M1. The particles is fed into the primary air tube, and transported into the center of the swirl burner by gravity and the airflow. The feeding rate of particles is measured by an electronic scale, WT1, which the screw feeder is placed upon.

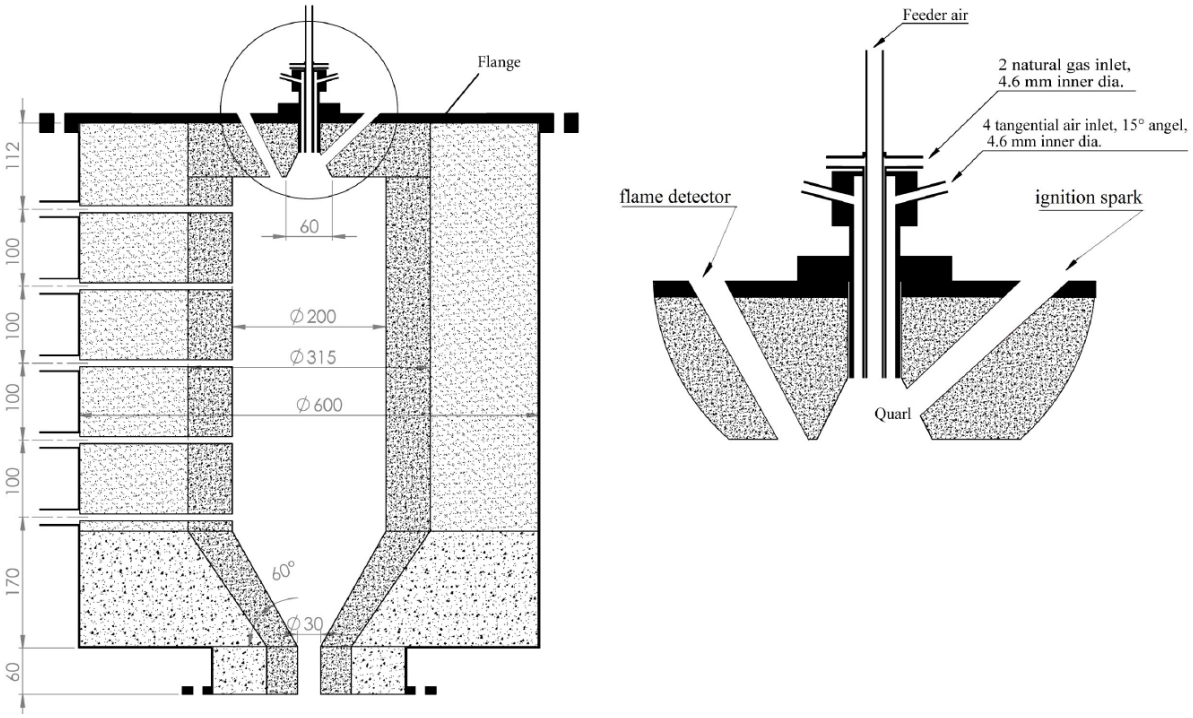

Figure 3.4: Illustration of the gas burner, (left) Full combustion chamber (right) swirl burner assembly (from [142])

3.1.1.2 Cyclone reactor

The inlet pipe, shown on the left in Figure 3.5, consists of a cylindrical elbow pipe with 30 mm in diameter, transitioning from vertical to horizontal. Before the cyclone, the pipe transitions into a rectangular pipe, with a width of 22 mm and a height of 55 mm, acting as a tangential inlet to the cyclone. There are three probe ports in the inlet section, one used for measuring the pressure drop over the cyclone, ΔPT31, one for temperature measurement, TE32, and one for reactant injection and gas sampling. The inlet section from the probe ports to the cyclone inlet with temperature measurement and reagent injection ports, are shown in Figure 3.6 B and C.

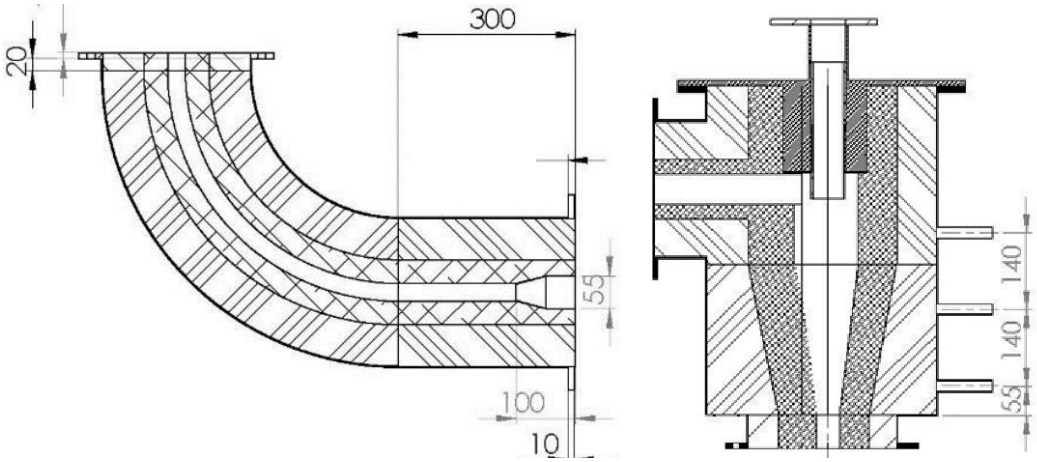

Figure 3.5: sketch of cyclone inlet section and cyclone chamber

The cyclone consists of a cyclone chamber, a dust bin for the solids outlet and a vortex finder as the gas outlet. A sketch of the cyclone is shown on the right of Figure 3.5. The cyclone geometry is a slightly modified Stairmand high efficiency cyclone with a diameter of 110 mm. All the chamber dimensions are shown in Figure 3.6 A, together with an overlaid coordinate

system used for reference in this thesis. An electrical heating jacket is mounted on top of the outer steel jacket of the cyclone assembly in order to reduce the heat loss from gas to the surroundings by lowering the temperature gradient in the cyclone.

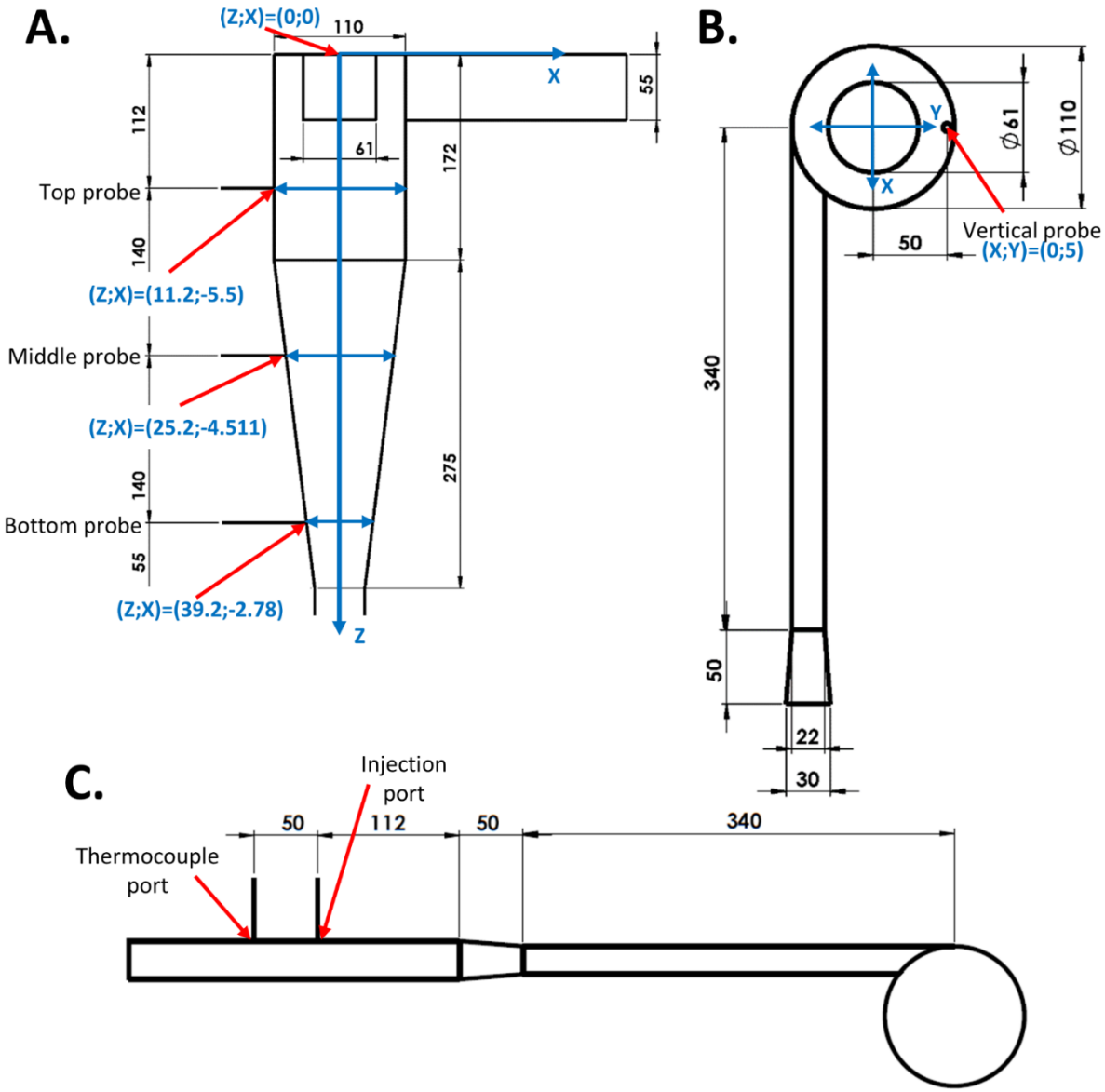

Figure 3.6: The cyclone reactor with detailed dimensions and probe positions: A. Cyclone side view with overlaid coordinates in centimeters; B. Cyclone top view with overlaid coordinates in centimeters; C. Cyclone inlet and injection system. All non-coordinate measurements is in millimeters

A comparison of the dimensional ratios for this cyclone reactor and a standard Stairmand High Efficiency cyclone is given Table 3.1. The main difference between the used setup and the standard design is an increase of the vortex finder diameter, De, and a slight increase in both total and cone length, H and h, respectively.

Table 3.1: Cyclone reactor dimensions and dimension ratios compared to standard Stairmand High Efficiency cyclone

Dimension	D	De	S	H	h	a	b	B
Value [mm]	110	61	55	447	173	55	22	42
Ratio	D/D	De/D	S/D	H/D	h/D	a/D	b/D	B/D
Cyclone reactor	1	0.55	0.50	4.06	1.57	0.50	0.20	0.38
Stairmand HE	1	0.50	0.50	4.00	1.50	0.50	0.20	0.38

The cyclone itself has three horizontal ports, marked in Figure 3.6 A, for temperature, TE33, and composition measurements as well as for ammonia injection in the cyclone. It also has one vertical probe port, marked in Figure 3.6 B, for temperature measurement, TE34.

The pure gaseous ammonia reagent for the SNCR reactions can be added either in the cyclone inlet section through the injection port, marked in Figure 3.6 C, or through any of the horizontal ports, marked in Figure 3.6 A. The ammonia gas flowrate is controlled by a mass flow controller MFC22, and a series of valves, V-26, V-27, and V28 are used to adjust where the ammonia is added. The ammonia is injected through a ceramic alumina tube, with an inner diameter of 4 mm and an outer diameter of 6.1 mm, inserted through the port. In order to improve the mixing at the injection point, nitrogen carrier gas can be added before the injection tube, its flowrate controlled by a separate mass flow controller, MFC51.

The gas exits the cyclone via the vortex finder, an alumna tube with and inner diameter of 56 mm and an outer diameter of 61 mm, inserted through the lid of the cyclone, exiting into a wider steel pipe. Immediately after the vortex finder, a probe port for outlet temperature, TE37, and the second connection for differential pressure, ΔPT31, is placed, followed by the post reactor flue gas treatment system.

3.1.1.3 Flue gas treatment system

Immediately after the cyclone reactor, the flue gas is cooled by a series of heat exchangers. First a quenching heat exchanger reduces the temperature to ~600 °C to stop the SNCR reactions, with the temperature after quenching measured by, TE38. Afterwards the gas is cooled further by two additional heat exchangers, bringing the gas below the dew point, close to ambient temperature, in order to condense most of the water. After the condenser a port for flue gas sampling is placed, used to withdraw flue gas for dry flue gas composition measurements. After cooling, the flue gas is filtered through a cartridge filter before the electrically driven fan, M2, which provides sub-atmospheric pressure in the entire setup from burner to the fan, exhausting into the central vent system. Throughout the flue gas treatment system the temperatures, TE38, TE35, and TE36, as well as the pressures, PT32, PT33, and PT34 is measured to ensure safe operation of the setup.

3.1.1.4 Measurement equipment

This section gives an overview of the measurement equipment used to conduct the various experiments in the cyclone reactor.

Temperature measurements

For temperature measurements, different thermocouples are used throughout the setup, chosen based on the relevant temperature range, and the available port size. Some of the temperature measurements are used to ensure safe operation and for control purposes and are not directly relevant to the experimental results. Hence, only the equipment for temperature measurements relevant to the reporting and interpretation of the experimental results are described here. 5 different types of thermocouples, shown in Figure 3.7, are used to measure the temperature in the cyclone reactor.

Thermocouples a and b are simple type K thermocouples with metal jackets with diameters of 3.1 and 6.1 mm respectively. Thermocouple c is a type S thermocouple with a 8.1 mm diameter ceramic jacket and a partially exposed thermal junction shielded by the ceramic, to protect it from the abrasion of particles in the gas stream. Thermocouple d is a long 3.1 mm S-type thermocouple supported in a 6.5 mm steel tube. The suction probe e have a 1.5 mm diameter type-s thermocouple inserted slightly retracted (8 mm) from the opening, meaning that when gas suction occurs, the suction probe can act as a form of primitive suction pyrometer.

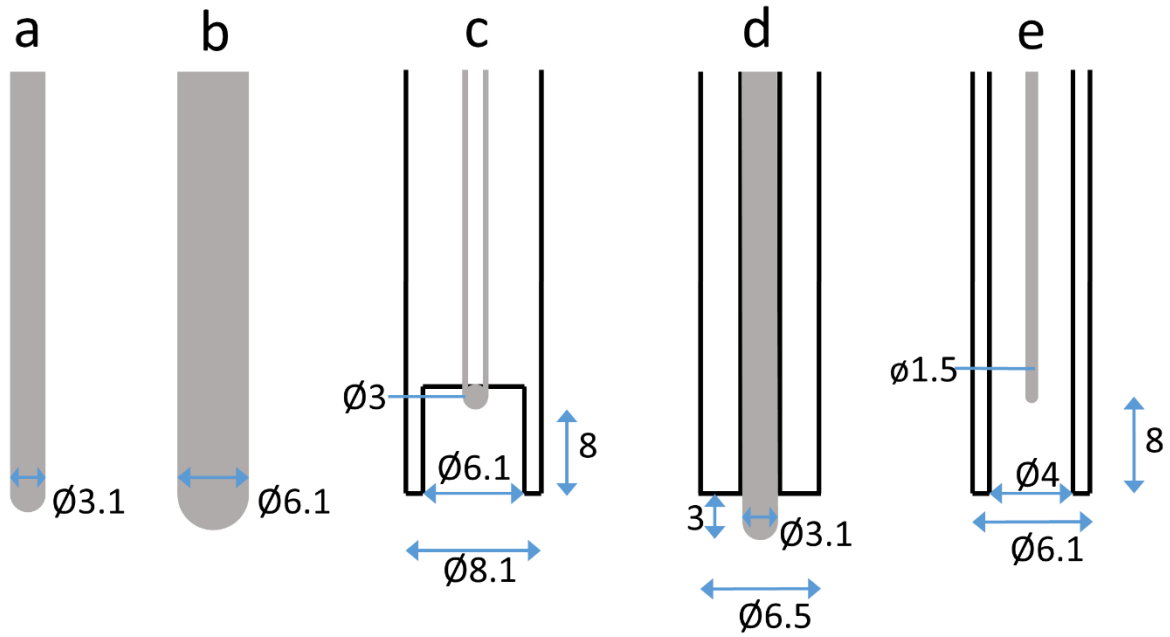

Figure 3.7: Illustration of the active end of the thermocouples and suction probe used for temperature measurements

Gas sampling system

Gas sampling is conducted using three different equipment configurations, two for wet NO, NO_2, and NH_3 analysis and one for dry flue gas analysis of O_2, CO, and CO_2.

For dry flue gas composition measurement, the flue gas sample is drawn from a sample port after the condenser, from where it flows in a pipe heat traced, at 80 °C, through a heat traced ceramic particle filter, and then into a low temperature (4 °C) condensation unit to remove any residual moisture. After the low temperature condensation unit the displacement pump driving the sample flow pumps the gas to the gas analysis equipment.

The gas sampling for wet flue gas analysis is drawn either directly from the probe port in the cyclone outlet pipe or from the gas suction probe described below. From here it goes from the sampling location via Teflon hoses heat traced at 80 °C to avoid condensation, through 2 heat traced ceramic particle filters placed in series, into the wet gas analyzer. After the gas analyzer is the displacement pump driving the flue gas into the exhaust.

The internal concentration profiles in the cyclone chamber are measured using a suction probe consisting of a ceramic alumina tube with an inner and outer diameter of 4 and 6 mm respectively. Alumina ceramic is used to avoid influence from catalytic surface reactions at the elevated temperatures inside the reactor. The gas suction probe is connected to the wet flue gas sampling system described above. A 1.5 mm thermocouple can be inserted into the ceramic suction tube, to form a crude suction pyrometer as shown in Figure 3.7 e.

Gas analyzers

The concentration of major flue gas species is measured by dry gas analysis using a Fisher-Rosemount NGA2000 analyzer measuring CO, CO_2, and O_2 using CLD (chemi-luminescence detector)

The NO_x and ammonia concentrations are measured by wet flue gas analysis using an ABB LIMAS 11 HW analyzer, measuring the NO, NO_2, and NH_3 content by Ultra Violet photometry at elevated temperature (70 °C) to avoid condensation.

3.1.2 Experimental procedures

Five experiment series were carried out in the pilot scale cyclone reactor, denoted as experimental series E1 through E5 from hereon. An experimental matrix summarizing the measurements and experiment type carried out for each experimental series is given Table 3.2.

Table 3.2: Experimental matrix for the different operating conditions

Experiment series	Mean inlet Temperature [°C]	Experiments conducted				
		Temperature profiles	Temperature measurement uncertainty	β influence on SNCR	Internal concentration profiles	Injection influence on SNCR
E1	866.0	X		X		
E2	936.2	X		X		
E3	981.7	X	X	X	X	
E4	1023.1	X		X	X	
E5	975.4	X		X		X

The temperature profiles were measured for all experimental series, in order to characterize the conditions for SNCR reactions. For Experimental series E3, temperature measurement uncertainty was also investigated. The overall SNCR performance dependence on the ammonia injection flowrate was measured in experimental series E1-E4 at different inlet temperatures from lowest E1 to highest E4. While E5 repeats the overall performance measurements at conditions close to E3, while also investigating the SNCR performances influence on mixing by changing the injection conditions, i.e. injection tube position and carrier gas flow.

Furthermore, E3-E4 measures the internal concentration profiles in the cyclone reactor during SNCR.

During each experimental series, the burner conditions were kept constant to ensure steady state operation. Throughout the experiments, the dry flue gas measurements for overall flue gas composition were performed and logged, to verify stable burner operation. The differential heat exchanger was moved in the burner chamber in order to achieve the desired steady state temperature. Once the setup had reached steady state with regards to temperature and flue gas composition, the desired NO concentrations were achieved by adjusting the ammonia dosing to the natural gas line.

3.1.2.1 Temperature measurements

During startup of the setup and during reaction experiments, the temperature was continuously measured in the inlet pipe and cyclone outlet. The inlet pipe temperature is measured using the ceramic shielded thermocouple illustrated in Figure 3.7 c, placed so the thermal junction is 2 mm into the bulk flow, to disturb the flow as little as possible. The outlet temperature was measured using a 3.1 mm diameter metal jacket thermocouple, illustrated in Figure 3.7 a, placed in the center of the outlet pipe.

Temperature profiles

Once steady state operation in the setup was reached, temperature profiles were measured one at a time in the cyclone reactor, both in the inlet tube and inside the cyclone chamber through the probe inlets detailed in Figure 3.6, using the thermocouples illustrated in Figure 3.7. The inlet pipe temperature profiles were measured using thermocouple c, the horizontal temperature profiles in the cyclone chamber were measured using thermocouple b, and the cyclone chamber vertical temperature profiles were measured using thermocouple d.

For each data point the thermocouple was moved to the measurement position. After a waiting for a steady temperature reading, the measurement was continued for at least 2 minutes with continuous data logging to get time averaged values.

Temperature measurement uncertainty

In order to investigate the uncertainty of the temperature measurement, the temperatures in the cyclone reactor setup were measured using different methods for the same temperature profiles.

The inlet temperature profile was measured under similar conditions to E3 and E5, using both thermocouple b and c as well as the suction probe e.

The horizontal temperature profiles in the cyclone reactor were measured for E3 using both thermocouple b as normal as well as the suction probe.

3.1.2.2 SNCR measurements

For the SNCR experiments, the ammonia injection tube was moved to the chosen position in the inlet pipe wall and the nitrogen carrier gas flow was set to the chosen flowrate. Before starting the SNCR process, the NO, NO_2 and NH_3 concentrations were measured without

ammonia injection in both inlet and outlet as background measurements, to confirm that no leaks were present, and to verify that no occurrence of re-burning of NO by any residual CO in the cyclone that would influence the outlet concentration.

The SNCR performance was then measured by increasing the ammonia flowrate to the injection tube stepwise, while measuring the concentration of NO, NO_2 and NH_3 in the cyclone outlet. The ammonia flowrate were held constant at each level until steady concentrations were measured for 5 minutes for data collection and time averaged data.

3.1.2.3 Internal concentration profiles

The internal concentration profiles, during SNCR, were measured for experiment series E3 and E4. The profiles were measured along the x-axis at the 3 horizontal probe ports. This was done using the ceramic suction probe described above. First the suction probe was fitted to a probe port and positioned with the probe end flush to the cyclone wall. For each level of ammonia flowrate, time was allowed for the concentrations in the cyclone to stabilize. Subsequently the suction probe was moved gradually inward in steps, for each position waiting for the measurements to stabilize, after which the position was held for 5 minutes for data collection. After all positions had been measured, the suction probe was moved back flush with the wall, the ammonia flowrate was readjusted and the procedure was repeated.

3.1.3 Experimental conditions

During the five experiment series, all burner settings, except the differential heat exchanger position and the ammonia dosing to the natural gas stream were kept the same. The measured gas flows to the burner and combustion chamber for experiment E1-E5 are shown in Table 3.3 together with the resulting flue gas flowrate and composition based on measurements and stoichiometric calculations.

Table 3.3: Burner operating conditions and the resulting wet gas phase composition and cyclone pressure loss

Condition	[unit]	Series					average±range‡
		E1	E2	E3	E4	E5	
Natural gas flowrate	[Nl/min]	15.4	15.9	14.8	15.1	15.1	15.3±0.6
Air flowrate	[Nl/min]	207	207	207	207	207	207
Nitrogen flowrate	[Nl/min]	40	40	40	40	40	40
Flue gas flowrate	[Nl/min]	255.3	255.6	254.9	255.1	255.1	255.2±0.4
O_2 *	[v%]	3.6	4.0	3.9	3.5	4.0	3.8±0.3
CO_2 *	[v%]	7.0	6.8	7.0	7.2	6.8	7.0±0.2
H_2O †	[v%]	9.9	10.3	9.6	9.8	9.8	9.9±0.4
N_2 *	[v%]	79.7	79.5	79.4	79.5	79.5	79.5±0.4

*calculated from dry gas measurements

†calculated from combustion stoichiometry

‡maximum deviation from average values

For all SNCR measurements the inlet NO concentration was set to 500 ppm. Due to the difference in temperature in the burner chamber the slight differences in combustion behavior required the ammonia dosing to the burner to be changed between experiments to achieve this.

As the gas flowrates were kept constant in all experiment series, the main difference in operating conditions is the inlet temperature. This will result in slightly different flow conditions inside the cyclone, as the inlet velocity is dependent on the volumetric flowrate and thereby the temperature, which also influences viscosity etc. The inlet velocities calculated based on the gas flowrates in Table 3.3 and the resulting pressure drop over the cyclone, measured during experiments are summarized in Table 3.4.

Table 3.4: calculated superficial inlet velocity† and measured cyclone pressure loss for different experimental series

Experimental series	E1	E2	E3	E4	E5
Mean inlet temperature [°C]	866.0	936.2	981.7	1023.1	975.4
Superficial inlet velocity† [m/s]	13.2	14.1	14.6	15.1	14.5
Pressure loss [Pa]	80	90	94	95	89

† calculated based on mean inlet temperature

For experiment series E1-E4, in the general SNCR performance measurements the ammonia injection tube was flush with the inlet pipe wall, while the carrier gas rate was constant at 1.5 Nl/min. For experiment series E5 the ammonia injection tube position was changed between three positions flush with the wall (0 mm), halfway in (15 mm), and all the way in (30 mm). While the carrier gas flowrate was varied between 0, 0.5, 1 and 1.5 Nl/min. Every combination of these settings was used in experiment series E5. The ammonia reagent flowrate in this work is reported as ammonia to NO molar ratio given as the initial ammonia to initial NO ratio $\beta = [\mathrm{NH_3}]_0/[\mathrm{NO}]_0$, as commonly used in literature. To calculate the actual flowrate, eq. 3.1 is used.

$$N_{NH_3} = N_{total} \cdot x_{NO,0} \cdot \beta \qquad \textit{eq. 3.1}$$

Here $\dot{N}_{NH_3}$ and $\dot{N}_{total}$ is the ammonia injection and total flue gas molar flowrates respectively and $x_{NO,0}$, is the inlet mole fraction of NO.

3.2 Results

3.2.1 Temperature profiles

The measured temperature profiles for the five different experimental series, E1-E5, are shown in Figure 3.8. The positions in the reactor and inlet pipe refers to those marked in Figure 3.6.

The inlet pipe temperature profiles for the different experimental series shown in Figure 3.8 D, show a non-uniform temperature distribution, which is to be expected. However, it is not the typical temperature profile expected from flow in a pipe with the highest temperature in the center and a decrease towards the wall, and the overall profile dependent on the degree of turbulence. Instead what can be observed is an increase in temperature moving from the probe inlet towards the opposite wall for all cases, with an increase of around 60 °C from the first to last measurement point. In order to categorize the experiment series by the inlet temperatures,

the mean temperature in the inlet, T_i, is calculated, giving 866 °C, 936.2 °C, 981.7 °C, 1023.1 °C, and 975.4 °C, for E1, E2, E3, E4, and E5 respectively.

Inside the cyclone chamber, the highest temperature for each case is measured in the vertical temperature profile, in Figure 3.8 E, at 5-7 cm below the cyclone roof, with temperatures of 818.7 °C, 870 °C, 925.6 °C, 971.8 °C, and 934 °C, for E1, E2, E3, E4, and E5 respectively. The temperature is not measured exactly at the point where the gas enters the cyclone. Hence, the maximum temperatures mentioned above is the best approximation for the cyclone inlet temperature. Using this gives a temperature reduction from the injection point to the cyclone between 40 and 60 °C. However, the temperature is still above 800 °C for all cases and therefore high enough for SNCR reaction.

From both the difference between the top and bottom horizontal temperature profiles and the vertical temperature profile, shown in Figure 3.8 A, C, and E respectively, large temperature changes of close to 400 °C from top to bottom of the cyclone chamber can be observed for all experimental conditions.

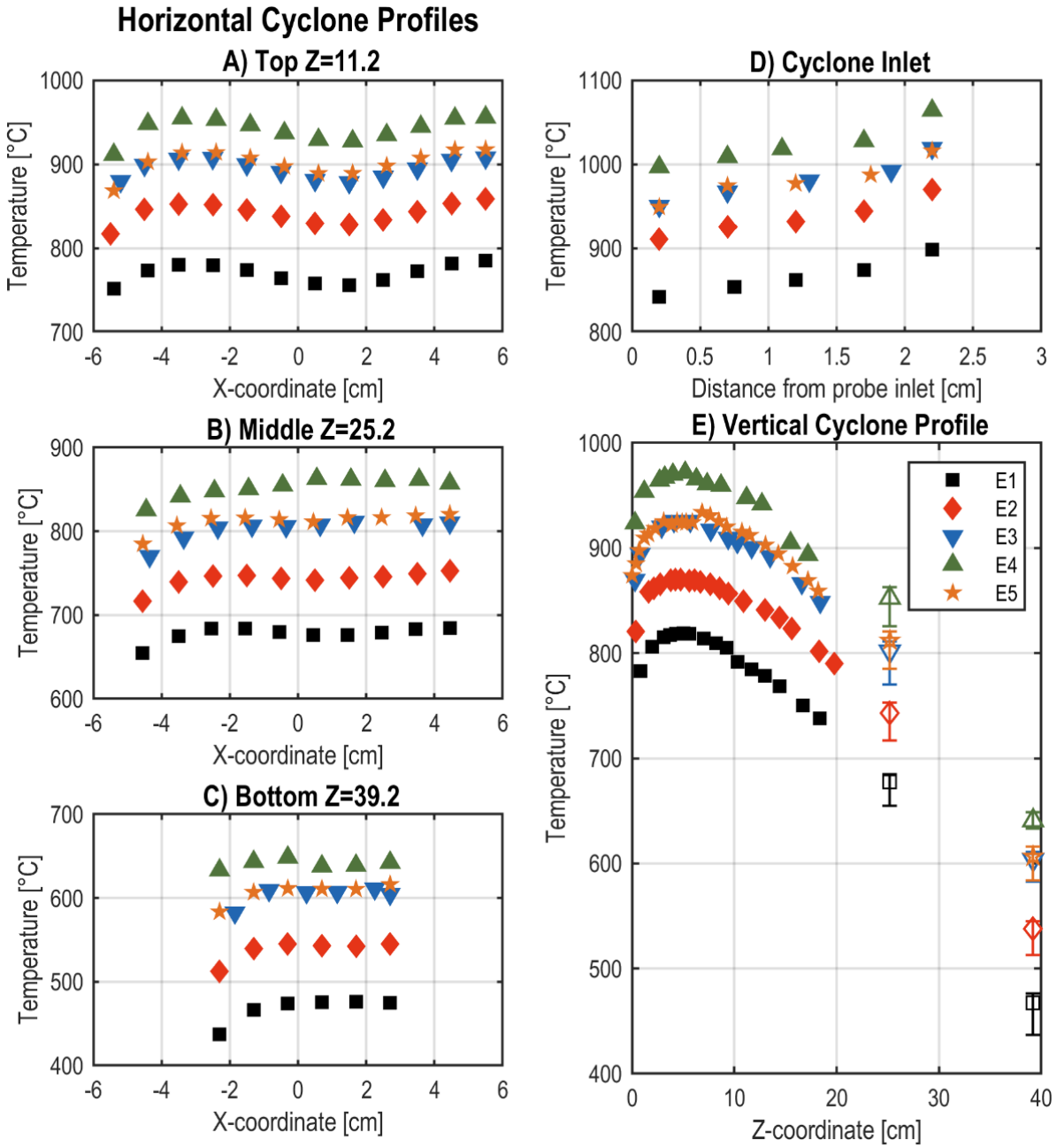

Figure 3.8: Measured temperature profiles for the 5 different experiment series, non-filled marker correspond to horizontal profiles mean values with error bars for the span

The top horizontal temperature profiles, in Figure 3.8 A, shows a distinctly shaped profile with a lower temperature near the center and a higher temperature in the outer region. This is related to the double vortex flow in reverse flow cyclones. However, this is not observed in the bottom horizontal profiles and only slightly in some of the middle horizontal profiles in Figure 3.8 B and C. The distinct shape of the temperature profile in the top is caused by the opposite vertical directions of the inner and outer vortex. As the gas travels down along the outer vortex it cools due to heat loss through the cyclone walls, as the gas enters the inner vortex and "reverse" flows upwards it causes a lower center temperature. The gas in the center at the top is still higher than the temperature measured below this point, ignoring radiation and conduction

through the gas, this can be explained by the gas gradually flowing from the outer to the inner vortex down through the cyclone. Due to this, the gas flowrate, both in terms of mass and volume reaching the lower parts of the cyclone is small compared to the total gas stream in and out of the cyclone. This also explains the low temperatures in the bottom of the cyclone, as the main mode of heat transport in the cyclone is convection. The reason the double vortex profile is not observed in the bottom and only slightly in some cases in the middle is likely also due to a high flow from outer to inner vortex compared to the vertical flow in the conical section and the overall low convective heat transport in the lower cyclone.

For all experiment series, except E1 with the lowest inlet temperature, the temperatures at the top horizontal probe position are above the lower limit (~800 °C) for SNCR reactions. For the middle horizontal probe position, the temperature for E2 is below 800 °C, while the temperatures for E3 and E5 are just above, at around 810-820 °C. While E4 with the highest inlet temperature is still ~850 °C. At the bottom position, the temperatures are too low (<650 °C) in all of the experimental series for SNCR reaction to happen at significant rates. From these temperature profiles and the general behavior of SNCR described in literature, it can be hypothesized that the main reactive zone in the cyclone reactor is in the inlet section and the upper part of the cyclone. While for cases E3-E5 the reactive zone extends down through most of the cyclone chamber although only low rates would be expected in the bottom.

An overall trend for all the measured temperature profiles is that the measured temperature is higher towards the opposite wall, as compared to close to the probe inlet. It is clear from the inlet temperature as described above, but it can also be seen in the horizontal temperature profiles where the first 1 or 2 data points deviates from the general trend. Furthermore, the temperatures measure in the very top of the cyclone have a very high gradient compared to the rest of the profile. This might be caused by measurement error due to thermal radiation and/or heat conduction through the probe. Generally the higher the immersion length of a thermocouple, the lower expected error is [143]. The uncertainty of the temperature measurement has been investigated by using different thermocouples and a suction probe to measure the temperature profiles, the results are shown in Figure 3.9 and Figure 3.10.

For the inlet pipe temperature profiles in Figure 3.9 the measurement results vary widely between thermocouple B and thermocouple C, over the entire range, while the suction probe show somewhat agreement with thermocouple C from the probe inlet until around the middle although with a slightly lower overall temperature. Thermocouple C and the suction probe measurements then diverges after approximately in the center, as the thermocouple C measurements increases sharply, while the suction probe measurements continues its relative flat profile. Thermocouple B and the suction pyrometer meet at the same maximum temperature at the wall opposite of the inlet where the influence of radiation to the colder environment (inside the probe port) is the smallest. The difference in the highest temperature between thermocouple C and both the suction probe and thermocouple B is ~25 °C.

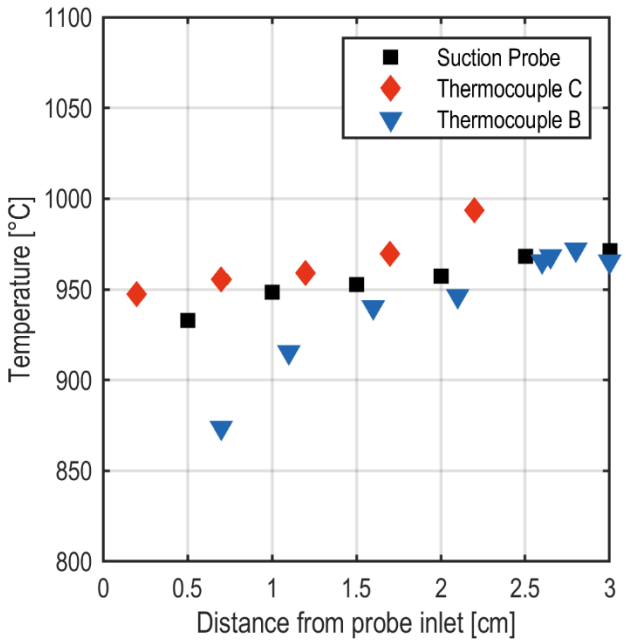

Figure 3.9: Comparison of inlet pipe temperature measurement with 2 different thermocouples and a suction probe

For the horizontal cyclone temperature profiles shown in Figure 3.10 the trends for the temperature measurement at all port positions are the same with the 2 measurement methods. Furthermore, the deviation between the methods very low, with the exception of the right side of the top horizontal temperature profile. On the right side the maximum measured temperature is 20 °C higher with the suction probe.

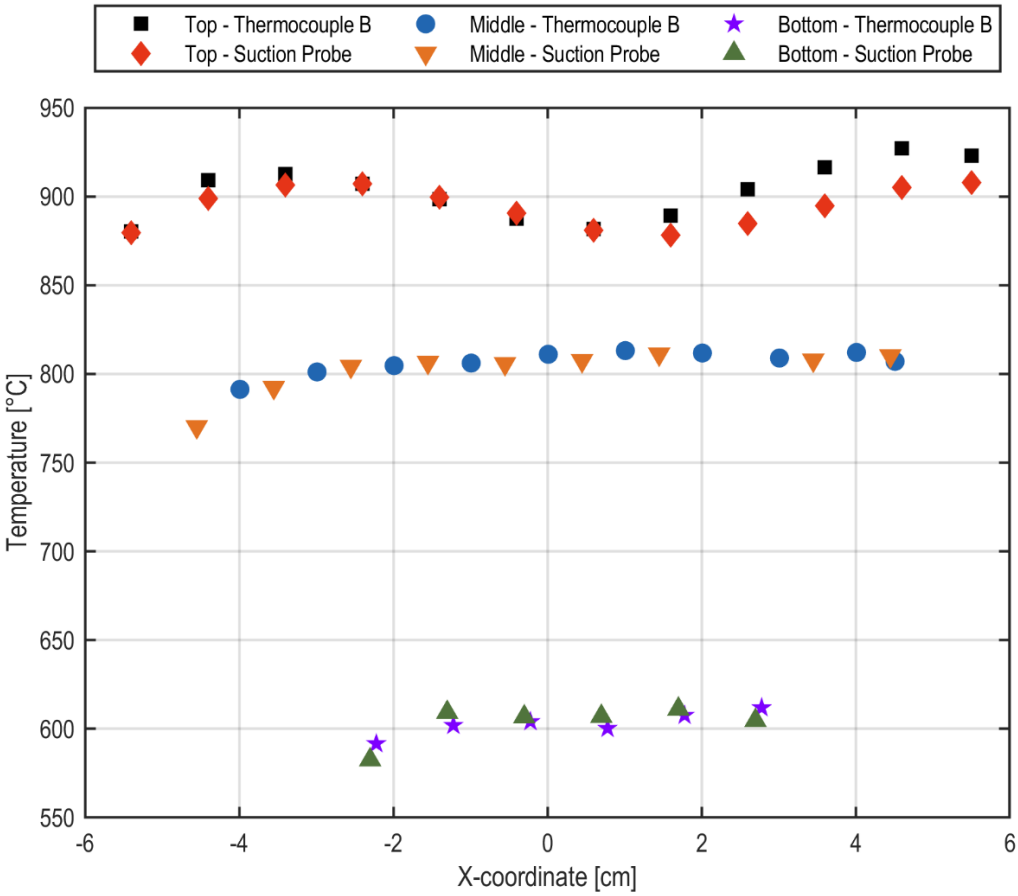

Figure 3.10: Comparison of horizontal temperature profile measurements in the cyclone chamber with a thermocouple and a suction probe for experimental case E3

3.2.2 SNCR experiments

The results for the different SNCR experiments and discussed in the following subsections.

3.2.2.1 Effect of stoichiometry

The experimental results for the overall SNCR performance in the cyclone reactor for the 5 different experimental series are shown in Figure 3.11 as the outlet NO and NH_3 concentrations dependency amount of ammonia injected, denoted by the stoichiometric ratio, β.

The overall behavior observed form the results match with what would be expected based on the established understanding of SNCR. The highest reduction of NO is achieved for the experimental series with inlet temperatures in the middle of the temperature range of 936-982 °C, i.e. E2, E3, and E5. While the lowest reduction is achieved for the low temperature conditions E1 due to low reaction rates, as seen from the high NH_3 slip, and for the highest temperature conditions E4 because of the low selectivity towards NO reduction. The highest NO reduction for a specific stoichiometric ratio is, achieved for E2, but comes at the cost of a high ammonia slip when β exceeds 1. At $\beta = 1.6$ an NO reduction of 77% can be achieved, but with an ammonia slip of 105 ppm. Although E3 and E5 have similar temperature conditions in the inlet (Figure 3.8 d), both the reduction in NO and the ammonia slip are slightly lower for E5, even with a slightly lower mean temperature. This is possibly due to slightly higher overall temperatures (10-20 °C) inside the cyclone. For these conditions 60-69 % reduction of NO is

achieved at a stoichiometric ratio of $\beta = 1.6$ with little to no ammonia slip (4 ppm for E3 and 0 ppm for E5). For series E4 with the highest inlet temperature, injection ratios of up to $\beta = 5.5$ can be utilized without ammonia slip, due to the high reaction rates and low selectivity at this stoichiometric ratio 79 % NO reduction is achieved.

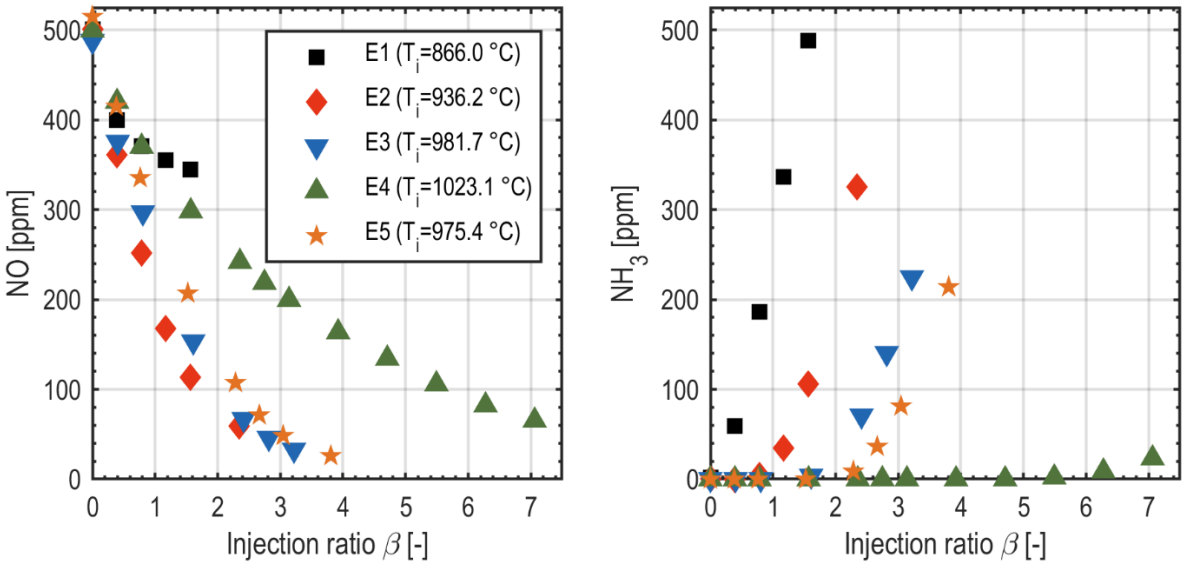

Figure 3.11 Measured outlet concentrations of NO and NH3 for SNCR in a cyclone reactor for the 5 different experimental series described in Table 3.2. With ammonia injection tube flush with inlet wall and 1.5 Nl/min N2 carrier gas.

3.2.2.2 Effect of temperature

In order to more clearly show the effect of temperature on the SNCR process, the NO and NH_3 outlet concentrations for series E1-E4 are plotted as a function of the inlet temperature for different injection ratios in Figure 3.12.

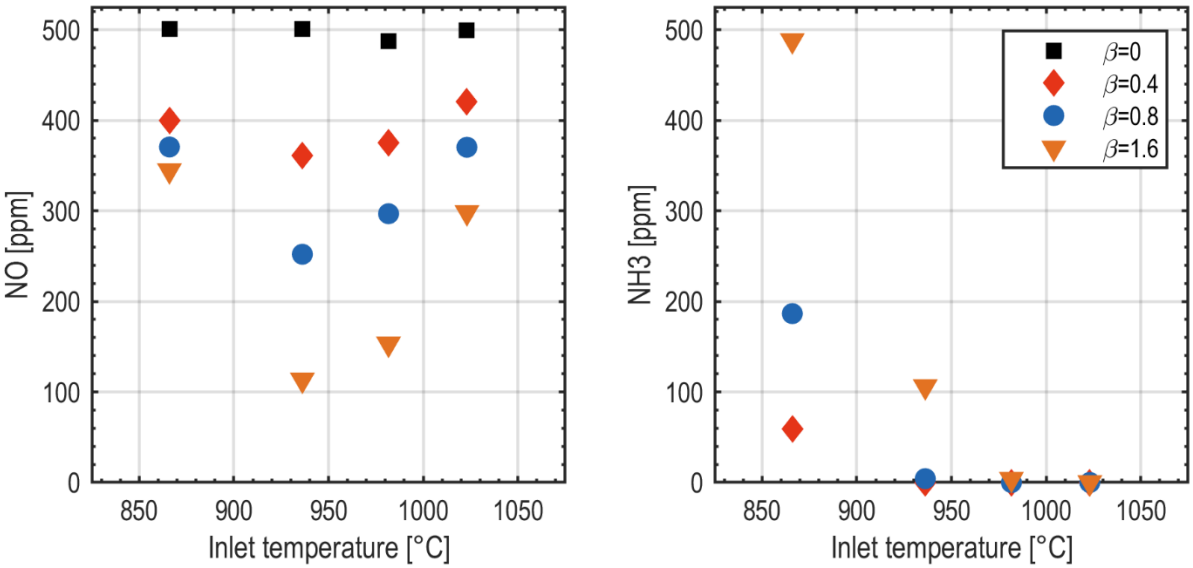

Figure 3.12 Measured outlet concentrations of NO and NH_3, dependence on inlet temperature for SNCR in a cyclone reactor for different stoichiometric ratios, β. With ammonia injection tube flush with inlet wall and 1.5 Nl/min N_2 carrier gas.

Figure 3.12 gives a clearer picture of the inlet temperatures effect on the SNCR process, showing the temperature window with an optimum at around 940 °C but with significant ammonia slip. The optimal operation conditions would seem to be those of E3 with an inlet temperature of ~980°C with $\beta = 1.6$ where the NO concentration can be reduced by 69 % to

153 ppm with only a negligible ammonia slip 4 ppm. Increasing the temperature further will result in lower NO reduction and decreasing it would increase the ammonia slip. These result fit well with various literature results with similar oxygen content. Which shows optimal temperatures to be 950-970, with NO reductions of 60-95 % depending on residence time, stoichiometric ratio, and scale of reactor [96].

3.2.2.3 Effect of mixing

The effect of mixing on the overall SNCR performance of the cyclone reactor was measured during experiment series E5, by changing injection conditions for the ammonia reagent, the results from this are shown in Figure 3.13. By changing the flowrate of the carrier gas, the total gas flowrate of the injected gas jet is changed, thereby changing the inertia and turbulence of the jet carrying the ammonia, while moving the injection tube changes where the jet is mixed into the bulk gas and the extent of disturbance of the injection tube to the bulk flow. Furthermore, increasing the carrier gas flowrate increases the amount of cold gas that needs to be mixed with and heated by the bulk gas flow.

The large influence of the injection conditions, and thereby the mixing, on the overall performance of the SNCR is evident from Figure 3.13. For all injection tube positions, an increase in NO reduction occurs when increasing the flow rate of the carrier gas, while the ammonia slip is also increased. This is in agreement with the behavior observed by Østberg et al. [133,141]. However, the influence on ammonia slip in their experiments was much less pronounced [133]. This behavior might be explained either by an improved mixing of the ammonia with the bulk gas, a cooling effect by the cold carrier gas or a combination of both. A higher inertia of the injected gas improves the mixing with the bulk flow [133], thereby leading to a more uniform distribution of ammonia in the flow. This would lead to locally lower reaction rates, but simultaneously favor the NO reduction pathway and increase selectivity. While a higher injection flowrate also leads to local cooling of the gas. Thereby the reaction is initially happening in a "colder" volume, favoring higher selectivity and lower reaction rates.

The position of the injection tube, seems to have a larger influence on the SNCR performance than the carrier gas flowrate. The farther into the bulk flow the injection tube is inserted, the lower the NO conversion and the ammonia slip are. This can also be explained by either a mixing effect or from the influence of the local reaction temperature. The lower NO conversion at higher insertion length can be explained by worse mixing, as the ammonia "jet" will only penetrate into the bulk flow in the part in front of the injection tube. Both the lower NO conversion and lower ammonia slip might be related to either higher local temperature towards the wall opposite of the probe inlet as seen in the measurements in Figure 3.8 d or some degree of preheating of the injected ammonia. As insertion of the injection tube will give a heat transfer surface from the bulk flow to the injected gas inside the tube. Thus the exit temperature of the injected gas will therefore be proportional to both insertion length and carrier gas flowrate. Hence, further insertion and reduced carrier gas flow leads to higher temperature in the local reaction volume increasing reaction rates and reducing selectivity. Interestingly at the worst mixing conditions, insertion length 1.5 and 3 cm and no carrier gas, the NO reduction is first

increased when increasing the ammonia dosing, after which it decreases to a point with close to no reduction, and finally at sufficiently high ammonia flowrate the NO reduction is increased again. What exactly causes this behavior is difficult to conclude without further investigation. One explanation for the decrease at sufficiently high injection ratio might be that the ammonia flowrate is reaching a level where it start improving the mixing due to higher momentum.

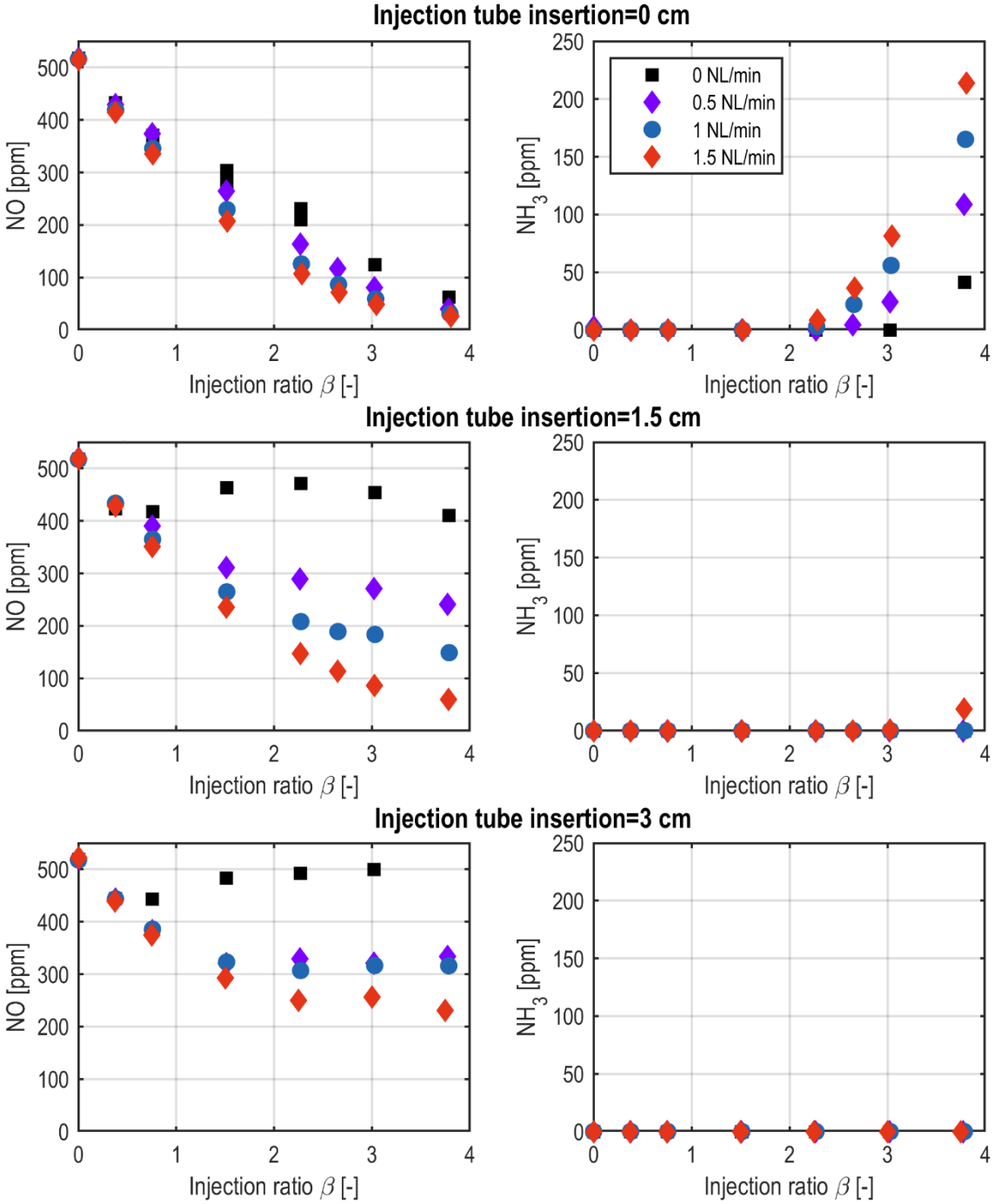

Figure 3.13: Measured outlet concentration for overall cyclone reactor SNCR efficiency dependency on injection conditions; carrier gas flowrate and injection tube position

3.2.2.4 Internal concentration profiles

The horizontal concentration profiles for NO and NH_3 inside the cyclone were measured during SNCR for experiment series E3 and E4, because these had sufficient temperature for SNCR

reactions in most of the cyclone as seen in Figure 3.8. The results for the concentration profiles are shown in Figure 3.14 and Figure 3.15, for E3 and E4 respectively.

For experiment series E3 (Figure 3.14) no ammonia is measured in the cyclone chamber before the injection ratio reach β =1.6, where a small amount of ammonia (6 ppm) is measured in the outer vortex at the top horizontal probe position. This is the same stoichiometric ratio at which 4 ppm ammonia is measured in the outlet. This shows that the main reaction zone is the inlet tube and the top of the cyclone, above the probe port, as was suggested from the temperature profiles. Above this point the majority of the conversion has already occurred and no further reaction occurs below as no ammonia is detected in middle and bottom probe port for this stoichiometric ratio.

For $\beta = 2.41$ and β =2.82, ammonia conversion occurs down through the cyclone chamber from 60 and 110 ppm in the outer vortex in the top to 0 and 20 ppm in the bottom respectively. While there is only a small NO reduction in the same path from 110 and 86 ppm NO in the outer vortex in the top to 96 and 66 ppm in the cyclone bottom. This shows that the conversion of NO mainly occurs in the inlet and in the upper part of the cyclone (cylindrical part), where temperatures are around 900 °C and above, with only slight conversion in the lower parts of the cyclone. Ammonia is converted through the whole volume of the cyclone even below the middle probe port, under which the temperature is below 800 °C, and therefore below the normal temperature window. This might be caused by the fact that a large part of the gas stream bypass this region, which leads to a long gas residence times in the bottom part. The high conversion of ammonia seen in the lower part of the cyclone without significant NO conversion is contrary with existing understanding of the SNCR process, where high selectivity towards NO reduction is expected at low temperatures.

For injection ratios β =2.41 and 2.82 the double vortex profile is easily distinguishable in the top horizontal NH_3 concentration profile, while only slightly noticeable for the NO measurements, with a slight drop in the center. Similar double vortex profile is not observed at the middle and bottom probe port. The distinct shape of the concentration profile in the top is caused by the double vortex flow in the same way as for the temperature profiles. High NO and NH_3 concentrations being transported downward in the outer vortex, while low concentration from below is transported upwards in the inner vortex, with reaction happening along the way in both the outer and inner vortex, instead of the heat loss primarily being from the outer vortex to the cyclone wall. The reason this type of shape is not observed for the profiles at the middle and bottom probe port, even with lower NH_3 concentration in the bottom is likely again due to the horizontal “inward” flow from outer to inner vortex being dominant over the vertical flow in the conical section.

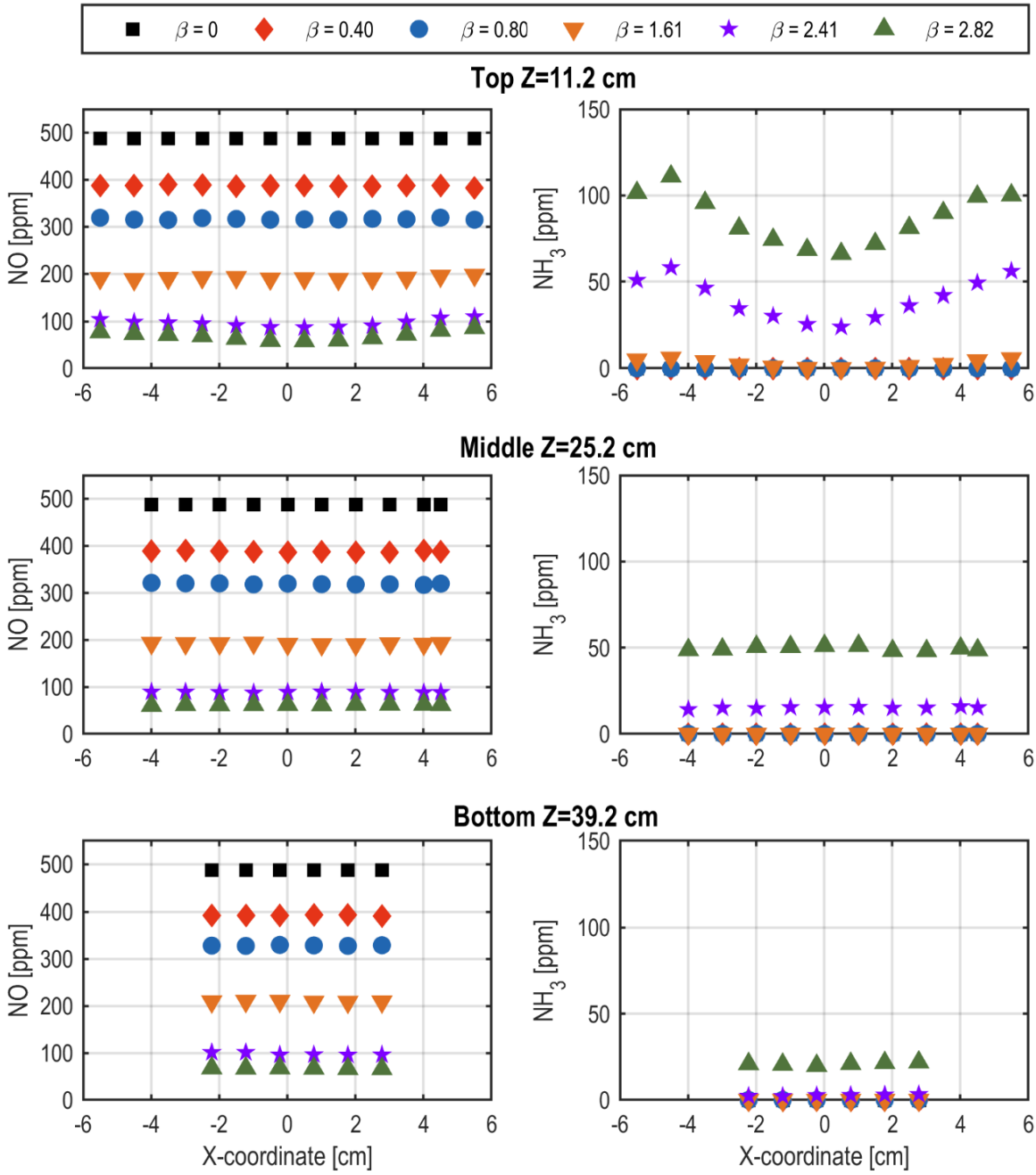

Figure 3.14: Measured profiles for the normalized NO concentration and the ammonia concentration inside the cyclone reactor during SNCR experiment E3

The concentration profile measurements for experiment series E4, in Figure 3.15, shows that there is only presence of ammonia at the top horizontal probe port position of the cyclone at a very high feed ratio of $\beta = 6.3$. Here ammonia is mainly found in the outer region corresponding to the downward flowing outer vortex. While no ammonia is present in the center, or at the middle and bottom probe port. This further confirms the observations that the main reaction zone is the inlet section and the upper cyclone, even with the higher temperatures in E4, due to the majority of the ammonia already being converted above the upper horizontal probe port. Due to the lack of ammonia in the cyclone chamber, no change in the NO concentrations between the top and middle probe port is observed.

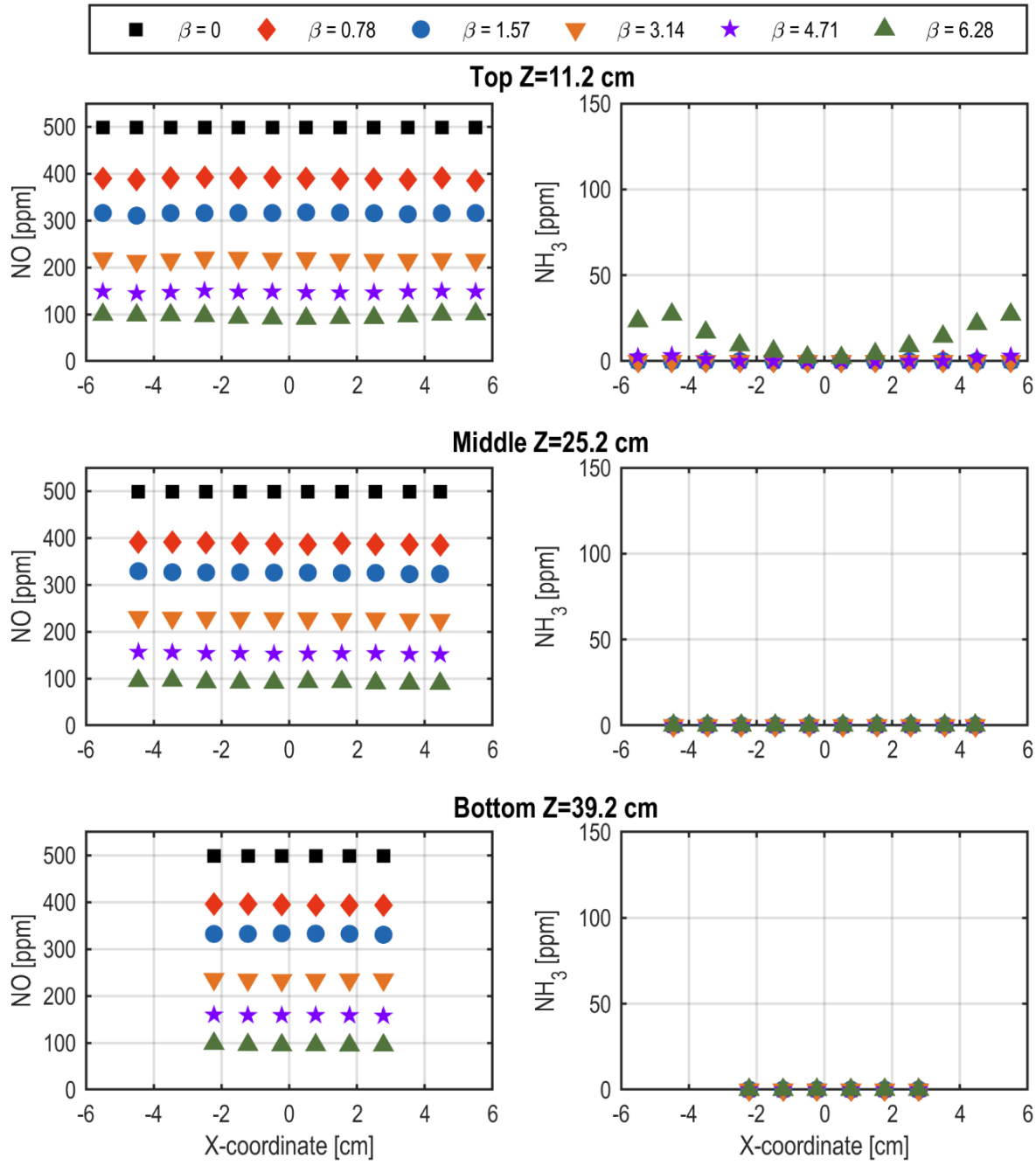

Figure 3.15: Measured profiles for the normalized NO concentration and the ammonia concentration inside the cyclone reactor during SNCR experiment E4

Overall from the internal concentration profiles measured for experiment series E3 and E4, the change in NO concentration between the top horizontal measurement point and the bottom is small or negligible, and thus the inlet section and the top part of the reactor volume contributes to the main part of the NO reduction. However, the ammonia concentration is reduced significantly from top to bottom in all the cases where ammonia is present inside the cyclone. This suggests that the lower part of the cyclone reactor mainly contributes to further reduction of the ammonia slip. However, without knowing the extent of mass transfer between the different parts of the cyclone the exact extent of the contribution of the lower parts of the cyclone reactor to the cyclone reactors total conversion is unknown.

The NO and NH_3 concentrations of the inner and outer vortex at the top horizontal probe position are compared with the outlet for the injection ratios, β, 2.41 and 2.82 in Table 3.5. Here the outer and inner vortex concentration is taken as the maximum and minimum values in the measured profiles respectively.

Table 3.5: NO and NH_3 concentrations measured in the upper part and the outlet of cyclone reactor during SNCR for experiment series E3

Injection ratio β	2.41		2.82	
Specie	NO [ppm]	NH_3 [ppm]	NO [ppm]	NH_3 [ppm]
Outer vortex†	110	58	86	111
Inner vortex‡	87	24	58	66
Outlet	67	70	46	140

† taken as the highest concentration measured at the top horizontal probe position

‡ taken as the lowest concentration measured at the top horizontal probe position

The higher concentration of ammonia in the outlet than both the inner and outer vortex suggest that a high fraction of the flue gas has entered the inner vortex before the top probe position, thereby bypassing most of the cyclone reactor volume. This bypass is a common cyclone phenomena called lip leakage. The outlet NO concentration is lower than both the inner and outer vortex concentrations showing that a significant NO reduction occurs in the upper part of the inner vortex and/or inside the vortex finder.

3.3 Conclusions

Five different experimental series have been conducted in a pilot scale cyclone reactor to study the effect of inlet temperature and ammonia injection conditions on SNCR performance and the internal profiles of temperatures and concentrations. The overall performance of SNCR and the temperature profiles in the cyclone reactor have been measured for a range of operating conditions, with inlet temperature between 866 and 1023 °C, inlet NO concentration of 500 ppm, and NH_3/NO feed ratios of up to $\beta = 7$, and various ammonia injection conditions. The concentration profiles inside the cyclone during SNCR have been measured using a suction probe for inlet temperatures of 982 and 1023 °C.

The measured temperature profiles showed large temperature drops of close to 400 °C from the top to the bottom of the cyclone, meaning that the main reaction zone is in the inlet section and top part of the cyclone chamber, while increasing inlet temperatures extents the reaction zone further down the cyclone. The horizontal temperature profiles in the top showed a distinct profile related to the double vortex flow structure in reverse flow structure, while this was not observed in the lower horizontal profiles.

Overall, the NO_x reduction was highest for an inlet temperature of 932 °C, but with a signicant ammonia slip. The most optimal conditions were an inlet temperature of 982 °C and injection ratio $\beta \approx 1.6$, with slightly lower NO reduction at 69 %, but with an ammonia slip of 4 ppmv.

The experiments with varying ammonia injection conditions, showed that an increase in carrier gas, which improves the mixing, leads to increased NO reduction but higher ammonia slip, while further insertion of the injection probe into the bulk flow showed the reverse behavior suggesting worse mixing with further insertion. This behavior with better mixing improving the NO reduction fits with literature results [133,141], while the effect on ammonia slip has only been seen to a smaller extent in literature [133].

The concentration profiles measured inside the cyclone reactor confirmed that the main reaction zone were in the inlet pipe and the upper part of the cyclone chamber. However, despite the low temperatures in lower parts of the cyclone, a significant conversion of ammonia occurred in this region. Due to this, the double vortex flow structure typical of a reverse flow cyclone could be observed clearly from the ammonia concentration profiles, in the top of the cyclone. Based on the concentrations measured in the outer and inner vortex and in the outlet it can be concluded that a significant fraction of the total gas flow bypass most of the volume of the cyclone, due to the phenomena lip leakage.

Chapter 4 – Pilot scale modelling

This chapter describes the modeling work conducted to test and develop models for gas phase reaction and in particular SNCR reactions in cyclone reactors.

4.1 Modelling methods

In order to model reactions in a flow systems both a reactor model and a kinetic model are needed. The reactor describes the flow pattern and mixing behavior, while the kinetic model describes chemical reactions. The most detailed ways to describe these phenomena is CFD, for the flow, mixing, and heat transfer in the reactor and detailed kinetics for the reactions. Despite advances in processing power and CFD methods, modelling flow and heat transfer in cyclones with CFD is already highly computationally demanding. Thus combining a full cyclone CFD model with a detailed chemical kinetic model for SNCR (with more than 100 separate species and 1000 different reactions) is still impractical due to the high computational cost. Others have worked with simplified and reduced kinetics in cyclone CFD models [123].

In this work simplified reactor network models combined with both detailed and simple kinetics are used to model the cyclone SNCR process.

Through the different models and reactor sections gas properties and the resulting residence times are calculated.

The residence times are calculated based on the volumetric gas flowrate at the chosen temperature as shown in eq. 4.1

$$\tau_k = \frac{V_k}{\dot{V}(T_k)} \qquad \textit{eq. 4.1}$$

Where V_k is the volume of the specific section, $\dot{V}(T_k)$ is the volumetric gas flowrate at temperature T_k, and subscript *k* denotes the section/volume described. The volumetric flowrate is calculated based on the overall molar flow rate, $\dot{N}$, and the molar volume, V_m, of the gas by eq. 4.1.

$$\dot{V}(T_k) = V_m(T_k) \cdot \dot{N} \qquad \textit{eq. 4.2}$$

Since the reacting components of the gas make up only a miniscule amount of the total flue gas flow the total molar flow rate is approximated as constant. The molar volume is calculated using the thermodynamics correlations in the kinetic scheme in Glarborg et al. [97]

4.1.1 Reactor models

In order to test the influence of the used reactor model and to find the best available model, different reactor models are used. Four different reactor models are used to model the cyclone reactor. Three different methods from literature are used, this includes the simplest ideal reactor models CSTR (continuously stirred tank reactor[2]) and PFR, as used by Leckner et al. [3] to model cyclone SNCR, and the reactor network model proposed by Lede et al. [111], described

[2] CSTR is also known as PSR (perfectly stirred reactor)

in Chapter 2, to model gas phase reaction in cyclone reactors. Finally a cyclone compartment model developed in this work is used.

For calculating the residence times in the different parts of the models, the volumes of the inlet section and the cyclone chamber is 501.3 cm^3 and 2965.3 cm^3.

4.1.1.1 Preexisting models

Inlet section

The inlet section between the ammonia injection point and the cyclone chamber is modelled as a PFR in all the reactor models. The temperature profile is assumed to be linear with time, between the mean temperature from the measured inlet pipe temperature profile and the maximum temperature measured inside the cyclone chamber. The residence time in the inlet section is calculated based the mean temperature between these. The conditions for modeling the inlet section for the 5 experimental series is summarized in Table 4.1.

Table 4.1: Reactor conditions for modeling the inlet section

Experiment series	T_{inlet} $[°C]$	$T_{cyclone}$ $[°C]$	$T_{inlet,mean}$	τ_{inlet} $[s]$
E1	866.0	818.7	842.4	0.0319
E2	936.2	870	903.1	0.0303
E3	981.7	925.6	953.6	0.0290
E4	1023.1	971.8	997.5	0.0280

In order to model conditions between these points and outside the range, linear correlations for the cyclone temperature and inlet residence time, given in eq. 4.3 and eq. 4.4 respectively, are used. The linear correlation fits can be found in Appendix.

$$T_{cyclone} = 1.0005 \cdot T_{inlet} - 52.939\ °C \qquad \textit{eq. 4.3}$$

$$\tau_{inlet} = -2.52 \cdot 10^{-5} \frac{s}{°C} \cdot T_{inlet,mean} + 5.305 \cdot 10^{-2} s \qquad \textit{eq. 4.4}$$

Cyclone chamber

The cyclone chamber is modelled using the three different preexisting reactor models.

The two simple ideal reactor models, CSTR and PFR, and the Lede model are modelled using a constant temperature equal to the highest measured temperature in the cyclone. For the CSTR and PFR model the residence time in the cyclone is calculated from the cyclone volume and chosen reactor temperature, the calculated residence times from this for each experimental series is summarized in Table 4.2.

For the Lede model separate residence times for the PFR volume and CSTR volume must be calculated based on volume fraction of each part and the bypass fraction of the gas, using eq. 4.5 and eq. 4.6. Using $\beta_{lede} = 0.42$, the residence time can be calculated as:

$$\tau_{pfr,lede} = \beta_{lede} \cdot \tau_{cyclone} \quad \textit{eq. 4.5}$$

$$\tau_{cstr,lede} = \frac{(1-\beta_{lede})}{\alpha_{lede}} \cdot \tau_{cyclone} \quad \textit{eq. 4.6}$$

The inlet Reynolds number, Re_0, is calculated based on the cyclone temperature. The Reynolds numbers, bypass fractions and the resulting residence times are summarized in Table 4.2.

Table 4.2: Reactor conditions for modeling the cyclone chamber using ideal reactors and the lede model

Experiment series	$T_{Cyclone}$ [°C]	$\tau_{cyclone}$ [s]	Re_0	α_{lede}	$\tau_{pfr,lede}$	$\tau_{CSTR,lede}$
E1	818.7	0.1927	4295	0.549	0.08093	0.2034
E2	870	0.1840	4169	0.558	0.07730	0.1915
E3	925.6	0.1755	4043	0.566	0.07371	0.1798
E4	971.8	0.1690	3944	0.573	0.07098	0.1710

To model conditions between these points and outside the range, a linear correlation for the cyclone residence time, given in eq. 4.7, is used. The linear correlation fit can be found in Appendix A.

$$\tau_{inlet} = -1.552 \cdot 10^{-4} \frac{s}{°C} \cdot T_{inlet,mean} + 0.3194\ s \quad \textit{eq. 4.7}$$

4.1.1.2 Cyclone compartment model

A compartment model has been developed in an effort to model the internal concentration profiles and account for the temperature profiles observed inside the cyclone reactor measured in the experimental work of this thesis.

The cyclone reactor is divided into 2 main parts; the inlet section and the cyclone chamber section. The inlet section corresponds to the volume from the ammonia injection point to where the pipe meets the cyclone chamber. The cyclone chamber denotes the full volume of the cyclone chamber from the inlet to where the conical section ends in the dust exit.

The inlet and outlet section are both modelled as a PFR, with the inlet using the same conditions as in the remainder of the models as summarized in Table 4.1.

The cyclone chamber section is divided into compartments based on the geometry of the cyclone and a simplified representation of the typical flow structure in a cyclone, as illustrated on the left in Figure 4.1. The double vortex flow structure with a downward flowing outer vortex and a upward flowing inner vortex is approximated by dividing the cyclone along a vertical partition extending from the vortex finder. Furthermore, a gradual flow from the outer vortex into the inner vortex down through the cyclone is known to occur [6,11]. Hence, the cyclone chamber is further divided horizontally into reactor compartments at intervals down through the height of the cyclone, allowed fraction of the gas from the outer compartment to flow into the inner compartments. Based on the cyclone flow field reported in literature [6,11]

and the residence time measurements from Lede [111] it is established that a large part of the gas can bypass most of the cyclone chamber directly at the lower edge of the vortex finder due to lip leakage. Thus the first horizontal partitions is placed just below the lip of the vortex finder. The next is placed where the cyclone chamber goes from cylindrical to conical. And the final partition is placed near the bottom of the conical section where the vortex reverse. The compartments are divided in such a way that the measuring points in the experimental setup corresponds to; C2 and C6 for the top horizontal profile, C3 and C5 for the middle horizontal profile, and C4 for the bottom horizontal profile. All the compartments in the cyclone chamber are modelled as CSTRs while the inlet and the outlet zones are modeled as PFRs as illustrated in Figure 4.1 on the right. The bypass fractions for each of the outer compartments, α_i, accounts for the flow of gas from the inner to the outer vortex in the interface between the corresponding compartments. These can be fitted either to the experimental data, or in the case of predictive modeling to either the residence time distributions from the Lede model, or CFD modeling of the flow field.

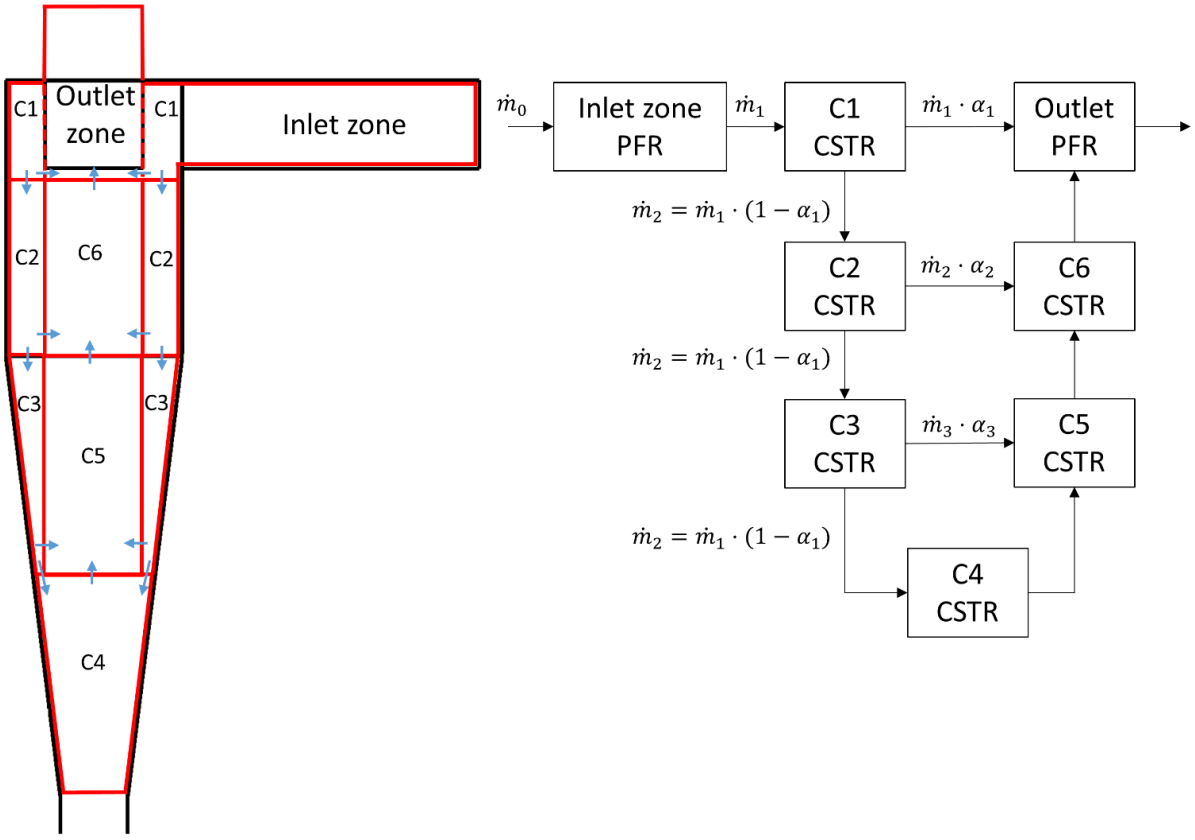

Figure 4.1: Illustration of cyclone reactor compartment model

The dimensions of the compartments when used for the pilot scale cyclone reactor setup used in this work are summarized in Table 4.3.

Table 4.3: compartment model dimensions

Compartment	Height [cm]	Inner diameter [cm]	Outer diameter 1 [cm]	Outer diameter 2 [cm]	Compartment volume [cm^3]
Inlet zone					501.3
Compartment 1	7	6.1	11	11	460.7
Compartment 2	10.2	6.1	11	11	671.2
Compartment 3	15	6.1	11	7.29	560.5
Compartment 4	12.5	0	7.29	4.2	331.9
Compartment 5	15	0	6.1	6.1	438.4
Compartment 6	10.2	0	6.1	6.1	298.1
Outlet	7	0	5.6	5.6	172.4

The temperatures in each compartment are selected as follows, compartment 1 uses the highest temperature measured on the vertical temperature profiles, compartments 2 and 3, are set to the highest measured temperature in the outer vortex at the top and middle probe ports respectively. Compartment 4 is set to the highest temperature measured in at the bottom horizontal probe position and compartments C5 and C6 are set to the minimum temperature measured in the middle at the middle and top probe positions respectively. 3 different cases was used to investigate how the overall flow pattern in the cyclone would affect the concentration profiles. Case 1 is an idealized case where all the gas flow down through the outer part of the cyclone reverses in the bottom and the flow up through the center. This is achieved by having all bypass fractions set to 0, $\alpha_1 = \alpha_2 = \alpha_3 = 0$. Case 2 simulates a flow pattern in which the gas flows gradually from the outer to the inner vortex down through the cyclone this is achieved by setting all bypass coefficients to $\alpha_1 = \alpha_2 = \alpha_3 = 0.5$ initially. Finally case 3 simulates that the majority of the gas leaks directly into the vortex finder, followed by no transfer from the outer vortex to the inner in the rest of the cylinder part of the cyclone, then followed by a larger transfer from the outer to the inner vortex when the conical shape starts. This is achieved by setting the bypass fractions to $\alpha_1 = 0.8$, $\alpha_2 = 0$ and $\alpha_3 = 0.8$. The temperatures and the corresponding residence time in each compartment, for experiment series E3, for the different cases for are summarized in Table 4.4.

Table 4.4: Temperatures and residence time in the compartments of the compartment model for different cases of bypass fractions

			Compartment						
			C1	C2	C3	C4	C5	C6	Outlet
			Temperature [°C]						
Bypass fraction			925.6	907.6	811.2	611.2	805.8	878.3	925.6
α_1	α_2	α_3	Residence time [s]						
0	0	0	0.0273	0.0403	0.0367	0.0266	0.0288	0.0184	0.0102
0.5	0.5	0.5	0.0273	0.0807	0.147	0.213	0.115	0.0368	0.0102
0.8	0	0.8	0.0273	0.202	0.183	0.666	0.144	0.0919	0.0102

4.1.2 Kinetics

In the modeling of the SNCR reactions three different kinetic models described in Chapter 2, section 2.3.3 are used, the full detailed kinetic model by Glarborg et al. [97]; the simple kinetic model by Duo et al. [1], with corrections for oxygen content; and the reduced mechanism by Brouwer et al. [94], converted to a simple kinetic model by only including the two reactions related to ammonia and NO conversion R2.28 and R2.29. The model calculation are carried out using the software Chemkin 17.1, for chemical reaction modeling with detailed kinetics.

4.1.3 Mixing

The mixing of the injected ammonia into the bulk gas have a significant influence on the performance of SNCR systems [132–134,140,141], as also described in Chapter 2 section 2.3.2.

To model the effect of mixing on the process a simple mixing model is used in which the main reactive species NO and NH_3 gradually mixes in the bulk gas. This is achieved by defining a series of pseudo components NO*, NO**, NO***. NH_3*, NH_3** and NH_3***. These are converted to their standard reactive forms through a series of first order pseudo reactions, with a constant non-temperature dependent reaction constant, as defined by R4.1 and R4.2:

$$NO^{***} \xrightarrow{k_{mix}} NO^{**} \xrightarrow{k_{mix}} NO^{*} \xrightarrow{k_{mix}} NO \qquad R4.1$$

$$NH_3^{***} \xrightarrow{k_{mix}} NH_3^{**} \xrightarrow{k_{mix}} NH_3^{*} \xrightarrow{k_{mix}} NH_3 \qquad R4.2$$

This approximates a linear mixing profile, for which the gradient can be adjusted to give a desired mixing time. The mixing time, t_{mix}, is defined as the time at which 95 % of the species have been converted to its reactive form. The mixing times used in the modeling of the experiment is chosen as $t_{mix} = 0.012\ s$ requiring a mixing constant of $k_{mix} = 550\ s^{-1}$ and $t_{mix} = 0.025\ s$ requiring $k_{mix} = 250\ s^{-1}$. This corresponds to approximately half and full residence time in the inlet section, dependent on the temperature.

4.2 Modeling results

4.2.1 Simple reactor model results

The model results for the three different simple reactor models used are shown in Figure 4.2 along with the SNCR performance measured during the experiments in terms of final NO over inlet NO [NO/NO_0] and NH_3 slip.

Overall the model results in Figure 4.2 follow a similar trend as the experimental results. The expected trend for SNCR is observed, with the highest NO reduction predicted in the middle of the temperature range, at T_{inlet} between 960 and 980 °C, and low reduction at high and low temperatures due to low selectivity and insufficient conversion respectively. The high NO reduction at the intermediate temperatures comes at the cost of incomplete ammonia conversion, with ammonia slip getting increasingly higher as the temperature gets lower and ammonia feed ratio gets higher.

The model predictions varies only little between the reactor types, the largest difference occurs when the ammonia feed ratio is high, in intermediate temperature range 950-1020 °C, where temperature is high enough for reaction in the cyclone chamber, but low enough that ammonia is still present here. When the temperature is lower there is only sufficiently high temperature for reaction in the inlet and when the temperature is too high all the ammonia is converted in the inlet, which in all cases are modelled as a PFR.

The quantitative predictions does not match the measured values, for the NO and NH_3 concentrations well. The ammonia slip is highly over predicted in the modeling results compared to the experimental results, with ammonia slips predicted at temperatures below 980 and 1020 °C for ammonia feed ratios, β, of 0.78 and 1.6 respectively, when in fact experimentally ammonia slips only occur at roughly 100 °C lower for the case of $\beta = 1.6$. The prediction of the lower threshold for onset of the SNCR reaction and the prediction of optimal temperature for NO reduction skewed towards higher temperatures with around with around 35-40 °C. The over prediction of the ammonia slip and the onset of reaction might be caused by model inaccuracies in the kinetics used or the temperature profile assumed based on measurements or a combination of both. For example the system contains roughly 10 % water in the gas phase, which is known to cause an overestimation of the lower threshold temperature for SNCR reactions when using the detailed kinetic scheme by Glarborg et al. [97] as described in Chapter 2 section 2.3.3. Furthermore, the NO conversion is highly over predicted for the inlet temperatures above 950 °C, which could be caused by either the ideal mixing assumption in the inlet or underestimation of the temperatures throughout the system.

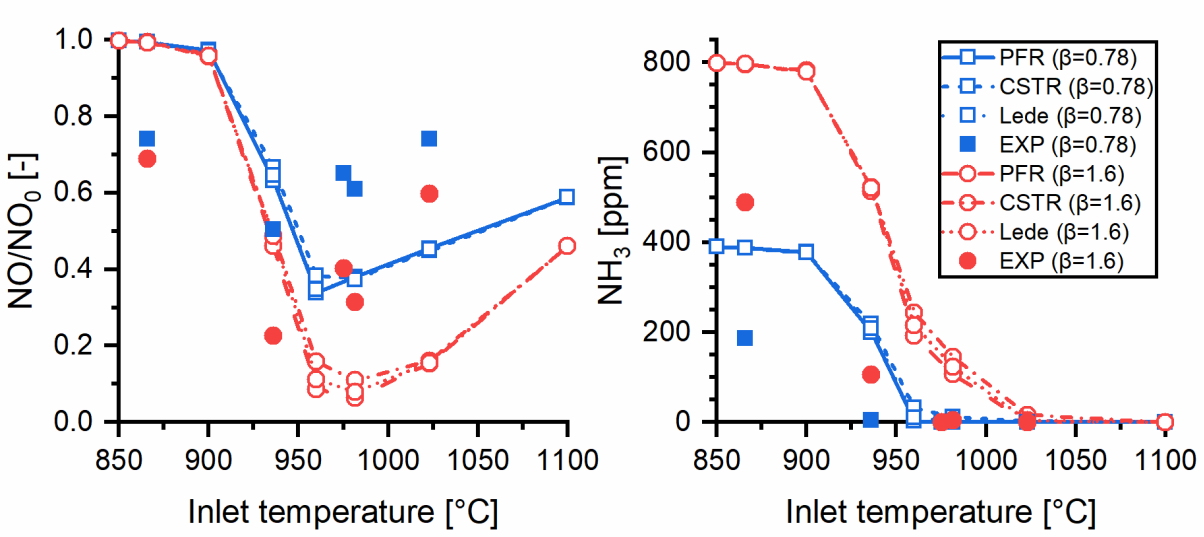

Figure 4.2: Experimental and modeling results for overall SNCR performance as a function of inlet temperature at 2 different ammonia injection ratios, $\beta \left[\frac{NH_{3,0}}{NO_0}\right]$, using detailed reaction kinetics and 3 different reactor models

In order to investigate the progress of the reaction and how it affects the outlet concentrations transient modeling results for experimental series E3 and selected β values using the detailed kinetics and both PFR & CSTR for the cyclone reactor are shown in Figure 4.3.

The transient concentration profiles show that the reason why the influence of reactor model only have a small effect on the model results, is that the majority of the conversion occur in the

inlet section. However, the temperature is still high enough, $T_{cyclone} = 925.6$ °C, for reaction in the cyclone reactor and thus the conversion continues quickly until enough NO has been converted to slow down the reaction, showing that in the kinetic model ammonia conversion is severely limited by the amount of available NO at temperatures below 1000 °C. While the experimental results for the concentration profiles from inside the cyclone in Figure 3.14 show that ammonia is still being converted down through the cyclone chamber even at temperatures below 800 °C, while little to no change in NO is observed. This shows that the kinetic model overestimates the selectivity of the NO reduction pathway, as more ammonia must be converted to N_2 and H_2O through a combination of the reduction and oxidation pathways, or possibly to N_2O which is not detected in the experiments. This would lead to faster consumption of the ammonia, thereby lower ammonia slip, and lower NO reduction. Possibly explaining why the ammonia slip is overestimated in the modeling results in general and NO conversion is overestimated at high temperatures. This is also exemplified by the models slight change in outlet NO concentration as ammonia injection rate is increased, while the experimental results show a much larger change while the opposite is observed with the ammonia slip.

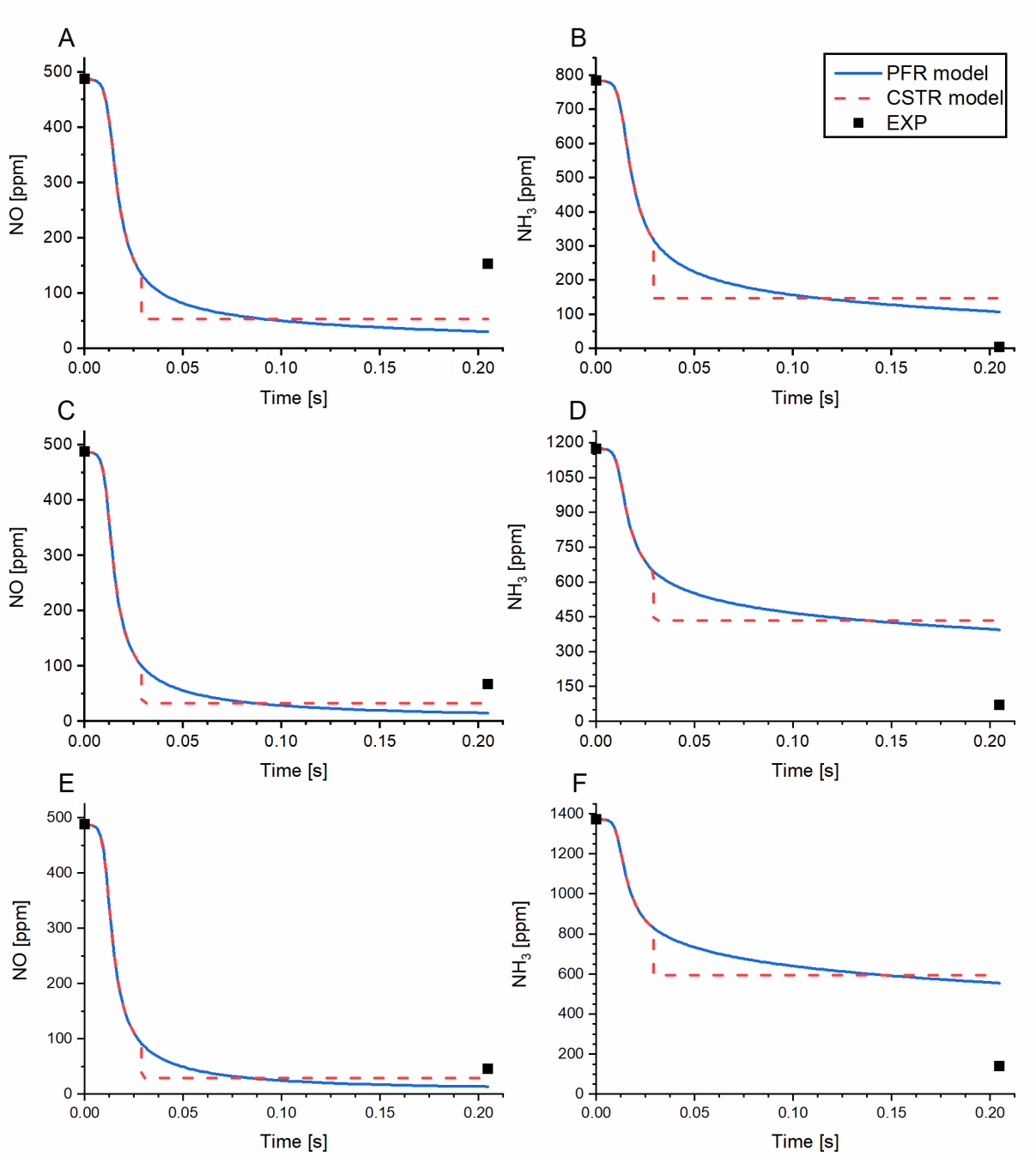

Figure 4.3: Transient model results for NO and NH_3 concentrations for operating conditions E3, using detailed kinetics and different reactor models for the cyclone chamber, at different ammonia injection ratios, $\beta \left[\frac{NH_{3,0}}{NO_0}\right]$ A & B $\beta = 1.6$, C & B $\beta = 2.41$, and E & F $\beta = 2.82$

The effect of mixing is investigated both as a function of temperature and as the transient conversion profile at the operating conditions related to experiments series E3, using the mixing model described in chapter 4.1.3.

Figure 4.4 shows the effect of mixing and its dependency on temperature using a PFR reactor model. Overall the effect of mixing in the model is small. However, the effect is highest for NO reduction at low inlet temperatures, where the temperature in the cyclone is too low for significant conversion and therefore any delay in mixing is detrimental. Interestingly with

higher mixing times the model leads to better NO reduction at higher inlet temperatures, as the reaction is delayed until a temperature with a better selectivity. Other investigations of the effect of mixing have shown similar results with modeling [141] while some have shown that NO reduction should still be improved with faster mixing at high temperatures [133,141].

In all cases the model shows increased ammonia slip with higher mixing times until the temperature is high enough for full conversion. Here no comparison with literature model results is possible, as the modeling results for ammonia is are generally not reported in the literature. The increased ammonia slip with high mixing times is expected modeling wise. However, it is not in accordance with the behavior observed in the experiments with different carrier gas flows and injection probe positions in Chapter 3 section 3.2.2.3, this might be due to the lack incorporation of the local cooling effect of the injected jet.

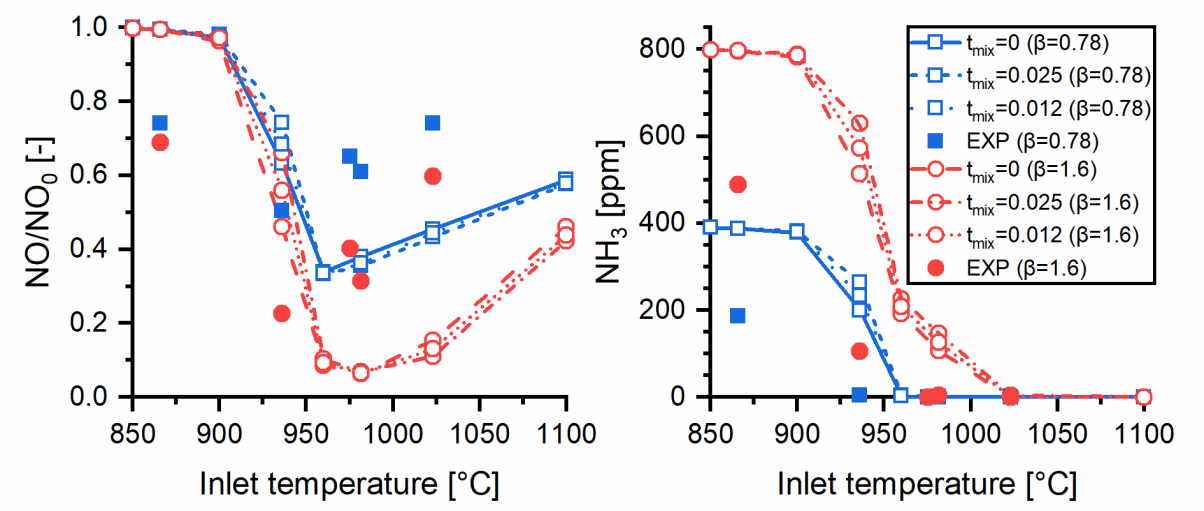

Figure 4.4: Effect of mixing time on the modeling results for overall SNCR performance as a function of inlet temperature at 2 different ammonia injection ratios, $\beta\left[\frac{NH_{3,0}}{NO_0}\right]$, using the detailed Glarborg kinetics with a simple mixing model and a PFR reactor model for the cyclone chamber

The transient model results for experimental series E3 with and without mixing, in Figure 4.5, show that the influence of reactor model, used for the cyclone chamber, is higher when mixing is implemented in the model. This can be observed by the higher difference between the PFR and CSTR results with and without mixing in all cases. It is caused by the mixing causing a delay in the reaction, which leads to a higher fraction of the conversion happening in the cyclone chamber.

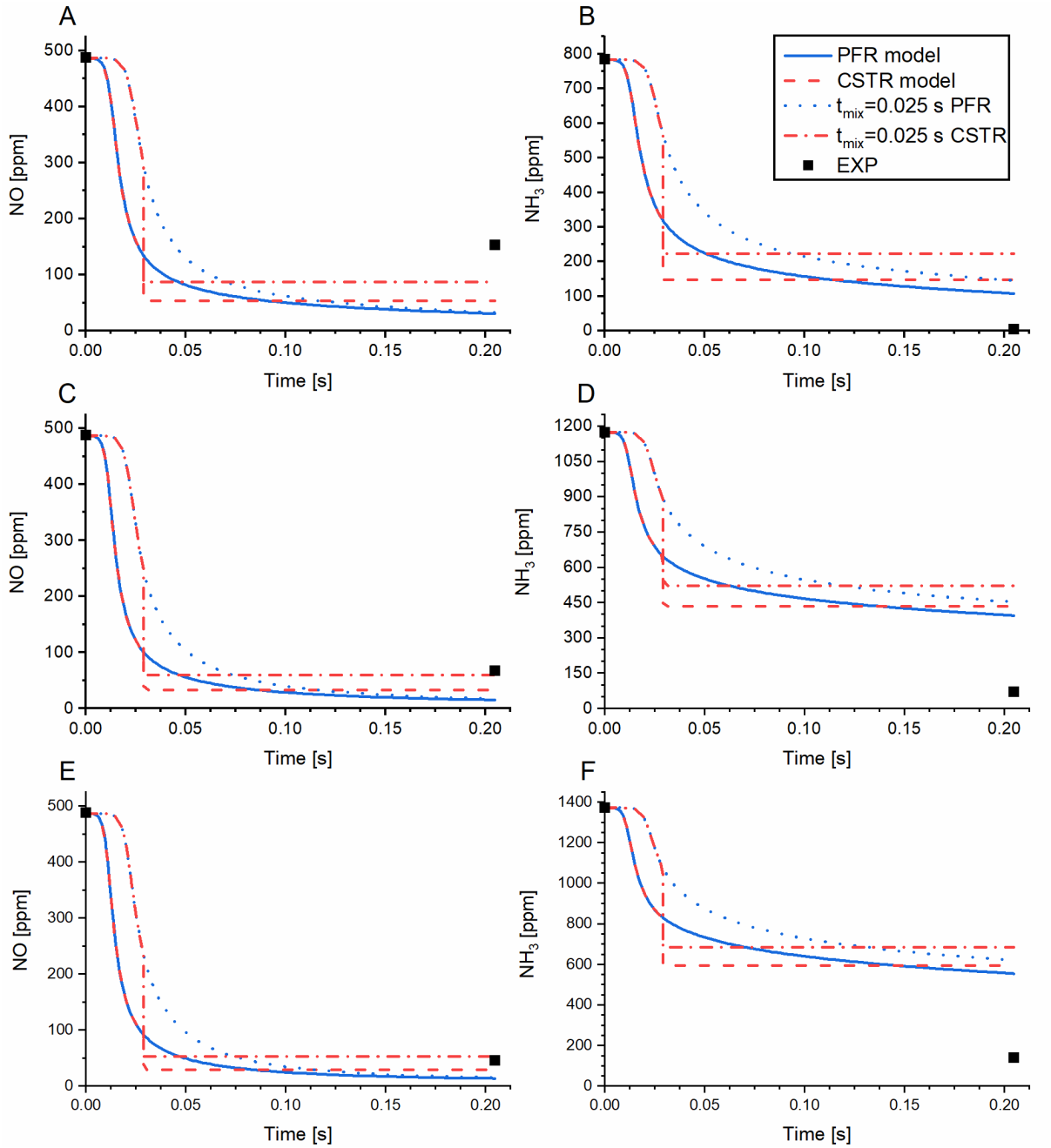

Figure 4.5: Transient model results for NO and NH_3 concentrations with and without mixing at different ammonia injection ratios, $\beta \left[\frac{NH_{3,0}}{NO_0}\right]$ A & B $\beta = 1.6$, C & B $\beta = 2.41$, and E & F $\beta = 2.82$ for operating conditions, E3 using different reactor models for the cyclone chamber

In order to investigate the influence of important reaction condition parameters, such as temperature and flue gas composition on the detailed kinetic model results a sensitivity study was conducted.

The models sensitivity to the measured temperatures is illustrated in Figure 4.6. Here the temperatures both in the inlet section and the cyclone is changed up and down by 35 °C, which is roughly the temperature variation measured across the width of the cyclone inlet pipe. The higher temperature model results do show an improved fit with the experimental data, both in the case of ammonia slip and NO concentration, while the low temperature model results show

a worse fit. However, the ammonia slip and the NO reduction are still overestimated for the high temperature model results. From this it is clear that the deviation between model and experimental results cannot be explained solely by an error in choice of temperature profile.

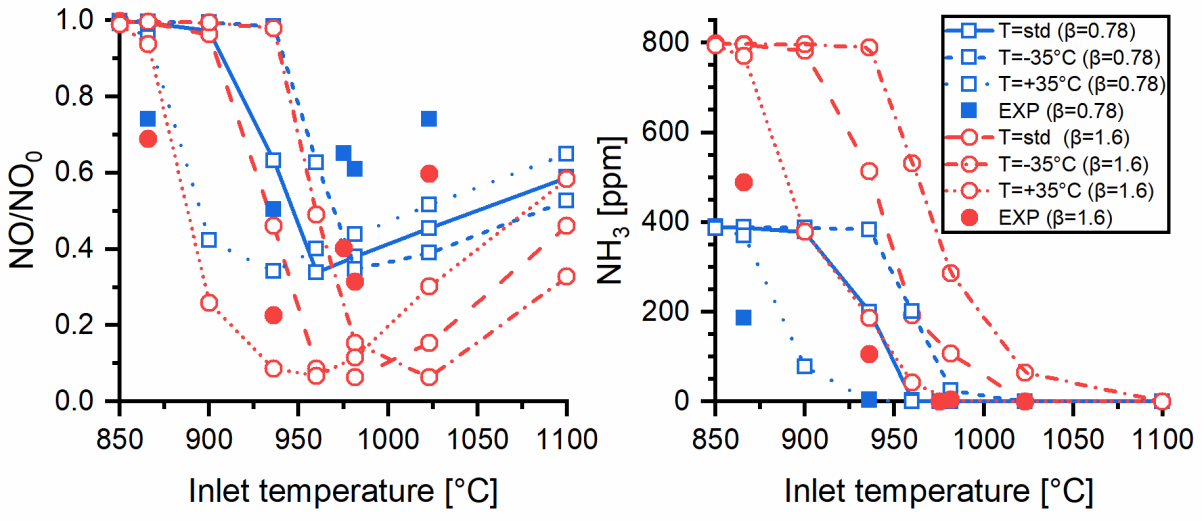

Figure 4.6: Model results sensitivity to temperature using detailed kinetics and a PFR reactor model.

The models sensitivity to the concentration water and CO in the flue gas is investigated in Figure 4.7. From this is it clear that water content, have a large impact on the predicted lower temperature for onset of reaction, which is lowered by ~50 °C, when no water is present in the model, bringing it closer to the experimentally observed trend. This is caused by the models tendency to overestimate the influence of gas water content on the temperature window, compared to experiments, due to interaction with the radical pool [97] as discussed in Chapter 2 section 2.3.3. The conversion of both NO and ammonia is still underestimated below 936 °C, while the selectivity is overestimated at temperatures for 936 °C and above, without water. Similar influence although to a lesser extent can be observed from the addition of 100 ppm CO in the model, with a lowering of the temperature for initial onset of reaction and a slight shift in the temperature window. While this effect is well known, no CO were measured in the flue gas during experiments.

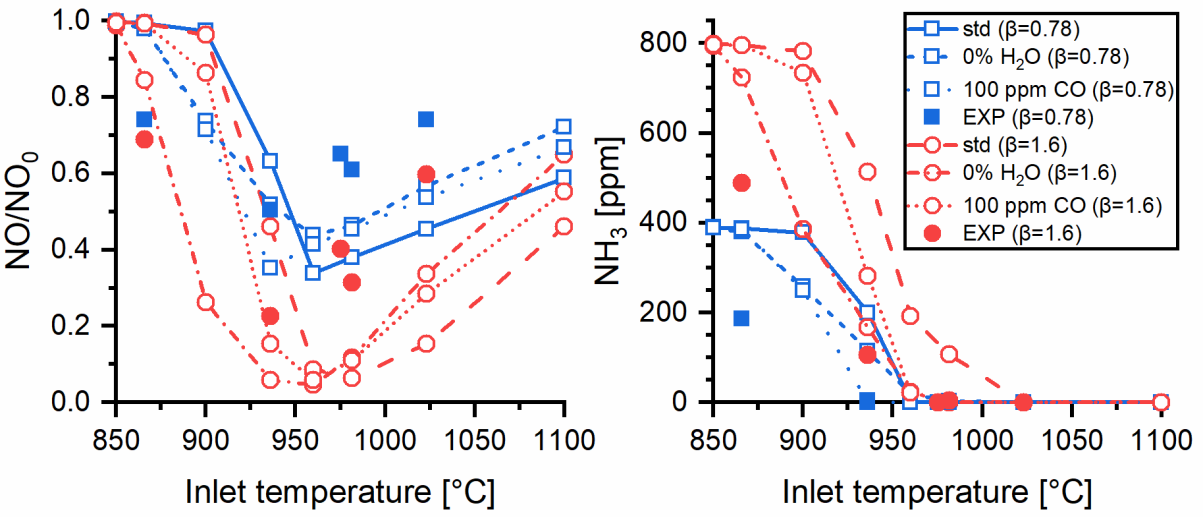

Figure 4.7: Model results sensitivity to composition changes using detailed kinetics and a PFR reactor model

To test the performance of the different kinetic models, the modeling results for different kinetic schemes using a PFR are shown in Figure 4.8 together with the experimental results. All the kinetic models show somewhat similar qualitative behavior with a similar optimal point for NO reduction at inlet temperatures around 960-980 °C and progressively lower ammonia slip as the temperature increases. The simple kinetics show reaction occurring at lower temperatures and a generally better fit with the experimental results as compared to the detailed kinetics. The simple kinetics from Duo et al. [1] have the overall best fit to the experimental data, while the Brouwer et al. [94] kinetics are closer to the detailed kinetics from Glarborg et al. [97]. However, generally once a temperature of ~950 °C is reached for the different kinetics, the NO reduction is overestimated for all the kinetics and the ammonia slip is over predicted. While the kinetics from Duo et al. [1] are the simplest, they were derived from data with conditions similar to the experiments in this work, with O_2 content of 4 % in N_2, and includes no influence from water [1], which influence is overestimated by the detailed kinetics [97].

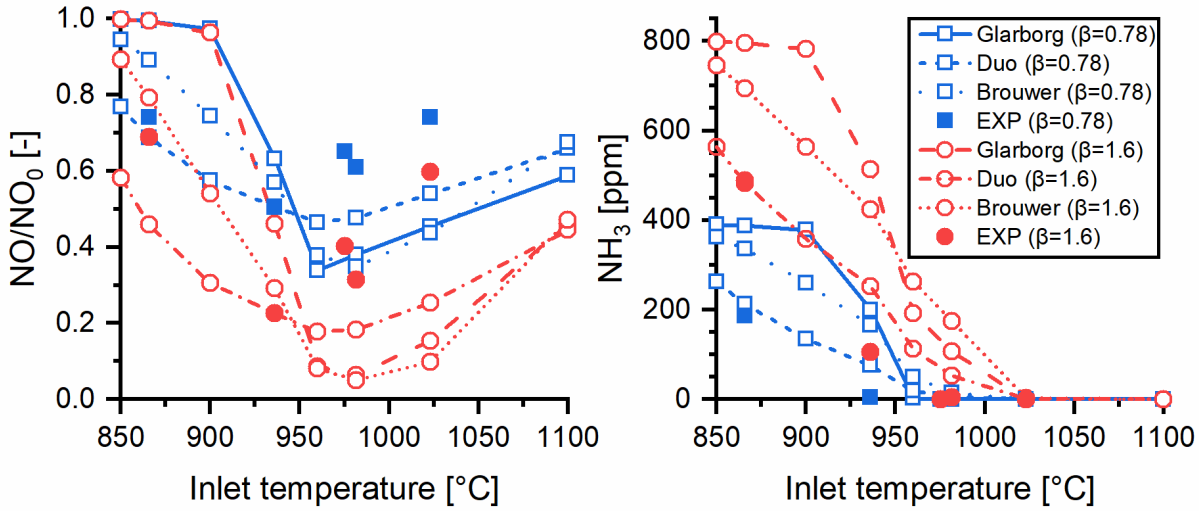

Figure 4.8: Modeling and experimental results for overall SNCR performance as a function of inlet temperature at 2 different ammonia injection ratios, $\beta\left[\frac{NH_{3,0}}{NO_0}\right]$, using 3 different kinetic models and a PFR reactor model

Based on the results in Figure 4.8 and the discussion above, the influence of reactor model when using simple kinetics by Duo et al. [1] is investigated in Figure 4.9. From this it is clear that the model used for the cyclone chamber have a much higher influence when using the simple kinetics as compared to the detailed kinetics results in Figure 4.2. This partly due to a much wider predicted temperature window, as even at low inlet temperatures, where plenty of ammonia is present in the gas at the cyclone inlet, the low cyclone temperatures are still within the temperature window predicted by the simple kinetics. As opposed to the detailed kinetics, where the beginning of the temperature window for SNCR is predicted to be at a much higher temperature than measured.

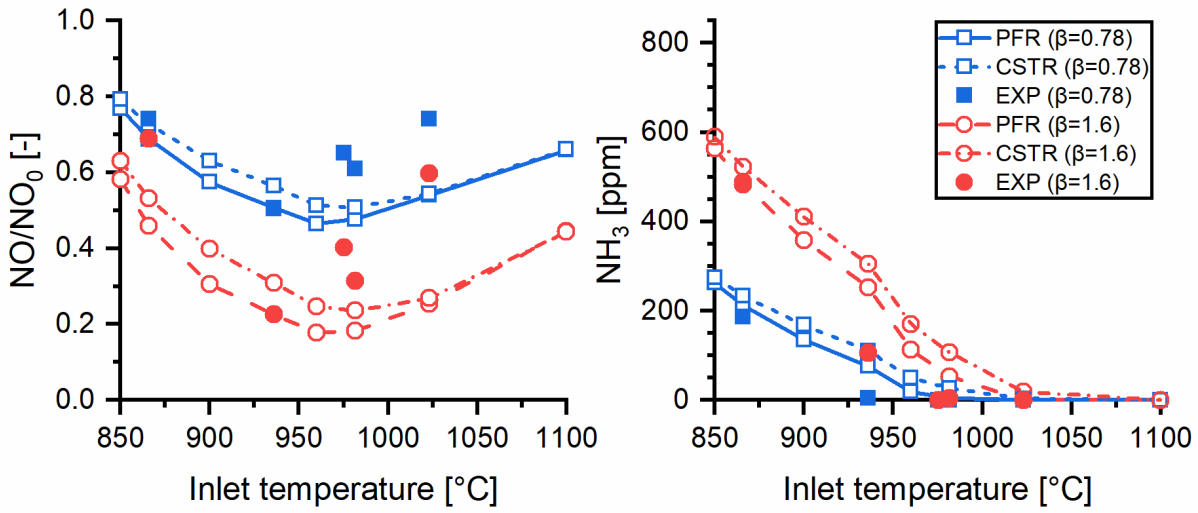

Figure 4.9: Experimental and modeling results for overall SNCR performance as a function of inlet temperature at 2 different ammonia injection ratios, $\beta\left[\frac{NH_{3,0}}{NO_0}\right]$, using simple reaction kinetics by Duo et al. [1] and 2 different simple reactor models

4.2.2 Compartment model results

The compartment model was developed in order to model the influence of the temperature distribution in the cyclone chamber and the reverse vortex flow, on both overall performance and internal concentration profiles, while using detailed reaction kinetics.

The model results for the internal concentration profiles for experimental series E3 with the ammonia injection stoichiometric ratio of $\beta = 2.82$, using detailed kinetics and the 3 different cases of bypass fractions given in Table 4.4, are shown in Figure 4.10. These operating conditions were chosen, as at these conditions reactions are happening throughout the majority of the reactor volume as seen from the experimental concentration profiles.

The results follow the general trend of the experimental data qualitatively, for all 3 cases of bypass fraction combinations. Both ammonia and NO is converted down through the chamber, with higher concentrations in the outer vortex than in the inner vortex. With the biggest difference in the top of the cyclone chamber. The highest concentrations of NO and ammonia at each height is observed for the ideal double vortex reverse flow assumption, with all bypass fraction set to $\alpha_1 = \alpha_2 = \alpha_3 = 0$. This is caused by the higher flow of gas into the lower parts of the cyclone giving a lower local residence time and therefore lower conversion. The lowest concentrations and the biggest difference between the inner and the outer vortex is observed for the model with a high initial bypass fraction $\alpha_1 = 0.8$, simulating high lip leakage, no bypass fraction for the cylindrical section, $\alpha_2 = 0$ and a high bypass fraction in the upper part of the conical section $\alpha_3 = 0.8$. This gives a low gas flow in most of the lower cyclone chamber providing ample residence time for further conversion even at lower temperatures. The case simulating a gradual transfer from the outer to the inner vortex through the entire cyclone, $\alpha_1 = \alpha_2 = \alpha_3 = 0.5$, show concentration profiles in between the results for the other cases.

The quantitative fit is poor showing too low NO concentrations already at the top measurement point and down through the cyclone reactor. It also shows too high ammonia concentrations down through the cyclone chamber. Both could be expected based on the observations from simple reactor model results using the detailed kinetics in chapter 4.2.1.

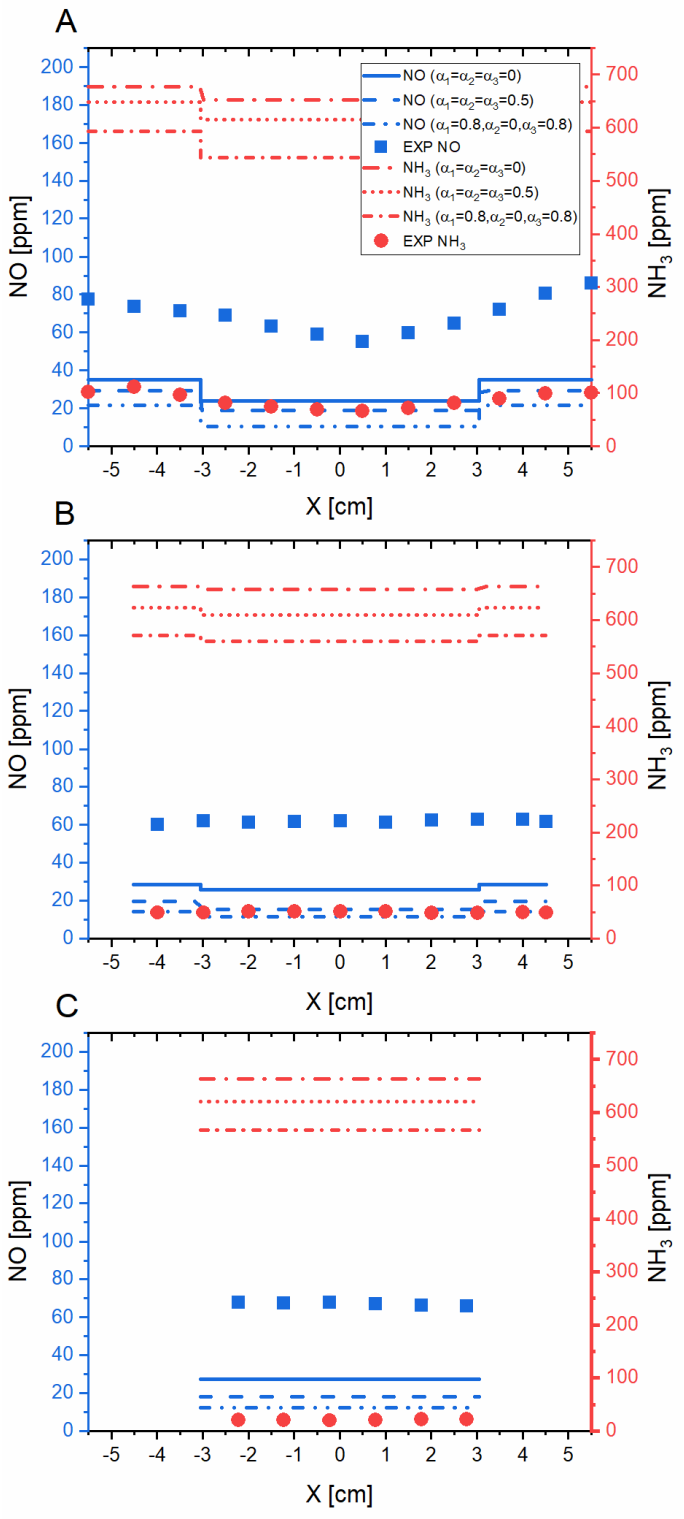

Figure 4.10: Compartment model results for internal concentration profiles using detailed kinetics for E3 at $\beta = 2.82$

The simple reactor model results using the simple kinetics by Duo et al. [1] had better agreement with the experimental results, compared to the detailed kinetics. As such the compartment model is tested using simple kinetics, using the reactor conditions described in Table 4.4. The results of this is shown in Figure 4.11. These also follow the general trend of the experimental data qualitatively, as described above for the detailed kinetics. While quantitatively the simple kinetics show a much better fit than the detailed kinetics. The NO concentrations, are close to the measured values, within 20 ppm in all cases with the best fit is obtained for the case with the ideal double vortex flow assumption with all bypass fractions set to 0, showing close to perfect agreement with the experimental results. The ammonia concentrations are still predicted too high for the model, in all cases. But the best fit for ammonia is case 3 with the high initial bypass fraction as this provides higher gas residence times in the cyclone with more time for ammonia conversion.

Slightly better agreement with the experimental results, for the internal concentration profiles, for both kinetic models might be achieved by fitting the bypass parameters using the measured profiles. However the main difference seems to be that the conversion of ammonia in the inlet section and the top of the cyclone is highly under predicted for both kinetic models. While for the detailed kinetics, the initial NO conversion is also highly over predicted. Despite the problems with modeling the conversion in the inlet section properly, the compartment model developed account for the complex double vortex flow structure and the temperature gradients in a cyclone reactor in a simple way, enabling the use of detailed kinetics in cyclone reactor modeling. However, further development of the modelling of especially the inlet section is needed. In order to use the compartment model itself, as a predictive tool instead of a descriptive model, bypass fractions might be fitted to surface flux calculations from CFD simulations or fitted to residence time measurements. As opposed to fitting it to the measured concentration profiles. Such a model may assist future modeling of other gas phase reactions for existing cyclone reactor applications, or model based evaluation of new cyclone reactor processes. To achieve such, the influence of the solid phase flow and cyclone design would have to be investigated and accounted for as these are an integral part of any cyclone process in terms main application as separation unit.

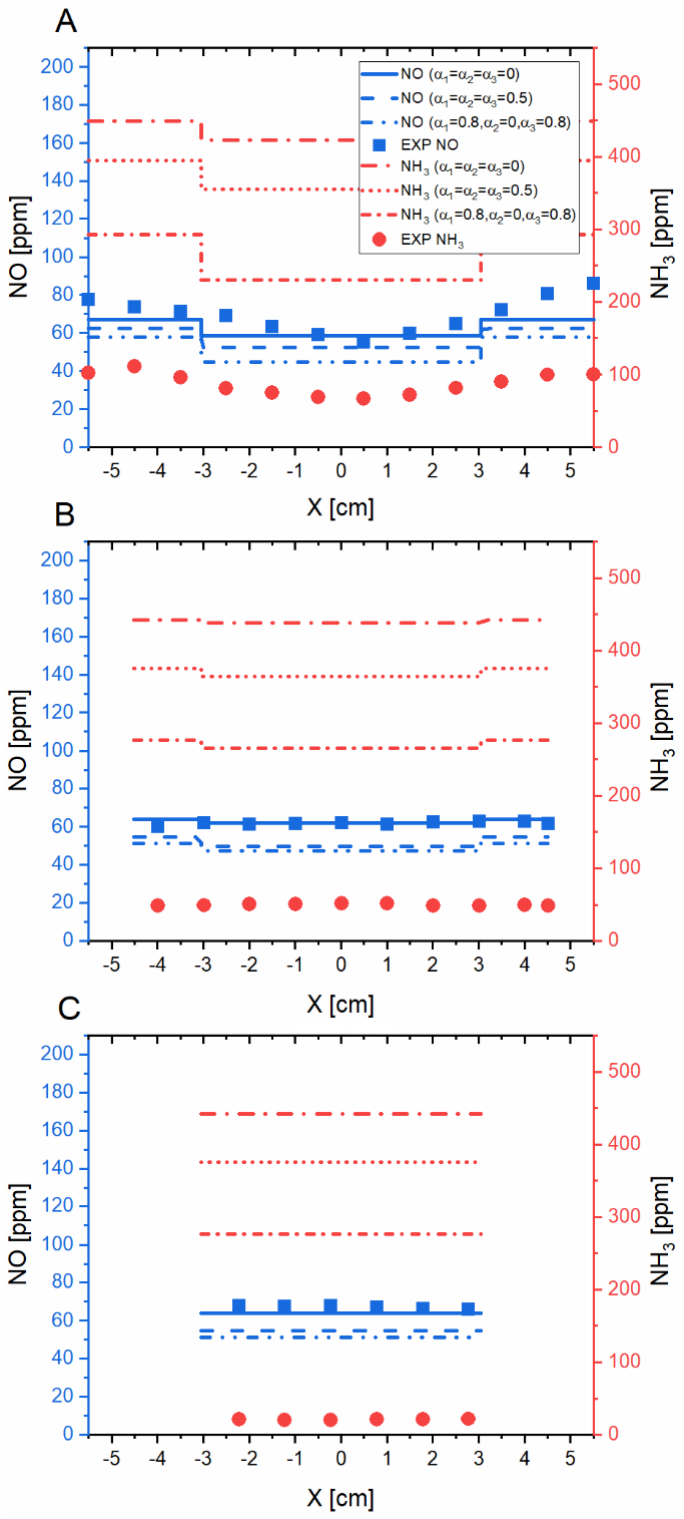

Figure 4.11: Compartment model results for internal concentration profiles using simple kinetics (Duo et al. [1]) for E3 at $\beta = 2.82$

4.3 Conclusions

The model prediction using existing kinetics and simple reactor models for the outlet NO concentration showed similar trends as the measured behavior. However, the NO reduction was overestimated in most cases. The ammonia slip over most of the investigated temperature range (up to 1023 °C) was highly over-predicted even with the assumption of constant temperature throughout the whole cyclone volume. The influence of reactor model, mixing modeling, temperature uncertainty, flue gas composition, and choice of kinetics were investigated. However, none of these were alone able to explain quantitative difference between the model and experimental results. The simple kinetics from Duo et al. [1] showed the best agreement with the experimental results.

A reactor network model consisting of multiple interconnected compartments each representing a volume of the cyclone was developed in order to make a simplified representation of the complex flow pattern inside a cyclone, and to reproduce the concentration profiles inside the cyclone. This model can be used with detailed reaction kinetics. The model was able to qualitatively reproduce the behavior of the internal concentration profiles caused by the double vortex flow in the cyclone reactor, using both detailed and simple kinetics. For the detailed kinetics the quantitative agreement were unsatisfactory for both NO and ammonia for all. For the simple kinetics, the predictions were quantitatively good for the NO concentrations, but unsatisfactory for the ammonia due to simplifications in the modeling of the inlet section and possibly insufficient accuracy of the kinetics.

Chapter 5 – SNCR in industrial cyclone preheater

This chapter describes the work conducted based on the application of SNCR in cyclones at an industrial scale. The studied case is the removal of NOx in a cyclone preheater system for a stone melting process used to produce mineral wool for insulation by Rockwool. The work includes a pre-study based on plant operation data from the company; an industrial measurement campaign, planned and carried out in collaboration with Rockwool; and modelling investigations of the process in general.

Note that much of the information in this chapter is based on knowledge from Rockwool and does not have public available references.

5.1 Introduction

Rockwool produce stone wool products at plants operating all around the world. While several different melting technologies are used by Rockwool, this work is based on the newer combustion based melting cyclone technology developed by Rockwool and patented in 2012 [100]. An overview of the melting process and flue gas treatment in plant using this technology is shown in Figure 5.1.

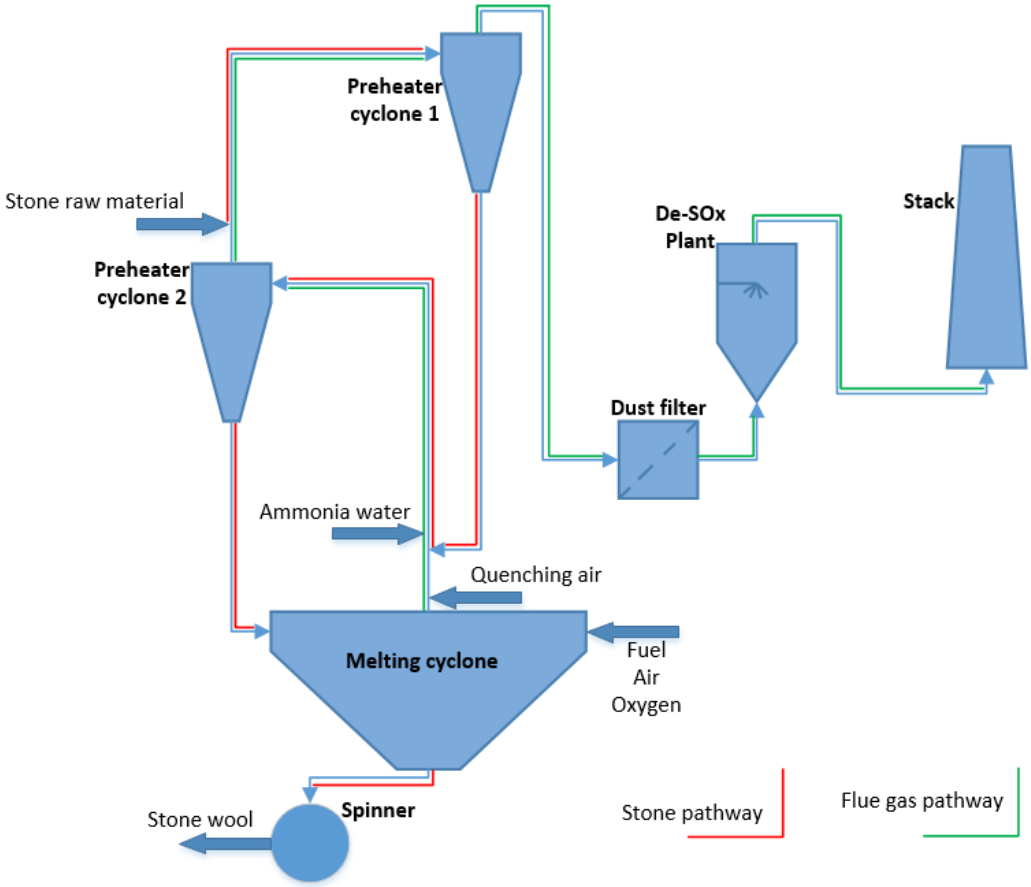

Figure 5.1: Process diagram for stone melting process and flue gas cleaning at Rockwool Cigacice

Due to the high temperatures, 1400-1700 °C, required in the melting cyclone a high amount of NO_x, is formed in the combustion process, typically in the range of 800-1200 mg/Nm^3 after quenching on dry basis. The current emission limits for mineral wool manufacturers using oxy-

fuel burners in the EU are given in Table 5.1 [144]. While normally emission limits are corrected for oxygen content to account for dilution, this method is inapplicable for oxyfuel burners. Instead the emission limit of NO_x for mineral wool production is also given in kg/tonne of melted stone [144].

Table 5.1: Current emission limits for mineral wool producers in the EU [144]

Unit	NO_x (as NO_2)	NH_3
mg/Nm^3 †	400-500	5-30
ppmv‡	195-244	7-40
$\frac{kg}{tonne\ melted\ stone}$	1.0-1.25	

†standard conditions is considered to be 273.15 K and 101.3 kPa dry basis

‡ dry basis

While, improvement of burner design, fuel substitution from coal to natural gas, and stabilizing the melting cyclone operation can help and already have helped to reduce NO_x emissions, secondary NO_x reduction measures are still needed in order to meet the current emissions limits shown in Table 5.1 and future emission limits. Currently selective non-catalytic reduction (SNCR) using a 24 wt% ammonia water solution as reduction agent is utilized in the preheater system for the melting cyclone. depending on operation conditions and production load, Rockwool is able to operate below the upper emission limits of ~240 ppmv NO_x and ~40 ppmv ammonia, during the majority of the time. When new emission standards is enacted or if local authorities decide that a new or existing plant must follow a lower limit, problems might arise in keeping within the new limits.

The cyclone preheater system where SNCR is applied is illustrated in Figure 5.2. Hot flue gas with a temperature of ~1400-1500 °C from the melting furnace, is cooled, first by mixing it with quenching air and then by adding raw material for the melting process in 2 steps where the particle and gas flow is in “counter current”. The hot flue gas is initially quenched by diluting with air and with water jackets on the side of the riser cooling it to around 1200 °C. Dried raw material at temperatures between 400-500 °C is then fed to the riser where it is mixed with the hot gas and subsequently separated in preheater cyclone 2, thereby heating the raw material, while cooling the flue gas. The partially cooled flue gas exits the cyclone, and is mixed with fresh cold raw material and again separated in preheater cyclone 1. This preheating process serves to recover and reuse energy from the flue gas to reduce fuel consumption and to assist the melting process by pre-heating the raw materials.

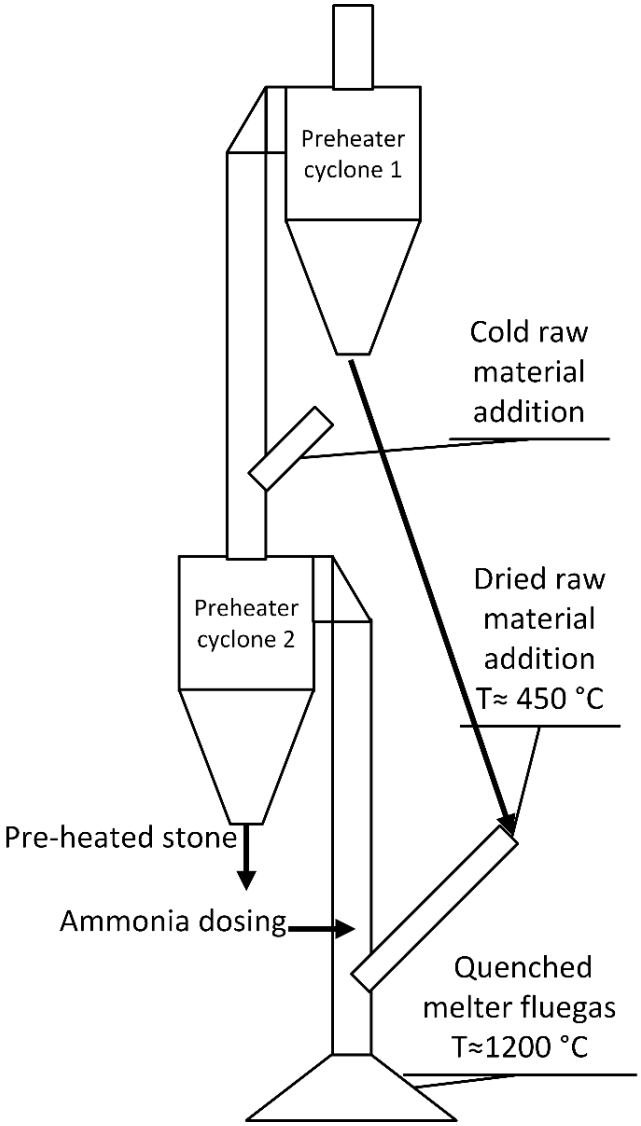

Figure 5.2: Illustration of cyclone preheater system

The zone where the gas temperature allow for the SNCR process to be possible is from the feeding point of the dried raw material, to the point where the cold raw material is fed, after the gas exit of preheater cyclone 2. In the current system, the reduction agent ammonia is injected as a 24 wt% ammonia-water solution through 3 atomizing nozzles placed around the circumference of the riser slightly above the raw material inlet, where the gas have been cooled slightly by the raw material, to ensure the right temperature for SNCR.

5.2 Pre study

This subchapter describes the initial data analysis and modeling work done in order to investigate the likely causes of the problems with SNCR experienced by Rockwool in their preheater systems for their melting furnaces. Their problem was that they are unable to get sufficiently low stable NO_x emissions, without getting a too high ammonia slip. Without any SNCR the NO_x emissions is at around 500 ppm varying depending on the operating conditions in the cyclone smelter. At the time, the efficiency of the SNCR allows Rockwool to reach NO_x emissions between 150 and 300 ppmv before the ammonia slip exceeded the emission limits

of 40 ppmv, with both the NO_x and ammonia emissions being highly unstable. This meant that on average the emission limits could be met, but with short periods of exceeding the limits. This study uses data from a specific Rockwool plant and the system description is based on this specific plant.

5.2.1 System description

The exact design of the system is confidential, but the overall dimensions are used to calculate the residence time used for the modeling. The conditions in the system can vary considerably due to changing thermal load of the burners in the melter, raw material feed rate and other process fluctuations. In order to model the system, base values for important parameters were obtained using operational data from the plant collected during SNCR tests carried out by Rockwool. From this data, the flue gas exit composition measured in the stack is used. Concentrations of the major flue gas (N_2, O_2, CO_2, H_2O) species were determined based on the averaged dry measurement and recalculated to wet values. The CO concentration is determined based on the average concentration in an interval with no ammonia addition and likewise recalculated to wet basis. The results for the base data are shown in Table 5.2.

Table 5.2: Calculated flue gas composition and flowrate data

Symbol	Value [unit]	Description
C_{O_2}	13 $[vol\%]$	Wet mole percentage†
C_{CO_2}	11 $[vol\%]$	Wet mole percentage†
C_{H_2O}	15 $[vol\%]$	Wet mole percentage
C_{N_2}	61 $[vol\%]$	Wet mole percentage
C_{CO}	62 $[ppm]$	Wet CO outlet concentration†

†Calculated based on dry gas measurement in the stack

The gas phase and particle temperature in the SNCR zone is uncertain, and no direct measurements is available. However, the gas phase temperature is in the range between the quenched flue gas temperature and the cyclone outlet temperature. Particle temperature is between particle inlet temperature and cyclone outlet temperature. This is summarized in Table 5.3.

Table 5.3: Known temperature data in the SNCR zone

Parameter	Temperature [℃]	Description
$T_{g,inlet}$	1200 [℃	Estimated gas temperature before particle inlet point
$T_{g,outlet}$	< 700	Gas temperature after cyclone outlet and cold raw material addition
T_g	<1200 ℃	Gas Temperature in the SNCR zone
$T_{p,inlet}$	~450 ℃	Estimated particle temperature at the particle inlet point
T_p	>450 ℃	Possible particle temperature range in the SNCR zone

5.2.2 Plant data analysis

The ammonia water flowrate and the NO_x, NH_3, and CO concentrations are measured values in the dataset received from the plant. These values for the entire dataset are shown in Figure 5.3. In order to obtain base conditions for modelling and data points to compare with, periods with stable ammonia injection and relative stable emission measurements are identified in the dataset.

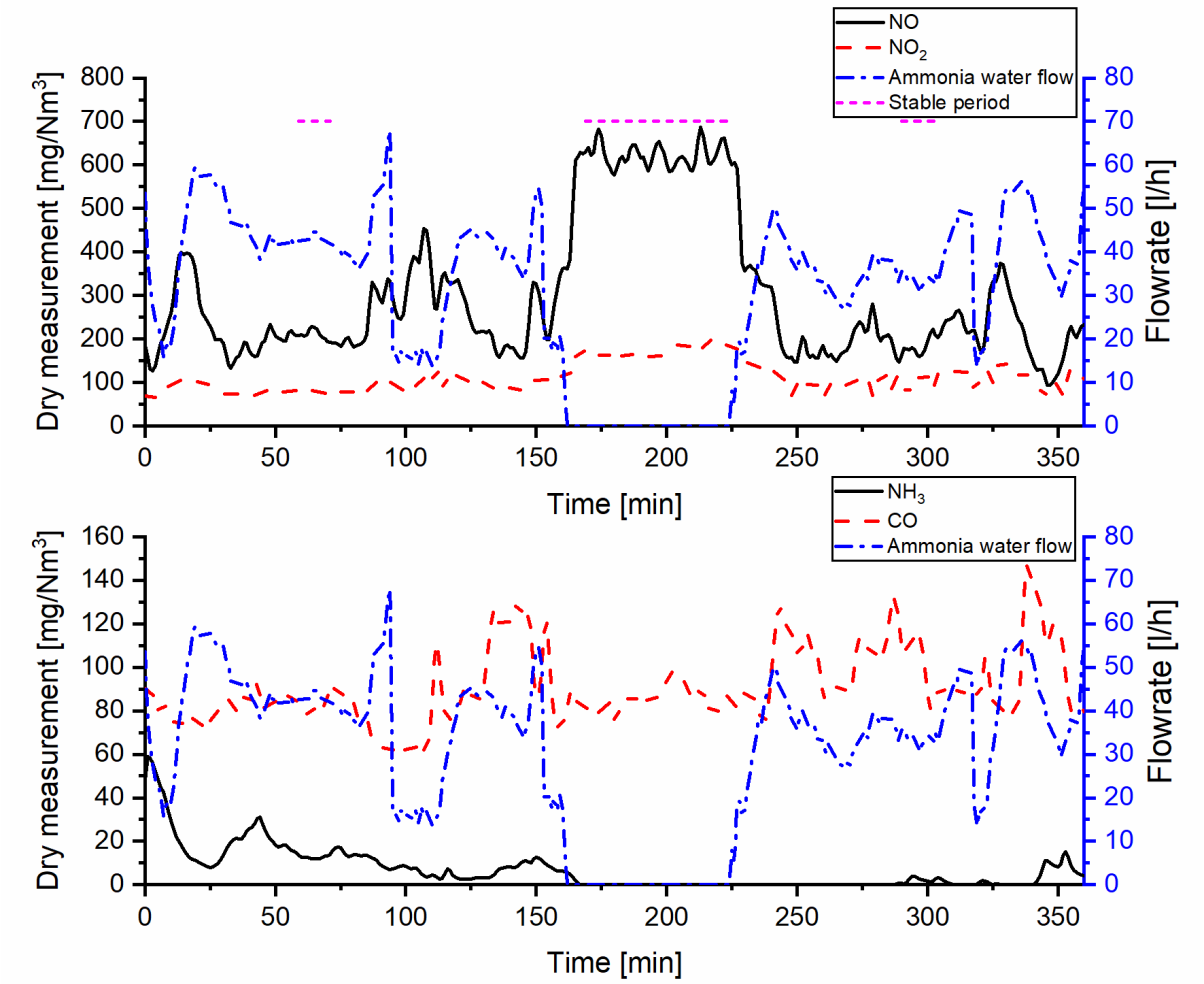

Figure 5.3: Rockwool Plant SNCR test emission data and 24% ammonia water dosing rate Top: Ammonia dosing, NO and NO_2 concentration and stable periods Bottom: Ammonia and CO concentration

From the data shown in Figure 5.3 it is clear that the ammonia water dosing was highly unstable. However, in the top part of Figure 5.3, three "stable" regions were identified and marked, including the region with no ammonia addition. These have been used as measurement points and averages of the composition in the periods have been used. With the one without ammonia addition used as the background/inlet values, this gives two data points with different ammonia addition rates, the emission data have been recalculated to wet gas concentration in ppmv and the ammonia addition has been converted to a molar feed ratio, defined as $\beta = \frac{[NH_3]_0}{[NO_x]_0}$, used to describe the inlet concentration of ammonia in relation to the NO_x concentration. The data obtained is shown in Table 5.4. Looking at the bottom part of Figure 5.3, it can be seen that the ammonia slip measurement takes a long time to change when the ammonia

addition changes. This behavior is caused by a combination of the ammonia sensor being placed in the stack, physically "far" from the injection point, with several unit operations, such as a bag filter for fines and a desulphurization unit, between the actuator and the measurement, and ammonias physical/chemical behavior. Ammonia has a high tendency to adsorb to "cold" surfaces [145], such as the inner surfaces of the plant downstream of the pre-heater system, the raw material particles in the fines filter, and the surfaces in the sampling equipment.

Table 5.4: Emission data used for simulations of the case

Symbol	Value [unit]	Description
$C_{NO,0,ppm}$	423 $[ppmv]$	Background NO concentration
$C_{NO_2,0,ppm}$	76 $[ppmv]$	Background NO_2 concentration
$\beta = 1$		
$C_{NO,ppm}$	123$[ppmv]$	Outlet NO concentration
$C_{NO_2,ppm}$	46 $[ppmv]$	Outlet NO_2 concentration
$C_{NH_3,ppm}$	3 $[ppmv]$	Ammonia slip
$\beta = 1.3$		
$C_{NO,ppm}$	143 $[ppmv]$	Outlet NO concentration
$C_{NO_2,ppm}$	35 $[ppmv]$	Outlet NO_2 concentration
$C_{NH_3,ppm}$	15 $[ppmv]$	Ammonia slip

Alternatively, the entire transient dataset can be used, by correlating the emissions directly to the ammonia dosing. However, the delay between actuation of the ammonia water dosing and the change in emission must be found and taken into account. This has been achieved by using the NO peaks from the top part of Figure 5.3 and the ammonia dosing "valleys" and vice versa. Examples of this correlation of peaks are shown in Appendix B.

The average time delay for the NO emission response to changes in ammonia injection were found to be 7 minutes. As discussed above, dynamics of the ammonia emission are much slower and many peaks in ammonia slip is not observed due to the fast changes in ammonia dosing. A delay in excess of 25 minutes can be observed for the ammonia from some of the peaks. However, in order to keep consistency in the data, the same time delay is used for both NO_x and ammonia. The results are shown in Figure 5.4. From this it is easy to spot the trend for decreasing NO_x emission and higher ammonia slip with increasing ammonia water flow. However, it is also clear that a large error is introduced from the zero measurements of ammonia.

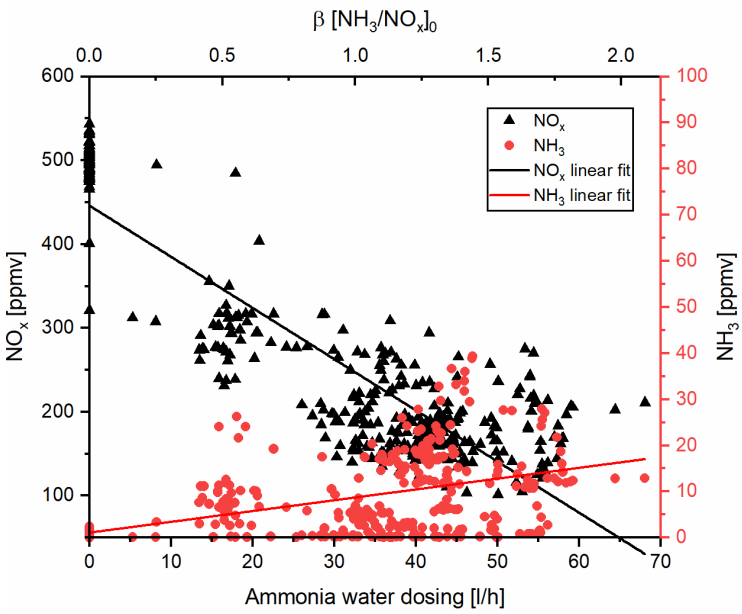

Figure 5.4: Time delay corrected NO_x and Ammonia emission correlated to Ammonia dosing

5.2.3 Modeling

The modeling in this work is based on simple reactor models and detailed reactor kinetics. The modeling is performed using the software program ChemKin 17.1 and the detailed SNCR kinetic model by Glarborg et al. 2018 [97].

The reactors are modeled as a combination of simple reactors, with the riser volume being modeled as a simple plug flow reactor (PFR) with a gas phase residence time of τ_{riser} and the cyclone is modeled as a CSTR with a residence time of $\tau_{cyclone}$ as illustrated in Figure 5.5.

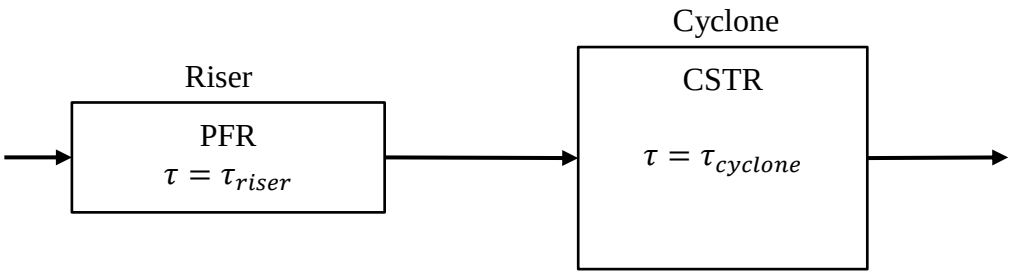

Figure 5.5: schematic illustration of reactor model setup

The residence times are calculated based on the particle free volumes of the riser and cyclone, the gas phase composition and gas flowrate from Table 5.2, and the assumed temperatures. The change in residence times as a function of temperature can be found in Appendix B.

5.2.4 Pre-study model results

The 2 experimental data sets shown in Table 5.4 are modeled using the model illustrated in Figure 5.5. To facilitate this a temperature profile in the system must be assumed. In order to simplify this a linear temperature profile of $T_{riser} = 1000 \rightarrow 900\ °C$ is assumed in the riser, resulting in a residence time of $\tau_{riser} = 0.068\ s$. While the temperature in the cyclone is assumed to be $T_{cyclone} = 840\ °C$ resulting in a residence time of $\tau_{cyclone} = 1.0\ s$.

Furthermore, it is assumed that the inlet concentration of all gas species are equal to the stack measurements given in Table 5.2 and Table 5.4 above. The results for the 2 different ammonia feed rates are shown in Figure 5.6. As seen on the graphs the majority of the conversion happens in the short timespan in the riser ending at $t = 0.068\ s$, while the cyclone according mainly acts to achieve full conversion of the ammonia according to the model. Note that of the cyclone residence time only the first 0.132 seconds are shown as the concentration is constant due to it being modelled as a CSTR.

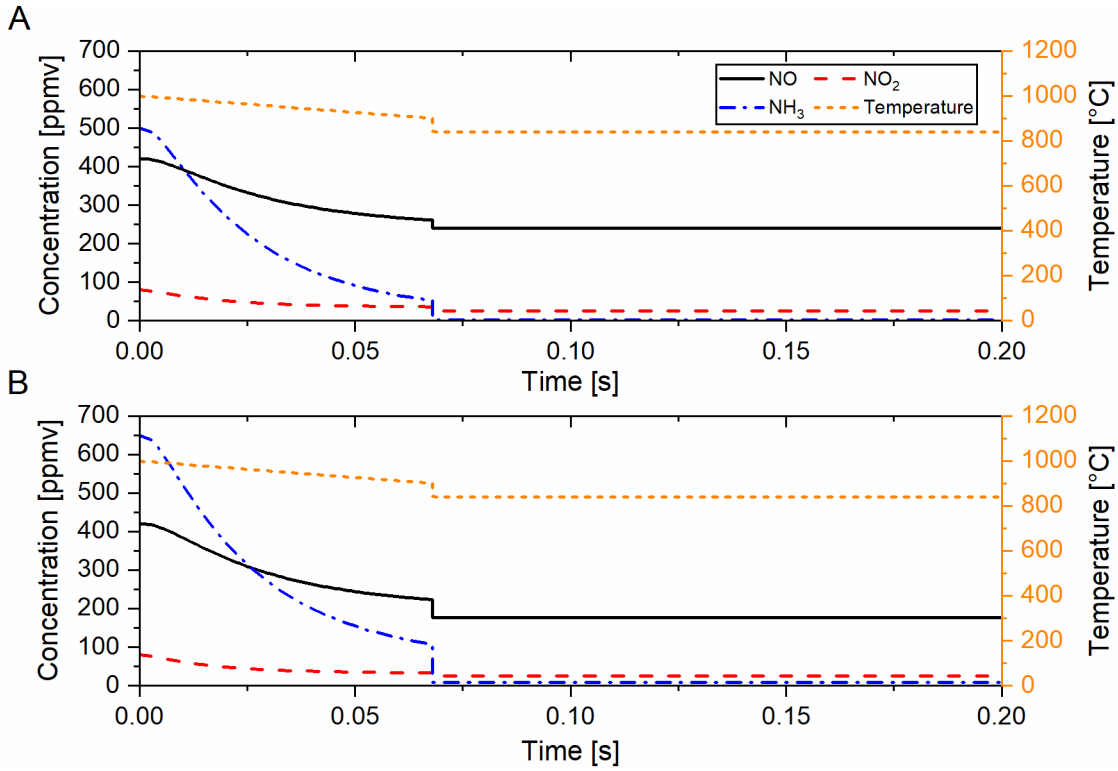

Figure 5.6: Modelled composition profiles in the SNCR zone for different ammonia feed ratios, β, A: $\beta = 1$ - B: $\beta = 1.3$, temperature profile is depicted, the residence time is $\tau_{riser} = 0.068\ sec$ & $\tau_{cyclone} = 1.0\ sec$, only the first 0.2 secs depicted

In order to evaluate the quality of the results the NO_x emission and NH_3 slip for, the model results are presented in Figure 5.7 together with the steady state results and the time corrected transient data results. To make the graph for the transient data more clear, the data has been collected in "bins" for each 5 L/h dosing of ammonia water and averaged and the standard deviations have been calculated and plotted. Note that the points for "bins" with only singular data points have been removed.

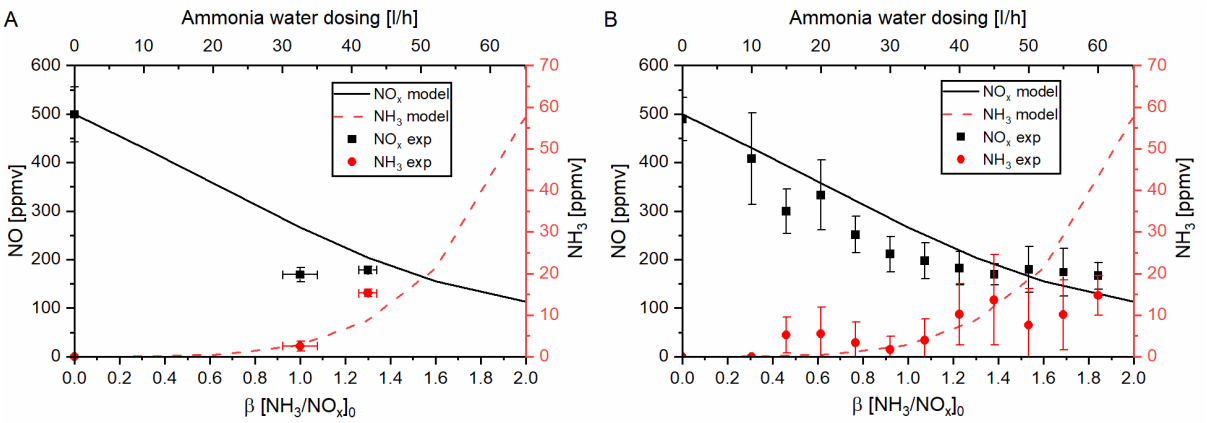

Figure 5.7: Modelled and measured NO_x and ammonia emissions for different ammonia feed ratios, and assumed temperature profile of $T_{riser} = 1000 \rightarrow 900\ °C$, $T_{cyclone} = 840\ °C$, and resulting residence times $\tau_{riser} = 0.068\ sec$ & $\tau_{cyclone} = 1.0\ sec$, A: stable measurement points B: time delay corrected results

Figure 5.7 A shows that the measured NO_x reduction level off with no further improvement when increasing ammonia feed rate from 1 to 1.3, while the model predicts this would not happen at the investigated feed rates. The ammonia slip fits well for $\beta = 1$ but after that increases more than the model predicts. From Figure 5.7 B it is seen that the measured reduction levels off before around $= 1.2$. The model results fit well with the time delay corrected transient data up until $\beta \approx 1.4$, after which the ammonia slip is over predicted. However, accounting for the problems with the ammonia data, the model most likely under predicts the actual steady state ammonia emissions connected with the used feed ratios. If taking the results for reliable, it should be possible to achieve sufficient NO_x removal without exceeding ammonia slip for feed ratios between $\beta = 1$ and $\beta = 1.3$, according to the model and both the representations of the plant data.

5.2.4.1 Sensitivity analysis

The modelling in this pre-study is based on the conditions in the riser. The sensitivity of the modeling results to the major assumptions are investigated below.

The temperatures at the inlet and the outlet of the SNCR zone in the model is based on the best estimations from the Rockwool engineers. However, the temperature is unknown between the point of particle injection and the outlet of preheater cyclone 2. To investigate the effect of the assumed temperature on the emission results, the effect of changing the temperature at the ammonia water injection point and the cyclone chamber is investigated. The temperature profile in the riser is still assumed linear, decreasing to 900 °C at the cyclone entrance, while the temperature in the cyclone chamber is assumed to be either 840 °C or 900 °C. The results for the outlet concentrations of NO_x and NH_3 are shown in Figure 5.8. From this it is evident that the model result for NO_x emission and ammonia slip is highly sensitive to the assumed temperature at the injection point, while it is only sensitive to the assumed cyclone temperature when the temperature at the injection points is below 1025 °C. Here the ammonia slip is much more sensitive to the cyclone temperature than the NOx emissions, this is caused by the behavior observed in Figure 5.6, where most of the NOx conversion occurs in the inlet section and the cyclone chamber acts mainly to convert the remaining ammonia.

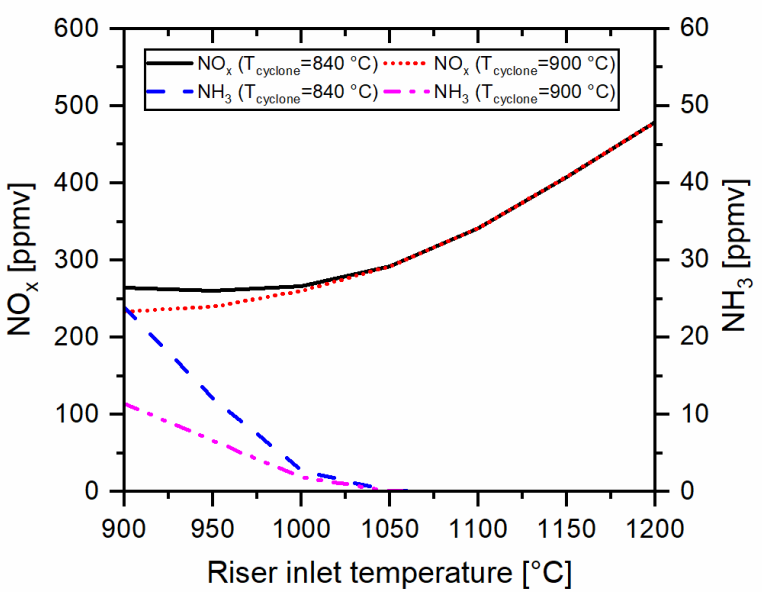

Figure 5.8: Model emission sensitivity for different riser start temperatures assuming linear decrease to 900 °C in the riser and different cyclone temperatures for $\beta = 1$, $\tau_{riser} = 0.068\ sec$ & $\tau_{cyclone} = 1\ sec$

The temperature profile in the riser is assumed to be linear with a constant cooling rate. To investigate the consequences of this assumption and the general effect of cooling rate on SNCR performance, 2 alternative riser temperature profiles is used. This is done using a fast and a slow cooling rate as well as the linear cooling rate used earlier, these are shown in Figure 5.9 B. These temperature profiles are used to model the NO_x and NH_3 emissions for different ammonia feed ratio, β, the results are given in Figure 5.9 A. The cooling rate does not have a big influence on the NO_x conversion, which seems to be mainly determined by the starting temperature, under the modelled conditions. However, the influence on the ammonia slip is quite high, and the slower the initial cooling rate, the lower the ammonia slip. This suggest that better overall SNCR performance can be achieved if the initial cooling rate is slowed.

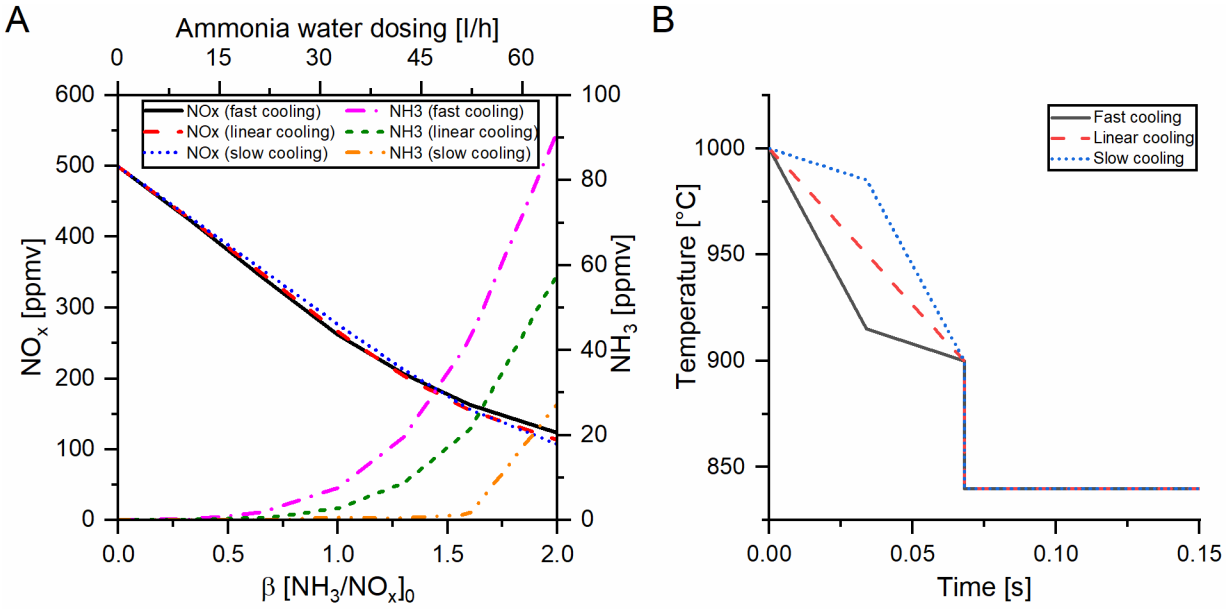

Figure 5.9: Model emission result sensitivity for different riser cooling rates τ_{riser}=0.068 sec, $\tau_{cyclone}$=1 sec A: Model emission as a function of feed ratio, β - B: Temperature profiles

The inlet CO and NO_x concentration is based on the outlet emission measurement while no ammonia is added. The measured CO concentration at the stack is likely lower than the value present at the injection point in the riser. Oxidation of CO will be ongoing under the conditions present in the system, especially in the high mixing flow in a cyclone. This might also be true for the NO_x species as unburned hydrocarbons and CO can "re-burn" and reduce NO_x throughout the system even without ammonia addition. It is known that CO has a high influence on the SNCR reactions and the effect on the modelled outlet concentrations is investigated in Figure 5.10.

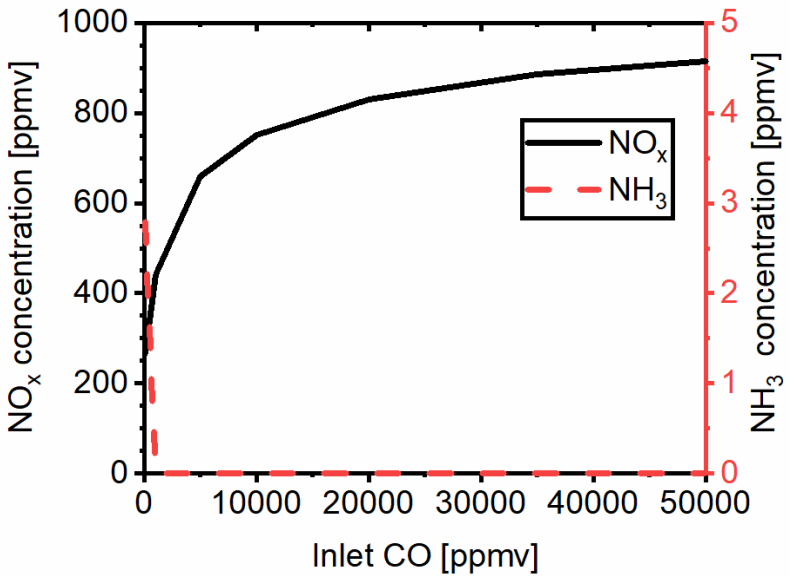

Figure 5.10: Modelled emission data for different inlet CO concentrations at $\beta = 1$ *,*$T_{riser} = [1000; 900]\ °C$, $T_{cyclone} = 840\ °C$, $\tau_{riser} = 0.06\ sec$ *&* $\tau_{cyclone} = 1\ sec$

From Figure 5.10 it is clear that the NO_x reduction is highly influenced by the CO content, and that knowing the concentrations of CO in the riser is important for accurate modelling of the process. It can also be observed that ammonia slip is completely eliminated as the CO concentration increases. Not shown in the figure is the outlet CO concentration as it was below 1 ppm in all cases and it is clear that even extremely high levels of CO in the inlet would not result in the CO measured in the stack from the raw data. This suggest either that the kinetic model is limited in its prediction of CO oxidization during SNCR or that there is a presence of unburned hydrocarbons or other phenomena contributing to the CO content measured in the stack.

5.2.5 Conclusions of pre-study

The conclusion will be divided into three parts. First conclusions are based on the analysis of the available plant data, then conclusions based on the modeling work and finally recommendations for future investigations and changes to improve the SNCR process.

5.2.5.1 Data analysis

The experimental data show large fluctuations and very few stable periods can be found. This reduces the possibility to verify the model predictions and the range of operation conditions the system can be investigated for. The transient data has been used to get a more complete picture of the influence of ammonia dosing rates. However, the results for ammonia slip are highly uncertain, due to the large time delay in stable ammonia measurements. Despite the quality of the data, the following overall conclusion can be drawn from the data:

- The time delay for the NO_x emission measurement are approximately 7 minutes while the time delay for stable ammonia measurements are 25 minutes or more
- The actuation of the ammonia water flow is much faster than the dynamics of emission measurements and highly unstable
- NO_x emissions is reduced with increased ammonia water flow. However, at feed ratio's, β, above 1 to 1.3 the added effect is insignificant
- NH_3 slip increase with increased ammonia water flow, but stays low until an ammonia/NO_x feed ratio, β, of ~1. This is also supported by the "steady state" data
- Looking mainly on the non-zero ammonia data, the ammonia slip is higher than or close to the slip limit of 40 ppm for feed ratios above 1.3
- Increased ammonia water flow increases the CO emissions

5.2.5.2 Modeling

Overall the simple reactor model and detailed kinetics captured the trend of the experimental data well. However, the uncertainty of especially the ammonia slip data should be noted. From the modeling work the following main conclusion can be concluded:

- NO_x reduction can ideally be increased slightly without exceeding ammonia slip limits
- The riser is the main reaction zone for NO_x reduction
- The cyclone chamber primarily acts to reduce the ammonia slip after close to full conversion in the riser
- The model is sensitive towards the assumed temperature and cooling rate, especially the ammonia slip
- The model is highly sensitive to the CO concentration at the injection point
- The CO concentration at injection point is different from measured value, the model cannot reproduce the CO concentration in the outlet

The sensitivity analysis shows that the results, especially for the ammonia slip are highly dependent on the temperature and composition, CO. Hence, measurement of the inlet conditions and measurements of composition and temperatures at several points in the riser and

possibly inside the cyclone, both with and without ammonia addition would be highly beneficial for further analysis.

5.2.6 Recommendations and suggestions

This section contains recommendations for increasing the reliability of the data, how to make the modelling of the cyclone preheater SNCR process more reliable and suggestions for alterations of the process that might achieve higher efficiency of the SNCR process with decreased ammonia slip.

5.2.6.1 Measurement campaign

Data for evaluation, modeling studies and process improvements should be gathered using open circuit experiments to avoid the high fluctuation in the ammonia dosing. Manual set-points for ammonia dosing, held for longer time, will achieve more stable results and will remove the insecurities caused by time delay.

In order to achieve more detailed and realistic modeling results some of the important conditions, that are unknown in the zone of interest could be measured. This includes measurements at several points in the riser, measurements inside the cyclone preheater and in the cyclone outlet. The following should be measured: temperature, NO, NO_2, NH_3, and CO concentrations with and without dosing of ammonia. Here it is important to use periods of stable ammonia injection and multiple data points without ammonia injection to give accurate background data.

5.2.6.2 Possible process alterations

This subsection describes a series of initial suggestions for alterations of the SNCR process in the cyclone preheater system. The alterations are purely based on understanding of the SNCR process, interpretation of the received data and the basic modeling work conducted in this report. There is no guarantee that any of them will work in practice and multiple of the alteration would be novel technology development.

Tuning of ammonia injection controller

The data series show that the change in emission due to the actuation of the ammonia dosing is much slower than accounted for by the controller, especially with regards to the ammonia slip. This is either due to human interference or a too tightly tuned controller. A more conservative control strategy should be implemented to achieve a better overall performance by avoiding overdosing followed by rapid decrease leading operation outside of the optimal range the majority of the time. Data from different plant operating conditions using the open circuit method suggested above might be used to tune such a controller.

Ammonia injection at increased temperature

The problems with ammonia slip can be reduced by increasing the temperature at which the reaction is initiated. This might be solved by moving the injection point closer to solid inlet, or even to the riser height as the solid inlet. Less air dilution might also help, but this might affect the operability of the preheater process due to molten particles.

Injection before solid inlet

To avoid problems with mixing caused by the dense particle flow in the riser and the limitations caused by ammonia slip, injection of ammonia water just beneath the particle feed might be considered. In order to not generate more NO_x due to the high temperature here, changing nozzles to increase the droplet size and/or lowering the concentration of the ammonia water might be needed.

Injection with solid feed

An alternative method for overcoming the mixing problems is to add the reduction agent to the particle stream before it enters the riser. This way the momentum of the particles should help ensure good mixing of reagent. The temperature if particle stream at ~450 °C should be high enough after preheater cyclone 1 to ensure fast vaporization of the reagent, but is not hot enough to initiate the SNCR reactions. Here the reagent could be either liquid (ammonia or urea in water) or solid in the form of solid urea etc. Additionally ammonia could be fed by wetting porous raw materials with ammonia water, the evaporation process would cause some time delay in the SNCR reaction.

Changing gas cooling profile

The problems with ammonia slip can be reduced by decreasing the rate of cooling of the gas phase in the riser thereby keeping high reaction rates for longer. This could be achieved either by splitting the solid feed into 2 stream and feeding part of it at a higher point. It could also be achieved by moving on of the cooling water panels from the bottom of the riser to the top of the riser.

Cyclone design changes

The ammonia slip might be caused by a small fraction of the gas stream, not yet fully reacted, going directly into the vortex finder due to lip leakage. This can be reduced by extending the vortex finder to below the lowest part of the cyclone inlet duct. This would normally increase the collection efficiency of the cyclone, but also increase the pressure drop. The effects on heat transfer efficiency in the cyclone is hard to predict.

5.3 Measurement campaign

In order to better understand and optimize the NO_x reduction by SNCR process, in the cyclone preheater system, and to find out what factors limit the performance, knowledge about the relevant conditions in the preheater section is needed. The data available in the pre-study were limited and consisted only of temperatures measured at the inlet of the preheater system and the cyclone exit, and gas composition measurements at the stack of the plant. In order to obtain more reliable data, a full measurement campaign was carried out at one of Rockwools plants. This was another plant than the one providing the original data for the pre-study. However, the general system is a similar design but with different dimensions.

Due to the high temperatures, and dense particle flows in the preheater system, accurate measurements of temperatures and gas phase composition are challenging. This section details the experimental work and methods used for the industrial measurement campaign and presents the experimental results, analysis hereof, and the main conclusions drawn from these.

Note that in the time period between the conduction of the pre-study and the measurement campaign, Rockwool had reduced the NO_x emissions through better control of the melting process, including further fuel substitution from coal to natural gas. Furthermore, the SNCR process had been improved by tuning the control system for injection of ammonia water for more stable flow ensuring even lower and more stable NO_x emissions.

5.3.1 Materials

This section describes the different equipment used during the measurement campaign.

5.3.1.1 Temperature measurement

For the temperature measurements several methods were tried, including suction pyrometer, a thermocouple array and large single thermocouples. Each of these are described below.

Suction pyrometer

To measure the gas phase temperature without errors caused by the influence of heat radiation a suction pyrometer can be used. The one used for this campaign is shown in Figure 5.11 A with a concept schematic shown in Figure 5.11 C. The suction pyrometer is 31 mm in diameter and 2.19 m in length. It consists of steel probe with an outer water cooled jacket and an inner tube for gas suction, in which a type-s thermocouple is placed through. A ceramic tip shown in Figure 5.11 B shields the thermocouple from radiative heat transfer, while allowing convective heat transfer from the gas sucked through a small opening in the side. The pyrometer need a cooling water supply and suction. The last of which is supplied by the Venturi ejector, which uses pressurized air and the venturi effect to create a low pressure facilitating suction, which can be controlled by a simple reduction valve. Due to the high solid loading in the riser and fairly large particles present, it was feared that the ceramic tip could be shattered on impact or immediately filled with particles and blocked. In order to counteract this a simple shield was made of a steel pipe to protect the ceramic tip. A picture of the suction pyrometer and the shield is shown in Figure 5.11 A and D respectively, while more technical drawings are given in Figure 5.11 B and C.

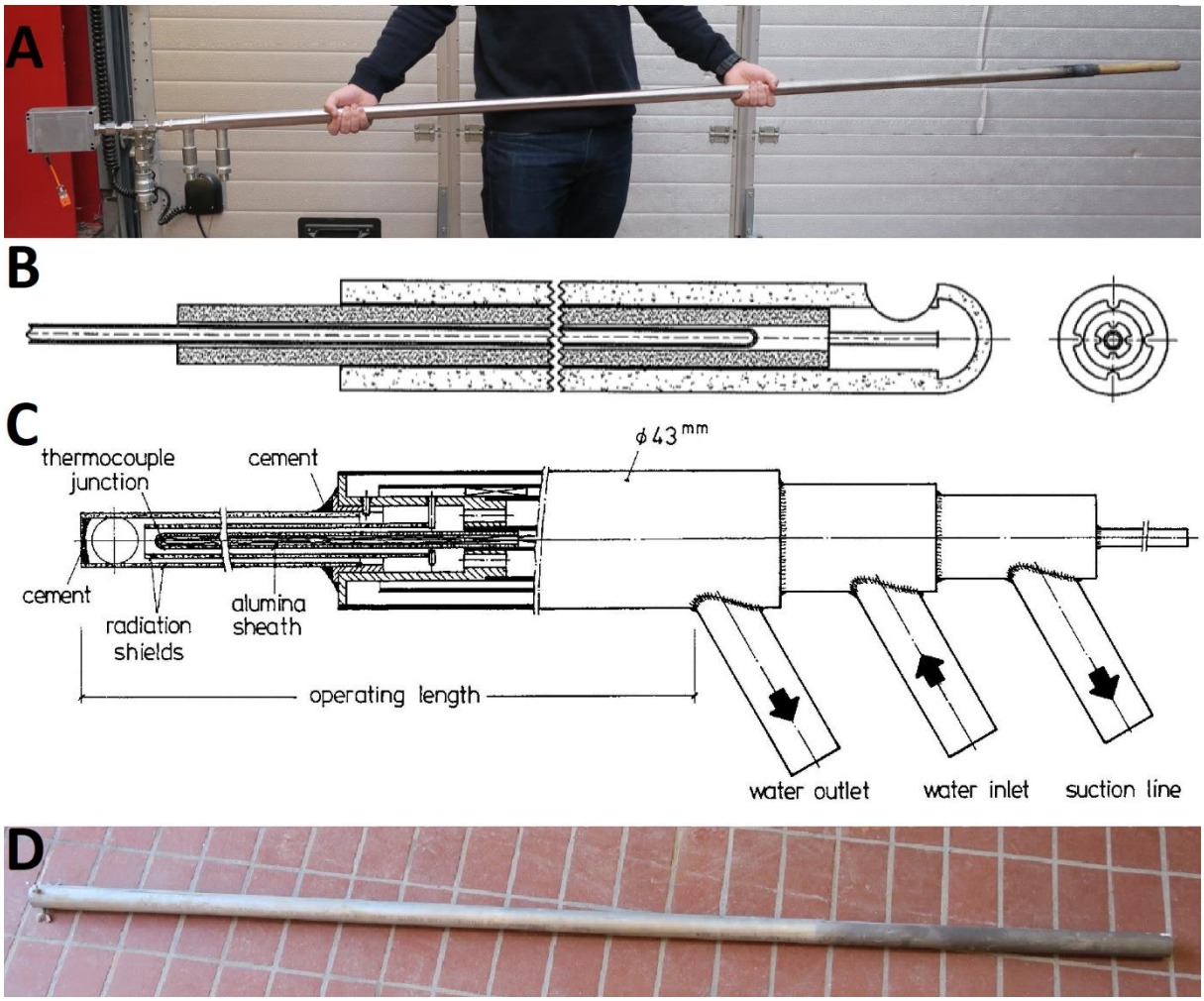

Figure 5.11: Suction pyrometer – A: Picture of the full pyrometer –B: Drawing of the ceramic tip – C: Concept schematic – D: Picture of suction pyrometer shield

Thermocouple array

As a backup to the suction pyrometer a thermocouple array was used to give several measurement points simultaneously. The thermocouple array support were built to place the thermocouples in and keep them in a fixed position during measurement. The support consisted of a V-shaped steel tray with small support struts welded across for structural strength and to hold the thermocouples. A picture of the thermocouple array assembled with both thermocouples and the support is shown in Figure 5.12. Three long Ø3mm n-type thermocouples were used, placed with their tips placed 25 cm apart.

Figure 5.12: Pictures of assembled thermocouple array

Large single thermocouples

In case the thermocouple array and the thin N-type thermocouples used with it did not work properly or broke during the campaign a couples of S- and K-type thermocouples for industrial use were brought as a back-up. One of these (k-type) is shown in Figure 5.13

Figure 5.13: Picture of large k-type thermocouple for industrial use

5.3.1.2 Gas composition measurement

The gas phase composition measurements were conducted by extracting flue gas with a suction probe and sending it through several gas analyzers. The equipment used for this is listed below:

- Gas suction probe
- Gas analyzers: ABB LIMAS 11 HW (NH3, NO, NO_2) and Fisher-Rosemount NGA2000 (CO, CO2, O2 & NO SO2) brought from DTU and a borrowed Horiba PG-250 analyzer from Rockwool
- Temperature controlled water supply
- Heated tubing and filters
- Gas conditioning unit – including pump
- Calibration gases

Gas suction probe

The gas suction probe consists of a water cooled steel probe with an outer diameter of Ø25 mm, with the inner annulus for gas flow having a diameter of Ø5 mm. The length of the cooled part of the probe is 1.70 m, while the full length is 2 m. The water for the cooling is supplied by an external pump connected via and inlet and an outlet hose. The gas annulus is connected via Swagelok fittings to the remainder of the gas system, a valve with an open connected can be used to attach pressurized air to clear blockages etc. A drawing and a picture of the probe can be seen in Figure 5.14.

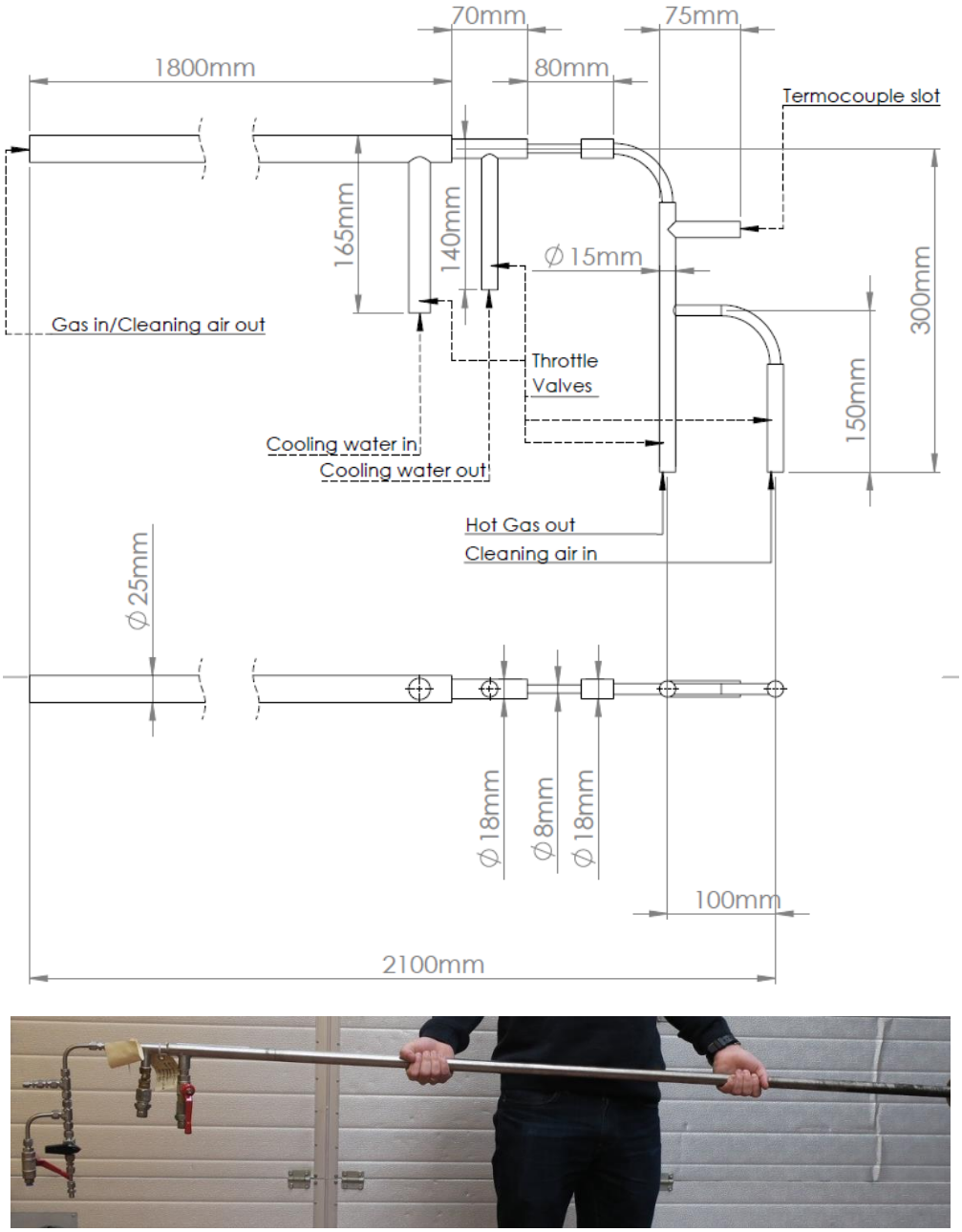

Figure 5.14: Drawing and picture of gas extraction probe

Gas analyzers

3 different gas analyzers were used for the gas composition measurements.

For the analysis of the main SNCR related species NH3, NO, and NO_2 measurements an ABB LIMAS 11 HW analyzer were initially used. This analyzer have a heated analysis chamber (70 °C) in order to measure wet gas concentrations, while avoiding condensation. The analysis method used is UV-spectrometry.

For the analysis of the background combustion gases, CO, CO_2 and O_2 a Fisher-Rosemount NGA2000 analyzer was used. This measures dry gas concentration and must therefore be placed after a gas conditioning unit. The measurement technique used is CLD (chemi-luminescence detector)

For a combined analysis of NO_x species a HORIBA-PG250 analyzer was borrowed from Rockwool Poland. This could measure various emission species, among which NO_x were measured using CLD.

Temperature controlled water supply
In order to avoid water condensation in the gas sampling probe, the cooling water used were heated to +70 °C. This was done by a heated water bath using 2 electric heating coils, a pump attached recirculated the hot cooling water from the bath to the gas extraction probe.

Heated tubing and filters
In order to avoid condensation of water from the extracted flue gas the tubing between the probe and the analyzers had to be heated. Furthermore, the gas had to pass through a fine particle filter, which also had to be heated. This was achieved through heat traced tubing and a special heat chamber for the filter housing all electrically heated and controlled to a temperature of ~80 °C.

Gas conditioning unit
Before dry gas composition measurements the water content in the flue gas had to be condensed, this was achieved in a portable gas conditioning unit, also containing the gas displacement pump used to drive the gas extraction.

Calibration gases
In order to calibrate the gas analyzer on-site, the calibration gases were shipped to location the in advance. The gasses used and their concentrations is given in Table 5.5.

Table 5.5: Gases used for gas analyzer calibration with their concentrations

Gas	Content (concentration)
Zero calibration	N_2 (100%)
Combustion gases low	CO (3800 ppm). CO_2 (3800 ppm), O_2 (4.5 vol%), N_2 (rest)
Combustion gases high	CO (4.5 vol%). CO_2 (18.9 vol%), O_2 (9.5 vol%), N_2 (rest)
NO_x calibration	NO (900 ppm) NO_2 (200 ppm) N_2 (rest)
NH_3 calibration	NH_3 (4000 ppm) N_2 (rest)

The ammonia gas was diluted with N_2 to 400 ppm NH_3 using pre-calibrated mass flow controllers.

5.3.2 Methods
This subsection describes the overall experimental procedure for the measurement campaign, as well as the individual measurement procedure for each type of measurement.

5.3.2.1 Experimental procedures
The measurements were performed during normal plant operation and the experiments had to follow the operational constraints the operator. 5 measurement series were conducted under different melting cyclone and preheater system operating conditions. For each measurement series, local temperature and gas phase composition measurements, as well as measurements

of the overall performance of the SNCR in the preheater system were performed. To the extent possible the operational conditions of the plant were kept constant during each measurement series. However, small deviations could and did occur when absolutely necessary based on operational needs of the plant. When the operation conditions were changed between series, time was given for the system to stabilize before starting the measurements. The SNCR system was manually controlled as part of the experiment, in order to achieve stable measurements of the emissions for each data point. However, the legislative emission limits could only be exceeded for a limited time in total, which meant that not all the data points had stable ammonia emissions due to the long time dynamics for ammonia.

3 different measurement positions were available in the preheater system, as access holes had been drilled prior to the campaign. The plant stack measurements make up a 4th position. The measurement position will be denoted as P1 through P4 going forward. The preheater system with the location of probe positions is shown in Figure 5.15. The probe locations has been selected based on importance with regards to future work with the results and the practical realities at the plant. P1 at the ammonia water injection point gives the inlet conditions to the system, while P2 at the preheater cyclone inlet gives the change in conditions through the riser, as well as the progress of the reactions up to this point. While P3 just above the cold raw material inlet after the preheater cyclone could be used to confirm if reaction stopped after the flue gas was quenched by the addition of the cold raw material. P4 could give the actual stack measurements which is what the plants emission limits are based on.

A summary of which measurements were conducted for the different measurement series is given in Table 5.6. Measurements series 1 was the most detailed and local composition measurements were performed in both P1 and P2, while temperature measurements were carried out in P1-P3. Due to equipment failure the composition measurements in P3 were never obtained. Measurement series 2-5 were less detailed than series 1 due to time constraints and local composition measurement were only performed in in the cyclone inlet, P2, so the reaction progress in the riser and the gas phase composition close to the SNCR system inlet could be measured. The temperature were measured in P1 and P2.

Table 5.6: Measurement matrix for the different measurement series

Measurement series		Series 1	Series 2	Series 3	Series 4	Series 5
Measurements conducted	Temperature P1	X	X	X	X	X
	Temperature P2	X	X	X	X	X
	Temperature P3	X				
	Composition P1	X				
	Composition P2	X	X	X	X	X
	Composition P4	X	X	X	X	X

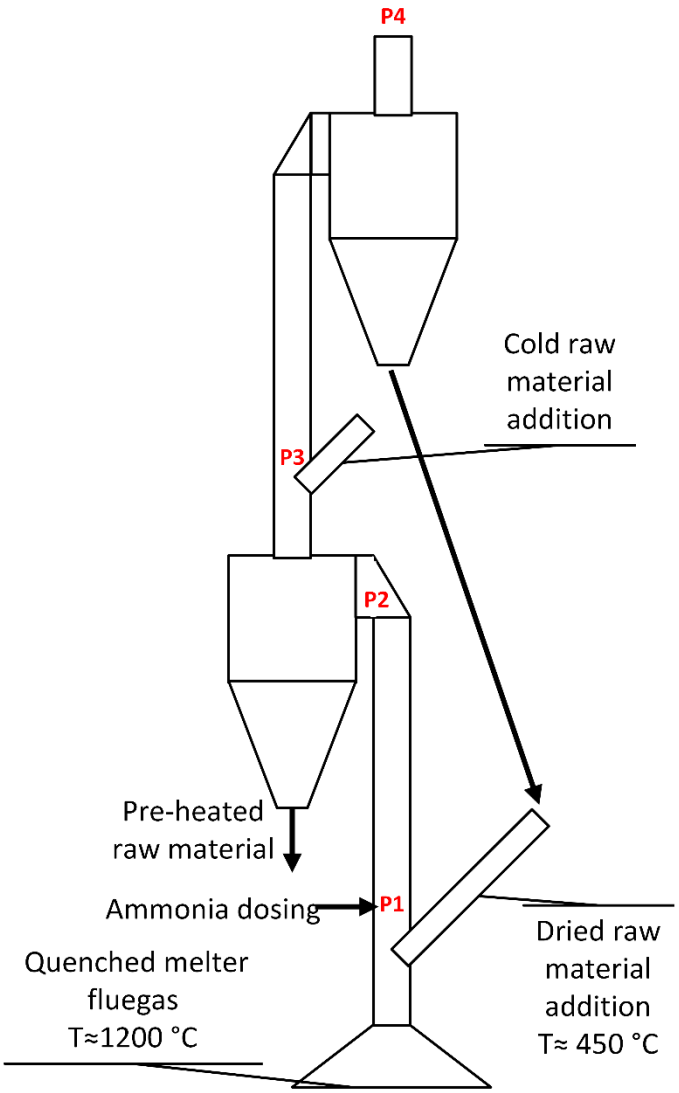

Figure 5.15: Illustration of cyclone preheater system (P1-P3 mark probe ports to be used and P4 marks the plants online stack measurement)

Temperature measurements

The original plan was to use both a suction pyrometer and thermocouples (thermocouple array) to measure the temperatures in the system in order to compare the results. However, due to the immediate failure of the suction pyrometer only the thermocouple array and single thermocouples were used.

In probe position P1 and P2 the thermocouple array were used. The thermocouples were connected to the data collection laptop and it was ensured that the thermocouple tips were in the prescribed positions. The data collection was started, after which the array was fully inserted into the probe port until touching the opposite wall. The measurement were continued until the measured temperatures had peaked and either reached stable values or started decreasing steadily due to slag buildup on the probe, at which point the array was pulled out and data logging stopped.

In probe position P3 the single type K thermocouple was used, as the thermocouple array did not fit the opening. The thermocouple was connected to the data collection laptop, the data collection was started, after which the thermocouple was inserted to the center of the riser. The measurement was continued until the measured temperatures reached stable values, at which point the array was pulled out and data logging stopped. No slag buildup occurred here, due to the much lower temperatures in this part of the preheater system.

Composition measurements.
Before starting composition measurements flow of heated cooling water were started, the heat tracing of tubing and the particle filter were turned on

For each experiment series background measurement was performed with the ammonia water dosing turned off, as well as several measurements with varying ammonia water dosing rates. First the change in dosing were made, and when stable concentration measurements were observed in the stack measurements were started. The suction probe were placed in the middle of the riser and the suction were turned on. When the measurements were stable the data logging were started.

5.3.3 Results

In this section, the experimental results and the interpretation of them will be presented in detail.

Plant operation data
During each series the ammonia dosing was changed and the effect on the NO_x emissions was measured. An example of a data series from this is shown in Figure 5.16. This shows the slow dynamics of the ammonia in the system, with ~10 minutes before the change is made to the ammonia emission change and upwards of 20-30 minutes before it stabilizes. While the NO_x stabilizes relatively fast after changing the ammonia water dosing. The results used for comparison of operation conditions and modeling are found by averaging over periods where the concentrations are stable, in case the ammonia did not reach stable conditions before a change were made no data point for ammonia concentration is recorded for the results. In some cases were a “stable” ammonia concentration might be estimated from the data based on the transient behavior after a change an approximated data point is recorded. This will be presented in a way that it is clear it is based on unsteady conditions.

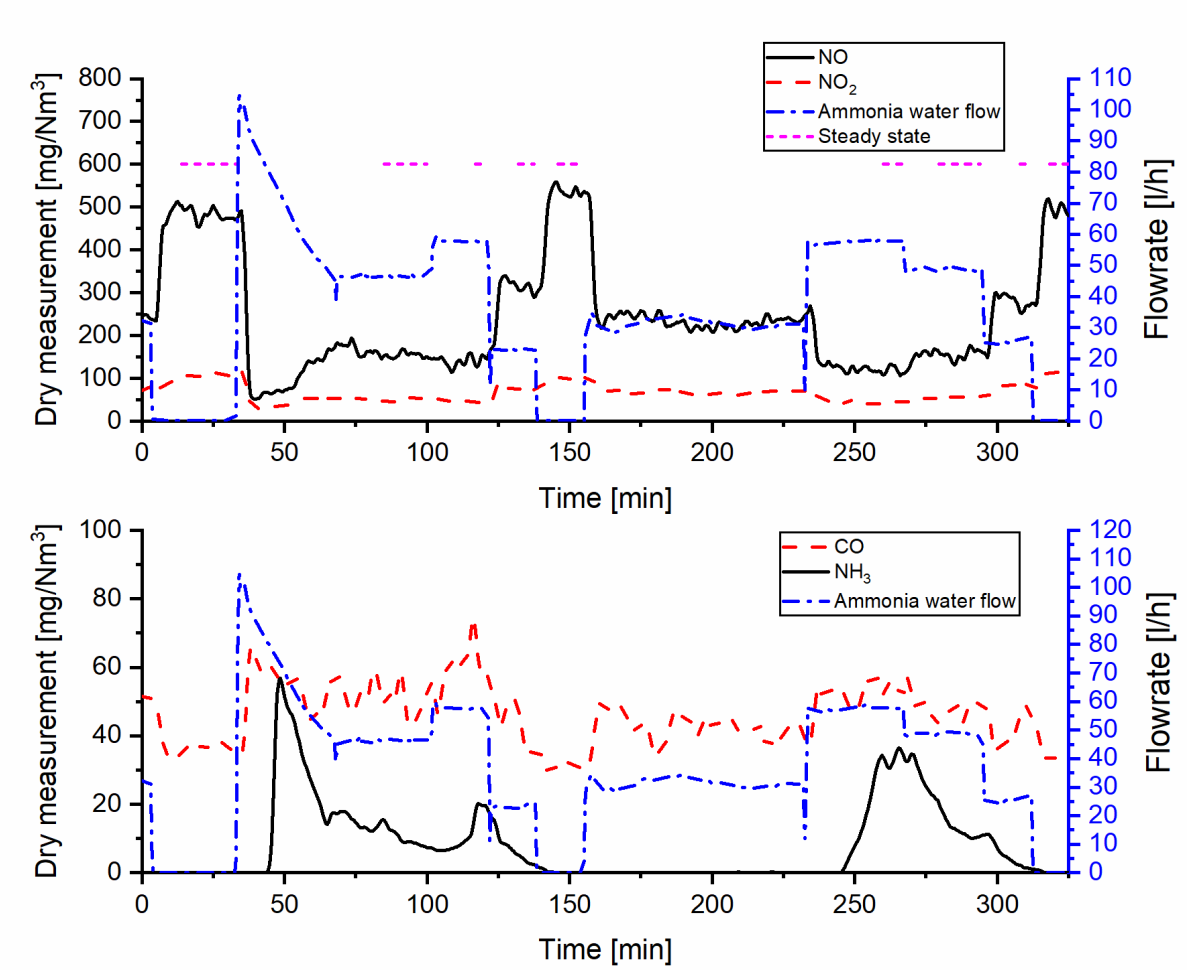

Figure 5.16: NOx and NH_3 concentration measurements in the stack with changing ammonia water dosing for measurement series 1

The main difference between operating conditions for the different measurement series were; total raw material dosing, waste fraction and the quenching air ratio measured indirectly in the flue gas amount. The operating conditions for each measurement series and the NO_X emission without SNCR active are summarized in Table 5.7. From this 2 trends can be observed. The main one is that a higher waste fraction reduces the NO_x emission, this can be observed from the difference between series 2 and all other series. This effect have also been observed by Rockwool engineers in earlier tests. The other trend is that increasing the flue gas flowrate decreases NO_x emission, even at the same raw material melting processing level. Both of these are illustrated for clarity in Figure 5.17.

Table 5.7: Overall plant operating conditions and the resulting NO_x emission and cyclone temperature

		Series 1	Series 2	Series 3	Series 4†	Series 5
Plant operating conditions	Raw materials dosing arbitrary scale [-]	0.879	0.966	0.972	0.971	0.969
	Wool waste fraction [-]*	0.342	0.156	0.309	0.309	0.284
	Flue gas flowrate at stack arbitrary scale [-]	0.938	0.748	0.981	0.955	0.845
Stack oxygen concentration [vol%]‡		15.5	13.1	15.4	15.6	14.9
NO_x Emission without SNCR	$\left[\frac{mg}{Nm^3}\right]$‡	878.5	1240.8	795.4	739.3	1035.4
	$\left[\frac{kg\ NO_x}{tonne\ melted}\right]$	1.30	1.40	1.08	1.02	1.26

* fraction of total raw material dosing

† the ratio between quenching air and combustion air/O_2 was higher for series 4 than the other measurement series to ensure lower temperatures in the preheater system

‡ Dry gas concentration

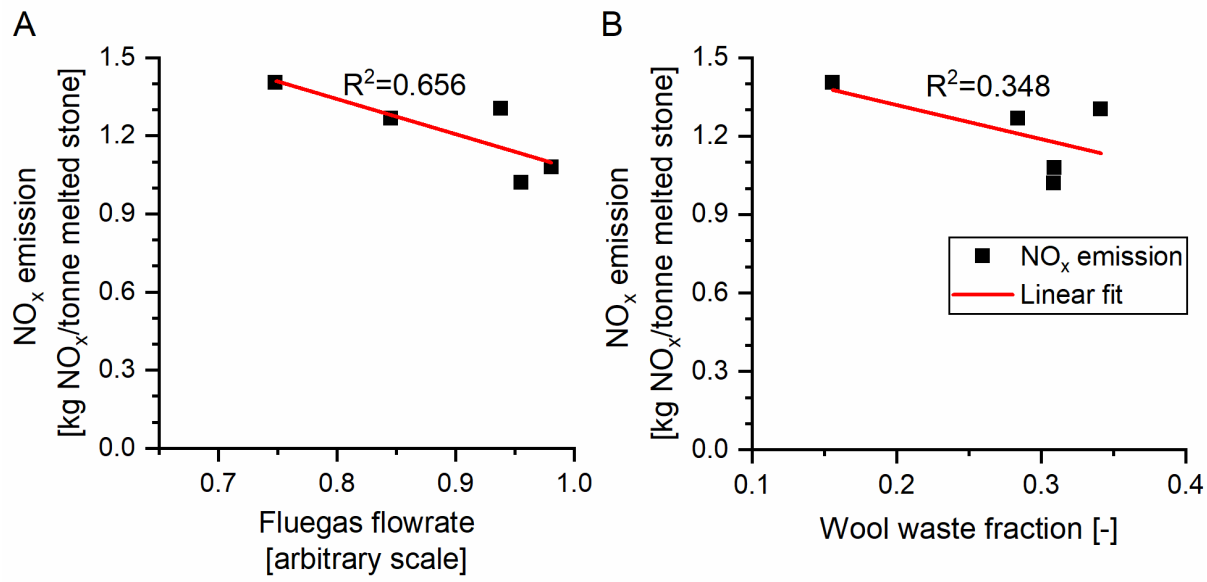

Figure 5.17: Correlation between operating conditions and NO_x emission

Temperature measurements with a suction pyrometer were quickly found to be impossible with the available equipment due to the high solid loading in the riser. Instead, the thermocouple array were used, despite the uncertainties caused by radiation and slag buildup. Figure 5.18 shows the time dependent data for the temperatures measured with the thermocouple array in the cyclone inlet for measurement series 2. After the initial heat up of the probes and holder, both small scale fluctuations as well as a large drop before rising steadily and dropping again can be seen. The large drops occurred due to buildup of slag on the probes and were un-avoidable with the method used. N-2 which were the middle thermocouple shows, after the

initial heat-up, consistently the highest temperature. This is due this being the thermocouple closest to the center of the flow, while the 2 other thermocouples are closer to each wall. From this graph the maximum temperature measured were taken as the temperature result for this position in the measurement series, as colder temperature were due caused by slag build-up. However, it is clear that there is a high degree of uncertainty due to the fluctuations and due to the fact that it's a high temperature system with colder particles in which high radiation influences can be expected and it is measured with thermocouples and not a suction pyrometer or other method.

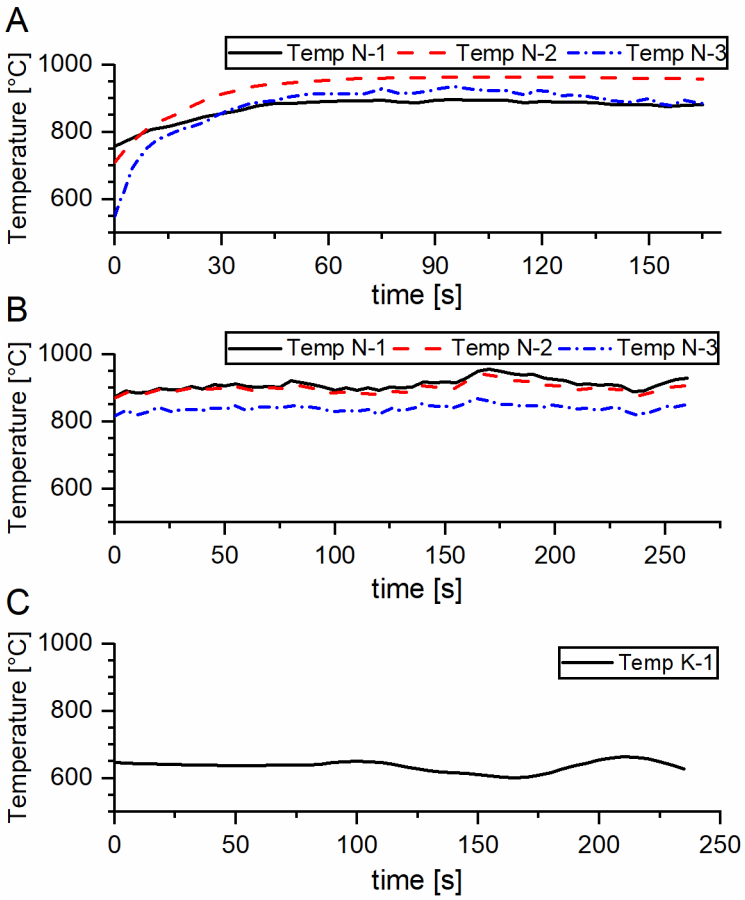

Figure 5.18: Temperature measurement data from measurement series 1 –A: ammonia water injection point P1 – B: Cyclone inlet P2 – C: cold raw material feeding point P3

The other temperature data were similar and treated in the same manner. For the cyclone outlet temperature the plant data were used and an average over the whole period of a measurement series were used instead. From Table 5.8 it can be observed that in most cases the temperature in the riser is measured to be around 950 °C at the cyclone injection point except for series 4 where it is measured to 922.2 °C. The measured temperature falls around 10-50 °C between the injection point and the cyclone inlet, with the exception of measurement series 3 and 4. The low measured change in temperature, and the fact that series 3 shows an increase, shows that the measurement using thermocouples is imprecise and that several measurements should be done for an measurement series to at least get reliable data. The low change in temperature is likely caused by the influence from radiation from the cold particles, which would be stronger

at the injection point than at the cyclone inlet, where the gas has partially cooled and the particles partially heated. Additionally, the tendency of slag buildup were more severe at the injection point as compared to the cyclone inlet, likely due to the presence of small amounts of molten droplets carried over from the melting cyclone. Despite the shortcoming of the measurement method the consequence of the measurement methods can clearly be seen in that fact that series 4, which is the one with higher quenching rate and lower burner load compared to the other series, shows significantly colder temperature measurements across the board.

Table 5.8: Summary of temperature measurement results

Measurement series	Injection point (position 1) temperature [°C]	Cyclone inlet (position 2) temperature [°C]	After raw material addition (position 3) temperature [°C]
1	963.3	955.2	664.4
2	954.4	940	-
3	940.2	946.3	-
4	922.2	852.2	-
5	956.6	906	-

The overall SNCR performance during the different measurement series is shown in Figure 5.19, detailing the stack measurements of NO_x, NH_3, and CO at different ammonia dosing stoichiometric ratios, β. Overall the NO_x concentration is progressively reduced as ammonia dosing is increased in all cases, while ammonia slip is detected at stoichiometric ratios above $\beta \approx 1$ depending on the measurement series. The NO_x concentration seems to flatten out at a level of 200 mg/Nm^3. Another observation is that as ammonia dosing increases, the CO emissions from the stack also increases, as also observed by Ljungdahl & Larfeldt [98] who suggested that it is caused by the competition for radicals needed for the SNCR process and the CO combustion [98].

The results for measurement series 1, the most extensive measurement series, seen in Figure 5.19 A, have the most data points and had stable ammonia measurements for most of the data points. Under the operating conditions it is possible to achieve NO_x emission 300 mg/Nm^3 with ammonia slip at 10 mg/Nm^3, which are both below the limits, at a stoichiometric feed ratio of around $\beta = 1.6$, corresponding to ammonia water dosing rates around 45-50 L/h. The ammonia slip breakthrough seems to roughly occur at a stoichiometric ratio, β between 1 and 1.5, the exact value being unknown. Although from the data in Figure 5.16 it can be observed that no ammonia slip is detected at a dosing rate of ~35, (period 160-230 minutes, where automatic control had been activated), which corresponds to roughly $\beta = 1.2$. Similar trends as those observed for measurement series 1 can be seen in measurement series 2-5 shown in Figure 5.19 B-E. For all measurement series the current NO_x emission limits can be reached at a stoichiometric ratio of around 1.5. It cannot be seen if the ammonia slip limit would be exceeded under stable measurements at these points and the breakthrough point for ammonia slip cannot be found for any of these from the data, as the stable data points for ammonia emissions are few. However, from the estimated data from unstable conditions it seems that for

series 2 and 3 the ammonia limits could be kept with no problem, even with the high initial NO_x emissions for series 2. For series for 4 it is highly unlikely, that the ammonia slip would not exceed the limits, this is likely caused by the lower temperature in the preheater system. Based on both the NO_x emission without SNCR and the achievable concentrations it seems that the operating conditions of series 1 and 3 are the optimal conditions reducing NOx emissions. While series 4 have lower "raw" emissions the low temperatures causes insufficient NO_x removal with SNCR without exceeding ammonia emissions limits.

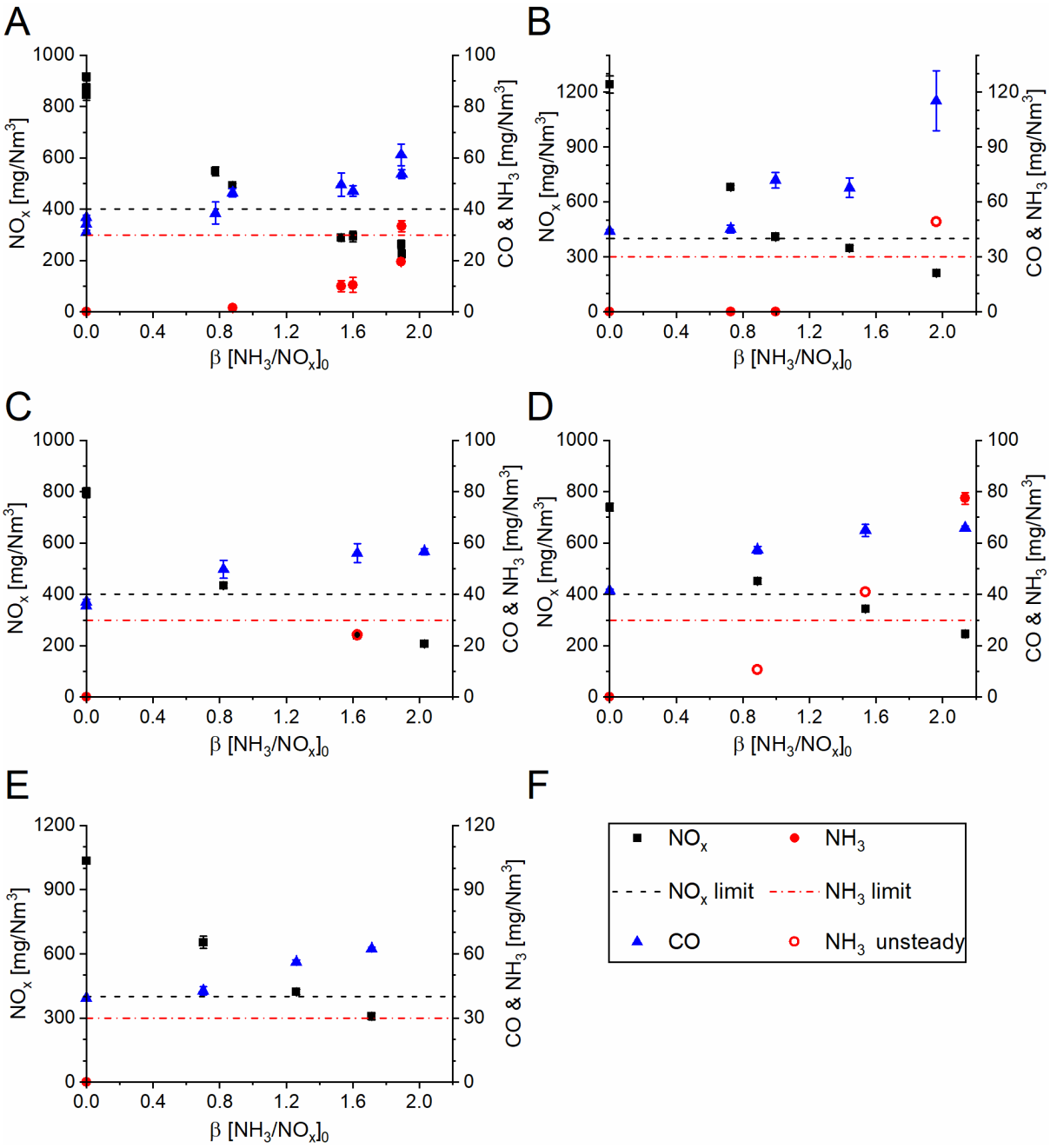

Figure 5.19: NO_x, NH_3 and CO emissions at different ammonia dosing rates for the different measurement series – A: measurement series 1 – B: measurement series 2 – C: measurement series 3 – D: measurement series 4 – E: measurement series 5 – F: legend

The measurement of the gas phase compositions inside the riser system were problematic due to leaks in the measurement equipment and the gas analyzer borrowed on-site for series 2-5.

Furthermore, the local ammonia concentration could not be measured due to cross sensitivity with the high SO_x content in the flue gas. However, assuming that the measurements during the period of each measurement series were subject to a constant error caused by the dilution, the local measurements relative difference during changing ammonia dosing can be used to analyze the behavior and in conjunction with the stack measurement to calculate absolute values for use in the modeling. The relative NO_x concentration to when SNCR is turned off is shown for the stack measurements (position 4) and the cyclone inlet (position 2) measurements in Figure 5.20.

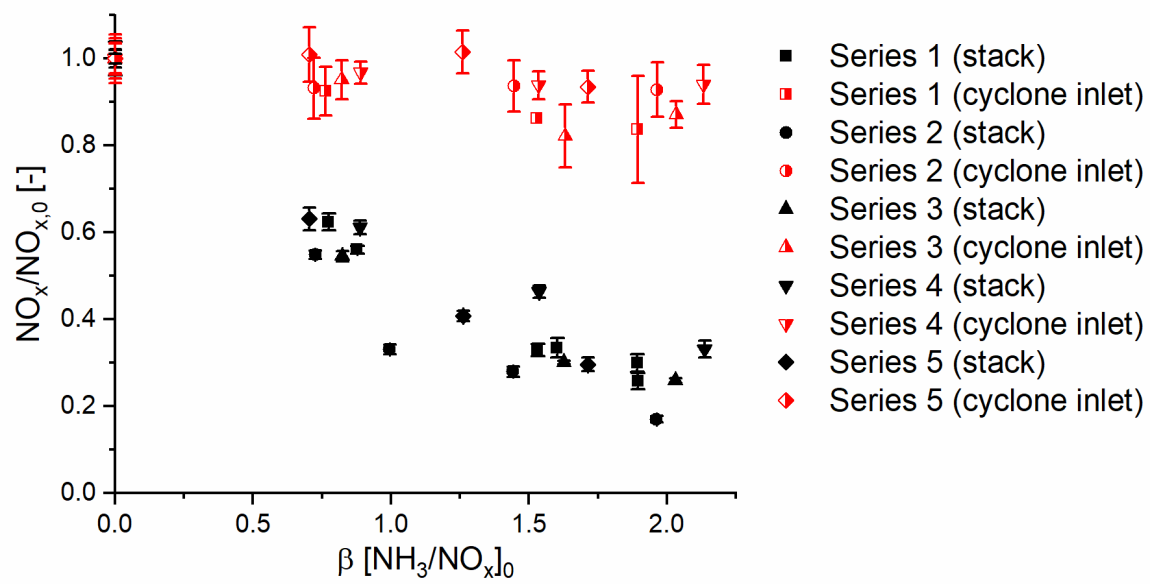

Figure 5.20: Relative NO_x concentration measured in the cyclone inlet and in the stack during SNCR for all measurement series

From Figure 5.20 it can be observed that little to no NO_x conversion occurs in the riser, before the cyclone inlet. The model work in the pre-study based on data from another Rockwool plant showed, that most of the NO_x reduction should have occurred in the riser with only a small change in the cyclone itself. This model work assumed perfect mixing at the injection point, which might explain the discrepancy. The delay in NO_x conversion can be caused by insufficient mixing, long droplet evaporation time for the injected ammonia water or alternatively by catalytic activity from the solid raw material favoring the oxidizing pathway at high temperatures, thereby causing a small to negligible selectivity towards NO_x reduction in the riser. However, most likely it is caused by poor mixing of the ammonia into the bulk gas due to the dense solid loading in the riser. Interestingly the relative NO_x removal for all the measurement series, despite operating conditions is quite similar with the same stoichiometric ratios.

Using the measured flue gas flowrates in the stack and the riser between preheater cyclones, the measured concentrations in the stack an in the riser the concentrations in the riser at the injection points when no SNCR is active is calculated based on the average data. To do this for dilution with both water from the moisture in the raw material and air in the riser and in the gas analysis equipment was accounted for the results are summarized in Table 5.9.

Table 5.9: Calculated gas phase composition at the ammonia water injection point, CO2, O2, H_2O and NO_x is based on stack measurements corrected for dilution in the system, CO is based on local measurements and corrected for dilution by the leak in measurement equipment

Measurement series	N2 Vol%	CO2 Vol%	O2 Vol%	H2O Vol%	CO [ppm]	NO [ppm]	NO2 [ppm]	NOx [ppm]
1	51.07	13.36	9.021	26.55	54.48	546.1	62.14	608.3
2	50.52	16.69	6.056	26.73	167.21	763.3	95.18	858.5
3	50.35	13.25	8.876	27.53	31.46	510.8	45.29	556.1
4	50.96	13.22	9.242	26.58	39.32	475.2	39.58	514.7
5	50.05	14.76	8.460	26.73	33.98	659.3	65.08	724.4

5.3.4 Experimental experience

The suction pyrometer cannot be used in an environment with that high particle loading, even with the impact shield jacket the ceramic tip shattered before even 1 temperature measurement could be made performed. Furthermore, the use of thermocouples gives a significant measurement error due to radiation and uncertainty due to the slag buildup. Better methods must be considered for temperature measurement. A simple way to improve the thermocouple measurements could be to have the thermocouples supported in a way so they are not placed in a tray like pocket, which possibly worsen the slag buildup. This will however, not solve the problem of radiation influence. Another method could be to use optical temperature measurement methods, which should be possible due to the high water content in the gas [146].

From the gas phase composition measurements an obvious conclusion is that a gas analyzer not cross sensitive to Sulphur should be used. Furthermore, it would be beneficial to have a somewhat rugged portable gas analyzer for NO_x and ammonia measurements. On the positive side, despite initial fears of fast clogging of the gas suction probe due to the dense particle loading in the riser it worked without issue for long and could be easily cleared when it finally clogged. The low flowrate ~1 Nl/min needed for gas analysis meant that the relatively large particles with a high velocity did not get sucked into the probe. When it finally clogged it was due to a tar like substance, likely from the combustion process.

5.3.5 Summary of experimental findings

From the experience and observations during the measurement campaign several conclusion and suggestions can be made for any future industrial experimental campaigns in the same or similar conditions.

From the stack emissions datasets it is clear that the dynamics of the system is very slow for ammonia, which should be accounted for in any future measurement campaign especially if reliant on stack measurements.

The raw NO_x emissions for different operating conditions show that high wool waste dosing and high flue gas flowrate decreases the NO_x coming from the melting cyclone. While high quenching air reduces the temperatures in the preheater systems. In order to optimize the SNCR process and achieve lowest possible NO_x emissions, the cyclone melter operating conditions

should ensure low initial NO_x formation, as high initial NO_x requires higher ammonia dosing to achieve the emission limits, which increases the ammonia slip. Furthermore, the temperature in the preheater zone should be kept sufficiently high, by controlling the quenching air addition, as low temperature in the preheater system gives problems with SNCR due to ammonia slip.

From the local gas composition measurements during SNCR it is observed that close to no conversion of NO_x occur in the riser. This is most likely due to severe mixing limitations in the riser from the ammonia injection point to the cyclone. Optimizing the injection method possibly help improve the SNCR performance. However, this have already been investigated by Rockwool.

5.4 Modeling industrial measurements

The modeling in this work is based on simple reactor models and detailed reactor kinetics. This report will not include a detailed investigation of the choice of various model assumptions and parameters, or a detailed sensitivity study, as that have already been reported in earlier work. Instead this work will include the model results of the SNCR process based directly on the input parameters from the industrial campaign. Even though this input comes with a certain degree of uncertainty as discussed in the experimental report, and the model itself has inherent uncertainties, the comparison between model and experimental result yields valuable insight into the behavior of the system and possibilities for optimization of both the practical SNCR system, the experimental methods and the models.

5.4.1 Kinetic model

To model the reaction the latest version of the detailed NO_x chemistry mechanism published by Glarborg et al. [97]. These kinetics are not optimized for any certain conditions, which in some cases could mean other models would give better results for the specific conditions they have been fitted under, at the cost of lack of flexibility and validation under vastly different conditions. The conditions in the preheater system vary significantly from many other SNCR systems due to the dilution of flue gas with quenching air (higher oxygen content) and the higher water content due to the use of natural gas and oxyfuel combustion. Therefore it is best to use a robust model that are not just fitted to very specific conditions. One thing to note though is the models tendency to overestimate the influence of water concentration on the temperature window for SNCR [97].

5.4.2 Reactor model

The model investigations in Chapter 4 have shown that the difference between the 2 simple reactor models PFR/CSTR, only have a minor influence on the results compared to the parameters with the highest influence, gas phase composition and temperature. Since the temperature measurements have a high degree of uncertainty, using a PFR with a temperature profile based on the available measurements to describe the whole system, is deemed optimal. As it is simpler and better than using PFR for the riser and CSTR for the cyclone having to assume a fixed temperature in the cyclone.

5.4.3 Mixing

Unless otherwise noted in the results, the modeling is performed with the assumption of perfect mixing at the injection point.

In order to investigate the influence of mixing from a modeling standpoint, the simple mixing model based on pseudo species of the main reactants NH_3 and NO introduced in Chapter 4 section 4.1.3 is used in part of the modeling.

Two different values of the mixing rate constant, $K_{mix} = 50$ and $K_{mix} = 25$, are used corresponding to mixing times of $t_{mix} = 0.12\ s$ and $t_{mix} = 0.24\ s$, defined as the time where 95% is mixed i.e. converted into its reactive forms, NO and NH_3 .

5.4.4 Model conditions

The time dependent temperature profiles in both parts of the reactor are assumed to be linear and the residence time is calculated based on the resulting mean temperature in each part; the flue gas flowrate; and the volume of the riser, between injection point and cyclone inlet, and in the cyclone in the specific plant. The correlations for residence time as a function of temperature in both the riser and the cyclone can be found in Appendix B. The reactor conditions for each measurement series are given in Table 5.10.

Table 5.10: Reactor conditions for modelling for each measurement series

Measurement series	series 1	series 2	series 3	series 4	series 5
Measured injection point temperature [°C]	963.3	954.4	940.2	922.2	956.6
Measured cyclone inlet temperature [°C]	955.2	940	946.3	852.2	906
Assumed cyclone outlet temperature [°C]	859.4	865.2	855.8	834.1	858.9
Riser mean temperature [°C]	959.3	947.3	943.3	887.2	931.3
Cyclone mean temperature [°C]	907.3	902.6	901.0	834.2	882.4
Riser residence time [s]	0.09672	0.1311	0.09243	0.1001	0.1102
Cyclone residence time [s]	0.4030	0.5427	0.3819	0.4135	0.4575

Each measurement series are modeling using ChemKin 17.1, with the reactor conditions in Table 5.10 and the gas phase concentrations given in Table 5.9. Furthermore, all NO_x is assumed to be NO at the injection point. The initial ammonia concentration is varied to correspond to the stoichiometric ratio, $\beta, \left[\frac{NH_3}{NO}\right]_0$.

5.4.5 Results

The model results for all the experimental cases are plotted together with the experimental results in Figure 5.21 where NO and NO_2 is summed to NO_x. The unsteady ammonia results have been added to the figure, where available and should only be used as a rough estimate, rather than a measured result.

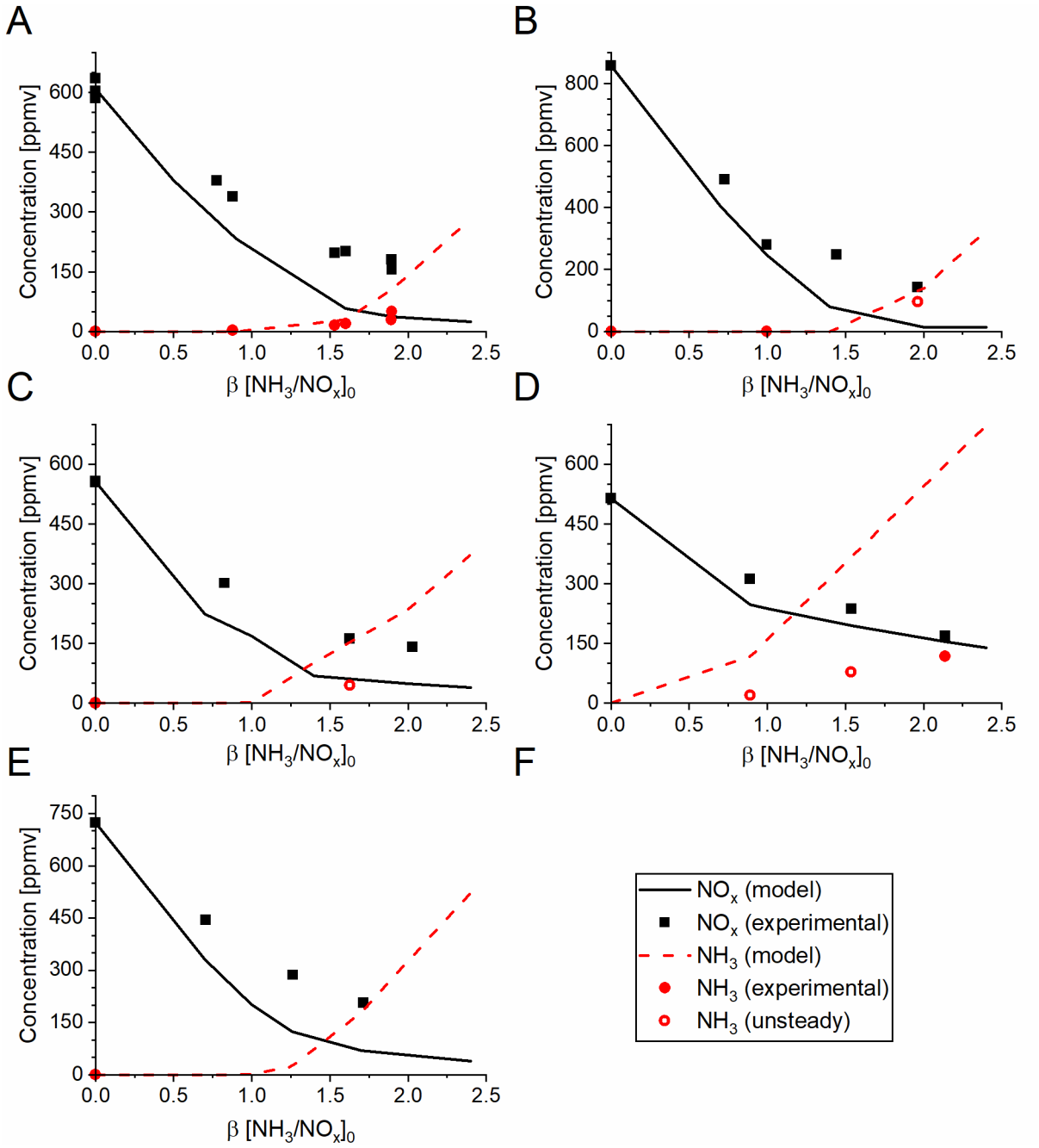

Figure 5.21: Model and experimental results for NO_x and NH_3 concentrations in the cyclone preheater system during SNCR for the different measurement series – A: measurement series 1 – B: measurement series 2 – C: measurement series 3 – D: measurement series 4 – E: measurement series 5 – F: legend

From the results for series 1 shown in Figure 5.21 A, it can be observed that the qualitative trend of the experimental results is well predicted. This includes both the decreasing NO_x emission with increased ammonia water dosing, which starts to flatten out between stoichiometric ratios of 1.5-2 as well as an accurate prediction of the breakthrough point for the ammonia slip. However, the selectivity for NO reduction is over predicted over the entire range as the predicted NO_x emissions are too low and the ammonia slip at $\beta = 1.8$ is too high. If this is due to; the unrealistic ideal mixing assumption, the measured temperatures being colder than the true gas phase temperature, un-accounted for surface activity of the solid raw material, general inaccuracy of the reactor or kinetic models, or a combination of several

reasons is unknown. However, it is likely a combination of mixing limitations and underestimated temperatures.

Similar observations can be made about the model predictions of the experimental results for measurement series 2, 3, and 5 shown in Figure 5.21 B, C, and E as were made for series 1. The trends are well predicted, but the NO_x reduction is over predicted. The ammonia slip breakthrough and its magnitude can only be compared with the unsteady estimate, for series 2 it seem to fit well, while it seems slightly overestimated for series 2. For measurement series 5 no ammonia data is available for comparison.

The model results for measurement series 4 in Figure 5.21 D gives a very good fit for the NO_x reduction both qualitatively and quantitatively, with much lower conversion caused by the low reactor temperature compared to the other cases. However, the ammonia slip is highly over predicted, much more so than in for series 1.

In the composition measurement results for the riser it was seen that the extent of NO_x reduction at this point was very low in all the measurement series as compared to the outlet measurements. In order to compare this with the model results, the modeled transient concentration profiles are plotted together with the measurement results for measurement series 1, for stoichiometric ratios $\beta = 0.9$ and $\beta = 1.6$. This can be seen in Figure 5.22. From this it is clearly seen that with the assumptions used in modeling the majority of the NO_x conversion should have occurred in the riser section up to $t \approx 0.1\ s$. As the temperature in the riser is more likely lower in the model than in the true gas temperature this is not caused by a too high temperature assumption. Most likely this is caused by either slow evaporation of the ammonia water droplets or bad mixing of the evaporated ammonia and the bulk gas.

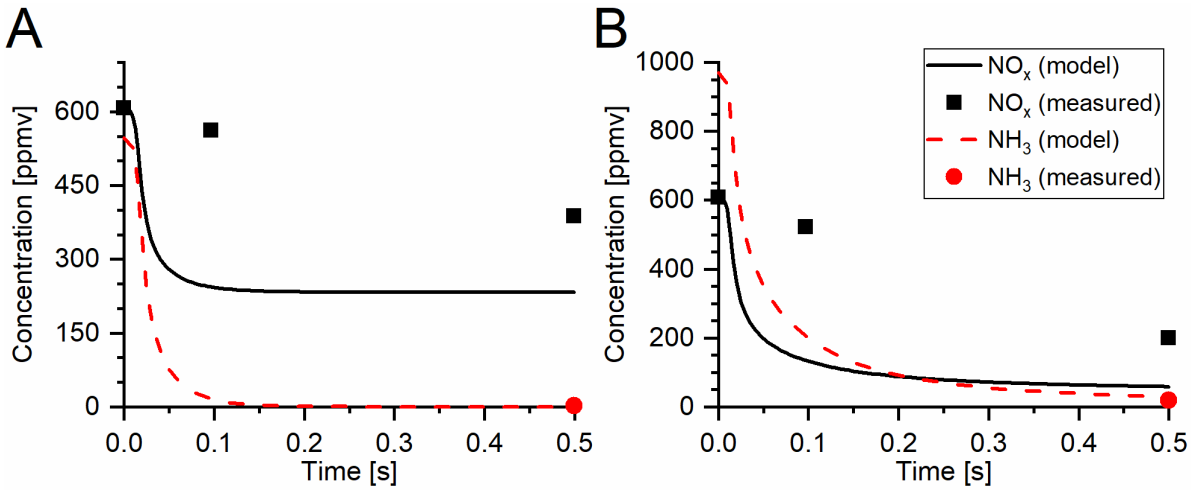

Figure 5.22: Transient model results for NO_x and ammonia concentration for measurement series 1 at stoichiometric ratios of A) $\beta = 0.9$ B) $\beta = 1.6$

In order to investigate the effect of mixing through modeling, the mixing model is used to simulate the same cases. The result of this is shown in Figure 5.23. From this it can be seen that the model results for NO_x at both the cyclone inlet and outlet are better for the mixing model, as the NO_x reduction is over predicted without mixing, and the mixing model results in delayed conversion and overall lower conversion. The mixing model with a mixing rate

constant of $K_{mix} = 25$, corresponding to a mixing time of $t_{mix} = 0.24\ s$, predicts the cyclone inlet NO_x concentration correctly. However, the outlet concentration is still under predicted. For a stoichiometric ratio of $\beta = 1.6$, in Figure 5.23 B, the ammonia slip prediction is worse for the mixing model. This supports the hypothesis that the low conversion in the riser is caused by mixing limitation, while the temperatures in the system is higher than measured. Both would increase the predicted NO_x emissions while an increased temperature would increase ammonia conversion.

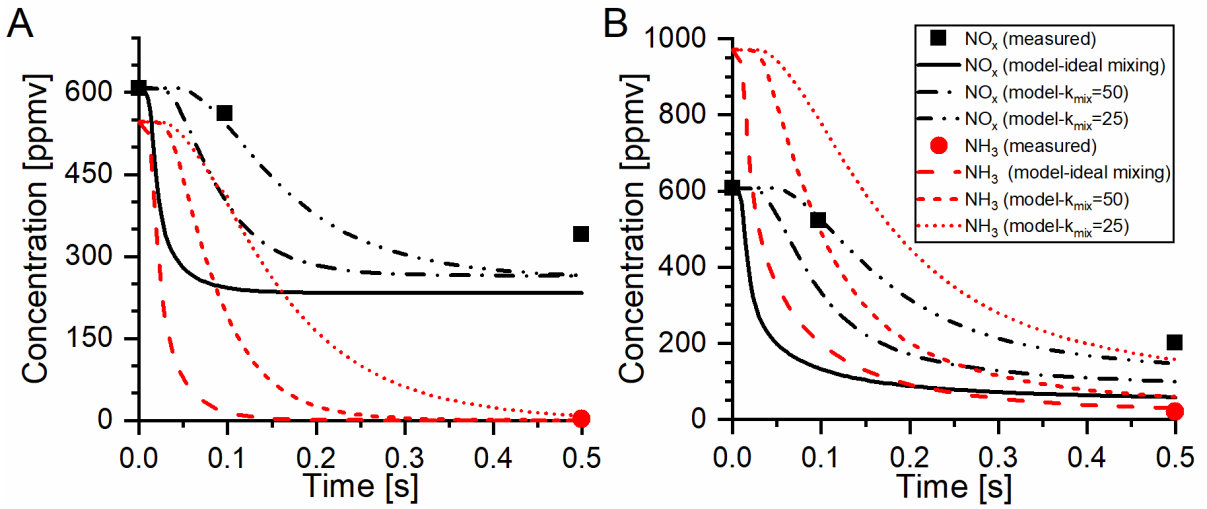

Figure 5.23: Transient model results with and without mixing for NO_x and ammonia concentration for measurement series 1 at stoichiometric ratios of A) $\beta = 0.9$ B) $\beta = 1.6$ Reactor conditions in Table 5.10

Based on the discussion above, the effect of mixing alone cannot explain the difference between the model predictions and the measurement. As discussed earlier there is a large uncertainty in the temperature measurements and the temperature profiles. Hence, the effect changing the temperature profile in the model is investigated. A higher gas temperature, 1000 °C, than the measured is assumed at the injection point, thereby accounting for the influence of radiation the cold particles have on the measurements. For the cyclone inlet, a temperature close to the measurements is assumed, 950 °C, as the gas would have cooled and the particles would have heated, reducing the error from radiation. A higher temperature than previously assumed in the cyclone is used, at 900 °C. The profiles between these points is assumed to be linear with residence time, and the residence time is calculated based on the average temperature. The temperatures and the resulting residence times are summarized in Table 5.11.

Table 5.11: Alternative temperatures and residence times for modeling measurement series 1

Injection point temperature [°C]	Cyclone inlet temperature [°C]	Cyclone outlet temperature [°C]	Riser mean temperature [°C]	Cyclone mean temperature [°C]	Riser residence time [s]	Cyclone residence time [s]
1000	950	900	975	925	0.0955	0.398

The transient results for the alternative temperature profile, given in Table 5.11, for $\beta = 0.9$ and $\beta = 1.6$ are shown in Figure 7.4 A and B, respectively. From Figure 7.4, the same behavior

as with the transient profiles for the original temperature profiles in Figure 5.23 can be observed. The highest mixing time predicts the NO_x concentration at the cyclone inlet, while all the models over predict the NO_x reduction through the rest of the system, although to a lesser degree than with the original temperature profiles. The NH_3 slip at high dosing ratio, $\beta = 1.6$, is over predicted for the with the high mixing time model, $k_{mix} = 25$, (which predict the delay correctly) and under predicted with no mixing implemented, while the intermediate mixing model, $K_{mix} = 50$, fits well.

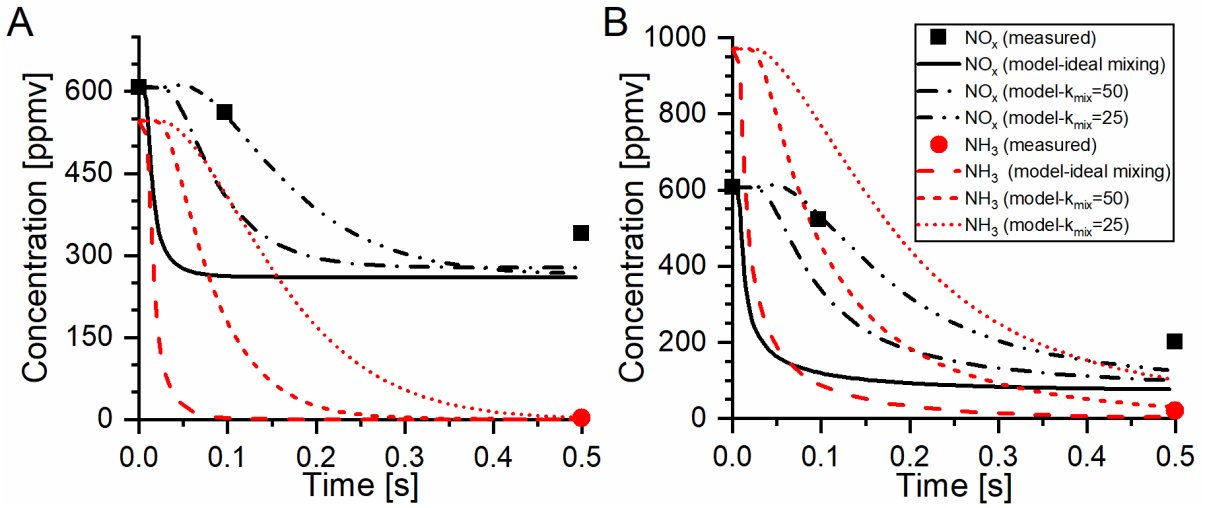

Figure 5.24: Transient model results with and without mixing for NO_x and ammonia concentration for measurement series 1 at stoichiometric ratios of A) $\beta = 0.9$ B) $\beta = 1.6$ Reactor conditions in Table 5.11

The outlet concentrations of NO_x and NH_3 for the two temperature profiles with and without the mixing model implemented are shown in Figure 5.25 A and B for the original and new temperature profiles given in Table 5.10 and Table 5.11 respectively. Comparing the two it is clear that the outlet results fit the experimental results better for the elevated temperature profile in Table 5.11, compared to the temperature profile based on measurements in the riser, given in Table 5.10. This is true for both the NO_x outlet concentration, which have increased due to the higher temperature, and the NH_3 slip which have decreased for the same reason. The NO_x reduction is still over predicted for all tested models, with the elevated temperature, but less so compared to the original. While the ammonia slip is now well predicted at high stoichiometric ratio's without mixing and over predicted with mixing. The improved predictions with the changed temperature profile and the fact that predictions of ammonia can be above and below the experiments with the mixing model, shows that some combination of temperature profile and simple mixing model could replicate the measured outlet concentrations. This supports the previous stated hypothesis' that the temperature in the riser is higher than measured, due to measurement error, that the cyclone temperature is higher than first assumed, and that there are severe mixing limitations in the riser.

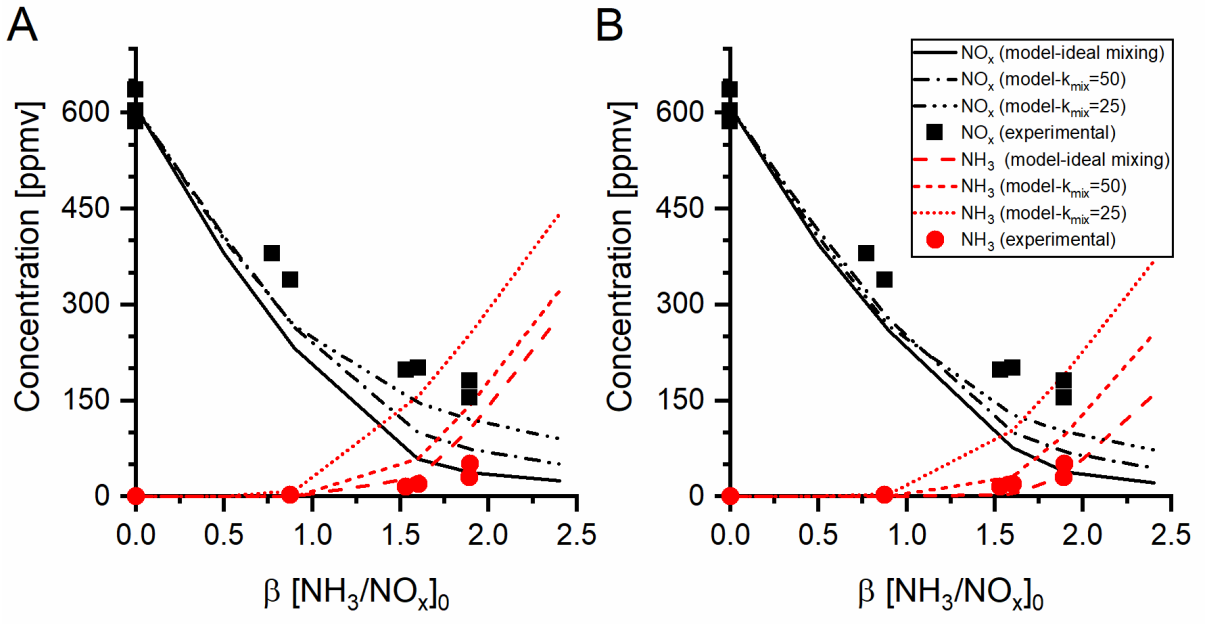

Figure 5.25: Model and experimental results for NO_x and NH_3 concentrations in the cyclone preheater system during SNCR for measurement series 1 with temperature profiles and residence times given in A) Table 5.10 and B)Table 5.11

5.4.6 Modeling summary

In general for the model results the trends are well predicted, while the quantitative accuracy is unsatisfactory in many cases, with under prediction of NO_x emissions and over prediction of ammonia slips. This can be explained by the measured temperatures being lower than the real gas phase temperatures. As increased temperatures for SNCR leads to higher ammonia conversion and lower selectivity for NO_x reduction. From the transient model results it is clear that there is severe mixing limitations in the riser and a simple mixing model can improve the model predictions for NO_x reduction at both the cyclone inlet and the outlet. However, implementing mixing alone would further worsen the prediction of the ammonia slip if no temperature correction were made.

5.5 Conclusions

A pre-study based on raw plant data and assumed reaction conditions have been conducted, followed by a full measurement campaign and modeling hereof.

5.5.1 Pre-study

Based on the pre-study the following conclusions and suggestions were made.

Data analysis:

The plant data for the pre-study showed large fluctuations and unstable operation, with the actuations of the ammonia water flow being much faster than the dynamics of the emission measurement, showing an over tuned control system. The response time delay in emission measurements were found to be approximately 7 minutes for the NO_x emissions and 25 minutes or more for the ammonia slip and therefore no stable data for ammonia slip were available.

NO_x emissions is reduced with increased ammonia water flow. However, at stoichiometric ratios, β, above 1 to 1.3 the added effect was insignificant, evening out at 60-70 % reduction. NH_3 slip increased with increased ammonia water flow, but stayed low until stoichiometric ratio of, $\beta \approx 1$. The ammonia slip exceeded the limit of 40 ppmv for feed ratios above 1.3. Increased ammonia water flow also increased the CO emissions.

Modeling:
The simple reactor model, describing the riser as a PFR and the cyclone as a CSTR, together with detailed kinetics, used to model the SNCR process captured the trend of the plant data well. From this model it could be concluded that the emission limits could be achieved under stable operation. Furthermore, the model results suggested that the riser was the main reaction zone for NO_x reduction, while the cyclone chamber primarily acted to reduce the ammonia slip after close to full conversion in the riser. This was later proven to be false by the measurement campaign.

The sensitivity analysis showed that the results, especially for the ammonia slip are highly dependent on the temperature and composition in regards to CO. Hence, measurement of the inlet conditions and measurements of composition and temperatures at several points in the riser and possibly inside the cyclone, both with and without ammonia addition would be highly beneficial for further analysis.

Suggestions:
Based on the pre-study a measurement campaign and series of process alterations were suggested to improve the efficiency of the SNCR process. Among the suggested process alterations were implementing a more conservative control strategy to achieve a more stable process, which Rockwool did, independently of the study, and improved their SNCR process yielding lower NO_x emissions and less ammonia slip. Other suggestions included changing the ammonia injection positions, ammonia injection methods and cyclone preheater design, none of these were been investigated further.

5.5.2 Measurement campaign
Based on the measurement campaign conducted at one of Rockwools plants, and the modelling hereof, the following conclusions were drawn.

Measurements
The local conditions in the cyclone preheater system, as well as the plant emissions at the stack were measured during a series of controlled SNCR experiments. From these the following conclusions can be drawn.

From the stack emissions datasets it was confirmed that the dynamics of the system is very slow for ammonia at around 20-30 minutes response time. Analysis of the plant data with SNCR turned off showed that a high wool waste fraction used in the melting process and high flue gas flowrate decreases the NO_x generation in the melting cyclone.

From the stack emission measurements at stable conditions during the SNCR experiments, the expected trends with decreasing NO_x emissions, increasing ammonia slip, and increasing CO emissions, when increasing the ammonia water dosing, were observed. The leveling off of the NO_x reduction did not occur until a stoichiometric ratio of β=1.6 or higher as compared to at 1-1.3 for the unstable conditions from the pre-study- From the results it can be concluded that operation within the NO_x emission and ammonia slip limits, of 195 and 40 ppmv respectively, could be achieved during stable operation at stoichiometric ratios, β, of 1.4-1.6, even with high initial NO_x concentration. The NO_x reductions at these conditions were 60-70%. However, decreasing the temperature in the preheater zone, by increasing quenching air, lead to lower NO_x reduction and higher ammonia slip and therefore lower achievable NO_x reduction. Hence, in the case with low temperatures in the preheater system, operating within the emission limits could not be achieved.

Gas composition measurements in the cyclone inlet showed only little conversion of NO_x in the riser, contrary to model results in the pre-study. This is caused by severe mixing limitation in the riser, meaning that the cyclone chamber itself is the main reaction zone. Meaning the mixing in the cyclone and its performance as SNCR reactor have a larger influence than the pre-study suggested.

Temperature measurements in the riser and cyclone inlet showed only little change over the riser length. However, this was attributed to measurement uncertainty.

Modelling

The SNCR process in the cyclone preheater system was modelled based on the measurement campaign, using a simple PFR reactor model and detailed kinetics.

The model results for the outlet concentrations captures the trends observed experimentally well, by simply using the measurement data as input and assumption where needed. However, the quantitative accuracy is insufficient, with under prediction of NO_x emissions and over prediction of ammonia slips.

Implementing a simple mixing model improved the predictions of the NO_x emission, while further increasing the over prediction of the ammonia slip.

The over predicted ammonia slip both with and without mixing model can be explained by either the uncertainty in the measured temperatures, inaccuracies of the kinetic model, or a combination of both. Increasing the temperatures used in the models leads to higher ammonia conversion and lower selectivity for NO_x reduction in the SNCR process, and together with the mixing models led to better quantitative model results, as compared with the experiments. This further support the experimental observation of mixing limitations and problems with temperature measurements.

The transient model results, predicted that without mixing limitations, the main reaction zone were in the riser, contrary to the experimental result. A mixing time corresponding to 0.25

seconds, roughly half the residence time in the riser and cyclone, gave accurate predictions of the extent of NO_x conversion in the riser.

Suggestions for emission reduction

Any control strategy implemented for the SNCR system should account for the slow dynamics of the ammonia slip measurements and placing an ammonia sensor closer to the preheater system would be beneficial for more efficient SNCR control.

In order to optimize the SNCR process and achieve lowest possible NO_x emissions, without changing the plant design, the cyclone melter operating conditions should ensure low initial NO_x formation, as high initial NO_x requires higher ammonia dosing. This can be achieved by optimization of the burner setting and by increasing wool waste dosage.

The temperature in the preheater zone should be kept high, by controlling the quenching air addition, as low temperature in the preheater system gives problems with SNCR due to ammonia slip.

Further optimization of the ammonia injection method could improve SNCR performance, by reducing the influence of mixing limitations in the riser. Another solution could be to improve mixing in the riser by inducing stronger turbulence. This could might achieved by using a small physical obstruction partway between the ammonia injection point and the cyclone inlet.

Alternatively the design of the cyclone might be changed to reduce lip leakage, as the cyclone have proven to be more important to cyclone SNCR processes than previously expected. However, these suggestions might have unintended consequences for the preheating process.

Chapter 6 – Conclusions and perspective

6.1 Conclusions

The objectives of this thesis were to improve the understanding of the SNCR process in cyclone reactors. This has been achieved through a review of the published literature, experimental work in both pilot and industrial scale cyclone reactors for SNCR, and modelling of these systems.

6.1.1 Literature

The literature study describes the state-of-the-art and knowledge gap in understanding and modelling cyclone reactors, as well as the SNCR process. The available literature on industrial applications of cyclone reactors shows that cyclone reactors are primarily used for high temperature processes, such as combustion, gasification, pyrolysis, pyro-metallurgical smelting processes, and flue gas cleaning by SNCR. Many other potential applications have been primarily investigated in laboratory or pilot scales.

A review of the typical reactors used for different applications shows that combustion and smelting processes use various different cyclone reactor configurations, while gasification, pyrolysis and SNCR are based on standard reverse flow cyclone configurations. The available literature on modeling of cyclone reactors, shows a big gap in the available models and the requirement for more detailed models and validation of existing models for cyclone reactors.

The literature on SNCR shows that a common limitation of both the experimental and model investigations is that the results for ammonia slip are generally not reported. This is a problem, with regards to model validation, as well as the industrial application of the research, as ammonia slip is a key limiting factor in the achievable NO_x reduction in industrial applications.

6.1.2 Pilot scale experiments

A pilot scale cyclone reactor for SNCR has been modified to allow the performed experiments. Five experimental series were conducted in the reactor under different reactor conditions. The temperature and concentration profiles in the cyclone reactor and the overall performance of SNCR have been measured. The inlet temperature has been varied between 866 and 1023 °C, with the inlet NO concentration kept at 500 ppmv. Ammonia gas was injected using nitrogen carrier gas, with the stoichiometry for the ammonia feed varied with a NH_3/NO molar ratio between 0 and 7. The ammonia injection tube position and carrier gas flow was varied, with the carrier gas varying between 0-1.5 Nl/min.

From the overall SNCR performance results, the highest NO reduction is achieved for an inlet temperature of 932 °C, but with significant ammonia slip, as such the most optimal conditions is found to be an inlet temperature of 982 °C and a stoichiometric ratio of $\beta \approx 1.6$, with an NO reduction of 69 %, with a small ammonia slip of 4 ppm.

The measured temperature profiles show large temperature drops of close to 400 °C from top to bottom of the cyclone, while the temperature is more uniform horizontally. This suggests

that the primary reaction zone of the cyclone reactor is the inlet section and the top part of the cyclone. This is confirmed by the measured concentration profiles, that show little to no NO reduction in the lower part of the cyclone. However, a significant ammonia conversion occurs in the lower cyclone, despite the low temperatures (600-800 °C). Based on the measured concentrations in the outer and inner vortex and the outlet it can be concluded that a large fraction of the total gas flow bypass most of the volume of the cyclone due to lip leakage.

The experiments with varying ammonia injection conditions, showed that an increase in carrier gas, which should improve the mixing, leads to increased NO reduction but higher ammonia slip, while further insertion of the injection probe into the bulk flow showed the reverse behavior.

6.1.3 Pilot scale modelling

The pilot scale experiments have been modelled using detailed and simplified kinetics, together with simple reactors and a reactor network model developed in this thesis.

The models are able to capture the qualitative trend of NO reduction and ammonia slip using detailed kinetics. However, the NO reduction and ammonia slip are significantly over-predicted for the majority of the temperature range.

The modeling results for the outlet concentrations are insensitive to the choice of reactor model and mixing model, but sensitive to temperature, gas composition and choice of kinetic model. The simple kinetics from Duo et al. [1] showed the best agreement with the experimental results, as well as a higher sensitivity towards the choice of reactor model.

The developed compartment model is able to adjust the flow pattern, as well as represent the temperature distribution in the cyclone reactor. The model is able to qualitatively reproduce the internal concentration profiles caused by the double vortex flow in the cyclone reactor, using both detailed and simple kinetics. The simple kinetics shows a good quantitative agreement for the NO concentrations, but unsatisfactory for the ammonia.

6.1.4 Industrial scale work

Industrial scale measurements of the SNCR process have been conducted in a preheater cyclone system. In the measurement campaign, raw NO_x emissions, flue gas composition, temperatures, and the performance of SNCR were measured. The system has been modelled using the measurement data, simple reactor models and detailed chemical kinetics.

The experimental results show that the SNCR process can achieve a NO_x reduction of up to 70 % without exceeding ammonia slip limits of 40 ppmv for the standard preheater conditions. When operating at low temperatures in the preheater system, the SNCR performance is insufficient for meeting the emission limits, due to high ammonia slips. Large mixing limitations are observed in the riser and only 0-15 % of NO_x conversion occurs in the riser, meaning the cyclone chamber is the largest contributor to the conversion.

The models can predict the overall trends of the SNCR process using the measured temperature and gas composition data as input. However, the NO_x removal and the ammonia slip is over-predicted, as also observed in the pilot scale results. The effect of mixing limitations on the NO_x concentrations in the riser could be replicated using the simple mixing model implemented.

By analyzing the emission plant data from a plant it was found that large delay times for the emission measurements, at ~25 minutes for the ammonia slip, which should be accounted for when tuning the control system.

6.2 Suggestions for future work

The design of a cyclone have a large effect on the flow patterns and thereby the mixing pattern and temperature distribution inside the cyclone. As suggested in this work, reducing the lip leakage in a cyclone reactor for SNCR might improve both NO_x reduction and reduce ammonia slip, thereby improving the performance of the SNCR process. Thus, an experimental investigation into this could be conducted, for example by changing the vortex finder length and evaluating the effect on SNCR performance. Design rules used for optimizing preheater cyclones and CFBC cyclones could be evaluated on their effect on the SNCR performance.

The presence of particles in the cyclone reactor influences both the gas flow and the temperature profiles. Some types of particles may also have a catalytic activity on the nitrogen chemistry. The influence of particles on these factors and their effect on SNCR have not yet been thoroughly investigated. Hence, a detailed study of the effect of different types of particles on the SNCR process could be carried out.

The compartment model should be further developed and its performance should be tested against other experiments. Suggestions for this is given below:

- Testing the developed model with parameters found from residence time distribution measurements or CFD calculations.
- Use the compartment model to evaluate design changes like vortex finder length etc. on the overall performance of the SNCR process using the parameters found above.
- Testing if the influence of particles can be described by the current model simply by accounting for the change in flow field and temperature profiles.
- Further develop the model to account for particles if necessary.
- Test the model for other cyclone reactor applications for gas phase reactions.

Bibliography

[1] W. Duo, K. Dam-Johansen, K. Østergaard, Kinetics of the Gas-Phase Reaction Between Nitric Oxide, Ammonia and Oxygen, Can. J. Chem. Eng. 70 (1992) 1014–1020. https://doi.org/10.1002/cjce.5450700525.

[2] S. Ouyang, Q.M. Mao, M. Rhodes, O.E. Potter, Short contact time gas-solid systems, Rev. Chem. Eng. 19 (2003) 133–228. http://en.scientificcommons.org/53784754.

[3] B. Leckner, M. Karlsson, K. Dam-johansen, C.E. Weinel, P. Kilpinen, M. Hupa, Influence of Additives on Selective Noncatalytic Reduction of NO with NH3 in Circulating Fluidized Bed Boilers, Ind. Eng. Chem. Res. 30 (1991) 2396–2404.

[4] J.M. Finch, Dust Collector, US325521, 1885. https://www.google.com/patents/US325521.

[5] O.M. Morse, Dust-Collector, US1029214, 1912.

[6] A.J. Hoffmann, L.E. Stein, Gas Cyclones and Swirl Tubes: Principles, Design, and Operation, 2nd ed., Springer, 2004.

[7] J. Mills, Dust Collector, US258099, 1882.

[8] N.P. Cheremisinoff, P.N. Cheremisinoff, Particulate capture from process gas streams, in: N.P. Cheremisinoff (Ed.), Encycl. Fluid Mech. - Vol. 4 Solids Gas-Solids Flows, Gulf Publishing Company, Houston, London, Paris Tokyo, 1986: pp. 1227–1279.

[9] D. Leith, D. Mehta, Cyclone performance and design, Atmos. Environ. 7 (1973) 527–549. https://doi.org/10.1016/0004-6981(73)90006-1.

[10] A.J. ter Linden, Investigations into Cyclone Dust Collectors, Proc. Inst. Mech. Eng. 160 (1949) 233–251.

[11] A.J. Hoekstra, Gas Flow Field and Collection Efficiency of Cyclone Separators, (2000) 1–165.

[12] J. Lede, H.Z. Li, F. Soulignac, J. Villermaux, Measurement of solid particle residence time in a cyclone reactor: A comparison of four methods, Chem. Eng. Process. 22 (1987) 215–222. https://doi.org/10.1016/0255-2701(87)85004-3.

[13] S.K. Kang, T.W. Kwon, S.D. Kim, Hydrodynamic characteristics of cyclone reactors, Powder Technol. 58 (1989) 211–220. https://doi.org/10.1016/0032-5910(89)80116-0.

[14] A.C. Hoffmannc, A. van Santen, R.W.K. Allen, R. Clift, Effects of geometry and solid loading on the performance of gas cyclones, Powder Technol. 70 (1992) 83–91. https://doi.org/10.1016/0032-5910(92)85058-4.

[15] C. Cortés, A. Gil, Modeling the gas and particle flow inside cyclone separators, Prog. Energy Combust. Sci. 33 (2007) 409–452. https://doi.org/10.1016/j.pecs.2007.02.001.

[16] J. Dirgo, D. Leith, Design of Cyclone Separators, in: N.P. Cheremisinoff (Ed.), Encycl. Fluid Mech. - Vol. 4 Solids Gas-Solids Flows, Gulf Publishing Company, Houston, London, Paris Tokyo, 1986: pp. 1281–1306.

[17] A.C. Hoffmann, M. De Groot, W. Peng, H.W.A. Dries, J. Kater, Advantages and risks

in increasing cyclone separator length, AIChE J. 47 (2001) 2452–2460. https://doi.org/10.1002/aic.690471109.

[18] F.A. Zenz, Cyclone Design, in: Fluid. Solids Handl. Process. Ind. Appl., Noyes Publications, 1989: pp. 773–816. https://doi.org/10.1016/B978-081551427-5.50014-4.

[19] F. Tan, I. Karagoz, A. Avci, The Effects of Vortex Finder Dimensions on the Natural Vortex Length in a New Cyclone Separator, Chem. Eng. Commun. 203 (2016) 1216–1221. https://doi.org/10.1080/00986445.2016.1160228.

[20] A. Kępa, The influence of a plate vortex limiter on cyclone separator, Sep. Sci. Technol. 51 (2016) 1–13. https://doi.org/10.1080/01496395.2016.1165249.

[21] S.C. Stultz, J.B. Kitto, Steam - its generation and use, 39th ed., Babcock & Wilcox, 1978.

[22] H.J. Kerr, J. Fletcher, G.A. Watts, L. Kooistra, Combustion Apparatus and Method, US2357303, 1944.

[23] H.J. Kerr, J. Fletcher, L. Kooistra, G.A. Watts, Fuel Burning Apparatus, US2594312, 1952.

[24] T.M. Nechvatal, T.J. Jansen, Converting Paper Mill SLudge or the like, US5549059, 1996.

[25] M.O. Dahl, H. Farzan, J.E. Granger, G.J. Maringo, Cyclone furnace for retrofit applications, US6021724, 2000.

[26] Z. Tian-cong, The Metallurgy of Antimony, Central South University of Technology Press, Changsha, 1988.

[27] G. Melcher, E. Muller, H. Weigel, The KIVCET cyclone smelting process for impure copper concentrates, J. Met. 28 (1976) 4–8.

[28] R.R. Moskalyk, A.M. Alfantazi, Review of copper pyrometallurgical practice: Today and tomorrow, Miner. Eng. 16 (2003) 893–919. https://doi.org/10.1016/j.mineng.2003.08.002.

[29] F. Sauert, U. Kerney, J. Pesl, Recycling EAF Dust with CONTOP Technology, in: FOURTH Int. Symp. Recycl. Met. Eng. Mater. Proc., 2000: pp. 427–441.

[30] B. Ruehl, A. Schulte, H. Traulsen, The Flame Cyclone Technology and Its Possible Application, in: Reinhardt Schuhmann Int. Symp. Innov. Technol. React. Des. Extr. Metall., Mackey, P. J., 1986: pp. 175–194.

[31] K. Emicke, The Development of the Flame Cyclone Reactor Technology at Norddeutsche Affinerie for Complex Copper Concentrates, in: P.J. Mackey (Ed.), Reinhardt Schuhmann Int. Symp. Innov. Technol. React. Des. Extr. Metall., 1986: pp. 195–208.

[32] J. Van Langen, K. Meijer, B. Corbett, G. Malgrarini, The cyclone converter furnace, Rev. Metall. 90 (1993) 363–368.

[33] A.C. Johansson, H. Wiinikka, L. Sandström, M. Marklund, O.G.W. Öhrman, J.

Narvesjö, Characterization of pyrolysis products produced from different Nordic biomass types in a cyclone pilot plant, Fuel Process. Technol. 146 (2016) 9–19. https://doi.org/10.1016/j.fuproc.2016.02.006.

[34] H. Wiinikka, P. Carlsson, A.C. Johansson, M. Gullberg, C. Ylipää, M. Lundgren, L. Sandström, Fast pyrolysis of stem wood in a pilot-scale cyclone reactor, Energy and Fuels. 29 (2015) 3158–3167. https://doi.org/10.1021/acs.energyfuels.5b00174.

[35] T.A. Gauthier, C.L. Briens, M.A. Bergougnou, P. Galtier, Uniflow cyclone efficiency study, Powder Technol. 62 (1990) 217–225. https://doi.org/10.1016/0032-5910(90)80108-B.

[36] R. Galiasso, Y. González, M. Lucena, New inverted cyclone reactor for flash hydropyrolysis, Catal. Today. 220–222 (2014) 186–197. https://doi.org/10.1016/j.cattod.2013.10.008.

[37] N. Syred, A.J. Griffiths, W. Fick, T. Fraser, Experimental and Numerical Studies of an Inverted Cyclone Gasifier - Isothermal Analysis, 13th Int. Symp. Appl. Laser Tech. to Fluid Mech. (2006).

[38] M. Lucena, Y. González, R. Galiasso, Model for the simulation of light naphtha cracking in an inverted cyclone reactor, J. Comput. Methods Sci. Eng. 17 (2017) 97–107. https://doi.org/10.3233/JCM-160665.

[39] W. Zhenbo, M. Yi, W. Jian, R. Xiangjun, W. Jianjun, L. Renxuan, J. Youhai, Axial-flow ultrashort contact cyclone reactor, CN102533311A, 2010.

[40] Y. chun Zhang, Z. bo Wang, Y. hai Jin, Simulation and experiment of gas-solid flow field in short-contact cyclone reactors, Chem. Eng. Res. Des. 91 (2013) 1768–1776. https://doi.org/10.1016/j.cherd.2013.03.015.

[41] Y. Zhang, Z. Wang, Y. Jin, Z. Li, W. Yi, CFD simulation and experiment of residence time distribution in short-contact cyclone reactors, Adv. Powder Technol. 26 (2015) 1134–1142. https://doi.org/10.1016/j.apt.2015.05.009.

[42] L. Zhu, A. Li, Z. Wang, Analysis of particle trajectories in a quick-contact cyclone reactor using a discrete phase model, Sep. Sci. Technol. 53 (2018) 928–939. https://doi.org/10.1080/01496395.2017.1386683.

[43] Y. chun Zhang, Z. bo Wang, Y. hai Jin, Z. he Li, W. ming Yi, Kinetic study of catalytic cracking on the effect of reaction parameters in short-contact cyclone reactors, Chem. Eng. Res. Des. 119 (2017) 188–197. https://doi.org/10.1016/j.cherd.2017.01.022.

[44] S.R. Turns, An Introduction to Combustion: Concepts and Applications, 3rd ed., McGraw-Hill, 2012.

[45] H.J. Kerr, J. Fletcher, G.A. Watts, L. Kooistra, Method of and apparatus for burning fuel, US2357302, 1944.

[46] J.S. Barnhart, N.M. Laurendeau, Pulverized coal combustion and gasification in a cyclone reactor. 1. Experiment, Ind. Eng. Chem. Process Des. Dev. 21 (1982) 671–680. https://doi.org/10.1021/i200019a024.

[47] S.Y. No, Combustion Characteristics of Anthracite In a Vertical Cyclone Combustor,

KSME J. 7 (1993) 295–302.

[48] N. Syred, J.M. Beér, Combustion in Swirling Flows : A Review, Combust. Flame. 23 (1974) 143–201. https://doi.org/http://dx.doi.org/10.1016/0010-2180(74)90057-1.

[49] K.A. Al-attab, Z.A. Zainal, Design and performance of a pressurized cyclone combustor (PCC) for high and low heating value gas combustion, Appl. Energy. 88 (2011) 1084–1095. https://doi.org/10.1016/j.apenergy.2010.10.041.

[50] H.R. Hoy, A.G. Roberts, D.M. Wilkins, Some investigations with a Small cyclone combustor, J. Inst. Fuel. 31 (1958) 429–457.

[51] D. Morgan, M. Biffin, S.Y. No, N. Syred, An analysis of the behaviour of non-slagging, coal fired, cyclone combustors using a phenomenological model, Symp. Combust. 22 (1989) 175–182. https://doi.org/10.1016/S0082-0784(89)80023-2.

[52] E.G. Bailey, H.J. Kerr, J. Fletcher, G.A. Watts, L. Kooistra, Fuel Burning Method and Apparatus, US2357301, 1944.

[53] L.L. Kalishevskii, B.G. Ganchev, A study of the Cyclone Process when Burning Solid Fuel, Therm. Eng. (1967) 70–74.

[54] Cyclone-Furnace Boilers, (n.d.). http://www.babcock.com/products/cyclone-furnace (accessed August 9, 2017).

[55] K. Luecke, E. Hartge, J. Werther, A 3D Model of Combustion in Large-Scale Circulating Fluidized Bed Boilers, Int. J. Chem. React. Eng. 2 (2004) 1–51.

[56] V.S. Sikarwar, M. Zhao, P.S. Fennell, N. Shah, E.J. Anthony, Progress in biofuel production from gasification, Prog. Energy Combust. Sci. 61 (2017) 189–248.

[57] H. Lu, W. Robert, G. Peirce, B. Ripa, L.L. Baxter, Comprehensive Study of Biomass Particle Combustion, Energy & Fuels. 22 (2008) 2826–2839. https://doi.org/10.1021/ef800006z.

[58] H. Perry, R.C. Corey, M.A. Elliot, Continuous gasification of pulverized coal with oxygen and steam by the vortex principle, Trans. ASME. 72 (1950) 599–610.

[59] M.A. Elliott, H. Perry, J. Jonakin, R.C. Corey, M.L. Khullar, Gasification of Pulverized Coal with Oxygen and Steam in a Vortex Reactor, Ind. Eng. Chem. 44 (1952) 1074-1082 ST-Gasification of Pulverized Coal wi. https://doi.org/10.1021/ie50509a044.

[60] K. Traenckner, Pulverized-Coal Gasification Ruhrgas Processes, ASME Trans. 75 (1953) 1095–1101.

[61] N.M. Laurendeau, Heterogeneous Kinetics of Coal Char Gasification and Combustion, Prog. Energy Combust. Sci. 4 (2006) 221–270.

[62] S. Yagi, D. Kunii, Studies on combustion and gasification of pulverized coal in a model cyclone generator, Symp. Combust. 6 (1957) 584–590. https://doi.org/10.1016/S0082-0784(57)80078-2.

[63] M. Gabra, E. Pettersson, R. Backman, B. Kjellström, Evaluation of cyclone gasifier performance for gasification of sugar cane residue - Part 1: Gasification of bagasse,

Biomass and Bioenergy. 21 (2001) 351–369. https://doi.org/10.1016/S0961-9534(01)00043-5.

[64] M. Gabra, E. Pettersson, R. Backman, B. Kjellström, Evaluation of cyclone gasifier performance for gasification of sugar cane residue — Part 2: gasification of cane trash, Biomass and Bioenergy. 21 (2001) 371–380.

[65] J.W. Cousins, W.H. Robinson, Gasification of Sawdust in an Air-Blown Cyclone Gasifier, Ind. Eng. Chem. Process Des. Dev. 24 (1985) 1281–1287.

[66] M. Gabra, A. Nordin, M. Öhman, B. Kjellström, Alkali retention/separation during bagasse gasification: A comparison between a fluidised bed and a cyclone gasifier, Biomass and Bioenergy. 21 (2001) 461–476. https://doi.org/10.1016/S0961-9534(01)00042-3.

[67] C. Fredriksson, Exploratory Experimental and Theoretical Studies of Cyclone Gasification of Wood Powder, PhD Thesis. (1999) 1–169.

[68] P.W. He, S.Y. Luo, G. Cheng, B. Xiao, L. Cai, J.B. Wang, Gasification of biomass char with air-steam in a cyclone furnace, Renew. Energy. 37 (2012) 398–402. https://doi.org/10.1016/j.renene.2011.07.001.

[69] J. Gao, Y. Zhao, S. Sun, H. Che, G. Zhao, J. Wu, Experiments and numerical simulation of sawdust gasification in an air cyclone gasifier, Chem. Eng. J. 213 (2012) 97–103. https://doi.org/10.1016/j.cej.2012.09.076.

[70] Y. Zhao, S. Sun, T. Zhang, H. Zhou, Experimental research on fuel staging cyclone gasification of wood powder, Fuel. 103 (2013) 53–57. https://doi.org/10.1016/j.fuel.2011.08.020.

[71] M. Risberg, O.G.W. Öhrman, B.R. Gebart, P.T. Nilsson, A. Gudmundsson, M. Sanati, Influence from fuel type on the performance of an air-blown cyclone gasifier, Fuel. 116 (2014) 751–759. https://doi.org/10.1016/j.fuel.2013.08.008.

[72] Y. Zhao, D. Feng, Z. Zhang, S. Sun, X. Zhou, J. Luan, J. Wu, Experimental study of cyclone pyrolysis – Suspended combustion air gasification of biomass, Bioresour. Technol. 243 (2017) 1241–1246. https://doi.org/10.1016/j.biortech.2017.07.065.

[73] S. Sun, Y. Zhao, H. Tian, F. Ling, F. Su, Experimental study on Autothermal cyclone air gasification of Biomass, J. Energy Resour. Technol. 140 (2018) 042001. https://doi.org/10.1016/j.biortech.2009.01.031.

[74] P.H. Jafari, A. Wingren, J.G.I. Hellström, B.R. Gebart, Effect of process parameters on the performance of an air-blown entrained flow cyclone gasifier, Int. J. Sustain. ENERGY. 39 (2020) 21–40. https://doi.org/10.1080/14786451.2019.1626858.

[75] P. Kallner, J. Fredriksson, B. Kjellstrom, Wood combustion and ash separation in a cyclone for gas turbine applications, Am. Soc. Mech. Eng. Int. Gas Turbine Inst. IGTI. 9 (1994).

[76] A. Vongsvarnrungruang, D. Atong, V. Sricharoenchaikul, Gasification of Furniture Waste Sawdust in a Cyclone Gasifier, IOP Conf. Ser. Earth Environ. Sci. 146 (2018). https://doi.org/10.1088/1755-1315/146/1/012041.

[77] J. Lédé, The Cyclone: A Multifunctional Reactor for the Fast Pyrolysis of Biomass, Ind. Eng. Chem. Res. 39 (2000) 893–903. https://doi.org/10.1021/ie990623p.

[78] M.I. Jahirul, M.G. Rasul, A.A. Chowdhury, N. Ashwath, Biofuels production through biomass pyrolysis- A technological review, Energies. 5 (2012) 4952–5001. https://doi.org/10.3390/en5124952.

[79] A. Demirbas, G. Arin, An Overview of Biomass Pyrolysis, Energy Sources. 24 (2002) 471–482. https://doi.org/10.1080/00908310252889979.

[80] F.L.P. Resende, Recent advances on fast hydropyrolysis of biomass, Catal. Today. 269 (2016) 148–155. https://doi.org/10.1016/j.cattod.2016.01.004.

[81] F.L.P. Resende, Recent advances on fast hydropyrolysis of biomass, Catal. Today. 269 (2016) 148–155.

[82] C.K. Choi, Process for the Pyrolysis of Carbonaceous Materials in a Double Helix Cyclone, US4151044, 1979.

[83] J. Lede, F. Verzaro, B. Antoine, J. Villermaux, Flash pyrolysis of wood in a cyclone reactor, Chem. Eng. Process. 20 (1986) 309–317. https://doi.org/10.1016/0255-2701(86)80009-5.

[84] J. Lédé, F. Broust, F.T. Ndiaye, M. Ferrer, Properties of bio-oils produced by biomass fast pyrolysis in a cyclone reactor, Fuel. 86 (2007) 1800–1810. https://doi.org/10.1016/j.fuel.2006.12.024.

[85] G. Brem, E.A. Bramer, PyRos: a new flash pyrolysis technology for the production of bio-oil from biomass residues, Proc. Int. Conf. Exhib. Bioenergy Outlook. (2007) 1–14.

[86] L. Sandström, A.-C. Johansson, H. Wiinikka, O.G.W. Öhrman, M. Marklund, Pyrolysis of Nordic biomass types in a cyclone pilot plant — Mass balances and yields, Fuel Process. Technol. 152 (2016) 274–284.

[87] L.C. Lin, F. V. Hanson, A.G. Oblad, J.D. Westhoff, The pyrolysis of bitumen-impregnated sandstone in short contact time reactors, I. Cyclone reactor, Fuel Process. Technol. 16 (1987) 173–190. https://doi.org/10.1016/0378-3820(87)90068-3.

[88] C.K. Choi, Pyrolysis of Carbonaceous Materials in a double helix cyclone, 1978.

[89] P.R. Taylor, R.W. Bartlett, M. Abdel-latif, Partial reduction of Particulate Iron Ores and Cyclone Reactor, 5,228,901, 1993.

[90] P.R. Taylor, M. Abdel-latif, R.W. Bartlett, Reduction of taconite concentrates in a cyclone reactor, Miner. Metall. Process. 11 (1994) 203–209.

[91] H. Hilbrans, M. Gamroth, G. Melcher, New features and developments in the application of the CONTOP cyclone smelting process, Pyrometallurgy. (n.d.).

[92] S. Demetrio, N. Santander, M. Solar, The copper smelters of the 2010 - a vision for the future, in: 4th Int. Conf. Copp. 99-Cobre 99, 1999: pp. 295–303.

[93] M. Gamroth, H. Hilbrans, G. Melcher, New applications of the Contop Process, Extr. Metall. (1985) 817–829.

[94] J. Brouwer, M.P. Heap, D.W. Pershing, P.J. Smith, A model for prediction of selective noncatalytic reduction of nitrogen oxides by ammonia, urea, and cyanuric acid with mixing limitations in the presence of CO, Symp. Combust. 26 (1996) 2117–2124. https://doi.org/10.1016/S0082-0784(96)80036-1.

[95] R.K. Lyon, J.E. Hardy, Discovery and development of the thermal DeNOx process, Ind. Eng. Chem. Fundam. 25 (1986) 19–24. https://doi.org/10.1021/i100021a003.

[96] M. Tayyeb Javed, N. Irfan, B.M. Gibbs, Control of combustion-generated nitrogen oxides by selective non-catalytic reduction, J. Environ. Manage. 83 (2007) 251–289. https://doi.org/10.1016/j.jenvman.2006.03.006.

[97] P. Glarborg, J.A. Miller, B. Ruscic, S.J. Klippenstein, Modeling nitrogen chemistry in combustion, Prog. Energy Combust. Sci. 67 (2018) 31–68.

[98] B. Ljungdahl, J. Larfeldt, Optimised NH3 injection in CFB boilers, Powder Technol. 120 (2001) 55–62. https://doi.org/10.1016/S0032-5910(01)00347-3.

[99] J.E. Johnsson, Formation and reduction of nitrogen oxides in fluidized-bed combustion, Fuel. 73 (1994) 1398–1415. https://doi.org/10.1016/0016-2361(94)90055-8.

[100] L. Elmekilde Hansen, L. Bøllund, An apparatus and method for making a mineral melt, WO2012028638A1, 2012.

[101] J. Horton, A. Linero, F.M.G. Miller, Use of SNCR to control emissions of oxides of nitrogen from cement plants, IEEE Cem. Ind. Tech. Conf. 2006 (2006) 316–344. https://doi.org/10.1109/citcon.2006.1635728.

[102] V.G. Chibante, A.M. Fonseca, R.R. Salcedo, Comparing the performance of recirculating cyclones applied to the dry scrubbing of gaseous HCl with hydrated lime, Ind. Eng. Chem. Res. 48 (2009) 1029–1035. https://doi.org/10.1021/ie800519x.

[103] W. Lin, J.E. Johnsson, K. Dam-johansen, C.M. Van den Bleek, Interaction between emissions of sulfur dioxide and nitrogen oxides in fluidized bed combustion, Fuel. 73 (1994) 1202–1208.

[104] A.M. Fonseca, J.J. Órfao, R.L. Salcedo, Dry Scrubbing of Gaseous HCl with Solid Lime in a Cyclone Reactor at Low Temperatures, Ind. Eng. Chem. Res. 40 (2001) 304–313. https://doi.org/10.1021/ie000634e.

[105] V. Chibante, A. Fonseca, R. Salcedo, Dry scrubbing of acid gases in recirculating cyclones, J. Hazard. Mater. 144 (2007) 682–686. https://doi.org/10.1016/j.jhazmat.2007.01.095.

[106] V.G. Chibante, A.M. Fonseca, R.R. Salcedo, Modeling dry-scrubbing of gaseous HCl with hydrated lime in cyclones with and without recirculation, J. Hazard. Mater. 178 (2010) 469–482. https://doi.org/10.1016/j.jhazmat.2010.01.106.

[107] G. Manenti, M. Masi, Simulation study of production of fine ceramic powders in a cyclone reactor, Chem. Eng. Process. Process Intensif. 50 (2011) 151–159. https://doi.org/10.1016/j.cep.2011.01.001.

[108] J. Lédé, H.Z. Li, J. Villermaux, The Cyclone - A Chemical reactor - Application to NaHCO3 Decarbonation, Can. J. Chem. Eng. 70 (1992) 1132–1142.

[109] J. Lédé, J. Mercadier, J. Villermaux, The cyclone, a reactor for sublimation: Sublimation of isocyanuric acid, Chem. Eng. J. 62 (1996) 13–21.

[110] S. Luidold, H. Antrekowitsch, R. Ressel, Production of niobium powder by magnesiothermic reduction of niobium oxides in a cyclone reactor, Int. J. Refract. Met. Hard Mater. 25 (2007) 423–432. https://doi.org/10.1016/j.ijrmhm.2006.11.002.

[111] J. Lede, H.Z. Li, J. Villermaux, Le Cyclone Réacteur Partie I: Mesure Directe de la Distribution des Temps de Séjour de la Phase Gazeuse - Lois d'Extrapolation, Chem. Eng. J. 42 (1989) 37–55.

[112] J. Lede, H.Z. Li, J. Villermaux, Le Cyclone Réacteur Partie II: Mesure Directe de la Distribution des Temps de Séjour de la Phase Solide - Lois d'Extrapolation, Chem. Eng. J. 42 (1989) 103–117.

[113] S.K. Kang, T.W. Kwon, S.D. Kim, Hydrodynamic Characteristics of Cyclone Reactors, Powder Technol. 58 (1989) 211–220.

[114] T. Saruchera, Measurement and Modelling of Particle Residence Time in a Return-Flow Cyclone, University of Canterbury, 1999.

[115] J. Szekely, R. Carr, Heat transfer in a cyclone, Chem. Eng. Sci. 21 (1966) 1119–1132.

[116] J. Lédé, H.Z. Li, F. Soulignac, J. Villermaux, Le cyclone réacteur III: Mesure de l'efficacité des transferts de chaleur et matière entre les parois et un gaz circulant seul, Chem. Eng. J. 45 (1990) 9–24. https://doi.org/10.1016/0300-9467(90)80021-4.

[117] J. Lédé, H.Z. Li, F. Soulignac, J. Villermaux, Le cyclone réacteur IV: Mesure de l'efficacité des transferts de chaleur entre les parois et les phases gazeuse et solide, Chem. Eng. J. 48 (1992) 83–99. https://doi.org/10.1016/0300-9467(92)85010-7.

[118] A. Jain, B. Mohanty, B. Pitchumani, K.S. Rajan, Studies on Gas-Solid Heat Transfer in Cyclone Heat Exchanger, J. Heat Transfer. 128 (2006) 761. https://doi.org/10.1115/1.2217748.

[119] G. Gronald, J.J. Derksen, Simulating turbulent swirling flow in a gas cyclone: A comparison of various modeling approaches, Powder Technol. 205 (2011) 160–171. https://doi.org/10.1016/j.powtec.2010.09.007.

[120] S. Obermair, J. Woisetschläger, G. Staudinger, Investigation of the flow pattern in different dust outlet geometries of a gas cyclone by laser Doppler anemometry, Powder Technol. 138 (2003) 239–251. https://doi.org/10.1016/j.powtec.2003.09.009.

[121] R.D. Luciano, B.L. Silva, L.M. Rosa, H.F. Meier, Multi-objective optimization of cyclone separators in series based on computational fluid dynamics, Powder Technol. 325 (2018) 452–466. https://doi.org/10.1016/j.powtec.2017.11.043.

[122] W. Zhong, A. Yu, G. Zhou, J. Xie, H. Zhang, CFD simulation of dense particulate reaction system: Approaches, recent advances and applications, Chem. Eng. Sci. 140 (2016) 16–43. https://doi.org/10.1016/j.ces.2015.09.035.

[123] Z. Kang, Q. Yuan, L. Zhao, Y.K. Dai, B. Sun, T. Wang, Study of the performance, simplification and characteristics of SNCR de-NOx in large-scale cyclone separator, Appl. Therm. Eng. 123 (2017) 635–645.

https://doi.org/10.1016/j.applthermaleng.2017.04.122.

[124] R. Atkinson, Atmospheric chemistry of VOCs and NO(x), Atmos. Environ. (2000). https://doi.org/10.1016/S1352-2310(99)00460-4.

[125] M.A. Wójtowicz, J.R. Pels, J.A. Moulijn, Combustion of coal as a source of N2O emission, Fuel Process. Technol. (1993). https://doi.org/10.1016/0378-3820(93)90061-8.

[126] EEA, European Union emission inventory report 1990-2017, Copenhagen, 2019. https://doi.org/10.2800/78220.

[127] J.B. Zeldovich, Oxidation of Nitrogen in Combustion and Explosion, Acad. Des Sci. L'urss -- Comptes Rendus. 51 (1946) 217–220. https://doi.org/10.1017/CBO9781107415324.004.

[128] G.A. Lavole, J.B. Heywood, J.C. Keck, Experimental and theoretical study of nitric oxide formation in internal combustion engines, Combust. Sci. Technol. 1 (1970) 313–326. https://doi.org/10.1080/00102206908952211.

[129] M. Abian, M.U. Alzueta, P. Glarborg, Formation of NO from N2/O2 mixtures in a flow reactor: Toward an accurate prediction of thermal NO, Int. J. Chem. Kinet. 47 (2015) 518–532. https://doi.org/10.1002/kin.20929.

[130] C.P. Fenimore, Formation of Nitric Oxide in Premixed Hydrocarbon Flames, Int. Symp. Combust. 13 (1971) 373–380.

[131] W. Duo, Kinetic studies of the reactions involved in selective non-catalytic reduction of nitric oxide, 1990.

[132] M. Østberg, K. Dam-Johansen, The droplet diffusion model-An empirical model for micromixing in reacting gas phase systems, Chem. Eng. Sci. 50 (1995) 2061–2067. https://doi.org/10.1016/0009-2509(95)00063-B.

[133] M. Østberg, K. Dam-Johansen, J.E. Johnsson, Influence of mixing on the SNCR process, Chem. Eng. Sci. 52 (1997) 2511–2525. https://doi.org/10.1016/S0009-2509(97)00069-9.

[134] M. Østberg, Influence of Mixing in High Temperature Gas Phase Reactions - The SNCR Process, The Technical University of Denmark, 1996.

[135] P. Glarborg, J.A. Miller, R.J. Kee, Kinetic Modeling and Sensitivity Analysis of Nitrogen Oxide Formation in Well-Stirred Reactors*, Combust. Flame. 65 (1986) 177–202.

[136] J.A. Miller, C.T. Bowman, MECHANISM AND MODELING OF NITROGEN CHEMISTRY IN COMBUSTION, Prog. Energy Combust. Sci. 15 (1989) 287–338.

[137] D. Wenli, K. Dam-Johansen, K. Østergaard, Widening the temperature range of the thermal DeNOx process. An experimental investigation, Symp. Combust. 23 (1991) 297–303. https://doi.org/10.1016/S0082-0784(06)80273-0.

[138] R. Rota, D. Antos, E.F. Zanoelo, S. Carrà, Experimental study and kinetic modelling of nitric oxide reduction with ammonia, Combust. Sci. Technol. 163 (2001) 25–47.

https://doi.org/10.1080/00102200108952150.

[139] F. Kasuya, P. Glarborg, J.E. Johnsson, K. Dam-johansen, The thermal DeNOx process: influence of partial pressures and temperature, Chem. Eng. Sci. 50 (1995) 1455–1466.

[140] M. Østberg, K. Dam-Johansen, Empirical modeling of the selective non-catalytic reduction of no: comparison with large-scale experiments and detailed kinetic modeling, Chem. Eng. Sci. 49 (1994) 1897–1904. https://doi.org/10.1016/0009-2509(94)80074-X.

[141] H. Røjel, A. Jensen, P. Glarborg, K. Dam-Johansen, Mixing effects in the selective noncatalytic reduction of NO, Ind. Eng. Chem. Res. 39 (2000) 3221–3232. https://doi.org/10.1021/ie000049d.

[142] Ahli-Gharamaleki, Selective Non-Catalytic Reduction of NOx in a cyclone reactor, Technical University of Denmark, 2018.

[143] F. Rinaldi, B. Najafi, Temperature Measurement in WTE Boilers Using Suction Pyrometers, (2014). https://doi.org/10.3390/s131115633.

[144] European Commission, (BAT) conclusions under Directive 2010/75/EU of the European Parliament and of the Council on industrial emissions for the manufacture of glass, Off. J. Eur. Communities. 55 (2012) L 70/1-70/98. http://eippcb.jrc.ec.europa.eu/reference/BREF/GLASSLexUriServ.pdf.

[145] K. Hjuler, K. Dam-Johansen, Design of a flue gas probe for ammonia measurement, Anal. Chim. Acta. 282 (1993) 703–709. https://doi.org/10.1016/0003-2670(93)80135-8.

[146] J.R. Tobiasson, S.C. Egbert, B.R. Adams, D.R. Tree, An optical method for the measurement of combustion gas temperature in particle laden flows, Exp. Therm. Fluid Sci. 98 (2018) 704–711. https://doi.org/10.1016/j.expthermflusci.2018.06.026.

Chapter 7 Appendix

Appendix A

This appendix contains the linear correlations used to find input parameters for modelling the SNCR process at points in between the experimental measurement points.

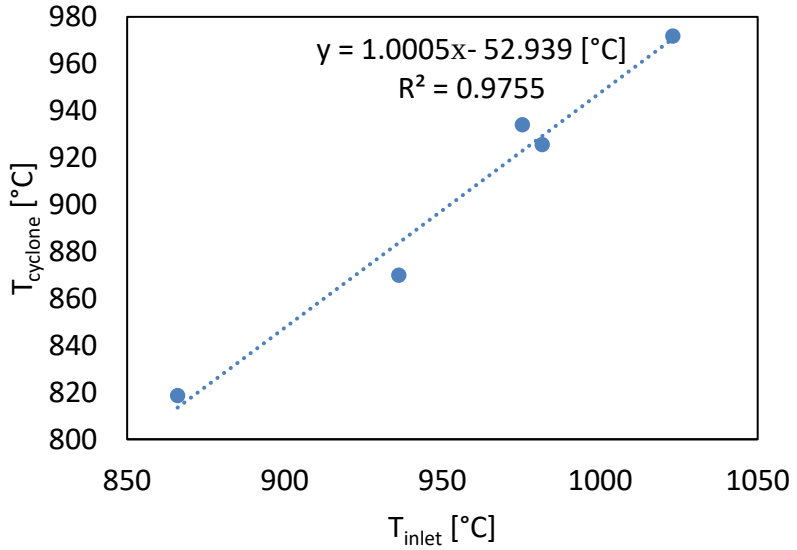

Figure 7.1: linear correlation between inlet temperature and cyclone temperature

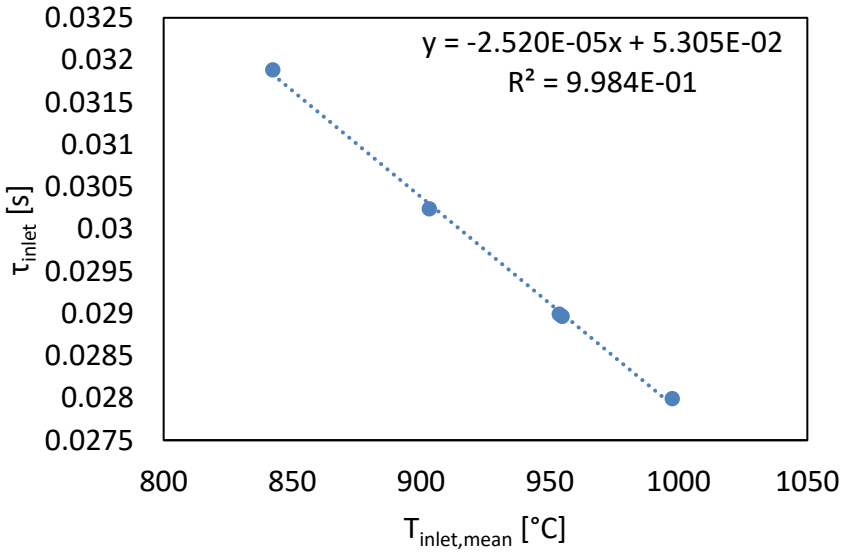

Figure 7.2: linear correlation between the mean temperature in the inlet section and the residence time in the inlet section

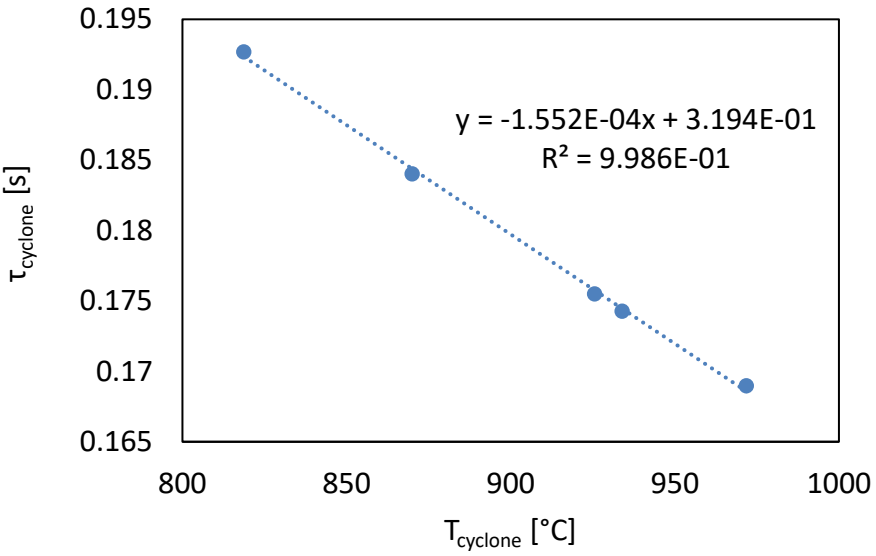

Figure 7.3: linear correlation between the cyclone temperature and the residence time in the cyclone

Appendix B

This appendix contains material used in the data treatment and modelling of the industrial scale measurements.

Figure 7.4 shows how the time delay between changes in ammonia addition and the resulting NO emissions are estimated

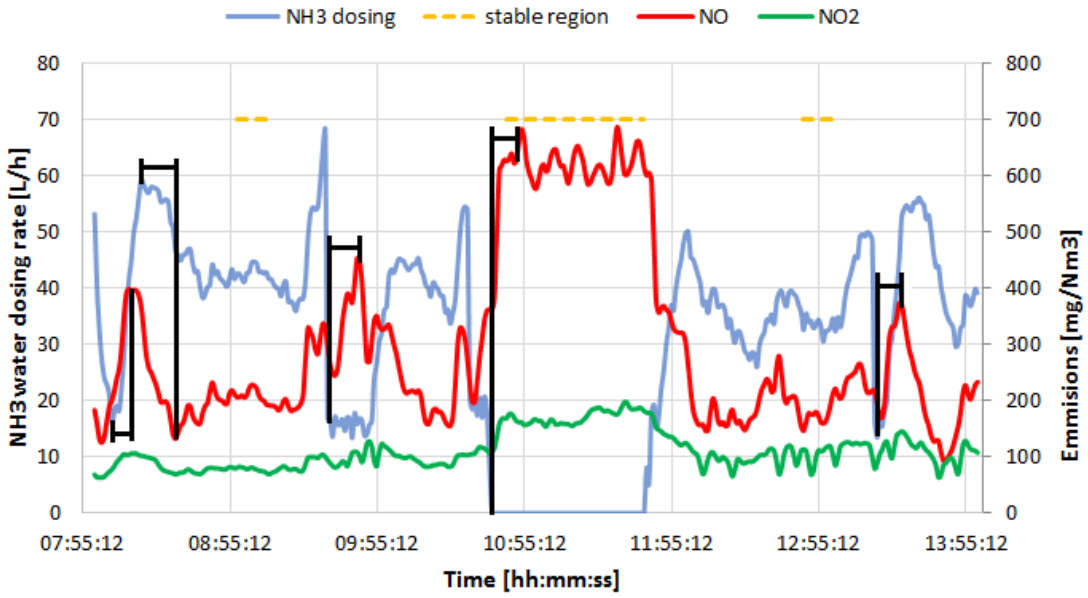

Figure 7.4: example of time delay for NO peaks/minimums caused by minimums/peaks in ammonia addition

Figure 7.5-Figure 7.10: Residence time estimates for the SNCR zone for measurement series 5 shows the dependence of the residence time in the riser and cyclone depends on the gas temperature.

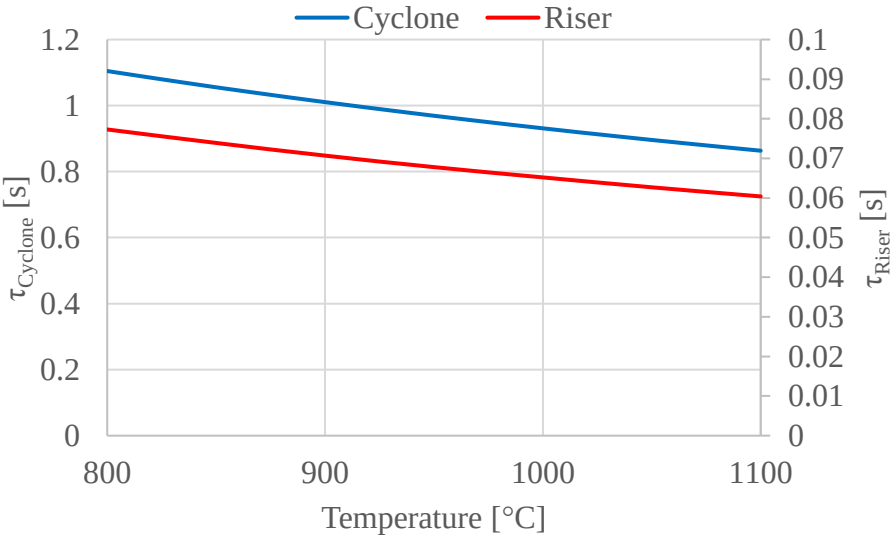

Figure 7.5: Residence time estimates for the SNCR zone in the pre-study

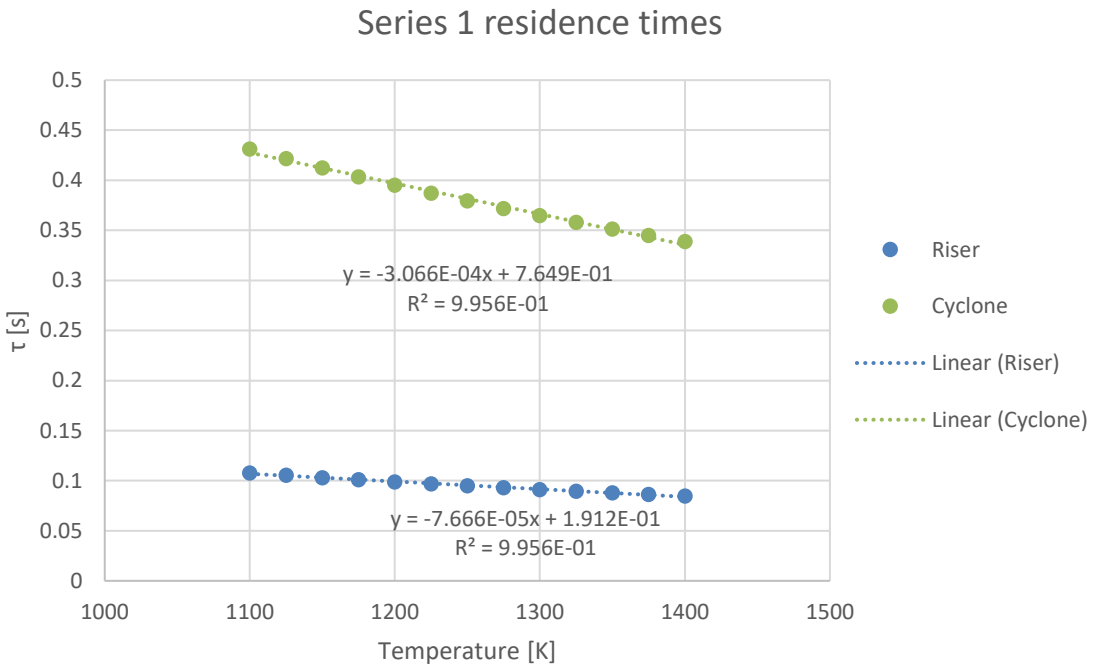

Figure 7.6: Residence time estimates for the SNCR zone for measurement series 1

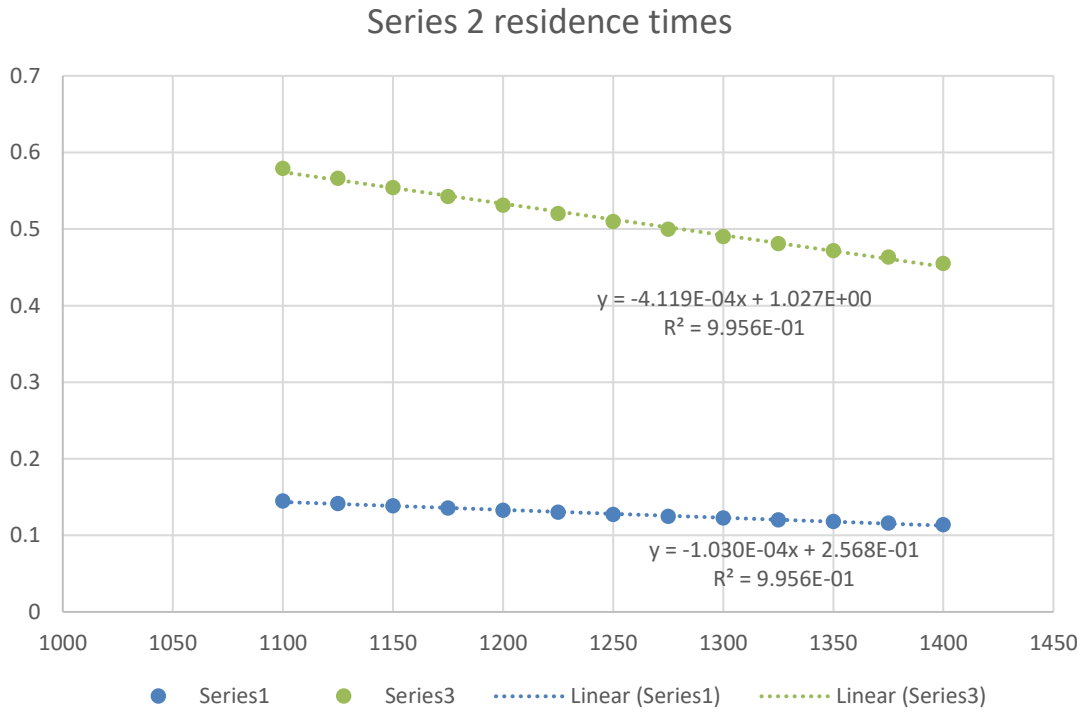

Figure 7.7: Residence time estimates for the SNCR zone for measurement series 2

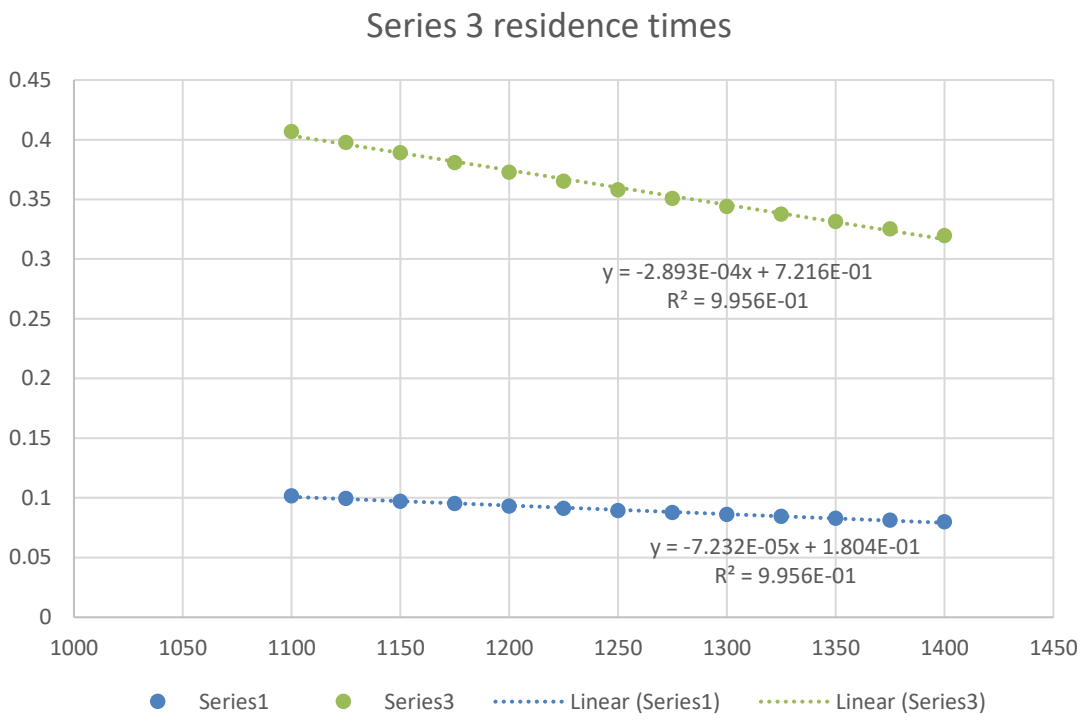

Figure 7.8: Residence time estimates for the SNCR zone for measurement series 3

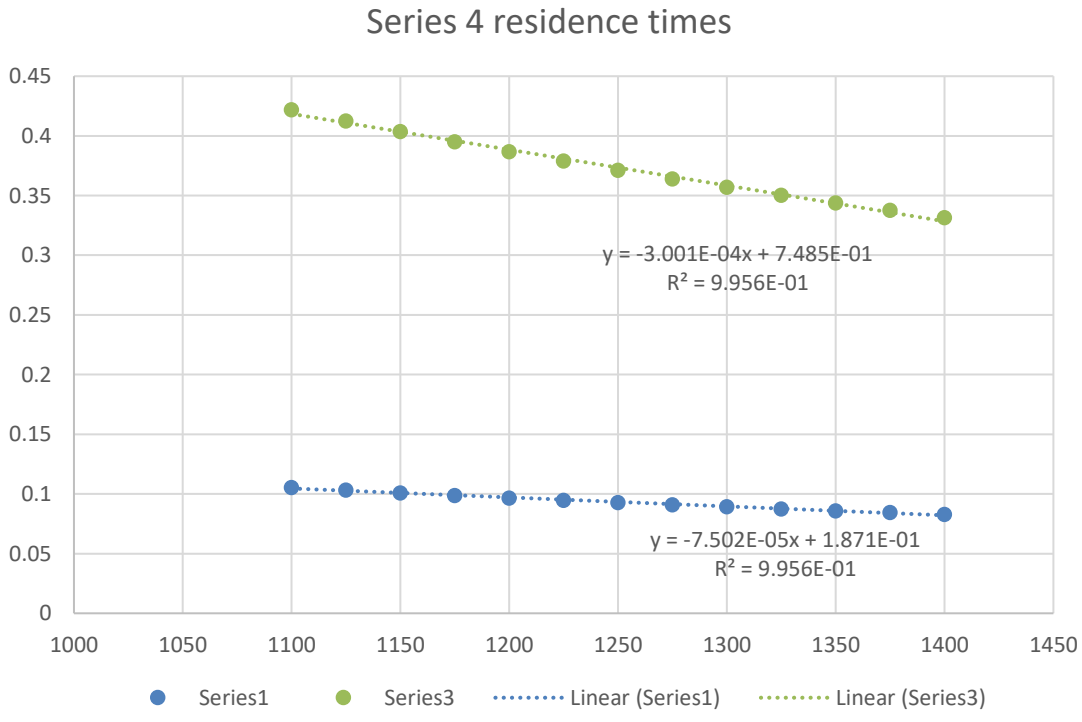

Figure 7.9: Residence time estimates for the SNCR zone for measurement series 4

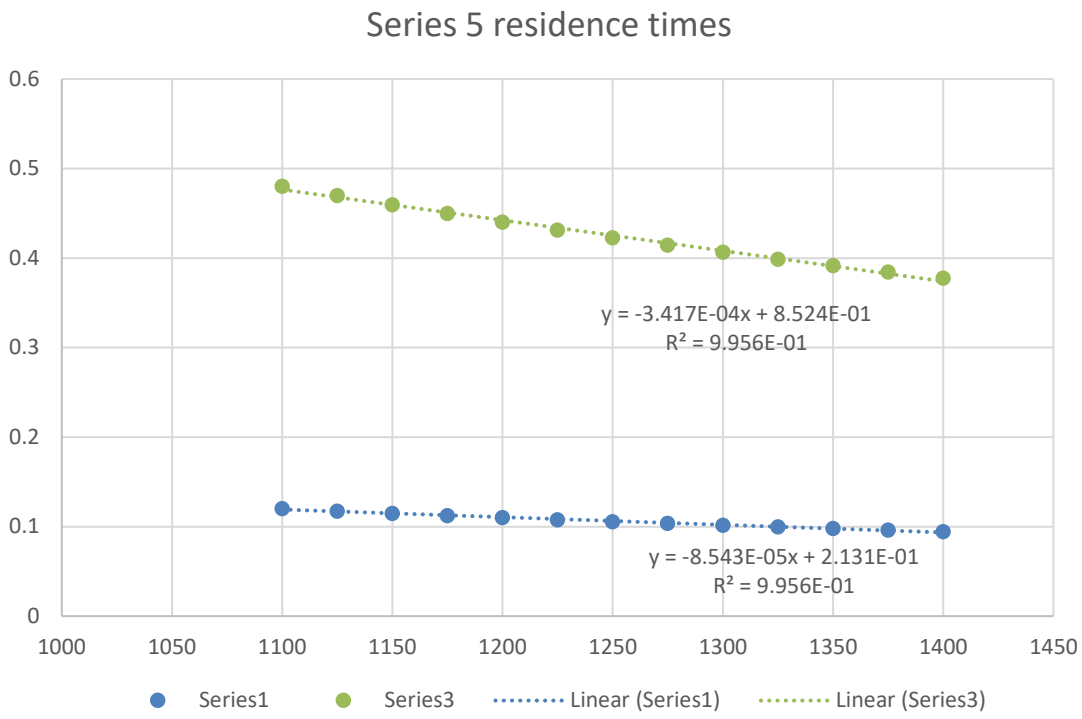

Figure 7.10: Residence time estimates for the SNCR zone for measurement series 5